PHOTOINDUCED REDOX PROCESSES IN SOME IRON PORPHYRINS STUDIED BY RESONANCE RAMAN SPECTROSCOPY

SYNOPSIS

SHANTHA P. K.
DEPARTMENT OF PHYSICS
SCHOOL OF PHYSICAL SCIENCES
NORTH-EASTERN HILL UNIVERSITY
SHILLONG

A THESIS
SUBMITTED FOR THE DEGREE OF

DOCTOR OF PHILOSOPHY

TO

THE NORTH-EASTERN HILL UNIVERSITY
SHILLONG - 793022
INDIA

JUNE 1995

DS
535.846
SHA

MEHU, LIBRARY
Acc.No. 102842
Acc.by. S.B Thakur
Date 15/1/97
Class by 23/10/2000
Sub Head.
Entry
Fra

S Y N O P S I S

Porphyrins and metalloporphyrins play important roles as prosthetic group in a wide variety of biological systems. The photosensitizer and redox chromophore in photosynthetic systems is a magnesium porphyrin. In hemeproteins the iron protoporphyrin IX functional group carries out diverse functions, i.e., as oxygen carrier and storage in hemoglobin and myoglobin,[1] as electron carrier in cytochromes[2] and as catalytic centre in peroxidases and catalases.[3] These manifold functions are controlled by the microenvironment of the heme group provided by the protein pocket. Changes in oxidation, ligation and spin states of the central iron atom with concomitant changes in the stereochemistry of the chromophore are responsible for the diverse physicochemical and biochemical functions of hemeproteins. The cooperative binding[4] of dioxygen to hemoglobin exemplifies the mode of action of these biomolecules. In an effort to understand the structure-function relationship of these complicated biomolecules, extensive studies on naturally occurring iron porphyrins and their model complexes have been carried out by a wide variety of techniques[5] at interdisciplinary level.

As the reduced state of iron is often an essential requirement in the functioning of most of the hemoproteins, a variety of techniques have been used to achieve this state in model and natural iron porphyrin systems including chemical,[6] electrochemical[7] and photochemical methods.[8] For a proper understanding of the functioning of hemeproteins and other porphyrin systems, it is necessary to elucidate the basic mechanism of redox processes under different environmental conditions.

The nature of chemical bonds and the geometrical structure of the molecules lend themselves to be effectively probed by vibrational spectroscopy. Selective enhancement of certain vibrational modes of the porphyrin chromophore by Resonance Raman (RR) technique provides unique and important information about the electronic excited states, chemical bonds, ligation states, core size, effects of environment and conformation of the molecules. Extensive investigations on well characterized porphyrins and metalloporphyrins have resulted in important correlations[9] between Raman frequencies and various stereochemical parameters such as oxidation (of the porphyrin ring or the central metal), ligation and spin states of the central metal atom, core size of the porphyrin ring etc,.

This thesis describes systematic RR and optical absorption studies carried out on model iron porphyrins in aqueous and organic solvents, in the presence of biologically relevant nitrogenous imidazole bases as axial ligands, in an effort to understand the mechanism of photoinduced redox reactions in these systems. The RR studies on the μ-oxo dimer of simple iron tetraphenylporphyrin, $(FeTPP)_2O$, formed on dissolution of FeTPPCl in alkaline detergent micelle have enabled us to characterize, for the first time, the oxoferryl porphyrin complex, $TPPFe^{IV}=O$, generated via photodisproportionation of the μ-oxo dimer at ambient and at low temperatures. Our studies on iron tetraphenylporphyrin chloride (FeTPPCl) have shown that under certain conditions reduction at the metal centre takes place on photoexcitation in the presence of specific ligands without the mediation of primary alcohols. Our detailed RR and absorption spectral studies have revealed the presence of an absorption band on the higher energy side of the Soret band in model iron porphyrin complexes under various ligation conditions which arises from a

photoreactive state responsible for photoreduction. This is a significant result for understanding the mechanistic details of photoreduction process in these systems. The studies on photoreduction of iron protoporphyrin (FePPCl, hemin) in ionic and non-ionic micellar media have shown interesting results. While in non-ionic and cationic micelles, photoreduction of hemin in anaerobic conditions in the presence and absence of added nitrogenous ligands was a facile process, in anionic micelle, the same phenomena was observed only in the presence of trace amounts of primary alcohol along with nitrogenous ligands. Individual chapters in this thesis provide details regarding the different aspects of these studies.

This thesis consists of seven chapters:

A general review of Resonance Raman and other related studies of porphyrins and metalloporphyrins form the main content of **Chapter 1.** Important studies on the photoreactivity of iron porphyrins have been discussed. Some of the pertinent photoredox reactions of iron porphyrins as well as related techniques for creating active intermediates capable of catalytic reactions and *in situ* monitoring of these processes by RR technique have been described.

Relevant theoretical aspects for an understanding of the electronic absorption and Resonance Raman spectra of iron porphyrins are dealt with in **Chapter 2.**

Details of various experimental techniques used in this study along with a brief description of the methods of sample preparation, the Laser Raman Spectrometer, relevant details of other instrumentation and

accessories are described in Chapter 3. A brief description of the micellar systems used in our work and preparation of samples in them are also given in this chapter.

In Chapter 4 we report[10] our studies on the photochemical behaviour of μ-oxo dimer, $(FeTPP)_2O$, obtained on dissolution of iron tetraphenylporphyrin chloride, FeTPPCl, in aqueous alkaline detergent micelle, Triton X-100 (TX-100), by RR and UV-VIS absorption studies under different experimental conditions. The 441.6 nm laser excitation of $(FeTPP)_2O$ in aerobic conditions in the absence of added bases at room temperature yielded the RR spectra typical of the μ-oxo dimer. The same sample in anaerobic conditions at room temperature showed Raman bands characteristic of two species: that of a five coordinated, high spin (5cHS) ferrous species as well as that of a low spin oxoferryl porphyrin complex. The latter was identified by the appearance of its characteristic RR marker bands at 1570 $cm^{-1}(\nu_2)$, 1370 $cm^{-1}(\nu_4)$ and a band at 843 cm^{-1} assignable to the $\nu(Fe^{IV}=O)$ axial stretching mode. These modes showed the expected enhancement at low temperature consistent with the higher thermal stability of oxoferryl porphyrin, $TPPFe^{IV}=O$, complex at low temperatures. The polarized nature of the 843 cm^{-1} mode (ρ = 0.4) lends further support for its assignment in accord with earlier observations. The enhancement in the intensity of these modes at lower laser powers along with the expected frequency shift on coordination of dimethylformamide trans to the ferryl oxygen have allowed us to assign the 843 cm^{-1} band unambigously to the $\nu(Fe^{IV}=O)$ stretching mode of oxoferryl porphyrin photoproduct, $TPPFe^{IV}=O$. In the absence of added imidazole bases, the 5cHS ferrous complex is inferred to be axially coordinated by a water molecule. To our knowledge, this is the first observation of an oxoferryl species of simple iron

porphyrin having been stabilized at room temperature in aqueous detergent micelle. The 441.6 nm laser excitation of $(FeTPP)_2O$ in anaerobic conditions in the presence of hindered nitrogenous imidazole bases like 2-methylimidazole (2-MeIm) and 1,2-dimethylimidazole (1,2-MeIm) at room temperature yielded RR spectra typical of a 5cHS ferrous species, or of a six coordinated, low spin (6cLS) ferrous species in the presence of N-methylimidazole (N-MeIm), suggesting that these complexes originate from the same initial ligand-free, four coordinated, intermediate spin ferrous species formed on photoexcitation of the ferric μ-oxo dimer.

In Chapter 5 we present[11] our detailed RR studies of photoreduction of FeTPPCl in CH_2Cl_2, DMSO and in neat 1,2-MeIm in the presence of 2-MeIm and 1,2-MeIm in the first two solvents. When the relative concentration X of 1,2-MeIm (X = [1,2-MeIm]/[FeTPPCl]) in a 1 mM solution of FeTPPCl in CH_2Cl_2 was low ($X \approx 500$), no photoreduction of the iron porphyrin was observed in anaerobic conditions unless trace amounts ($\leq$ 1%) of methanol was simultaneously present. However, in the presence of low concentrations of 2-MeIm ($X \approx 100$), photoreduction of FeTPPCl in CH_2Cl_2 was observed on irradiation at either 441.6 or 406.7 nm under anaerobic conditions. On the other hand, at higher concentrations of 1,2-MeIm in CH_2Cl_2 ($X > 500$) or in neat 1,2-MeIm, clean photoreduction was observed in aerobic conditions on excitation at 441.6 nm even in the absence of methanol. In DMSO, however, low concentrations of 1,2-MeIm ($X \approx 100$) sufficed to effect photoreduction of FeTPPCl even in the absence of methanol. A systematic study of the absorption spectra of FeTPPCl in the above solvent systems under experimental conditions similar to those used for RR work revealed the presence of a new absorption band in the 315-340 nm region in those complexes for which photoreduction was observed in our

RR study. The apprearance of this new absorption band indicates coordination of hindered imidazole(s) or of methoxy group to iron depending on the experimental conditions. We infer that this absorption band, whose most likely origin is a charge transfer (CT) transition from the axial ligand to iron, arises from a photoreactive state responsible for photoreduction. Almost complete photoreduction of FeTPPCl in CH_2Cl_2 in the presence of 2-MeIm observed with 406.7 nm excitation compared to that with 441.6 nm excitation due to higher absorption of the complex at the lower excitation wavelength lends further support for our interpretation.

In Chapter 6 we present[12] detailed RR and optical absorption studies of iron protoporphyrin IX chloride (hemin) solubilized in aqueous non-ionic Triton X-100 (TX-100), cationic cetyltrimethylammonium bromide (CTAB) and anionic sodium dodecyl sulphate (SDS) detergent micelles, where we have employed RR technique for the first time to monitor the photoreduction of hemin under excitation at 441.6 and 457.9 nm. We have observed that in TX-100 and CTAB in anaerobic alkaline conditions hemin is photoreduced under 441.6 and 457.9 nm excitations leading to the formation and stabilization of four-coordinated, intermediate spin (4cIS), ferrous species along with the presence of 5cHS, ferric and ferrous species in minor quantities. While absorption spectra did not reveal any evidence of axial ligation of the hindered imidazoles to ferric hemin in any of the micellar systems used at alkaline pH conditions, their coordination to the 4cIS ferrous species formed by laser excitation of hemin in TX-100 and CTAB in anaerobic conditions is indicated by the RR spectra characteristic of the 5cHS or 6cLS ferrous complexes in the case of 2-MeIm and imidazole ligands respectively. However, in SDS photoreduction of hemin was observed only in the simultaneous presence of 2-MeIm and trace amounts of ethanol

(≈ 1%). This is interpreted as due to the formation[13] of an ethoxy moiety in the presence of 2-MeIm and hemin and its coordination at the axial position trans to the hydroxyl moiety in the ferric complex and transfer of charge from the ethoxy group to the iron centre on photoexcitation.

From a study of the photoreduction process as a function of concentration of the detergent and pH, it has emerged that the hydroxyl ion coordinated monomeric hemin encapsulated within the micelle is the photoreducible species and that in TX-100 and CTAB photoexcitation at $\lambda \leq$ 458 nm results in electron transfer from the hydroxyl ion to iron yielding the ferrous species. Attempts have been made to rationalize the observed absence of photoreduction of hemin in SDS under otherwise identical experimental conditions as in the other two micelles, from the point of view of possible effects of the lesser hydrophobicity of SDS micelle, the proximity of the negative surface charges to the iron centre, the deprotonated carboxylic groups of iron-protoporphyrin and of the known effects of alcohol in coordinating to the iron centre in hemin in the presence of 2-MeIm. Absence of photoreduction of hemin on excitation at λ > 458 nm in the micellar systems indicates a possible link of the process to the high energy Soret transition or a nearby charge transfer transition.

Chapter 7 summarizes the work carried out in this thesis for understanding the mechanism involved in the photoinduced redox processes of iron porphyrins under various experimental conditions. Suggestions for possible future studies as extention of our work and confirmation of the proposed mechanisms and other aspects in this study are also discussed.

REFERENCES

1. Gibson, Q.H. *The oxygenation of Hemoglobin.* In *The Porphyrins*; Dolphin, D., Ed.; Academic Press: New York, 1979; Vol.5, Part C, pp 153.

2. Fergusson-Miller, S.; Brautigan, D.L.; Margoliash, E. In *The Porphyrins*; Dolphin, D., Ed.: Academic Press: New York. 1979; Vol.7, part B, pp 149.

3. Hewson, W.D.; Hager, L.P. In *The Porphyrins*; Dolphin, D., Ed.; Academic Press: New York, 1979; Vol.7, part B, pp 295.

4. Perutz, M.F. *Nature* (London), 1972, 237, 495.

5. (a) *Iron Porphyrins*, Lever, A.P.B. and Gray, H.B., Eds.; Addison-Wesley: Reading, MA. 1983; Part I and II.
   (b) *The Porphyrins*; Dolphin, D., Ed.; Academic Press: New York, 1978; Vol. 1 to 7.

6. (a) Collman, J.P. *Acc. Chem. Res.* 1977, 10, 265.
   (b) Donhoe, R.J.; Atamian, M.; Bocian, D.F. *J. Am. Chem. Soc.* 1987, 109, 5593.

7. Kadish, K.M. *Iron Porphyrins*, Lever, A.P.B. and Gray, H.B. Eds.; Addison-Wesley Publishing Company: Reading, 1983; Part II, pp 161.

8. (a) Bartocci, C.; Maldotti, A.; Varani, G.; Battioni, P.; Carassiti, V.; Mansuy, D. *Inorg. Chem.* 1991, 30, 1255.
   (b) Peterson, M.W.; Rivers, D.S.; Richman, R.M. *J. Am. Chem. Soc.* 1985, 107, 2907.
   (c) Suslick, K.S.; Bautista, J.F.; Watson, R.A. *J. Am. Chem. Soc.* 1991, 113, 6111.

9. Spiro, T.G.; Li, X.-Y. In *Biolgical Applications of Raman Spectroscopy*. Spiro, T.G., Ed.; Wiley-Interscience: New York, 1988; Vol. 3, Chapter. 1.

10. Shantha, P.K.; Verma, A.L. *J. Am. Chem. Soc.* (submitted).

11. Shantha, P.K.; Verma, A.L. *Chem. Phys. Lett.* (submitted).

12. Verma A.L.; Shantha P.K. (To be published).

13. Uno, T.; Hatano, K.; Nishimura, Y. *J. Am. Chem. Soc.* 1994, 116, 4107.

PHOTOINDUCED REDOX PROCESSES IN SOME IRON PORPHYRINS STUDIED BY RESONANCE RAMAN SPECTROSCOPY

SHANTHA P. K.
DEPARTMENT OF PHYSICS
SCHOOL OF PHYSICAL SCIENCES
NORTH-EASTERN HILL UNIVERSITY
SHILLONG

A THESIS
SUBMITTED FOR THE DEGREE OF

DOCTOR OF PHILOSOPHY

TO

THE NORTH-EASTERN HILL UNIVERSITY
SHILLONG - 793022
INDIA

JUNE 1995

DS
535.846
SHA

LIBRARY
102842
S.P. Thakur
15/1/97
23/10/2000

पूर्वोत्तर पर्वतीय विश्वविद्यालय
पू० प० विवि० परिसर, शिलांग-७९३०२२ (मेघालय)
North-Eastern Hill University
NEHU Campus, Shillong-793022 (Meghalaya)

Phone :
Grams : NEHU

Prof. A. L. Verma
Department of Physics

C E R T I F I C A T E

I certify that the thesis entitled "**PHOTOINDUCED REDOX PROCESSES IN SOME IRON PORPHYRINS STUDIED BY RESONANCE RAMAN SPECTROSCOPY**" submitted by Smt. Shantha P.K. for the Degree of Doctor of Philosophy of the North-Eastern Hill University, Shillong, embodies the record of original work carried out by her under my supervision.

She has been duly registered and the thesis is worthy of being considered for the Award of Ph.D. Degree.

This work has not been submitted to any other University for any Degree.

A Verma
5.6.95

(Prof. A. L. Verma)

Thesis Supervisor

June, 1995.

Shillong.

पूर्वोत्तर पर्वतीय विश्वविद्यालय
पू० प० विवि० परिसर, शिलांग-७९३०२२ (मेघालय)
Phone :
Grams : NEHU
North-Eastern Hill University
NEHU Campus, Shillong-793022 (Meghalaya)

Department of Physics

5-6-1995

This is to certify that Ms. Shantha P. K. has cleared the following courses as a requirement for the Ph.D. programme and obtained the indicated grades:

	Courses	Grade	G.P.A.
1.	Many-Body Theory	A	6.5
2.	High Energy Physics	A	6.5
3.	German Language	O	9.6
4.	Numerical Methods with Applications to Computer Programming.	A	6.5

(K.Kumar)
Professor and Head
Department of Physics
School of Physical Sciences
North-Eastern Hill University
Shillong-793022

A C K N O W L E D G E M E N T

It is with great happiness that I wish to express my deep sense of gratitude to Prof. A.L. Verma *for not only introducing me to this subject and his constant guidance and supervision at every stage of this work but also to his kind words of encouragement and help without which this work would not have been completed.*

I wish to take this opportunity to thank Prof. K. Kumar, Prof. C.S. Shastry *and other faculty members of the Department of Physics, NEHU for their constant encouragement during the entire course of my work.*

My sincere thanks goes to Drs. N.K. Chaudhury, G.S.S. Saini, R. Das, T. Chakraborthy, A. Ghosh, L. Santra, B. Dey *and all my colleagues and friends in the Department of Physics for their friendly cooperation and* constant help. *I also thank* Mr. A.K. Rathore *for his invaluable help with the Raman experiments.*

I would like to utilize this opportunity to thank Dr. D.T. Khathing *and the staff of RSIC for their help in providing the UV-VIS Spectrophotometer facility. I would also like to sincerely thank* Prof. S.N. Bhat *and other faculty members of the Department of Chemistry, NEHU for their kind encouragement and help during the course of this work.*

I am extremely grateful to NEHU for giving me the opportunity to undertake and successfully complete this work. I acknowledge with gratitude the financial assistance from the University Grants Commission and the Department of Science and Technology, New Delhi during the period of this programme.

It gives me immense pleasure to acknowledge the constant help, encouragement and affection I have recieved from Ms. Prasuna, Mr. T.N. Gopalakrishna, Dr. T. Mukherjee, Mrs. Ganguly, Mrs. S. Chudamani and Mrs. S. Rukmini *from among the many family members and friends who have extended immeasurable moral support all along and kept my spirits from faltering during the long and ardous years. I also take this opportunity to sincerely acknowledge the various acts of kindness and concern, words of encouragement, love and hope from my* parents, Mr. M.R. Bhashyam, Dr. M.R. Seshadri, Dr. A. Rawat and Mr. P. Ramesh *to name only a few.*

Words are inadequate to convey my very special thanks, love and appreciation to my daughter, Vidhya, *for bearing with extraordinary patience and understanding the many hardships and inconveniences during these many years and for being a constant source of love, comfort and care.*

Shantha PK
2/5/95
(Shantha P.K.)

C O N T E N T S

SYNOPSIS

S Y N O P S I S

Porphyrins and metalloporphyrins play important roles as prosthetic group in a wide variety of biological systems. The photosensitizer and redox chromophore in photosynthetic systems is a magnesium porphyrin. In hemeproteins the iron protoporphyrin IX functional group carries out diverse functions, i.e., as oxygen carrier and storage in hemoglobin and myoglobin,[1] as electron carrier in cytochromes[2] and as catalytic centre in peroxidases and catalases.[3] These manifold functions are controlled by the microenvironment of the heme group provided by the protein pocket. Changes in oxidation, ligation and spin states of the central iron atom with concomitant changes in the stereochemistry of the chromophore are responsible for the diverse physicochemical and biochemical functions of hemeproteins. The cooperative binding[4] of dioxygen to hemoglobin exemplifies the mode of action of these biomolecules. In an effort to understand the structure-function relationship of these complicated biomolecules, extensive studies on naturally occurring iron porphyrins and their model complexes have been carried out by a wide variety of techniques[5] at interdisciplinary level.

As the reduced state of iron is often an essential requirement in the functioning of most of the hemoproteins, a variety of techniques have been used to achieve this state in model and natural iron porphyrin systems including chemical,[6] electrochemical[7] and photochemical methods.[8] For a proper understanding of the functioning of hemeproteins and other porphyrin systems, it is necessary to elucidate the basic mechanism of redox processes under different environmental conditions.

The nature of chemical bonds and the geometrical structure of the molecules lend themselves to be effectively probed by vibrational spectroscopy. Selective enhancement of certain vibrational modes of the porphyrin chromophore by Resonance Raman (RR) technique provides unique and important information about the electronic excited states, chemical bonds, ligation states, core size, effects of environment and conformation of the molecules. Extensive investigations on well characterized porphyrins and metalloporphyrins have resulted in important correlations[9] between Raman frequencies and various stereochemical parameters such as oxidation (of the porphyrin ring or the central metal), ligation and spin states of the central metal atom, core size of the porphyrin ring etc,.

This thesis describes systematic RR and optical absorption studies carried out on model iron porphyrins in aqueous and organic solvents, in the presence of biologically relevant nitrogenous imidazole bases as axial ligands, in an effort to understand the mechanism of photoinduced redox reactions in these systems. The RR studies on the μ-oxo dimer of simple iron tetraphenylporphyrin, $(FeTPP)_2O$, formed on dissolution of FeTPPCl in alkaline detergent micelle have enabled us to characterize, for the first time, the oxoferryl porphyrin complex, $TPPFe^{IV}=O$, generated via photodisproportionation of the μ-oxo dimer at ambient and at low temperatures. Our studies on iron tetraphenylporphyrin chloride (FeTPPCl) have shown that under certain conditions reduction at the metal centre takes place on photoexcitation in the presence of specific ligands without the mediation of primary alcohols. Our detailed RR and absorption spectral studies have revealed the presence of an absorption band on the higher energy side of the Soret band in model iron porphyrin complexes under various ligation conditions which arises from a

photoreactive state responsible for photoreduction. This is a significant result for understanding the mechanistic details of photoreduction process in these systems. The studies on photoreduction of iron protoporphyrin (FePPCl, hemin) in ionic and non-ionic micellar media have shown interesting results. While in non-ionic and cationic micelles, photoreduction of hemin in anaerobic conditions in the presence and absence of added nitrogenous ligands was a facile process, in anionic micelle, the same phenomena was observed only in the presence of trace amounts of primary alcohol along with nitrogenous ligands. Individual chapters in this thesis provide details regarding the different aspects of these studies.

This thesis consists of seven chapters:

A general review of Resonance Raman and other related studies of porphyrins and metalloporphyrins form the main content of **Chapter 1.** Important studies on the photoreactivity of iron porphyrins have been discussed. Some of the pertinent photoredox reactions of iron porphyrins as well as related techniques for creating active intermediates capable of catalytic reactions and *in situ* monitoring of these processes by RR technique have been described.

Relevant theoretical aspects for an understanding of the electronic absorption and Resonance Raman spectra of iron porphyrins are dealt with in **Chapter 2.**

Details of various experimental techniques used in this study along with a brief description of the methods of sample preparation, the Laser Raman Spectrometer, relevant details of other instrumentation and

accessories are described in Chapter 3. A brief description of the micellar systems used in our work and preparation of samples in them are also given in this chapter.

In Chapter 4 we report[10] our studies on the photochemical behaviour of μ-oxo dimer, $(FeTPP)_2O$, obtained on dissolution of iron tetraphenylporphyrin chloride, FeTPPCl, in aqueous alkaline detergent micelle, Triton X-100 (TX-100), by RR and UV-VIS absorption studies under different experimental conditions. The 441.6 nm laser excitation of $(FeTPP)_2O$ in aerobic conditions in the absence of added bases at room temperature yielded the RR spectra typical of the μ-oxo dimer. The same sample in anaerobic conditions at room temperature showed Raman bands characteristic of two species: that of a five coordinated, high spin (5cHS) ferrous species as well as that of a low spin oxoferryl porphyrin complex. The latter was identified by the appearance of its characteristic RR marker bands at 1570 $cm^{-1}(\nu_2)$, 1370 $cm^{-1}(\nu_4)$ and a band at 843 cm^{-1} assignable to the $\nu(Fe^{IV}=O)$ axial stretching mode. These modes showed the expected enhancement at low temperature consistent with the higher thermal stability of oxoferryl porphyrin, $TPPFe^{IV}=O$, complex at low temperatures. The polarized nature of the 843 cm^{-1} mode (ρ = 0.4) lends further support for its assignment in accord with earlier observations. The enhancement in the intensity of these modes at lower laser powers along with the expected frequency shift on coordination of dimethylformamide trans to the ferryl oxygen have allowed us to assign the 843 cm^{-1} band unambigously to the $\nu(Fe^{IV}=O)$ stretching mode of oxoferryl porphyrin photoproduct, $TPPFe^{IV}=O$. In the absence of added imidazole bases, the 5cHS ferrous complex is inferred to be axially coordinated by a water molecule. To our knowledge, this is the first observation of an oxoferryl species of simple iron

porphyrin having been stabilized at room temperature in aqueous detergent micelle. The 441.6 nm laser excitation of $(FeTPP)_2O$ in anaerobic conditions in the presence of hindered nitrogenous imidazole bases like 2-methylimidazole (2-MeIm) and 1,2-dimethylimidazole (1,2-MeIm) at room temperature yielded RR spectra typical of a 5cHS ferrous species, or of a six coordinated, low spin (6cLS) ferrous species in the presence of N-methylimidazole (N-MeIm), suggesting that these complexes originate from the same initial ligand-free, four coordinated, intermediate spin ferrous species formed on photoexcitation of the ferric μ-oxo dimer.

In **Chapter** 5 we present[11] our detailed RR studies of photoreduction of FeTPPCl in CH_2Cl_2, DMSO and in neat 1,2-MeIm in the presence of 2-MeIm and 1,2-MeIm in the first two solvents. When the relative concentration X of 1,2-MeIm (X = [1,2-MeIm]/[FeTPPCl]) in a 1 mM solution of FeTPPCl in CH_2Cl_2 was low ($X \approx 500$), no photoreduction of the iron porphyrin was observed in anaerobic conditions unless trace amounts ($\leq$ 1%) of methanol was simultaneously present. However, in the presence of low concentrations of 2-MeIm ($X \approx 100$), photoreduction of FeTPPCl in CH_2Cl_2 was observed on irradiation at either 441.6 or 406.7 nm under anaerobic conditions. On the other hand, at higher concentrations of 1,2-MeIm in CH_2Cl_2 ($X > 500$) or in neat 1,2-MeIm, clean photoreduction was observed in aerobic conditions on excitation at 441.6 nm even in the absence of methanol. In DMSO, however, low concentrations of 1,2-MeIm ($X \approx 100$) sufficed to effect photoreduction of FeTPPCl even in the absence of methanol. A systematic study of the absorption spectra of FeTPPCl in the above solvent systems under experimental conditions similar to those used for RR work revealed the presence of a new absorption band in the 315-340 nm region in those complexes for which photoreduction was observed in our

RR study. The apprearance of this new absorption band indicates coordination of hindered imidazole(s) or of methoxy group to iron depending on the experimental conditions. We infer that this absorption band, whose most likely origin is a charge transfer (CT) transition from the axial ligand to iron, arises from a photoreactive state responsible for photoreduction. Almost complete photoreduction of FeTPPCl in CH_2Cl_2 in the presence of 2-MeIm observed with 406.7 nm excitation compared to that with 441.6 nm excitation due to higher absorption of the complex at the lower excitation wavelength lends further support for our interpretation.

In Chapter 6 we present[12] detailed RR and optical absorption studies of iron protoporphyrin IX chloride (hemin) solubilized in aqueous non-ionic Triton X-100 (TX-100), cationic cetyltrimethylammonium bromide (CTAB) and anionic sodium dodecyl sulphate (SDS) detergent micelles, where we have employed RR technique for the first time to monitor the photoreduction of hemin under excitation at 441.6 and 457.9 nm. We have observed that in TX-100 and CTAB in anaerobic alkaline conditions hemin is photoreduced under 441.6 and 457.9 nm excitations leading to the formation and stabilization of four-coordinated, intermediate spin (4cIS), ferrous species along with the presence of 5cHS, ferric and ferrous species in minor quantities. While absorption spectra did not reveal any evidence of axial ligation of the hindered imidazoles to ferric hemin in any of the micellar systems used at alkaline pH conditions, their coordination to the 4cIS ferrous species formed by laser excitation of hemin in TX-100 and CTAB in anaerobic conditions is indicated by the RR spectra characteristic of the 5cHS or 6cLS ferrous complexes in the case of 2-MeIm and imidazole ligands respectively. However, in SDS photoreduction of hemin was observed only in the simultaneous presence of 2-MeIm and trace amounts of ethanol

($\approx$ 1%). This is interpreted as due to the formation[13] of an ethoxy moiety in the presence of 2-MeIm and hemin and its coordination at the axial position trans to the hydroxyl moiety in the ferric complex and transfer of charge from the ethoxy group to the iron centre on photoexcitation.

From a study of the photoreduction process as a function of concentration of the detergent and pH, it has emerged that the hydroxyl ion coordinated monomeric hemin encapsulated within the micelle is the photoreducible species and that in TX-100 and CTAB photoexcitation at $\lambda \leq$ 458 nm results in electron transfer from the hydroxyl ion to iron yielding the ferrous species. Attempts have been made to rationalize the observed absence of photoreduction of hemin in SDS under otherwise identical experimental conditions as in the other two micelles, from the point of view of possible effects of the lesser hydrophobicity of SDS micelle, the proximity of the negative surface charges to the iron centre, the deprotonated carboxylic groups of iron-protoporphyrin and of the known effects of alcohol in coordinating to the iron centre in hemin in the presence of 2-MeIm. Absence of photoreduction of hemin on excitation at λ > 458 nm in the micellar systems indicates a possible link of the process to the high energy Soret transition or a nearby charge transfer transition.

Chapter 7 summarizes the work carried out in this thesis for understanding the mechanism involved in the photoinduced redox processes of iron porphyrins under various experimental conditions. Suggestions for possible future studies as extention of our work and confirmation of the proposed mechanisms and other aspects in this study are also discussed.

REFERENCES

1. Gibson, Q.H. *The oxygenation of Hemoglobin.* In *The Porphyrins*; Dolphin, D., Ed.; Academic Press: New York, 1979; Vol.5, Part C, pp 153.

2. Fergusson-Miller, S.; Brautigan, D.L.; Margoliash, E. In *The Porphyrins*; Dolphin, D., Ed.: Academic Press: New York. 1979; Vol.7, part B, pp 149.

3. Hewson, W.D.; Hager, L.P. In *The Porphyrins*; Dolphin, D., Ed.; Academic Press: New York, 1979; Vol.7, part B, pp 295.

4. Perutz, M.F. *Nature* (London), 1972, 237, 495.

5. (a) *Iron Porphyrins*, Lever, A.P.B. and Gray, H.B., Eds.; Addison-Wesley: Reading, MA. 1983; Part I and II.
   (b) *The Porphyrins*; Dolphin, D., Ed.; Academic Press: New York, 1978; Vol. 1 to 7.

6. (a) Collman, J.P. *Acc. Chem. Res.* 1977, 10, 265.
   (b) Donhoe, R.J.; Atamian, M.; Bocian, D.F. *J. Am. Chem. Soc.*, 1987, 109, 5593.

7. Kadish, K.M. *Iron Porphyrins*, Lever, A.P.B. and Gray, H.B. Eds.; Addison-Wesley Publishing Company: Reading, 1983; Part II, pp 161.

8. (a) Bartocci, C.; Maldotti, A.; Varani, G.; Battioni, P.; Carassiti, V.; Mansuy, D. *Inorg. Chem.* 1991, 30, 1255.
   (b) Peterson, M.W.; Rivers, D.S.; Richman, R.M. *J. Am. Chem. Soc.* 1985, 107, 2907.
   (c) Suslick, K.S.; Bautista, J.F.; Watson, R.A. *J. Am. Chem. Soc.* 1991, 113, 6111.

9. Spiro, T.G.; Li, X.-Y. In *Biolgical Applications of Raman Spectroscopy*. Spiro, T.G., Ed.; Wiley-Interscience: New York, 1988; Vol. 3, Chapter. 1.

10. Shantha, P.K.; Verma, A.L. *J. Am. Chem. Soc.* (submitted).

11. Shantha, P.K.; Verma, A.L. *Chem. Phys. Lett.* (submitted).

12. Verma A.L.; Shantha P.K. (To be published).

13. Uno, T.; Hatano, K.; Nishimura, Y. *J. Am. Chem. Soc.* 1994, 116, 4107.

CHAPTER

I N T R O D U C T I O N

The studies on structural and dynamic properties of porphyrins and metalloporphyrins constitute an interesting and important research area in their own right. However, the presence of such species as prosthetic groups in important classes of biomolecules like hemeproteins, chlorophylls, etc., has generated enormous interest on detailed studies of porphyrins and metalloporphyrins by almost all the available experimental techniques and theoretical tools in the roles of models for the active site of such complex systems.

Porphyrins and their metal derivatives are tetrapyrrole systems with π-conjugated double bonds having different groups attached at the periphery. The planar structure of the large porphyrin ring conferred by the strong π-electron interaction over the entire ring is responsible for the rigidity of the ring system. Many metals displace the two central hydrogen atoms and form metalloporphyrins, which may be labile ion complexes or stable porphyrin complexes depending on whether the interaction between the metal and the porphyrin anion is primarily electrostatic or predominently covalent type. The former type are found with metals like Na^{+}, K^{+}, Ca^{2+} etc., while the latter complexes are formed with metals such as Fe^{2+}, Fe^{3+}, Ni^{2+}, Co^{2+}, Zn^{2+}, Mn^{3+} etc. Fig. 1.1a shows the basic tetrapyrrole structure with peripheral substituent patterns in some specific porphyrin complexes.

Important biological functions like photosynthesis in green plants and electron transfer in respiratory chain are mediated by porphyrins and their metal derivatives. Thus, chlorophylls[1] are magnesium complexes of the modified porphyrin ring of the chlorin family, the hydroporphyrin, found in green plants in several forms. The cobalt porphyrin forms the active site of vitamin B_{12} in which the two pyrrole rings are linked directly (Fig. 1.1b). Iron porphyrins form the active site in reversible oxygen transport proteins like hemoglobin, myoglobin[2], in reversible electron transfer proteins like cytochromes[3] and in enzymes such as oxidases, catalases and peroxidases[4] which are involved in irreversible, covalent transformation of substrates. Oxidation or reduction of metalloporphyrins can occur at the central metal or at the porphyrin ring (π-cation or π-anion formation) or at both locations depending on various factors. The oxidized or reduced metalloporphyrins serve as transient intermediate species in the catalytic cycle[1-4] of heme peroxidases, catalases, as well as in the bacterial photoreaction centres[5] of the special pair bacteriochlorophyll *a* dimer in which the two porphyrin rings may share the radical character.

Biomedical interests in porphyrins span the areas of drug metabolism, treatment of diseases like porphyria[6], application of photo chemo and photodynamic therapy of cancerous tumours using hematoporphyrin derivatives in combination with laser irradiation[7]. On the technological side, the vast potential of porphyrins in solar energy harvesting[8] devices, photoconducors, semi and super conductors[9], lasers[10] and chemical catalysis[11] has stimulated great deal of research activity. Several structural synthetic analogues of porphyrins such as phthalocyanines are used as dyes[12] in textile and other industries, processing in the

production of heavy isotopes,[13] and in oxidation-reduction indicators.[14]

Metalloporphyrins perform their biological and catalytic functions only within the protein environment. The elucidation of structure-function relationtionships in these biological macromolecules presents formidable problems due to the sheer size and complexity of these systems. In an effort towards understanding the functions of such complex systems on a molecular basis, simple model compounds that exhibit some of the salient physical or spectroscopic properties of the active site of the proteins have been extensively used. Such models permit one to focus attention on specific structure-function relationships on a considerably reduced scale and under conditions permitting greater flexibility in applying systematic perturbations to the system. The information derived from the model compounds may, under favourable circumstances, be applied directly to an understanding of the molecular basis of the functioning of certain proteins. Although natural porphyrins should serve as best models for proteins, it has been found that certain distinct advantages are gained by studying the synthetic porphyrins[15] in many circumstances. One of the main advantages of utilizing the meso-aryl substituted porphyins is that they tend to aggregate considerably less[16a-c] than do the natural porphyrins.[16d] Synthetic porphyrins also provide the possibility of introducing a wide variety of variations in certain properties of the ligand that shed light on the role of the chemical nature and arrangements of the peripheral substituents in the natural porphyrins. The low symmetry of natural porphyrins was found in many cases to severely limit the spectral resolution and details. The synthetic derivatives provide, on the other hand, idealized four-fold or higher symmetry to the structure. The pyrrole substituted porphyrins with methyl, ethyl, vinyl, propionic acid

and acetic acid groups model the naturally occuring porphyrins, whereas porphyrins with the phenyl groups substituted at the meso carbon positions are purely synthetic in origin.

The absorption spectra of all metalloporphyrins have some common features. These features include a very intense band between 380 and 420 nm called Soret, or γ band and a weaker band between 500 and 600 nm called Q(0,0) or α band, along with an associated side band Q(1,0) or β band, on the shorter wavelength side of the β band. Typical absorption spectra of metalloporphyrins are shown in Fig. 1.2. The electronic transitions of the delocalized π electrons, having maximum density above and below the porphyrin molecular plane are responsible for the observed absorption spectra of metalloporphyrins. The σ electrons are not expected to contribute in this region of the spectrum as they are strongly localized between the nuclei. In certain metalloporphyrins like Mn(III) porphyrins and iron (III) porphyrins, the absorption spectra become complicated due to charge transfer transitions, metal d-d transitions and configuration interactions between the porphyrin excited triplet and singlet states and the charge transfer transitions.[17] The theoretical details of the absorption spectra will be dealt with in Chapter 2.

The same prosthetic group, the iron protoporphyrin IX (Fig. 1.1) present in most of the hemeproteins like hemoglobin, myoglobin, cytochromes, peroxidases, catalases etc., carry out a variety of biological functions. The diversity of these functions are associated with varying degree of change in the heme environment, extending from subtle conformational variations to changes in axial ligands, spin and oxidations states of the iron atom etc., apart from the nature of the polypeptide

chain. In the resting ferrous state of Hb and Mb, the axial ligands are most frequently the imidazole group of nearby histidine residue, and either another histidyl imidazole, methionine sulphur, water or dioxygen. However, hemeproteins with other axial ligands like halide, azide, cyanide and CO are also known and well characterized[2]. In the resting state of most cytochromes, the iron is in the ferric state and attached to two endogenous axial ligands, frequently, an imidazole and a mercaptide moiety.

The process of binding of dioxygen directly to the iron centre in hemoglobin, trans to the histidyl imidazole triggers the process of cooperativity[18] exhibited by hemoglobin, whereby, the iron atom being in its native ferrous state in one subunit changes from a high spin ($S = 2$) deoxy state to a low spin ($S = 0$) oxygenated state. This causes the motion of the proximial histidine and consequent rearrangement of the protein chain which extends to another subunit. The one electron transfer in cytochromes occurs by reversible oxidation-reduction reactions between ferrous and ferric states. Oxidation of substrates by cytochrome P-450 occurs, by transfer to them, of an oxygen atom directly bound to the iron. Peroxidases and catalases form intermediates involving oxygen atom binding directly to the heme group.

A variety of experimental techniques have been used to study iron porphyrins in relation to their various spin, oxidation and axial ligation states[19], and also the intermediate states in the enzymatic cycle in hemeproteins. In the studies on binding of ligands such as O_2 and CO to porphyrins[20] and hemeproteins[21], the nature of the complex multistep process involving movement of iron into the porphyrin plane and the change

in the spin state of the resulting complex to a diamagnetic ground state has been revealed. Further, investigations of the multiple steps of cytochrome P-450, peroxidase, catalase in the oxidation of substrates have also been carried out with model compounds[22a] and intact proteins.[22b,c]

As mentioned before, numerous experimental techniques have been employed to study the various intrinsic physical and chemical properties of model porphyrin complexes that have direct association with their biophysical and biochemical functions. These include, electronic and luminescence spectroscopy,[23] X-ray studies,[24] ESR,[25] NMR,[26] Mössbauer,[27] IR,[28] magnetic susceptibility measurements[29] and Raman Spectroscopy.[30,31] A variety of theoretical approaches including quantum mechanical calculations have helped rationalize the many experimental results.[32]

The extreme sensitivity of the vibrational frequencies of these molecules to the bonding and geometric arrangements of localized groups lends itself for studies of the intermolecular interactions of these systems in a continual effort for an understanding of the mode of functioning of biosystems. In the last two decades, Raman Spectroscopy has emerged as a very powerful technique in the area of vibrational spectroscopy, aided by the development of lasers and great strides in the pulse counting and detection technology. A brief account of the salient features of Resonance Raman (RR) technique is given below.

The interaction of electromagnetic radiation with matter resulting in inelastic scattering of the incident radiation from different excitations in the scattering medium constitutes the basis of Raman Spectroscopy. Intense monochromatic, polarized, tunable lasers and pulsed lasers have enabled the principles of Resonance Raman effect to be applied

in probing the structural details of biological chromophores at physiologically relevant concentrations without interference from other chromophores or their protein environment transparent to the incident radiation. When the energy of the exciting radiation coincides (is in resonance) with the optically allowed electronic transition of the system, selective enhancement of those vibrations occurs which involve mainly the motion of the atoms in that part of the chromophore responsible for the electronic transition. Enhancement in intensity of the Raman bands of the order of 10^3 - 10^6 is possible under resonance conditions compared to the normal Raman scattering where the excitation is far from any of the electronic transition. The peak positions of vibrational modes in the RR spectra are characteristic property of the electronic ground state, while their intensities are strongly dependent on the properties of the excited as well as the ground electronic states.

The extended π-congugated system gives rise to a relatively small HOMO-LUMO energy gap ($\approx$ 2eV) and consequently metalloporphyrins absorb light strongly in the near UV and visible regions of the spectrum. The enhancement of certain vibrations in the RR spectra due to selective excitation in different spectral regions has enabled the proper classification and assignments of the vibrational modes according to their origin and provided a direct monitor of the nature of the electronic states involved in the scattering process. While X-ray diffraction studies have provided detailed crystal structure in the solid state, monitoring dynamic structural changes due to biochemical transformations both in solid and in solution under physiological conditions have been possible with spectrosopic techniques. In combination with IR spectroscopy, RR data can provide detailed information about molecular symmetry and structure.

The peripheral substituents on the porphyrin macrocycle as well as the metal influence the biological and chemical properties of the metalloporphyrins. The π-conjugated electronic system of the chromophore functions as a reservior of electrons in controlling the reactivity at the axial ligand positions of the metal. The planarity of the metal with respect to the porphyrin plane, the external side chain substituents and the axial ligands etc., have also been shown to cause profound changes in the RR spectra of metalloporphyrins and heme proteins.[31c,d] As the prominent bands in the RR spectra of hemeproteins and metalloporphyrins arise mainly from the in-plane vibrations of the heme group,[33] any alterations in the π-conjugation due to substituents are reflected in the RR Spectra.[33b-d]

The variation of intensity of Raman bands with the excitation frequency gives the Raman excitation profile (REP). Important information[31c] regarding the nature of the electronically excited states have been drawn using the REPs. These include the enhancement mechanism of metal-axial ligand stretching modes and of the internal modes of the bound axial ligands. Thus, a charge transfer transition at $\approx$ 490 nm has been identified as being responsible for the enhancement of the $\nu[Fe\text{-}N(Py)_2]$ (Py = Pyridine) symmetric stretch and some internal modes of the axially bound pyridine.[34a,b] Similar enhancement has also been observed in pyridine adducts of Ru^{II} and OS^{II} porphyrins,[34c] the ν(Fe-Cl) stretching mode in FeTPPCl,[31c] the $\nu(RS^{-}\text{-}Fe^{III})$ mode in cytochrome P-450,[34c] the $\nu(Fe\text{-}N_3^{-})$ in the azide bound metmyoglobin,[34d] the $\nu(O\text{-}O_2)$ and ν(O-O) stretching modes in the oxy-cobalt myoglobin. RR enhancement due to charge transfer transitions from filled porphyrin π orbitals to metal d orbitals have been shown to be responsible for the appearance of $Fe\text{-}F^{-}$ and $Fe\text{-}OH^{-}$

stretching modes in metmyoglobin[35a] and in Mn^{III} porphyrins[35b] from a study of their REPs. Fig. 1.3 illustrates the REPs of some Raman modes in a metalloporphyrin.

Observation of dispersion in the depolarization ratio with the excitation frequency have been correlated with transformation of the structure of the molecule in solution.[36] The Raman bands in hemeproteins and metalloproteins constituted the first experimental evidence of antisymmetric vibrational scattering leading to inverse polarization, although this phenomena was first predicted long back by Placzek.[37]

The markedly different RR spectra exhibited by hemeproteins[38a,b] and metalloporphyrins in different chemical states in early studies attracted attention on identification of the RR marker bands corresponding to the oxidation and spin states of the iron centre. The frequency of the oxidation state RR marker band $\nu_4(C_\alpha\text{-}N)$ pyrrole half-ring stretch is known to depend upon the electron density in the $e_g(\pi^*)$ orbital of the porphyrin core. The electron density in this orbital decreases on π-backbonding from axial ligands increasing the frequency of this mode. RR study of etioporphyrin[38c] anion radicals also supported the above electron density changes in $e_g(\pi^*)$ orbitals. A similar upshift of the spin state marker[34a,39] bands depending on the oxidation state of the metal, was attributed to the withdrawal of the d_π electrons from the $e_g(\pi^*)$ orbitals due to competition from the axial ligand π^* orbitals. The spin state marker bands were first thought to be due to doming of the porphyrin ring.[39b] Spaulding et al[40a] suggested that one of the spin marker bands, the anomalously polarized ν_{19} mode, showed consistent correlation with the porphyrin core size. Further studies established that all skeletal modes

above 1450 cm^{-1} show inverse linear correlation with the core size[39c,40b] including the ν_{19}, and two other spin state marker bands,[31c,d] ν_3 and ν_{10}. Systematic deviations have been observed for domed porphyrins[39c] which are thought to arise from loss in π-conjugation due to tilting of the pyrrole rings. The core size dependence was inferred to result from changes in methine bridge force constants as the porphyrin contracts or expands.[40c] Changes in the core size were expected to be accommodated by alterations in methine bond angles and bond lengths.[40d] Fig. 1.4 illustrates the core size correlation with various porphyrin skeletal modes.

The axial coordination site of metalloporphyrins is the catalytic site of chemical reactions in model complexes as well as in biological systems. Several RR studies were addressed to explore the mode of of interaction between the metal and the axial ligand. The assignment of the Fe-histidine stretching (ν_{Fe-His}) RR band of hemoglobin by Kitagawa et al[41a] focussed general attention in connection with the strain model for hemoglobin cooperativity.[41b] Hori and Kitagawa[42a] first assigned an RR band at 206 cm^{-1} due to the iron-imidazole stretching mode in Fe^{II}PP(2-MeIm) complex. The solvent sensitivity[42b] of this mode is shown by a decrease in its frequency to 205 cm^{-1} in the hydrophobic environment of a detergent micelle, or in benezene solution, but an increase to 220 cm^{-1} in aqueous medium and on deprotonation of the coordinated imidazole at N_δ position, to 239 cm^{-1}. Such changes in the $Fe-N_{axial}$ stretching frequency have been attributed to the effect of hydrogen bonding between the N_δ-proton and the H-bond acceptor molecule, increasing this frequency with increasing H-bonding interaction. Based on these observations the higher frequency of the Fe-histidine stretching mode for the peroxidase than for hemoglobin was attributed to strong H-bonding of proximal

histidine and the resultant strong σ-basicity of an imidazole-like ligand.[42c] Other examples of such H-bonding have been found in deoxyMb and deoxyHb as well.[41a,42b] It has been recently found that the hindered imidazoles, 2-MeIm and 1,2-MeIm, bind to the iron centre in two different configurations, tilted and vertical, with respect to the porphyrin plane in iron protoporphyrin dimethyl ester and iron octaethylporphyrin complexes.[43] The metal-ligand bond at the fifth coordination site of hemeproteins plays a key role in their functions. The RR mode arising from the metal-ligand stretching is thus a sensitive probe for monitoring the coordination state of the axial ligands.

It has been known for long that photoexcited porphyrins and related compounds like chlorophyll can function as net electron donor or acceptor or otherwise mediate electron transfer.[44a,b] The dual function of chlrophylls as both electron acceptor and donor forms the cornerstone of photosynthesis.[44] Irradiation of chlorophyll, porphyrins and metalloporphyrins in polar solvents in the presence of electron acceptors often leads to production of detectable transients or permanent products due to net electron transfer. Formation of exciplexes having some charge transfer contribution can provide an alternate channel for reaction in certain systems. In polar solvents, both triplet and singlet excited electronic states of metalloporphyrins yield free ions that recombine to yield the starting materials at rates near the diffusion controlled limit, whereas in non-polar solvents quenching of metalloporphyrin triplet states lead to long-lived triplet exiplexes, which do not decay to free ions for long durations.[44a,c]

A useful model of electron distribution in the porphyrin macrocycle in understanding both the photooxidations and photoreduction of porphyrins and metalloporphyrins was proposed by Woodward.[45] Each of the pyrrolenine units (Fig. 1.5a) of the porphyrin macrocycle contains five π-electrons which on removing electron density from the methine bridge C_m positions achieve an aromatic sextet. Fig. 1.5b shows the extreme resonance structure. The methine bridges carry partial positive charge when no electron transfer has taken place between the metal and the porphyrin and no redox reaction has taken place on the porphyrin ring. These nucleophilic type additions occur readily. However, the change in electron density at methine position is pronounced while it is very little on the aromatic system of the pyrrole rings when electrons are donated from either the central metal or externally (reduction of the ligand). The variable redox behaviour of the central metal induces great diversity in the reactivity of the methine bridges.[46]

The photochemistry and photophysics of porphyrins and metalloporphyrins are also of interest from the point of view of conversion of solar light energy to chemical energy, photodynamic therapy in treatment of malignant tumours, in applications in chemical industries etc,. Porphyrins with low oxidation potentials are found to be easily oxidized and those with high oxidation potentials are easily reduced. While an electron is added with difficulty it is easily removed[47a] from the porphyrin ring as the central metal atom distributes its negative charges mostly within the porphyrin ligand. The site of redox reactions are influenced by many factors such as the spin and oxidation states of the metal, perphiral substituents at the porphyrin ring, nature of axial ligands, solvents, temperature, the proximity of the donor acceptor pairs

etc. The oxidation and reduction of porphyrins and metalloporphyrins by chemical, electrochemical and photochemical methods, its mechanism and characterization by various techniques have been extensively reviewed.[47] From electrochemical and ESR studies of metalloporphyrins the general pattern emerged that while metals with low third ionization potentials (Fe, Co, Ni) were oxidized to the +3 state and then the ring was oxidized in two one-electron transfer steps, copper and zinc porphyrins underwent only two ring oxidations but not a change of oxidation state of the central metal. In electrochemical studies of redox processes the electron donor/acceptor is the metal electrode. Specific information on the ground state properties which relate to the variation of the redox potential as a function of the basicity of the porphyrin ligand or axial ligand, the nature of peripheral substituents and also of the solvent systems used have been obtained.[47c,d] Both metal and ring centred reductions of these compounds have been observed. The electrochemical and RR studies on metalloporphyrins (M = Zn, Mg, Ni, Cu)[48] have revealed that either the a_{1u} or a_{2u} type radicals were generated depending upon whether the electrons were added to or removed from a_{1u} or a_{2u} orbitals of the porphyrin π-system. In the case of iron porphyrins, strongly coordinating solvents shift the Fe(III)/Fe(II) reduction potential anodically while strongly coordinating anions shift the potential cathodically.[47d] However, no structural information was revealed in these studies.

In heme derived porphyrins, the unsaturated vinyl side chains are shown to be selectively photooxidized by molecular oxygen in organic solvents like pyridine.[49] In magnesium porphyrin, photooxidation under aerobic conditions leads to destruction of the conjugated double bonds and irreversible addition of oxygen with formation of magnesium formyl

biliverdin.[50] The studies on π-cation radicals on oxidation of the porphyrin ring have direct relevance due to the fact that the π-cation radical of chlorophyll is the primary photochemical product in photosynthesis[51a] and the π-cation radicals of ferrylporphyrins in compound I of catalase and peroxidase.[51b] Resonance Raman studies of photooxidation of H_2TPP and ZnTPP in the presence of electron acceptors have been carried out to explore the mechanism of electron transfer under selective laser excitation.[52]

Photochemical methods of study of the redox processes avoids complications and interference from other chemicals used in chemical reduction processes. The identification and characterization of transient intermediate species in the redox processes become easier in the photochemically induced redox reactions for the concentration of such species can be varied as a function of electron donors and acceptors and other parameters. In fact, a combination of these techniques have contributed greatly to a better understanding of the structure-function relationship of metalloporphyrins.

Photoreduction of free-base porphyris in protic solvents yield phlorin complexes.[53] The long lived triplet excited state was proposed as being responsible for the photoreaction. Metalloporphyrins undergo photoreduction either at the metal centre or at the porphyrin ring. Photoreduction of zinc porphyrin in the presence of ascorbic acid leading to the formation of corresponding chlorin complex was demonstrated by Seely and Talmadge.[54] Photoreduction of the metal centre in metalloporphyrins in various solvent systems has been reported.[55-59] Imamura et al[55a] reported photoreduction of metal centres in Zn(III),

Fe(III), Co(III), and $Mo^{V}O$ tetraphenylporphyrin in organic solvents. From absorption and ESR studies they concluded that the electron transfer from the coordinated halogen to the metal in the excited state led to photoreduction via cleavage of the metal-halogen bond followed by radical abstraction by the solvent. A negative linear correlation of the rates of photoreduction of Fe(TPP)Cl with solvent bond dissociation energy was demonstrated by Hendrickson et al.[55c] They also showed that in these solvent systems clean photoreduction of Fe(TPP)X (X = I, Br, Cl, F) occured on irradiation into the LMCT band in the 350-400 nm range in anaerobic conditions. Photoreduction in metalloporphyrins by homolytic σ-bond cleavage following electron transfer from the coordinated axial ligands on excitation with light of wavelength less than 500 nm in both solution and in matrix isolated conditions[55b] and in substituted benzene solvents[55d,e] have been reported by various workers. The axial ligands[55b] included NO_2, SO_4, NO_3, Cl, OH and ClO_4.

In early studies, photoreduction of the iron centre was observed in several hemeproteins.[56] Some of these studies also showed the wavelength and power dependence of the photoreduction phenomena, the yield of photoreduced species increasing at shorter wavelengths and higher powers.[56b] More recently the indispensability of primary alcohols as an essential constituent of the solvent systems used in the photoreduction of iron porphyrins has been demonstrated.[57a,b] The photoreduction of ferric deuteroporphyrin in benzene, water or micellar solutions containing primary alcohols led the authors[57b] to propose an electron transfer mechanism whereby the axially coordinated alcoholate ligand transfers its charge to the iron centre on photoexcitation in the $\approx$ 265 - 350 nm range. The diverse solvent compositions used, however, did not allow a complete

correlation of the observed phenomena. Studies by Bartocci et al[57c] suggested that photoreduction of chlorohemin in pure pyridine occured via the charge transfer from the monocoordinated pyridine to the iron centre under photoexcitation in the 400-450 nm range.

Recently several reports of RR studies on photoreduction of iron porphyrins in non-coordinating solvents in the presence of hindered imidazole ligands like 2-MeIm and 1,2-MeIm have appeared.[58,59] The presence of primary alcohol in trace amounts was found indipensable for the observation of photoreduction of iron octaethylporphyrin[58a-c] and iron protoporphyrin[59a] complexes in CH_2Cl_2. No photoreduction was observed[58a,b] on irradiation into the CT band (alcohol—>Fe) at ≈ 585 nm although the RR band of ν(Fe-MeOH) stretching mode at 524 cm^{-1} was enhanced at this excitation wavelength. Irradiation at shorter wavelengths led to progressively higher photreduction yields but now along with competition with photooxidation process.[58d] Time-resolved RR studies[58c] indicated the possibility of both 2-MeIm and alcohol coordinated simultaneously to the iron centre as electron donors in the photoexcited state depending on their relative concentrations. A recent report by Uno et al[60a] suggest that in the simultaneous presence of methanol and 2-MeIm the axial ligand coordinated to the ferric porphyrin is the methoxide species and not 2-MeIm. On the other hand, photoreduction of ferric protoporphyrin dimethylester in DMSO at room temperature and low temperatures in the presence of 1,2-MeIm supports the coordination of this nitrogenous ligand in the photoreducible species.[59b]

The observation of photoreduction of FeTPPCl in pure ethanol only under conditions conducive to the formation of the "base" form, in which both an ethoxo and an ethanol moiety are coordinated[60b] to the iron centre only on irradiation within the proposed CT transition at ≈ 335 nm and not at λ_{exc} = > 400 nm, coupled with the absence of photoreduction[60b] in the bis-ethanol complex (lacking this band at 335 nm) of Fe^{III}(TPP) confirms the importance of the ethoxo moiety as well as that of the wavelength of excitation in this process.

The studies of iron porphyrin complexes under conditions approaching the physiological state seem useful for a thorough understanding of their physicochemical properties which play dominant role in the functioning of related biological systems. It is well known that the heme prosthetic group, the ferrous protoporphyrin IX, is distributed as monomer units in the α and β chains of the tetrameric hemoglobin within the hydrophobic pocket provided by the protein chains.[61,19b] The role of the hydrophobic pocket in preventing the oxidation of Fe(II) porphyrin and access to protons has been recognized.[61] Iron porphyrins aggregate in alkaline aqueous medium, leading to the formation of μ-oxo dimer or higher aggregates. However, mono dispersion of iron porphyrins in aqueous detergent micelles has been achieved[62] and has found extensive application in the study porphyrin complexes[63] and of iron porphyrins.[64] However, only few studies of photoreduction of iron porphyrins in micelles are reported,[57b] although reduction of iron porphyrins solubilized in micelles by pulse radiolysis technique has been observed.[65] Most biological reactions require the reduced state of iron. Thus characterization of the reduced iron porphyrins and identification of transient intermediate species, if any, in the photoreduction process in different micellar media

through vibrational studies by RR technique in relation to their structural properties become important.

High oxidation states of transition metal complexes are of considerable importance as major source of metal oxidants. The dioxygen activation of iron (II) porphyrins has attracted much attention in relation to elucidation of the catalytic functions of various heme enzymes[66b] such as peroxidases, catalases, cyt P-450, apart from the mechanism of epoxidation of olefins by oxoferryl porphyrins. Thus, the oxo-iron(IV)porphyrin radical cation formalism (Compound I) has been assigned for peroxidases, whereas oxo-iron(IV) porphyrin structure without radical character has been assigned to Compound II. The successive reduction of Compound I regenerates the enzyme via formation of an enzyme intermediate called Compound II. During the catalytic cycle, the cyt P-450 forms the dioxygen adduct which is converted to a ferryl species (akin to compound I) via the O-O bond cleavage. The nature and reactivity of these enzyme intermediates have been extensively reviewed.[66] Model synthetic iron porphyrins containing iron(IV) species have been generated by autooxidation of Fe(II) porphyrins, by electrochemical, chemical and photochemical methods[67-70] at low temperatures and characterized by various spectroscopic techniques. The stability of the iron(IV) porphyrin complexes at only low temperatures ($<30^{\circ}C$) in organic solvents had confined all studies of this species, till recently, to low temperatures. Room temperature stabilization and characterization, however, has been possible in only a few synthetic porphyrins and natural enzyme systems.[69b,c,71] RR technique[69-71] has also been used to identify and characterize several oxoferryl species. An important observation that has emerged from these studies is the significant variation of Fe^{IV}=O

stretching frequencies between the hemeprotein and model porphyrin complexes (Table 1.1). The studies have also established a low spin d^4 electronic configuration[68b,72] for the oxoferryl species and a relatively short iron-oxygen bond.[70b]

In the oxoferryl structure, strong interaction between the oxygen lone pair and the metal d_{z^2} orbital, and strong overlap between oxygen π orbitals and metal d_π (i.e. d_{xz} and d_{yz}) orbitals results[73,70b] in electron donation from O^{2-} ligand to the Fe^{IV} atom. The trans ligand effect of a strong σ and π donor ligand is to reduce the charge donation from the oxo ligand to the iron atom and weaken the Fe^{IV}=O bond decreasing its frequency. Table 1.1 gives some of the iron-oxygen stretching frequencies in synthetic iron porphyrins and hemeproteins. Resonance enhancement of the $\nu(Fe^{IV}=O)$ stretching mode in the 780-852 cm^{-1} region with 406.7 nm Soret excitation has been attributed to a charge transfer (CT) transition (oxygen ⟶ Fe) from a filled σ or π ligand orbital to the vacant orbital of the metal[70b] although direct coupling of the $\nu(Fe^{IV}=O)$ mode to the in-plane electronic transition has also been suggested.[31b,70b]

Transient absorption studies of photodisproportionation of the μ-oxo dimer, $(FeTPP)_2O$ and $(FeTPPS)_2O$ in anaerobic organic solvents and aqueous buffer media respectively, on irradiation in the Soret region have been reported to yield[73] a ferrous and an oxoferryl porphyrin as photoproducts following homolytic cleavage of the Fe-O-Fe bond. The formation of oxoferryl species was inferred by its chemical reaction on easily oxidizable substrates added to the solution. However, no RR studies of this process have so far been reported. Other homolytic β bond cleavage of oxoanions of manganese (III) porphyrin (nitrate and nitrite) in

solution leading to the formation of $Mn^{IV}(TPP)O$ species have been reported by Suslick et al.[74]

The structure of iron porphyrins used in our studies presented in this thesis is shown in Fig. 1.6. In this thesis we describe our systematic RR studies on μ-oxo dimer of simple iron tetraphenylporphyrin, $(FeTPP)_2O$, in aqueous detergent micelle in the absence and presence of nitrogenous ligands. The RR scattering from the photodisproportionated products generated by laser irradiation was monitored to study the nature of the photoproducts under different experimental conditions of laser power, solvent composition etc,. From the dependence of the intensity of RR modes on laser power we have identified the oxoferryl porphyrin complex as one of the photoproducts. An enhancement in intensity of the $\nu(Fe^{IV}=O)$ stretching mode at low temperature and a shift in its frequency on coordination by a σ donor ligand in the sixth coordination position further confirmed the nature of this complex. The other photoproduct was identified as a ferrous porphyrin.

Another aspect of our study described in this thesis pertains to the photoreduction of FeTPPCl in some organic solvents like CH_2Cl_2, DMSO and neat 1,2-MeIm in the presence of hindered nitrogenous ligands in the first two solvents. Systematic optical absorption studies in these solvents under conditions similar to those where photoreduction was observed in our RR work revealed the existence of a photoreactive state in the 315-340 nm range. This may be linked to a charge transfer transition from the coordinated axial ligand to the iron centre responsible for the photoreduction process observed in the high spin ferric porphyrin species studied.

Detailed RR and optical absorption spectroscopic studies of iron protoporphyrin IX chloride (hemin) solubilized in ionic and non-ionic detergent micelles under various experimental conditions form another aspect of our studies reported in this thesis. Observation of photoreduction of hemin in non-ionic and cationic micelles in the absence of added hindered imidazole ligands have led us to propose electron transfer from axially coordinated hydroxo moiety to the iron atom under alkaline pH conditions on near Soret photoexcitation. In anionic micelle, however, photoreduction was not observed in the presence of 2-methylimidazole unless trace amounts of ethanol was present. A photoreduction mechanism has been proposed whereby an electron transfer from the coordinated ethoxy group to the iron centre under excitation at 441.6 nm takes place followed by stabilization through axial coordination of imidazole ligand(s). It was further observed that only the monomeric high spin hemin coordinated by the hydroxyl moiety in alkaline conditions is photoreducible under near Soret excitation.

REFERENCES

1. (a) Falk, J.E. In *Porphyrins and Metalloporphyrins*; Elsevier: Amsterdam, 1964.
   (b) Fajer, J.; Davis, M.S. In *The Porphyrins*; Dolphin, D., Ed.; Academic Press: New York, 1979; Vol. 4B, pp 167.

2. (a) Antonini, E.; Brunori, M. in *Hemoglobin and Myoglobin in their Reactions with Ligands*; North-Holand: Amsterdam, 1971; pp 73.
   (b) Hewson, W.D.; Hager, L.P. In *The Porphyrins*; Dolphin, D., Ed.; Academic Press: New York, 1979; Vol. 7, pp 295.

3. (a) Davies, H.S.; Forman, A.; Fajer, J.; *Proc. Natl. Acad. Sci. U.S.A.* 1979, 76, 1476.
   (b) Harbury, H.A.; Marks, R.H.L. In *Inorganic Biochemistry*; Eichhorn, G., Ed.; Elsevier: Amsterdam, 1973; Vol. 2, Chapter 1.
   (c) *The Porphyrins*; Dolphin, D., Ed.; Academic Press: New York, 1979; Vol. 7. Chapters 1-7.

4. Schonbaum, G.R.; Chance, B.; In *The Enzymes*; Boyer, P.D., Ed.; Academic Press: New York, 1976; Vol. 13, pp 363.

5. (a) Parson, W.W.; Ke, B. In *Photosynthesis: Energy Conversion by Plants and Bacteria*; Grovindijee., Ed.; Academic Press: New York, 1983.
   (b) Norris, J.R.; Sheer, H.; Katz, J.J. In *The Porphyrins*; Dolphin, D., Ed.; Academic Press: New York, 1979; Vol. 4, pp. 159.

6. Golderg, A.; Remington, C. In *Diseases of Porphyrin Metabolism*; Thomas: Springfield, 1962.

7. (a) Jori, G. In *Laser in Photomedicine and Photobiology*; Pratesi, R. Sacchi, C.A., Eds.; Springer: New York, 1980; pp 58.
   (b) Jori, G. In *Primary Photoprocesses in Biology and Medicine*; Benasson, R.V.; Jori, G.; Land, E.J.; Truscott T.G., Eds.; Plenum: New York, 1985; pp 349.

8. (a) Alt, H.; Binder, H.; Sandstede, G. *J. Catalysis.* 1973, 28, 8.
   (b) Derwent, J.R.; Douglas, P.; Harriman, G.; Porter, G; Ricoux, M.C. *Coord. Chem. Rev.* 1982, 44, 83.

9. Haak, F.; Nolta, J. *J. Chem. Phys.* 1963, 38, 2648.

10. Berezin, B.D. In *Coordination Compounds of Porphyrins and Phthalocyanines*; John Wiley: New York, 1981; Chapter 1.

11. Fleischer, E.B.; Krishnamurthy, M. *J. Am. Chem. Soc.* 1972, 94, 1382.

12. Patterson, D. In *Pigments, an Introduction to their Physical Chemistry*; Elsevier: New York, 1964; pp 44.

13. Lever, A. *Advances. Inorg. Radiochem.* 1965, 7, 27.

14. Cerny, P. *Chem.* Zvesti. 1955, 9, 94.

15. (a) Whitlock, H.W.; Hanauer, R. *J. Org. Chem.* 1968, 33, 2169.
(b) Adler, A.D.; Longo, F.R.; Finarelli, J.F.; Goldmacher, J.; Assour, J.; Korsakoff, L. *J. Org. Chem.* 1967, 32, 476.

16. (a) Fulton, G.P.; La Mar, G.N. *J. Am. Chem. Soc.* 1976, 98, 2119.
(b) Walker, F.A. *J. Mag. Resonance*, 1974, 15, 201.
(c) Snyder, R.V.; La Mar, G.N. *J. Am. Chem. Soc.* 1977, 99, 7178.
(d) White, W.I. In *The Porphyrins*; Dolphin, D., Ed., Academic Press: New York, 1979; Vol. 5, pp 303.

17. Kobayashi, H.; Yanaga, Y.; Osada, H. *Bull. Chem. Soc.* Jpn. 1973, 1471.

18. (a) Perutz, M.F. *Nature* (London) 1970, 228, 726.
(b) Perutz, M.F.; TenEyck, L.F. *Cold Spring Harbor Symp. Quant. Biol.* 1971, 36, 295.

19. (a) Collman, J.P.; Hoard, J.L.; Kim, N.; Lang, G.; Reed, C.A. *J. Am. Chem. Soc.* 1975, 96, 2676.
(b) Collman, J.P. *Acc. Chem. Res.* 1977, 10, 265.
(c) Jamesson, G.B.; Molinaro, F.S.; Ibers, J.H.; Collman, J.P.; Brauman, J.L.; Rose, E.; Suslick, K.S. *J. Am. Chem. Soc.* 1980, 102, 3224.
(d) Caron, C.; Mitscher, A.; Riviere, L.R.; Schappachar, M.; Weiss, R. *J. Am. Chem. Soc.* 1979, 101, 7401.

20. Traylor, T.G.; Berzinis, A.P. *Proc. Natt. Acad. Sci.* 1980, 77, 3171.

21. (a) Satterlee, J.D.; La Mar, G.N.; Bold, T.J. *J. Am. Chem. Soc.* 1977, 99, 1088.
(b) Austin, R.H.; Beeson, K.W.; Eisenstein, L.; Frauenfelder H.; Gunsalus, I.C. *Biochemistry* 1975, 14, 5355.

22. (a) Groves, J.T.; Nemo, T.E.; Myers, R.S. *J. Am. Chem. Soc.* 1979, 101, 1932.
(b) Oertling, W.A.; Babcock, G.T. *Biochemistry*. 1988, 27, 3331.
(c) Egawa, T.; Miki, H.; Ogura, T.; Makino, R.; Ishimura, Y.; Kitagawa, T. *FEBS. Lett.* 1992, 305, 206.

23. (a) Gouterman, M. In *The Porphyrins*; Dolphin, D. Ed.; Academic Press: New York, 1978; Vol. 3, pp 1.
(b) Owens, J.W.; O'Connor, T. *Coord. Chem. Rev.* 1988, 84, 1.
(c) Smith, D.W.; Williams, R.J.P. *Struct.Bonding* (Berlin) 1970, 7, 1
(d) Adar, F. In *The Porphyrins*; Dolphin, D., Ed.; Academic Press: New York, 1978; Vol. 3, pp 167.

24. (a) Gans, P.; Buisson, G.; Duée, E.; Marchon, J.C.; Erler, B.S.; Scholz, W.F.; Reed, C.A. *J. Am. Chem. Soc.* 1986, 108, 1223.
(b) Collins, D.M.; Countryman, R.; Hoard, J.L. *J. Am. Chem. Soc.* 1972, 94, 2066.

25. (a) Subramaniam, J. In *Porphyrins and Metalloporphyrins*, Smith, K.M., Ed.; Elsevier: Amsterdam, 1975; pp 555.
(b) Palmer, G. In *The Porphyrins*; Dolphin, D., Ed.; Academic Press: New York, 1979; Vol. 4, pp 313.

26. (a) Janson, T.R.; Katz, J.J. In *The Porphyrins*; Dolphin, D., Ed.; Academic Press: New York, 1979; Vol. 4, pp 1.
(b) La Mar, G N.; Walker, F.A. In *The Porphyrins*; Dolphin, D., Ed.; Academic Press: New York, 1979; Vol. 4, pp 61.
(c) Scheer, H.; Katz, J.J. In *Porphyrins and Metalloporphyrins*; Smith, K.M., Ed.; Elsevier: Amsterdam, 1975, pp 399.

27. (a) Sams. J.R.; Tsin, T.B. In *The Porphyrins*; Dolphin, D., Ed.; Academic Press: New York, 1979; Vol. 4, pp 425.
(b) Hambright,P.; Bearden, A.J. In *Porphyrins and Metalloporphyrins*; Smith, K.M., Ed.; Elsevier: Amsterdam, 1975, pp 539.

28. Alben, J.O. In *The Porphyrins*; Dolphin, D., Ed.; Academic Press: New York, 1978; Vol. 3, pp 323.

29. Mitra, S. In *Iron Porphyrins*; Lever, A.P.B.; Gray. H.B., Eds.; Addison-Wesley: Reading, MA, 1983; part 2, pp 1.

30. Verma, A.L. *Indian J. Phys.* 1980, 54b, 54.

31. (a) Felton, R.H.; Yu, N.-T In *The Porphyrins*; Dolphin, D., Ed.; Academic Press: New York, 1978; Vol. 3, pp 347.
(b) Spiro. T.G. In *Iron Porphyrins*; Lever, A.P.B.; Gray. H.B., Eds.; Addison-Wesley: Reading, MA, 1983; part 2, pp 91.
(c) Spiro, T.G.; Li, X.Y. In *Biological Applications of Raman Spectroscopy*; Spiro, T.G., Ed.; Wiley-Interscience: New York, 1988; Vol. 3, Chapter 1.
(d) Kitagawa, T.; Ozaki, Y. *Struct. Bonding* (Berlin) 1987, 64, 71.

32. (a) Loew, G.H. In *Iron Porphyrins*; Lever, A.P.B.; Gray. H.B., Eds.; Addison-Wesley: Reading, MA, 1983; part 1, pp 1.
(b) Antipas, A.; Gouterman, M. *J. Am. Chem. Soc.* 1983, 105, 4896.

33. (a) Spiro T.G. *Biochim. Biophys. Acta.* 1975, 416, 169.
(b) De Vito, L.V.; Asher, S.A. *J. Am. Chem. Soc.* 1989, 111, 9143.
(c) Sarkar, M.; Verma, A.L. *J. Raman. Spectroscopy.* 1986, 17, 407.
(d) Verma, A.L.; Mendelsohn, R.;Bernstein, H.J. *J. Chem. Phys.* 1974, 61, 383.

34. (a) Spiro, T.G.; Burke, J.M. *J. Am. Chem. Soc.* 1976, 98, 5482.
(b) Wright, P.G.; Stein, P.; Burke, J.M.; Spiro, T.G. *J. Am. Chem. Soc.* 1978, 101, 3531.
(c) Champion, P.M.; Gunsalus, I.C. *J. Am. Chem. Soc.* 1977, 99, 2000.
(d) Tsubaki, M.; Srivastava, R.B.; Yu, N.-T. *Biochemistry.* 1981, 20, 946.

35. (a) Asher, S.A.; Schuster. T.M. *Biochemistry*, 1979, 18, 5377.
(b) Asher, S.A.; Sauer, K. *J. Chem. Phys.* 1976, 64, 4115.

36. Verma, A.L.; Bernstein, H.J. *J. Chem. Phys.* 1974, 61, 2560.

37. Placzek, G. In *Rayleigh and Raman Scattering:* UCRL. Trans. No. 526(L) for *Handbuch der Radiologie*; Marx, E., Ed.; Akademishe Verlagsgesselschaft: Leipzig, 1934; Vol. 6, part 2, pp 205.

38. (a) Brunner, H.; Mayer, A. Sussner, H. *J. Mol. Biol.* 1972, 70, 153.
(b) Verma, A.L., Bernstein, H.J. *J. Raman. Spectroscopy.* 1973, 2, 163.
(c) Ksenofonotova, N.M.; Maslov, V.G.; Sidorov, A.N.; Bobovich, Y, S. *Opt. Spectrosc.* 1976, 40, 462.

39. (a) Kitagawa, T.; Ozaki, Y.; Kyogoku, Y. *Adv. Biophys. Acta.* 1978, 11, 153.
(b) Spiro, T.G.; Strekas, T.C. *J. Am. Chem. Soc.* 1974, 96, 338.
(c) Choi, S.; Spiro, T.G.; Langry, K.C.; Smith, K.M.; Budd, D.L.; La Mar, G.N. *J. Am. Chem. Soc.* 1982, 104, 4345.

40. (a) Spaulding, L.D.; Chang, C.C. Yu, N-T.; Felton, R.H. *J. Am. Chem. Soc.* 1975, 97, 2517.
(b) Choi, S.; Spiro, T.G.; Langry, K.C.; Smith, K.M.; *J. Am. Chem. Soc.* 1982, 104, 4337.
(c) Abe,M.; Kitagawa, T.; Kyogoku, Y. *J. Chem.Phys.* 1978, 69, 4526.
(d) Warshel, A. *Ann. Rev. Biophys. Bioeng.* 1977, 6, 273.

41. (a) Kitagawa, T.; Nagai, K. Tsubki, M. FEBS Lett. 1978, 104, 376.
(b) Perutz, M.F. *Nature* (London), 1972, 273, 495.

42. (a) Hori, H.; Kitagawa, T. *J. Am. Chem. Soc.* 1980, 102, 3608.
(b) Stein, P.; Mitchell, M.; Spiro, T.G. *J. Am. Chem. Soc.* 1980, 102, 7795.
(c) Teraoka, J.; Kitagawa, T. *J. Biol. Chem..* 1981, 256, 3969.

43. Verma, A.L.; Chaudhury, N.K.; Saini, G.S.S. *Spectrochim. Acta.* 1978, 104, 376.

44. (a) Roy, J.K.; Whitten, D.G. *J.Am. Chem. soc.* 1972, 94, 7162.
(b) Harbour, J.R.; Tollin, G. *Photochem. Photobiol.* 1974, 19, 147.
(c) Roy, J.K.; Carrol, F.A.; Whitten, D.G. *J. Am. Chem. Soc.* 1974, 96, 6349.

45. Woodward, R.B. *Ind. Chim. Belge.* 1962, 2, 1293.

46. Fuhrhop, J.H. *Struct. Bonding* (Berlin) 1974, 18, 1.

47. (a) Felton, R.H. In *The Porphyrins*; Dolphin, D., Ed.; Academic Press: New York, 1978; Vol. 5, pp 53.
(b) Caestro, C.E. In *The Porphyrins*; Dolphin, D., Ed.; Academic Press: New York, 1978; Vol. 5, pp 1.
(c) Davis, D.G. In *The Porphyrins*; Dolphin, D., Ed.; Academic Press: New York, 1978; Vol. 5, pp 127.

(d) Kadish. K. M. In *Iron Porphyrins*; Lever, A.P.B.; Gray. H.B., Eds.; Addison-Wesley: Reading, MA, 1983; part 2, pp. 161.

48. Kim, D.; Miller, L.A.; Rakhit, G.; Spiro, T.G. *J. Phys. Chem.* 1986, 90, 3320.

49. Inhoffen, H.H,; Brockman, H.; Bliesener, K.M. *Justus. Liebigs. Ann. Rev.* 1969, 730, 173.

50. Fuhrhop, J.H.; Kadish, K.; Davis, D.G. *J. Am. Chem. Soc.* 1973, 95, 5140.

51. (a) Borg. D.C.; Fajer, J.; Felton, R.H. *Proc. Natl. Acad. Sci. U.S.A.* 1970, 67, 813.
(b) Dolphin, D.; Forman, A.; Borg, D.C. *Proc. Natl. Acad. Sci. U.S.A.* 1971, 68, 614.

52. (a) Saini. G.S.S; Chaudhury, N.K.; Verma, A.L. *Photochem. Photobiol.* 1992, 55, 815.
(a) Saini. G.S.S; Chaudhury, N.K.; Verma, A.L. *J. Chem. Soc., Farad. Trans*, 1992, 88, 2853.

53. Mauzerall, D. *J. Am. Chem. Soc.* 1962, 84, 2437.

54. Seely, G.R.; Talmadge, K. *Photochem. Photobiol.* 1964, 3, 195.

55. (a) Imamura, T.; Jin, T.; Suzuki, T.; Fujimoto, M. *Chem. Lett.* 1985, 847.
(b) Suslick, K.S.; Bautista, J.F.; Watson, R.A. *J. Am. Chem. Soc.* 1991, 113, 6111.
(c) Hendrickson, D.N.; Kinnaird M.G.; Suslick, K.S. *J. Am. Chem. Soc.* 1987, 109, 1243.
(d) Tohara, A.; Sato, M. *Chem. Lett.* 1989, 153.
(e) Maldotti, A.; Bartocci, C.; Amadelli, B.; Polo, E.; Battioni, P. Mansuy, D. *J. Chem. Soc., Chem. Commun.* 1991, 1486.
(f) Harriman, A.; Porter, G. *J. Chem. Soc., Farad. Trans.* 1979, 75, 1543.

56. (a) Kitagawa, T.; Nagai, K. *Nature*, 1979, 281, 503.
(b) Kitagawa, T.; Chihara, S.; Fushitani, K.; Morimoto, H. *J. Am. Chem. Soc.* 1984, 106, 1860.
(c) Adar, F.; Yonetani, Y. *Biochim. Biophys. Acta.* 1978, 502, 80.
(d) Ogura, T.; Yoshikawa, Kitagawa, T. *Biochemistry.* 1985, 24, 7746.

57. (a) Bartocci, C.; Scandola. F.; Ferri, A.; Carassiti, V. *J. Am. Chem. Soc.* 1980, 102, 7067.
(b) Bizet, C.; Morliere, P.; Brault, D.; Delgado, O.; Bazin, M.; Santus, R. *Photochem. Photobiol.* 1981, 34, 315.
(c) Bartocci, C.; Maldotti, A.; Traverso, O.; Bignozzi, C.A.; Carassiti, V. *Polyhedron.* 1983, 2, 97.

58. (a) Fidler, V.; Ogura, T; Sato, S.; Aoyagi, K; Kitagawa, T. *Bull. Chem. Soc. Jpn.* 1991, 64, 2315.
(b) Ogura, T.; Fidler. V.; Ozaki, Y.; Kitagawa, T. *Chem. Phys. Lett.* 1990, 169, 457.

(c) Sato, S.; Kamogawa, K.; Aoyagi, K.; Kitagawa, T. *J. Phys. Chem.* **1992**, 96, 10676.
(d) Gu, Y.; Li, P.; Sage, T.; Champion, P.M. *J. Am. Chem. Soc.* **1993**, 115, 4993.

59. (a) Verma, A.L.; Chaudhuri, N.K. *J. Raman. Spectrosc.* **1991**, 22, 427.
(b) Chaudhuri, N.K.; Saini, G.S.S.; Verma, A.L. *Inorg. Chem.* **1994**, 33, 346.

60. (a) Uno, T.; Hatano, K.; Nishimura, Y. *J. Am. Chem. Soc.* **1994**, 116, 4107.
(b) Hoshino, M.; Ueda, K.; Takahashi, M.; Yamaji, M.; Hama, Y. *J. Chem. Soc., Farad. Trans.* **1992**, 88, 405.

61. James, B.R. In *The Porphyrins*; Dolphin, D., Ed.; Academic Press: New York, 1978; Vol. 5, pp 205.

62. (a) Simplicio, J. *Biochemistry*, **1972**, 11, 2525 and 2529.
(b) Simplicio, J.; Schwenzer, K. *Biochemistry*, **1973**, 12, 1923.

63. (a) Kadish, K.M.; Maiya. G.B.; Aruallo, C. Guillard, R. *Inorg. Chem.* **1989**, 28, 2725.
(b) Ravikanth, M.; Reddy, D.; Chandrasekhar, T.K. *J. Chem. Soc., Dalton. Trans.***1991**, 2103.

64. (a) Medhi, O.K.; Mazumdar, S.; Mitra S. *Inorg. Chem.* **1989**, 28, 3243.
(b) Mazumdar, S. *J. Chem. Soc., Dalton. Trans.* **1991**, 2091.
(b) Mazumdar, S. *J. Phys. Chem.* **1990**, 94, 5947.

65. (a) Evers, E.L.; Jayson, G.G.; Swallow, A.J. *J. Chem. Soc., Farad. Trans. 1.* **1978**, 74, 418.
(b) Brault, D.; Bizet, C.; Morliere, P.; Rougee, M; Land, E.J.; Santus, R; Swallow, A.J. *J. Am. chem. soc.* **1980**, 102, 1015.

66. (b) Groves, J.T. In *Cytochrome P-450: Structure, Mechanism and Biochemistry*; Ortiz de Montellano, P.R , Ed.; Plenum: New York, 1986; Chapter 1.
(b) *Metal Ion Activation of Dioxygen*; Spiro, T.G., Ed.; Wiley: New York, 1980.
(c) *The Enzymes*; Boyer, P.D., Ed.; Academic Press: New York, 1975; Vol. 12.

67. Ghosh, A.; Almlöf, J.; Lawrence, Q.(Jr). *J. Phys. Chem.* **1994**, 98, 5576.

68. (a) Ozawa, S.; Watanabe, Y.; Nakashima, S.; Kitagawa, T.; Morishima, I. *J. Am. Chem. Soc.* **1994**, 110, 634.
(b) Chin, D.H.; La Mar, G.N.; Balch, A.L. *J. Am. Chem. Soc.* **1980**, 102, 1446 and 5945.
(c) Paeng, I.R.; Nakamoto, K. *J. Am. Chem. Soc.* **1990**, 112, 3289.

69. (a) Czernuszewicz, R.S.; Macor, K.A.; *J. Raman. Spectrosc.* **1988**, 19, 553.
(b) Rodgers, K.T.; Reed, C.A.; Su, Y.O.; Spiro, T.G. *J. Am. Chem. Soc.* **1992**, 31, 2688.

(c) Shedbalkar, V.P.; Modi, S.; Mitra, S. *J. Chem. Soc., Chem. Comm.* 1988, 12, 38.
(d) Groves, J.T.; Gross, Z.; Stern, M.K. *Inorg. Chem.* 1994. 33, 5065.
(e) Schappacher, M; Chottard, G.; Weiss, R. *J. Chem. Soc., Chem. Commun.* 1986, 93.

70. (a) Proniewicz, J.M.; Bajdor, K.; Nakamoto, K. *J. Phy. Chem.* 1986, 90, 1760.
(b) Hashimoto, S.; Tatsuno, Y.; Kitagawa, T. *J. Am. Chem. Soc.* 1987, 109, 8096.
(c) Oertling, W.A.; Kean, R.T.; Wever, R.; Babcock, G.T. *Inorg. Chem.* 1990, 29, 2633.
(d) Gold, A.; Jayaraj, K.; Doppelt, P.; Weiss, R.; Chottard, G.; Bill, E.; Ding, X.; Trautwein, A.X. *J. Am. Chem. Soc.* 1988, 110, 5756.
(e) Oertling, W.A.; Kean, R.T.; Wever, R.; Babcock, G.T.; *Inorg. Chem.*1990, 29, 2633.
(f) Oertling, W.A.; Hoogland, H.; Babcock, G.T.; Wever, R. *Biochemisty*, 1988, 5395.

71. (a) Terner, J.; Sitter, A.J.; Reczek, C.K. *Biochim. Biophys. Acta.* 1985, 828, 73.
(b) Sitter, A.J.; Reczek, C.M.; Terner, J. *Biol. Chem.* 1985, 260, 7515.
(c) Hashimoto, S.; Tatsuno, Y.; Kitagawa, T. *Proc. Natl. Acad. Sci. USA.* 1986, 83, 2417.
(d) Hashimoto, *S.*; Teraoka, J.; Inubushi, T.; Yonetani, T.; Kitagawa, T. *J. Biol. Chem.* 1986, 261, 11110.
(e) Sitter, A.J.; Reczek, C.K. Terner. J. *Biochim. Biophys. Acta.* 1985, 828, 229.

72. Büchler, J.W.; Kökisch, W.; Smith, W. *Struct. Bonding* (Berlin) 1978, 34, 79.

73. (a) Peterson, M.W.; Rivers, D.S.; Richman, R.M. *J. Am. Chem. Soc.* 1985, 107, 2907.
(b) Richman, R.M.; Peterson, M.W. *J. Am. Chem. Soc.* 1982, 104, 5795.
(c) Peterson, M.W.; Richman, R.M. *Inorg. Chem.* 1985, 24, 722.
(d) Guest C.R.; Straub, K.D.; Hutchins, J.A.; Rentzepis, P.M. *J. Am. Chem. Soc.* 1988, 110, 5276.

74. Suslick, K.S.; Watson, R.A. *Inorg. Chem.* 1991, 30, 912 and 2311.

TABLE 1.1: Iron-Oxygen stretching frequencies (cm^{-1}) of oxoferryl porphyrins and hemeproteins.

Species	$\nu(Fe^{IV}=O)$	Solvent: Temp.(°C)	Ref.
$Fe^{IV}=O$(TPP)	852	Ar:-250	70a
$Fe^{IV}=O$(OEP)	852	Ar:-258	70a
$Fe^{IV}=O$(TMP)	843	Toluene:-80	70b
$Fe^{IV}=O$(TMP)	845	Toluene:-46	68c
$Fe^{IV}=O$(TMP)	841	CH_2Cl_2: -40	69a
(THF)$Fe^{IV}=O$(2,6-ClTPP)	841	THF: -50	70d
(DMF)$Fe^{IV}=O$(2,6-ClTPP)	829	THF: -50	70d
(1MeIm)$Fe^{IV}=O$(2,6-ClTPP)	818	THF: -50	70d
(1MeIm)$Fe^{IV}=O$(PPDME)	820	Toluene:-120	70e
(N-MeIm)$Fe^{IV}=O$(TPivPP)	807	THF: -50	69e
(1-MeIm)$Fe^{IV}=O$(TPP)	820	Toluene: -120	70e
(1-MeIm)$Fe^{IV}=O$(OEP)	820	Toluene: -120	70e
(THF)$Fe^{IV}=O$(TpivPP)	829	THF: -50	69e
(OH)$Fe^{IV}=O$(TMPyP)	763	H_2O: pH 13, RT	69b
Protein	$\nu(Fe^{IV}=O)$	pH, Temp.(°C)	Ref.
Mb=O	797	8.5 : 20	71a
HRP-II	775	7 : RT	71a
HRP-II	787	11 : RT	71c
MPO-II	782	11.5 : 5	70f
CCP-I	767,753	4-7 : RT	71e

Abbreviations: TMP, tetramesitylporphyrin: TpivPP, tetrakis(o-pivalolyl-phenylporphyrin: Mb=O, oxo-ferryl myoglobin: MPO-II, myeloperoxidase Compound II: CCP-I cytochrome *c* peroxidase compound I or ES: RT, room temperature.

Porphyrin Dianion Ligands

Pp	protoporphyrin (2- and 4- substituents are $-CH=CH_2$)
Mp	mesoporphyrin (2- and 4- substituents are $-C_2H_5$)
Dp	deuteroporphyrin (2- and 4- substituents are $-H$)
Diacetyl Dp	diacetyldeuteroporphyrin (2- and 4-substituents are $-COCH_3$)

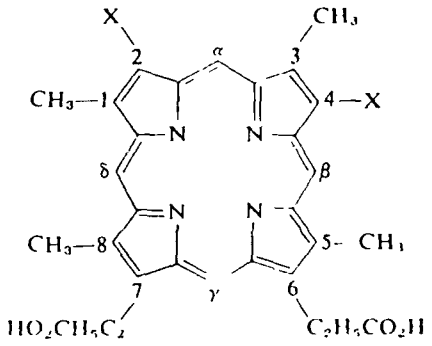

DME	dimethyl ester of a particular porphyrin, e g , PpDME
DEE	diethyl ester of a particular porphyrin, e g , PpDE
OEP	octaethylporphyrin, with $-C_2H_5$ substituents at positions 1–8
TPP	tetraphenylporphyrin, with phenyl substituents at bridging α,β,γ,δ positions and pyrrole 1–8 positions unsubstituted

Fig. 1.1a Illustration of the basic tetrapyrrole and peripheral substituent pattern of some synthetic porphyrins. Metalloporphyrins have a single metal atom in the centre.

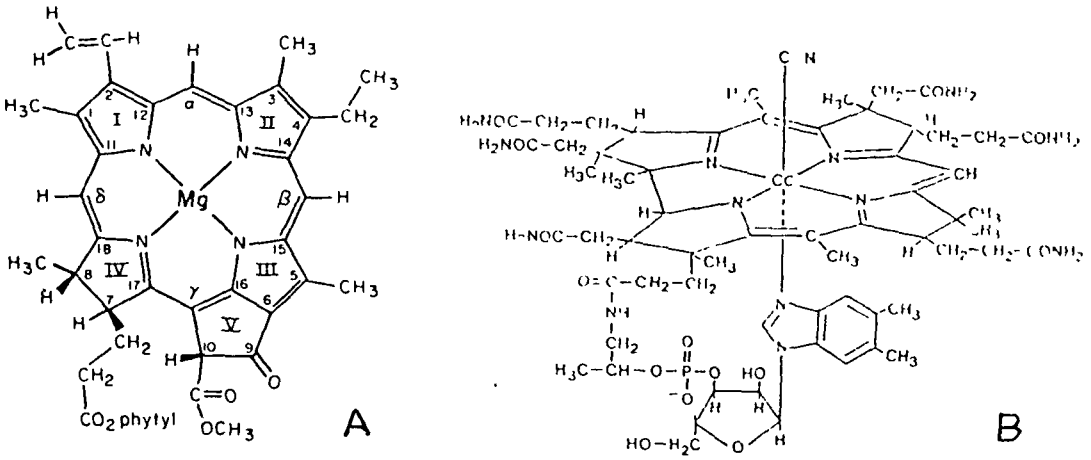

Fig. 1.1b Diagrams showing the basic molecular structure of (A) chlorophyll *a* and (B) Vitamin B_{12} (Cyanocobalamin)

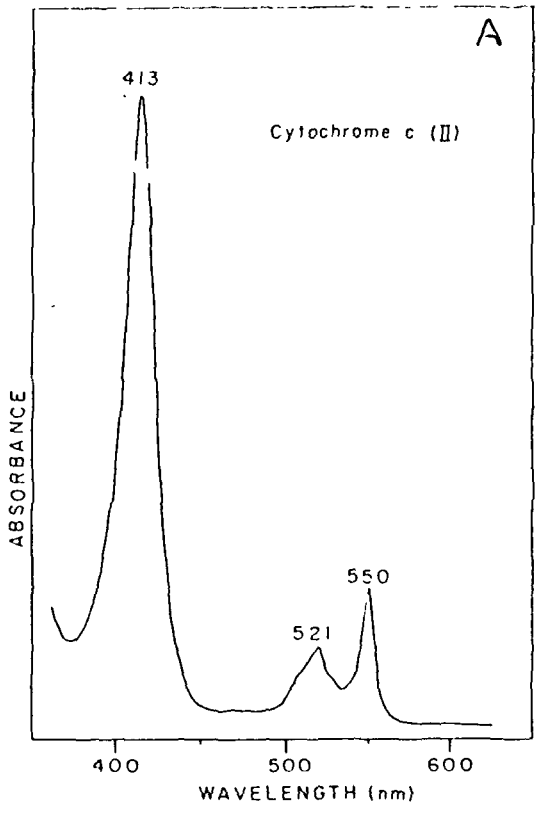

Absorption spectrum of reduced cytochrome *c*.

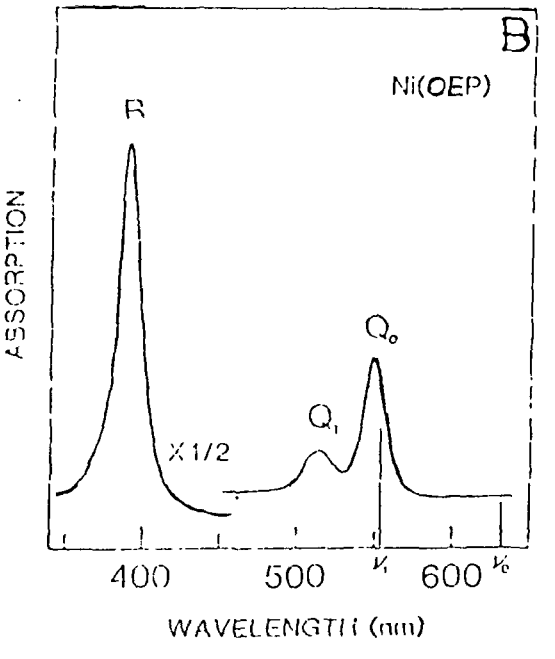

Visible absorption spectrum of octaethylporphyrinatonickel(II), Ni(OEP), in CH_2Cl_2

Fig. 1.2 Typical absorption spectra of heme protein (A) and a synthetic metalloporphyrin (B).

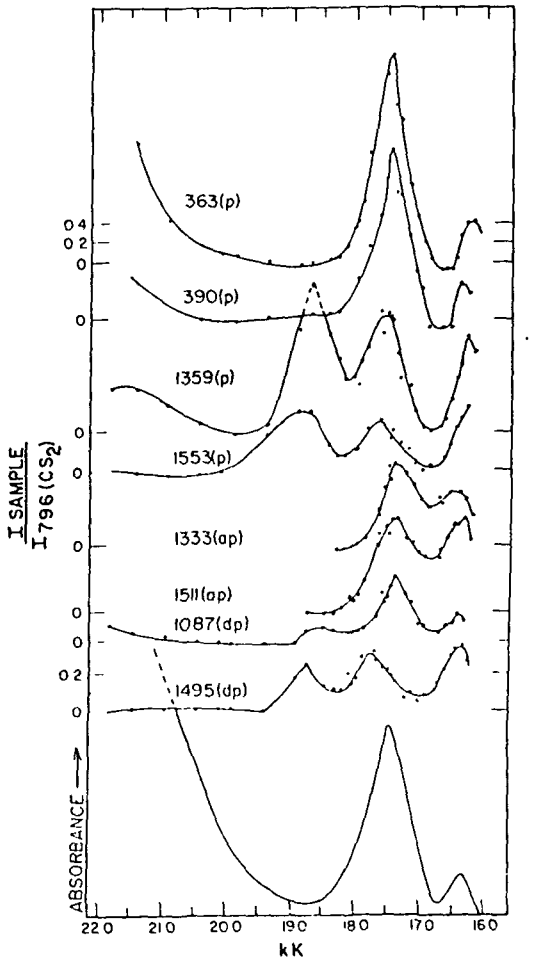

Resonance Raman excitation profiles of [Fe(TPP)]$_2$O. The visible absorption spectrum is shown at bottom of figure.

Fig. 1.3 Illustration of Raman excitation profiles (REP) of some Raman bands in metalloporphyrin.

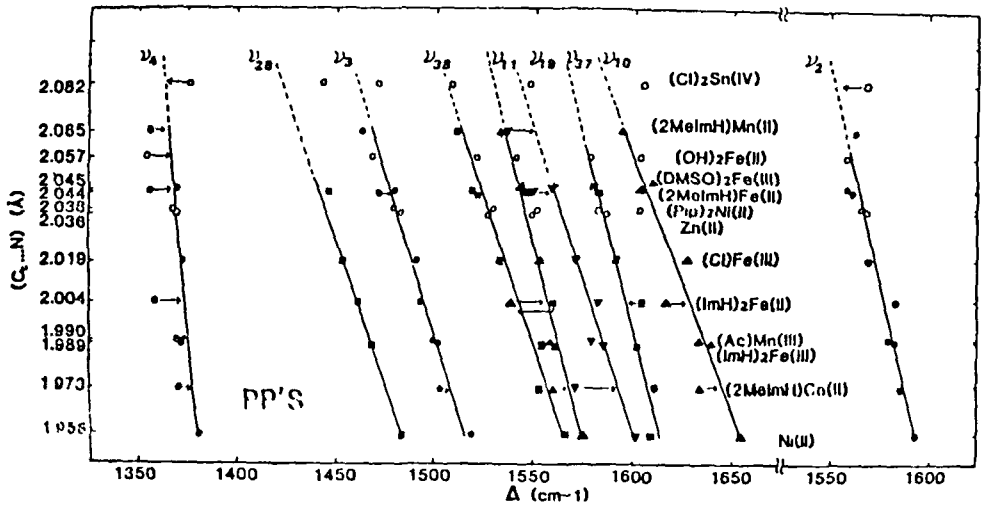

Fig. 1.4 Core size vs. skeletal mode frequencies plotted for indicated metalloporphyrin complexes.

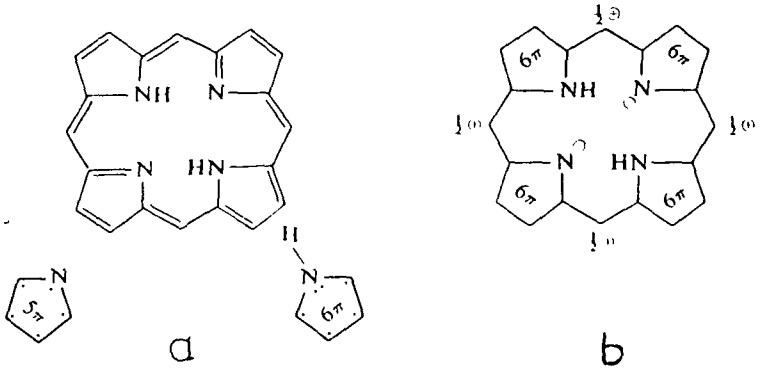

Fig. 1.5 Model for porphyrin electron distribution as proposed by Woodward.

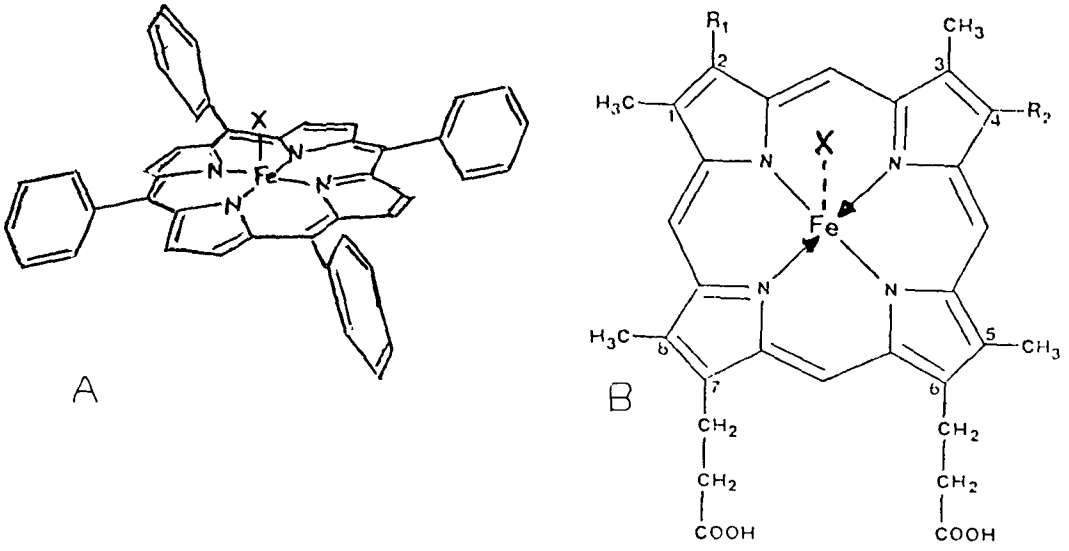

Fig. 1.6 Diagrams illustrating the molecular structure of (A) ferric tetraphenylporphyrin chloride (X = Cl): (B) ferric protoporphyrin (IX) chloride (X = Cl; R_1, R_2 = $CH{=}CH_2$)

CHAPTER 2

THEORETICAL ASPECTS OF ELECTRONIC ABSORPTION AND RESONANCE RAMAN SPECTRA

In this chapter, the relevant theoretical aspects of the electronic absorption spectra of porphyrins in general, and iron porphyrins in particular, are discussed. A brief background of the theory of Resonance Raman scattering is also described.

2.1 Structure and Nomenclature

The basic porphyrin ring is shown in Fig. 2.1.1. This cyclic tetrapyrrole structure was first suggested by Küster.[1] The four pyrrole rings (A to D) are linked through methine bridges at α, β, γ, and δ positions. The ring is structured with a basic fourfold symmetry including nitrogen atoms directed towards the centre. If all the positions labelled 1 to 8, and α to δ are occupied by hydrogen atoms and if there are two hydrogen atoms at the centre, the structure so formed is termed "free-base porphin" or H_2P. If the central core is occupied by a metal, then it is called a metalloporphyrin.

Porphyrins are formally derived from porphin by substitution of some or all of the peripheral hydrogens with various side-chains. In such cases, occupancy by two hydrogen atoms or a metal at the centre yields "free-base" porphyrin or a metalloporphyrin (MP). Depending on the nature of the substituents at the periphery of the ring and at the methine positions, the complexes are known by specific nomenclature. Figure 2.1.1. also gives the structure and nomenclature of some of the commonly known porphyrins. If any one or more of the double bond structure is lost due to

additional substituents at the pyrrole or the methine carbon positions, the resulting complexes are no longer conjugated porphyrins but are termed hydroporphyrins or chlorins. The structure of some of these with their names are shown in Fig. 2.1.2.

2.2. Absorption Spectra

The optical absorption spectra of all metalloporphyrins are dominated by a very intense band between 380 nm and 420 nm known as Soret or B(0,0) or γ band with extinction coefficient $\approx$ 2 to 4 $\times$ 10^5 $M^{-1}cm^{-1}$. A vibronic side band, B(0,1), attributed to addition of one mode of vibrational excitation and separated from B(0,0) by $\approx$ 1250 cm^{-1} towards blue region is also observed in some spectra. Further weaker bands to the blue of the Soret band around 325 nm (N band), 215 nm (M band) and also much weaker L band between these two are exhibited by metalloporphyrins.

In the visible region, the absorption spectra of metalloporphyrins show two bands between 500 and 600 nm designated as α or Q(0,0) and β or Q(0,1) bands, with molar exctinction coefficient of $\approx$ 10^4 M^{-1} cm^{-1}. The lower energy α band is the electronic origin of the lowest energy excited singlet state. The β band which is higher in energy, is vibronic in origin and includes one mode of vibrational excitation.[3a] The vibronic nature of the β band was originally identified from the constant relative energy gap between the Q(0,1) and Q(0,0) bands. The absorption spectra of free-base porphyrins differ from that of the metalloporphyrins in that the visible bands show a four banded (D_{2h} type) structure in the former compared to the two banded structure (D_{4h} type) in the latter. The doubly degenerate in-plane transition Q(0,0) in the D_{4h} symmetry gives

rise to transitions polarized along each of the inequivalent axes in the D_{2h} symmetry of the free-base porphyrins, resulting in the $Q_x(0,0)$ and $Q_y(0,0)$ components. As each has its own vibronic envelope, $Q_x(0,1)$ and $Q_y(0,1)$, there are four bands in the visible region. All these bands of both porphyrins and metalloporphyrins are interpreted as (π, π^*) transitions for their origin. Fig. 2.2.1 shows the typical absorption spectrum of a free-base porphyrin and its metal complex.

In general, the electronic absorption spectra of porphyrins and metalloporphyrins show variation in band positions and intensities depending on the nature of the various substituents at the macrocyclic periphery and the nature of the chromophoric system. Electron withdrawing groups like vinyl, formyl etc., cause a red shift of the bands due to decreased electron density at the pyrrole nitrogen atoms. This, in turn, decreases the porphyrin ligand basicity. Stern et al[2] and other workers[3] have correlated the nature of the substituents with the absorption spectra of porphyrins.While electron donating groups at the porphyrin periphery tend to move the absorption bands to higher energy, unsaturated substituents have the opposite effect. They also tend to increase the intensity of the α-band relative to the β-band. An extreme example of this is seen in the spectra of heme *a*. For a given porphyrin bound to a divalent metal, the bands move to higher energy with increasing electronegativity of the metal. The effect of the axial substituents is usually small except that the α-band can be greatly intensified by a good σ or π donor ligand.[4]

Metalloporphyrins also show additional features in their absorption spectra which arise due to (CT) charge transfer transitions,

metal d-d transitions or some other type of transitions. These bands arise for those metalloporphyrins where there is strong configuration interaction between the energy levels of the metal electrons and those of the porphyrin ring.

2.3. Theoretical Description of Absorption Spectra

Considering the inner 16 membered ring with 18π electrons (each of the 16 atoms of the inner ring contribute one π electron with the imine nitrogens contributing two each) as the delocalization pathway for the electrons, Simpson[5] proposed the first theoretical treatment to explain the optical spectra of the porphyrins. Fig. 2.3.1 shows the π electron system for a free-base porphyrin. His free electron model predicted that the lower energy transitions would be forbidden whereas the higher energy transition would be allowed. In analogy with benzene, the electrons were placed in orbitals of increasing angular momentum. Allowing for the two spin states of each electron, the distribution of two electrons in the lowest level $l_z = 0$ and four electrons in each of the levels $l_z = 1, 2, 3$ and 4, results in the lowest energy excited states by promoting one of the four electrons to the highest filled orbital with angular momentum $l_z = \pm 4$ to the empty orbital with angular momentum $l_z = \pm 5$. The change in the orbital angular momentum would then be either ± 1 or ± 9 and the pairs of the transitions would be allowed or forbidden respectively. Hund's rules predict the lower energy state to correspond to a change in angular momentum $\Delta l_z = \pm 9$. This predicts, as observed, that the longer wavelength transitions are much weaker than the UV-transitions. Simpson accounted for the two sets of visible bands observed in the free-base porphyrins as arising from the two tautomers of the free-base. However, the extra

spectral features of the free-base porphyrins are due to the large distortions from square-planar symmetry of the porphyrin ligand as the free-base porphyrins have protons on opposite nitrogens. On the other hand, the metal substitution at the centre restores the D_{4h} four fold axial symmetry and collapses the four visible bands into two.[3a]

The failure of the Simpson's model to account for many quantitative features of the absorption spectra of porphyrins was a result of the assumed cylindrical symmetry $D_{\infty h}$ instead of the actual D_{4h} or D_{2h} symmetry for these molecules. Expressing molecular orbitals of the π system as linear combinations of atomic orbitals, Longuet-Higgins et al[7] applied the Hückel LCAO treatment and showed that this results in the top-filled orbitals designated as $3a_{2u}(\pi)$ and $1a_{1u}(\pi)$ and the lowest empty degenerate orbital $4e_g(\pi^*)$. Fig. 2.3.2a shows the orbital coefficients of these orbitals. The Q(0,0) and the B(0,0) bands accordingly were associated with the $3a_{2u}(\pi) \longrightarrow 4e_g(\pi^*)$ and $1a_{1u}(\pi) \longrightarrow 4e_g(\pi^*)$ transitions respectively. That the intensity of the Soret band is an order of magnitude larger than that of the Q transitions, however, could not be accounted for by these calculations as the interactions between the singly excited configurations was not taken into account.

These factors were taken into account by Gouterman[3b,6] who developed a theory for explaining the absorption spectra of porphyrins termed as the "four-orbital model", where he incorporated the salient features of both the free-electron model[5] and the LCAO-MO description.[7] He considered only the two lowest empty and the two highest filled orbitals of the porphyrins in the ground state. The highest filled orbitals are designated as a_{1u} and a_{2u} in the D_{4h} symmetry, while the lowest empty

orbitals to which the electrons can be promoted are designated as e_g (Fig. 2.3.2a). The transitions take place due to excitation of an electron from either the a_{2u} or a_{1u} to the e_g orbital. These excited state configurations of E_u symmetry are depicted as $(a_{1u}e_g)$ and $(a_{2u}e_g)$ and mix together by Coulomb repulsion due to their identical symmetry, their overlap being weighted by a finite Coulomb repulsion energy. Such configuration interaction produces the high intensity Soret band in which the transition dipole moments add up and the weak intensity Q band where the transition dipole moments nearly cancel. The a_{1u}, a_{2u} and e_g orbitals are analogous to the free electron orbitals with $l_z = \pm 4$ and $l_z = \pm 5$ respectively in the Simpson's model.[8] Fig. 2.3.2b illustrates the four-orbital model in a schematic manner for a metalloporphyrin.

The singly excited state configurations $(a_{2u}e_g)$ and $(a_{1u}e_g)$ are not adequate descriptions of the excited states as their overlap due to Coulomb repulsion is finite. Let H_{eff} be the Hamiltonian of the pure configurations and if their interaction via Coulomb repulsion between electrons be represented by $H' = \frac{e^2}{r_{ij}}$, then the total Hamiltonian of the system can be written as

$$H = H_{eff} + H' \qquad (2.3.1)$$

The coefficients for the mixed states can be calculated by defining the parameters as follows:

$$A'_{1g} = \frac{1}{2}\left[E(a_{1u}e_{gx}) + E(a_{2u}e_{gy})\right] \qquad (2.3.2)$$

$$A_{1g} = \frac{1}{2}\left[E(a_{2u}e_{gy}) - E(a_{1u}e_{gx})\right] \qquad (2.3.3)$$

$$A''_{1g} = \int (a_{2u}e_{gx})\ H\ (a_{1u}e_{gy})\ dv \qquad (2.3.4)$$

$$R_{1y} = \int (a_{1u} e_{gx})\ y\ \Psi_o\ dv \qquad (2.3.5)$$

$$R_{2y} = \int (a_{2u} e_{gx})\ y\ \Psi_o\ dv \qquad (2.3.6)$$

Since $R_1 \approx R_2$, we have

$$R = \frac{1}{\sqrt{2}} (R_1 + R_2) \qquad (2.3.7)$$

where A'_{1g} is the centre of gravity of the two configurations before interaction, A_{1g} is the splitting between them, A''_{1g} is the configuration interaction and the R's are the transition dipole moments. Table 2.3.1 gives the matrix for Y-polarized mixed states. The X-polarized mixed states would be similar due to the X-Y degeneracy. The rows of the table represent approximate mixtures for the case in which configuration interaction is much larger than the splitting between the pure states. A weak Q band and a minimum in the energy difference E(Soret) – E(Q) which is observed in the absorption spectra of metalloporphyrins is predicted by the case (c). This case also predicts that

$$E_B - E_Q \approx 2\ A'_{1g} = \text{constant} \qquad (2.3.8)$$

and

$$q_B^2 \approx R^2 = \text{constant} \qquad (2.3.9)$$

A plot of E_B vs E_Q gives a slope of 1. Since the oscillator strength of the Soret band is given by

$$f_B \approx E_B\ q_B^2 \qquad (2.3.10)$$

is predicted to be nearly constant as E_B is fairly constant. This is borne out by the data on the absorption spectra of the metalloporphyrins. The removal of degeneracy of the B and the Q bands by configuration interaction has been the major result of this calculation.

About 10% of the intensity is borrowed by the lower energy transition from the higher energy transition (Soret) through vibronic coupling with the formation of a vibronic side band called the β or the Q(0,1) band on the higher energy side of the α band such that

$$\nu_{\beta}^{max} = \nu_{\alpha}^{max} + \nu_{vib} \qquad (2.3.11)$$

where ν_{vib} is the frequency of the vibrational modes in the excited electronic state which are responsible for the vibronic coupling.

It is necessary to apply degenerate perturbation theory to linear combinations of the degenerate components as the electronic states of the metalloporphyrins are degenerate. Since only those vibrations contained in the cross product of the symmetries of the two excited states would be active and as both Q and B states originate from configurations of E_u symmetry, vibronic coupling between the two states can occur by the vibrations having symmetry species given by:

$$\Gamma_{vib} \subset E_u \times E_u = A_{1g} + A_{2g} + B_{1g} + B_{2g} \qquad (2.3.12)$$

It is argued that A_{1g} modes will not be vibronically active if the cyclic polyene model is strictly applicable to metalloporphyrins.[9] Thus in the D_{4h} point group, the only modes vibronically active are those belonging to B_{1g}, B_{2g} and A_{2g} symmetry species.

While the vibrational structure that can be resolved in the Soret band region of the porphyrin spectra can be assigned to the Franck-Condon activity of the symmetric vibrations, the vibrational transitions in the Q(0,1) or the β band region have been attributed to the vibronic borrowing from the Soret band.[9-12] Experimental evidence of the

correctness of this model came from Resonance Raman experiments,[13-15] where it was shown that under Q band resonance excitation of porphyrin complexes, the A_{2g}, B_{1g} and B_{2g} vibrational modes are strongly enhanced, identified by their depolarization ratios. The theoretical section on RR scattering in this chapter will cover further details on the vibronic coupling, Herzberg-Teller activity and the Raman activity of the non-totally symmetric vibrations based on group theoretical and other considerations.

2.4 Absorption Spectra of Iron Porphyrin complexes

The iron porphyrins belong to the d-type hyperporphyrins similar to those of transition metals having an electronic configuration d^m, $1 \leq m \leq 6$ that have vacant $e_g(d_\pi)$ metal orbitals and relatively stable lower oxidations states. The requirement for the vacant $e_g(d_\pi)$ orbitals excludes the low spin (S = 0) ferrous complexes. The hyper type absorption spectra have extra absorption bands in addition to the Q, B and the N bands in the region $\lambda > 320$ nm. The iron porphyrins and hemeproteins show the characteristic spectra with intense Soret band around 400-420 nm and a weak pair of Q bands (α, β) in the 550-600 nm visible region. These electronic transitions are polarized in the plane of the porphyrin ring. Ferric high spin porphyrins show complicated absorption spectra. The visible spectra contain extra bands which are attributed to CT or metal d-d transitions and some other type of transitions. Generally, porphyrins form complexes with various transition metals. The transition metals and porphyrins interact strongly due to the proximity of energy levels and favourable symmetry character of the electronic orbitals. This results in molecular orbitals containing mixtures of metal and porphyrin orbitals.

The coordination of other ligands to the metal along the axial direction affects the energy levels of the metalloporphyrins and also introduce additional molecular orbitals capable of mixing with porphyrin orbitals or metal orbitals. In a spherically symmetric field, the five d orbitals of iron are degenerate. These orbitals split when the metal is complexed to the porphyrin because different d orbitals will interact with the porphyrin to varying degrees depending on the geometry of the orbital lobes relative to the porphyrin orbitals. Fig. 2.4.1 shows in a schematic way the splitting of the iron 3d orbitals, when perturbed by the crystal field created by the porphinato macrocycle and the axial ligands. It also shows how the orbitals are split by the decrease in symmetry from octahedral to tetragonal and then to rhombic. The electronic configuration for the ferric porphyrins with the resultant spin equal to S = 1/2, S = 3/2 and S = 5/2 are also shown in Fig. 2.4.2.

Many five coordinated ferric porphyrins with various axial ligands X (X = N_3^-, F^-, Cl^-, OCH_3^-) are high spin (S = 5/2) complexes. The cyanide complex (CN^-) is a low spin species (S = 1/2). For high spin complexes, the iron atom is shifted out of the porphyrin plane towards the axial ligand. In five coordinated low spin species the ferric atom is closer to the porphyrin plane. The axial ligands which produce low spin species create strong crystal field and provide better overlap with the metal orbitals via strong σ interaction and/or π acceptor ability. The net result is shorter iron-ligand bond length. The axial ligands which produce high spin species are often good σ donors or π donors and lengthen the metal axial ligand bond resulting in the displacement of the iron away from the porphyrin plane.

The iron porphyrins with intermediate spin state are generally found when the axial ligand is very weak; e.g., the large radius anions ClO_4^-, BF_4^-. The weak σ donor characteristic of these ligands increase the bond length with the shrinking of the porphyrin core radially. The crystal field anisotropy (x, y $\gg$ z) causes the depopulated $d_{x^2-y^2}$ orbital to be raised in energy higher than other d orbitals and its restoration to an antibonding state.[17] The overall effect is the S = 3/2 state. Fig. 2.4.3 and Fig 2.4.4 illustrate the formation of various spin state species in ferric and ferrous porphyrins respectively. The X-Y axes in metalloporphyrins are defined to coincide with the Fe-N direction. The d_{xy} (b_{2g} in D_{4h} symmetry) orbital interaction with the porphyrin is much less than that of the $d_{x^2-y^2}$ (b_{1g}) orbital and the latter is antibonding and higher in energy. The d_{z^2} orbital is sensitive to the presence of axial ligands and is relatively higher in energy. In the tetragonal field, the d_{xy} (b_{2g}) and d_π (d_{xz} and d_{yz}) orbitals are split due to their different interactions with the porphyrin nitrogen orbital and the axial ligand orbital.

In ferrous porphyrins with no axial ligands, the iron is in the plane of the porphyrin. The d_{xy}, d_{yz}, d_{zx} and d_{z^2} orbitals are quite close in energy giving the d^6 configuration an intermediate (S = 1) spin state (Fig.2.4.4). When the iron is moved out of the porphyrin plane, the $d_{x^2-y^2}$ orbital is lowered in energy to give a high spin state but the d_{z^2} orbital is not high enough to cause a low spin state, when water, a weak field ligand is added as a fifth ligand. Strong field ligands like CO and imidazole raise the d_{z^2} orbital in energy and the low spin state is

achieved with the iron moving into the porphyrin plane to assume a lower energy configuration.

From the above it is clear that except for ferrous low spin porphyrin complexes, all the other complexes have a vacancy in the $e_g(d_\pi)$ orbitals. Therefore allowed CT transitions from $a_{1u}(\pi)$ and $a_{2u}(\pi)$ orbitals to $e_g(d_\pi)$ orbital is possible. The $a_{1u}(\pi)$ —> $e_g(d_\pi)$ transition is weaker than the $a_{2u}(\pi)$ —> $e_g(d_\pi)$ transition as the electron density is more on the nitrogen atoms in the a_{2u} orbital (Fig.2.3.2a). In the ferric high spin complexes, the CT transitions are responsible for strong visible bands. In ferric low spin cases, the CT transitions have been identified at low energy, $\approx$ 6500 cm^{-1}. In ferrous high spin cases they would be expected at higher energy.

The CT bands arise due to excitation of an electron from one atom or group of atoms to another different atom or group of atoms. These bands are weak as the molecular orbitals are located in different regions of the complex. In ferric porphyrins, this occurs as a result of porphyrin—>iron electron transfer (i.e., porphyrin (π)—>Fe(d_π) CT transitions) regardless of spin state. Figs. 2.4.5 illustrates the various types of charge transfer transitions in iron porphyrins. Apart from these, there are CT transitions observed in both low spin and high spin complexes which are of the type porphyrin (π) —> Fe(d_{z^2}).[18] The position of the a_{1u} —> d_{z^2}, and a_{2u}, a_{1u} —> d_π CT bands emphasize the importance of metal d orbital splittings on the energies of the CT bands.[19] The larger ligand field splittings of low spin porphyrins (t_{2g} —> e_g) accounts for the low energy of the a_{2u}, a_{1u} —> d_π transitions ($\approx$ 1300 nm). The same transition occurs around 600 nm and 800 nm for high spin species, While metMbCN, a

low spin ferric complex, exhibits a CT band at 488 nm attributed to the $a_{2u} \longrightarrow d_{z^2}$ transition, the $e_g(\pi) \longrightarrow d_\pi$ CT band near 800 nm has been found characteristic of all the low spin ferric porphyrins. Because of its z-polarized character, Makinen and Churg[18] have postulated that the position of this band is important in estimating the degree of mixing of metal and the axial ligand orbitals.

Most ferric high spin porphyrins show one or two CT bands between 550 and 600 nm and between 600 and 800 nm.[4,11,18] depending on the axial ligand. These CT bands assigned to porphyrin $(\pi) \longrightarrow Fe(d_\pi)$ transitions are usually intense due to mixing of the porphyrin $e_g(\pi^*)$ and the metal $e_g(d_\pi)$ orbitals. The latter are raised in energy and are non-degenerate in high spin complexes which allow for increased mixing and high intensity of the CT bands. Charge transfer transitions are expected to occur at higher energy for π donating ligands because these would increase electron density at the metal centre and would require more energy for the transfer of an electron from porphyrin ring to the metal. The opposite is true for π accptor ligands like CN and imidazole. The 631 nm band in high spin hemeoctapeptide is assigned to a CT band, $a_{2u} \longrightarrow d_\pi$ transitions, while a band between 570 and 580 nm has been assigned to the $a_{1u} \longrightarrow d_\pi$ CT transition in ferric protoporphyrin.[19]

The d-d transitions are forbidden in D_{4h} symmetry as being g—>g transition but can be observed if the symmetry is lowered by distortion created by ligation of two different ligands. However, for high spin ferric hemes, all transitions are both spin and symmetry forbidden. In low spin hemes the transitions become allowed by a reduction in symmetry.

Thus levels responsible for the optical spectra of iron-porphyrins are very complicated owing to the presence of filled and empty d orbitals in the same energy region as the top-filled π and π^* orbitals. Thus the spectra are strongly perturbed by small shifts of the d levels which are, in turn, influenced by the out of plane distance of the metal. This is decided by the axial ligands and hence by the spin state.

Ferric high spin complexes exhibit B bands near 400 and 380 nm with the Q(0,1) and Q(0,0) bands near 500 and 545 nm respectively. Low spin complexes exhibit B bands near 420 and 400 nm with the Q(0,1) and Q(0,0) bands near 540 and 575 nm respectively. The intensity of the Q(0,1) band is independent of both the nature of the axial ligand and metal oxidation state. The enhanced intensity of this band in both the high and low spin porphyrins is attributed to intense vibronic coupling to the B band.[18] However, the intensity of the Q(0,0) band is known to be dependent on the heme group structure.[18] In high spin ferric complexes, location of the iron atom out of the plane causes mixing of the d_π orbitals with the a_{2u} orbitals and also removes the degeneracy of the $e_g(\pi^*)$ orbitals. This results in increased intensity of the Q(0,0) band for the high spin porphyrins. On the other hand, the Q(0,0) band is generally weak in low spin porphyrins, and is more often buried in the more intense Q(0,1) band. The planar position of the iron atom in these complexes causes less structural changes in a low spin state.

Iron complexes exhibit a large number of different spectra of both the hypso and hyper type. They not only show various spin states in usual valency states of +2 and +3, but also show unusual valency states of +1 and +4 under different conditions.

While the absorption spectra of iron porphyrins are very complicated, their emission spectra are too simple. All iron porphyrins are radiationless. Only very weak flourescence ($\phi \approx 10^{-6}$) has been found in hypso complexes and in hyper iron porphyrins no emission has been detected.[20a] Based on the intensity of RR spectrum and absorption linewidth observed at low temperature, the iron $Q(\pi,\pi^*)$ state was estimated to have a lifetime of 15 fs.[20b]

2.5 Raman Scattering

The interaction of the electric field of electromagnetic radiation with the charge distribution of an atom or a molecule induces an oscillating dipole in the latter. The induced dipole becomes a source of secondary radiations, emitting at the frequency incident primary radiation. The interference of these primary and secondary radiations is responsible for the phenomena of reflection, refraction and scattering. Raman scattering refers to the observation of frequencies in the scattered radiation which are greater and lesser than that of the incident radiation due to modulation of induced dipole by excitations of the medium.

In the process of Raman scattering, the inelastic collision between the photon and the molecule decreases or increases the energy of the scattered photon due to exchange of energy by amounts equal to the quantized increments corresponding to the vibrational or rotational energy of the molecule.[21] After momentary excitation to an unstable virtual state, the molecule may return to a higher vibrational level of the ground electronic state giving rise to Stokes-Raman scattering. If the exciting photon interacts with a molecule already in the higher vibrational state,

the photon may gain energy giving rise to the anti-Stokes Raman scattering. when the molecule returns to the ground vibrational level. The elastic collision, however, leaves the frequency of the scattered radiation unchanged giving rise to Rayleigh scattering.

Photon scattering giving rise to the Raman effect is extremely weak - only about 10^{-8} of the incident light appears as Raman scattered signal. The high intensity monochromatic laser, however, overcomes this difficulty in detection of weak Raman lines. In nonresonant Raman scattering, the frequency of the exciting monochromatic radiation is far removed from the stationary energy states of the system and is not sufficient to excite the system to a higher electronic level. The intermediate state is not associated with any particular eigenstate as such and is considered to be a statistical superposition of a large number of excited electronic states of the system. As the frequency of the exciting radiation approaches an elecronic absorption band, the intermediate state dominates the summation term. Thus the pre-resonance and Resonance Raman scattering conditions are achieved by tuning the incident exciting frequency through the electronic absorption band (Fig. 2.5.1). The intermediate state becomes dominated by a few vibronic levels in the same energy range as that of the incident energy. Resonance Fluorescence is observed when the incident energy coincides with a single sharp level of the excited electronic state.

While both Resonance Raman and Resonance fluorescence involve excitation and emission in the electronic absorption band, the two processes differ considerably. The line shapes of the states of photon and that of the molecule as also their energy difference affect the resonant

scattering process. In Resonance Fluorescence, the molecular state is much sharper than the photon state and is thus completely in resonance with the incident beam. The scattering may be described, then, as a rapid population of the excited state followed by slow decay characterised by the life time of this excited state. The photon state, on the other hand, is better defined, in the Resonance Raman scattering process, than the molecular state and thus is in resonance with only a small part of it. In this case, two emission processes can be visualized: a fast one with the life time of the incident photon state and a slower one with the excited state life time. The former represents the resonant contribution, while the latter, the non-resonant part of the scattering process. Thus the reemission life time is characteristic of either the excited state or of the incident radiation, whichever has the narrower line width. Resonance Fluorescence is attributed to the latter situation and Resonance Raman to the former.[22] The physical process, however, remains the same inspite of this distinction between the two phenomena.

2.6 Theory of Resonance Raman Scattering

The secondary radiations from the dipole induced in a molecule due to its interaction with the periodically varying electric field of the electromagetic wave incident on it forms the basis of the scattering phenomena. The polarizability of the molecule fluctuates due to the oscillating induced dipole moment and gives rise to frequency changes in the scattered radiation. This simple classical treatment is insufficient to explain the precise nature of interaction of radiation with matter or the important phenomena like Resonance Raman scattering or Stimulated Raman scattering. A fully quantum mechanical treatment was first applied

by Jacon[23] to understand RR scattering process, while a semi-classical treatment of Kramer and Heisenberg[24] which correlates the scattering tensor to the wavefunctions and energy levels of the scatterer gave correct results for the RR scattering. In this model, the incident radiation, treated classically, is regarded as a source of perturbation of the energy levels of the scattering system and quantum mechanical techniques are applied to investigate transitions between quantized energy levels of the perturbed system. Later workers extended this approach.[25-30]

Consider a non-rotating molecule at the origin of a space-fixed co-ordinate system interacting with an oscillating electromagnetic field which can be represented as

$$\bar{E}_\sigma = \bar{E}^o_\sigma \quad \exp\, i(\bar{k}.\bar{r} - \omega t) \qquad (2.6.1)$$

where $\bar{k}$ and ω are the direction of propogation and angular frequency respectiely. The oscillating electric dipole moment of the molecule may then be expressed as

$$(\bar{\mu}_\rho)_{mn} = (\bar{\alpha}_{\rho\sigma})_{mn}\, \bar{E}_\sigma \qquad (2.6.2)$$

where

$$(\bar{\mu}_\rho)_{mn} = \langle \psi_m | \bar{e}_\rho | \psi_n \rangle \qquad (2.6.3)$$

is the amplitude of the transition moment and ψ_m and ψ_n are the time independent wavefunctions of the initial and final states respectively. $(\bar{\alpha}_{\rho\sigma})_{mn}$ is the polarizability tensor for the transitions from m to n and ρ and σ are the molecular cartesian coordinate axes of the scattering tensor. The scattered light intensity I_{mn} in terms of photons per molecule per second scattered into a solid angle 4π after averaging over all the orientations of the molecule can be expressed as,[31]

$$I_{mn} = \frac{128\pi^5}{9c^4} (\nu_o \pm \nu_{mn})^4 I_o \sum_{\rho,\sigma} |(\alpha_{\rho\sigma})_{mn}|^2 \qquad (2.6.4)$$

where $|m\rangle$ and $|n\rangle$ are the initial and final vibronic states, ν_o and I_o, the frequency and the intensity of the plane polarized incident radiation, $(\nu_o \pm \nu_{mn})$ the frequency of the scattered radiation and ν_{mn} is the frequency of the vibration involved in the Raman scattering, c is the velocity of light and $\alpha_{\rho\sigma}$ $(\rho,\sigma = x,y,z)$ is the $\rho\sigma^{th}$ component of the polarizability tensor.

From the above equation it is seen that the intensity of the scattered radiation depends on the fourth power of the frequency of the incident radiation and more critically on the square of the polarizability tensor component $(\alpha_{\rho\sigma})_{mn}$. As a result, the main effort in developing the Raman theory has been to provide a theoretical frame work for calculating the polarizability tensor component $(\alpha_{\rho\sigma})_{mn}$ in terms of the molecular parameters.

In order to determine the polarizability, the distortion of the wavefunction due to the periodic perturbation by the electromagnetic wave has to be calculated. Using time dependent perturbation theory, the transition dipole moments can then be evaluated using the new wavefunctions. The time dependent Schrödinger equation is given by

$$i\hbar \frac{\partial}{\partial t} |\psi\rangle = (H_o + H')|\psi\rangle \qquad (2.6.5)$$

where H_o is the unperturbed Hamiltonian satisfying the equation,

$$i\hbar \frac{\partial}{\partial t} |\psi_k^o\rangle = H_o |\psi_k^o\rangle \qquad (2.6.6)$$

The time dependency of the wavefunction can be incorporated through

$$|\psi\rangle = \sum_k a_k(t)\,|\psi_k^o\rangle \tag{2.6.7}$$

where

$$|\psi_k^o(t)\rangle = |\psi_k^o\rangle \exp\left[-\frac{iH_o t}{h}\right] \tag{2.6.8}$$

is the solution when H' = 0. The perturbation by the electric field of the incident electromagnetic radiation can be represented by

$$H' = -\frac{1}{2}\left[\mu_\rho E_\rho^o \{\exp(i\omega t) + \exp(-i\omega t)\}\right] \tag{2.6.9}$$

where μ_ρ is the component of the electric dipole moment in the direction ρ given by

$$\mu_\rho = \sum e_j \rho_j \tag{2.6.10}$$

where e_j and ρ_j represents the charge and the dipole moment of the j^{th} particle of the system. The above equations represent the salient parts of the interaction of the molecule with the electromagnetic radiation.

The $(\rho\sigma)^{th}$ component of the molecular polarizability for the transition from $|m\rangle$ to $|n\rangle$ is given by the second order perturbation theory as given by Kramer-Heisenberg-Dirac equation:[25,32]

$$(\alpha_{\rho\sigma})_{mn} = \frac{1}{h}\sum_e \left[\frac{\langle n|\mu_\sigma|e\rangle\langle e|\mu_\rho|m\rangle}{\nu_{em} - \nu_o + i\Gamma_e} + \frac{\langle n|\mu_\rho|e\rangle\langle e|\mu_\sigma|m\rangle}{\nu_{en} + \nu_o + i\Gamma_e}\right] \tag{2.6.11}$$

where μ_ρ and μ_σ are the dipole moment operators and the summation is over all the excited eigenstates $|e\rangle$ of the molecule. $i\Gamma_e$ is the damping term related to the width of the excited state $|e\rangle$. When $\langle e|\mu|m\rangle$ is finite for a real state, $|e\rangle$, the transition from $|m\rangle$ to $|e\rangle$ is accompanied by light absorption which would have the centre frequency ν_{em} and full width at half maximum of $2\Gamma_e$, and its maximum intensity would be proportional to $|\langle e|\mu|m\rangle|^2$. If the exciting frequency ν_o is close to the frequency of

electronic transition ν_{em}, the first term of $(\alpha_{\rho\sigma})_{mn}$ and hence of I_{mn} would be very large. This is termed Resonance Raman scattering. Only those modes which are involved in the chromophore of the absorption band gain resonance enhancement of Raman intensity.

To extract the vibronic information accessible by Raman effect, Albrecht[16] and Tang and Albrecht[33] applied the Born-Oppenheimer approximation where the electronic and vibrational wavefunctions are separated as $|m\rangle = |g\rangle\,|i\rangle$, $|n\rangle = |g\rangle\,|j\rangle$ and $|e\rangle = |r\rangle\,|v\rangle$ with $|i\rangle$, $|j\rangle$ and $|v\rangle$ as the vibrational wavefunctions for the quantum numbers i, j and v, and $|g\rangle$ and $|r\rangle$ as the electronic wavefunctions for the electronic ground and excited states respectively. The wavefunctions $|m\rangle$, $|n\rangle$ and $|e\rangle$ depend on both the nuclear and electronic co-ordinates. It is postulated that the vibrational wavefunctions in the electronic ground and excited states are the same except for the shift in origin of the coordinates, that is, the equilibrium structure of the molecules differs between the two states. The change in the electronic wavefunction due to the origin shift is incorporated with the Herzberg-Teller expansion. The main terms contributing to the scattering tensor (equation 2.6.11) under resonance with a particular electronic state $|r\rangle$, are the following two terms obtained from the leading terms of the Taylor expansion of the Raman polarizability with respect to the normal coordinate Q.

$$(\alpha_{\rho\sigma})^{r}_{ij} = (A_{\rho\sigma})^{r}_{ij} + (B_{\rho\sigma})^{r}_{ij} \qquad (2.6.12)$$

where

$$(A_{\rho\sigma})^{r}_{ij} = \frac{M^{gr}_{\sigma}\, M^{gr}_{\rho}}{h} \sum_{v} \frac{\langle j|v\rangle\langle v|i\rangle}{\nu_{rg} + (v - i)\Delta\nu_{a} - \nu_{o} + i\Gamma_{r}}$$

and

$$(B_{\rho\sigma})^{r}_{ij} = \frac{M_{\sigma}^{gr}\ h_{a}^{ra}\ M_{\rho}^{ag}}{h^{2}(\nu_{r} - \nu_{a})} \sum_{v} \frac{\langle j|Q_{a}|v\rangle\langle i\rangle}{\nu_{rg} + (v-i)\Delta\nu_{a} - \nu_{o} + i\Gamma_{r}}$$

$$+ \frac{M_{\sigma}^{ga}\ h_{a}^{ar}\ M_{\rho}^{rg}}{h^{2}(\nu_{r} - \nu_{a})} \sum_{v} \frac{\langle j|v\rangle\langle v|Q|i\rangle}{\nu_{rg} + (v-i)\Delta\nu_{a} - \nu_{o} + i\Gamma_{r}}$$

where $M_{\sigma}^{gr} = \langle g^{o}|\mu_{\sigma}|r^{o}\rangle$, $h\nu_{rg}$ is the energy separation between the $|r\rangle$ and $|g\rangle$ states, and $h_{a}^{ra} = \langle r|(\partial H/\partial Q_{a})|s\rangle$ is the vibronic coupling operator that mixes the two electronic states via a given normal mode Q_{a} and $\Delta\nu_{a}$ is the frequency of the normal mode Q_{a}.

Several features of the Raman scattering of the fundamental are discernible upon examination of the A and B terms. When the Raman spectra are obtained with excitation in the electronic absorption band, the vibrational modes which are expected to show resonance enhancement are those which contribute to the electronic spectrum, i.e., they are vibronically active and are of two types: (1) modes which connect the ground and excited electronic states involved in resonance through the Franck-Condon overlap (A term), (2) modes which mix the resonant electronic state $|r\rangle$ to another one of higher energy $|s\rangle$ (B term). The potential energy curve of the excited electronic state is shifted in the Franck-Condon effect so that the vibrational wavefunctions are not orthogonal. Raman scattering from modes due to Franck-Condon effect can arise only when the orthogonality between the ground state and the excited vibrational wavefunctions is removed. That is, the overlap integral is non-zero if there is considerable origin shift or if the vibrations are totally symmetric. A-term enhancement varies directly with the strength of the electronic transition and inversely with its bandwidth and also directly on the magnitude of the overlap integral, $\langle j|v\rangle\langle v|i\rangle$. These

increase with the increase in displacement of the excited state potential well along the normal coordinate, i.e., the A-term modes gain intensity via origin shift. Hence the extent of excited state distortion determines the degree of enhancement of a given totally symmetric vibration. There is no enhancement via Frank-Condon term for the non-totally symmetric modes as the origin shift is zero for these modes upon electronic excitation and the Franck-Condon term is zero.

Non-totally symmetric modes, however, gain intensity via the B-term because of Q-dependent vibrational integrals. The contribution of $\langle 1|Q|0\rangle\langle 0|0\rangle$ and $\langle 1|1\rangle\langle 1|Q|0\rangle$ terms are significant to the B-term for vibrational modes differing by one quantum. Therefore the B-term becomes important in situations where a forbidden or weakly allowed transition gains intensity from vibronic mixing with a strongly allowed transition. The mixing modes are then enhanced in the RR spectrum when excited at the weak transition. The enhancement depends on the magnitude of the mixing integral and on the frequency separation of the electronic states $|r\rangle$ and $|s\rangle$. The active vibrations are those that are effective in mixing the two states and depend on their geometries. The allowed symmetries are given by the cross product of the electronic transition representations. When the two electronic states are degenerate we have the limiting case, Jahn-Teller effect. The mixing vibrations (Jahn-Teller active modes) are strongly enhanced.

2.7 The Polarizability Tensor and Depolarization Ratio

As mentioned earlier, when electromagnetic radiation interacts with the charge distrubution of a molecule, the polarization of the charge

cloud induced by the electric field of the incident radiation results in an induced dipole moment. The dipole moment so induced is proportional to the electric field and to the polarizability α for smaller electric field strengths:

$$\bar{\mu} = \alpha \, \bar{E} \tag{2.7.1}$$

For an isotropically polarizable molecule, the induced dipole moment vector, $\bar{\mu}$, is in the same direction as that of the electric field vector $\bar{E}$. However, for an anisotropic molecule, the induced dipole moment in any direction is given by

$$\bar{\mu}_{ij} = \sum_{j} \alpha_{ij} \, \bar{E}_{j} \tag{2.7.2}$$

where i,j = x, y, z. The polarizability tensor α_{ij} can be expressed as

$$\alpha_{ij} = \begin{bmatrix} \alpha_{xx} & \alpha_{xy} & \alpha_{xz} \\ \alpha_{yx} & \alpha_{yy} & \alpha_{yz} \\ \alpha_{zx} & \alpha_{zy} & \alpha_{zz} \end{bmatrix} \tag{2.7.3}$$

The elements of α_{ij} generally depend on the frequency of the incident radiation, apart from the wavefunctions and electronic properties of the molecular systems. However, certain combinations of the polarizability tensor elements remain invariant with respect to change of coordinate system and are given by

$$(\bar{\alpha})^2 = \frac{1}{9} \left[\alpha_{xx} + \alpha_{yy} + \alpha_{zz} \right]^2 \tag{2.7.4}$$

$$\gamma_s^2 = \frac{1}{2} \left[(\alpha_{xx} - \alpha_{yy})^2 + (\alpha_{yy} - \alpha_{zz})^2 + (\alpha_{zz} - \alpha_{xx})^2 \right] + \frac{3}{2} \left[(\alpha_{xy} + \alpha_{yx})^2 + (\alpha_{yz} + \alpha_{zy})^2 + (\alpha_{zx} + \alpha_{xz})^2 \right] \tag{2.7.5}$$

$$\gamma^2_{as} = \frac{3}{4}\left[(\alpha_{xy} - \alpha_{yx})^2 + (\alpha_{yz} - \alpha_{zy})^2 + (\alpha_{zx} - \alpha_{xz})^2\right] \qquad (2.7.6)$$

where $\bar{\alpha}$, γ_s, and γ_{as} represent the isotropic, symmetric isotropic and the antisymmetric anisotropic tensor invariants.

The coordinate system employed for observation of scattered light intensity is shown in Fig.2.7.1, where the incident light is propogating along the Y-axis and the scattered light is observed at 90° along the Z-axis. In this geometry the depolarization ratio is defined as

$$\rho_l(\theta = 90^\circ) = \frac{I_\perp}{I} \qquad (2.7.7)$$

of the invariants, the depolarization ratio ρ_l can be expressed as

$$\rho_l = \frac{3\gamma^2_s + 5\gamma^2_{as}}{45(\bar{\alpha})^2 + 4\gamma^2_s} \qquad (2.7.8)$$

Under normal non-resonance Raman effect, the scattering tensor is symmetric, that is , $\alpha_{ij} = \alpha_{ji}$, so that

$$\rho_l = \frac{3\gamma^2_s}{45(\bar{\alpha})^2 + 4\gamma^2_s} \qquad (2.7.9)$$

Thus equation (2.7.5) reduces to

$$\gamma^2_s = \frac{1}{2}\left[(\alpha_{xx} - \alpha_{yy})^2 + (\alpha_{yy} - \alpha_{zz})^2 + (\alpha_{zz} - \alpha_{xx})^2\right] + 6\left[(\alpha_{xy})^2 + (\alpha_{xz})^2 + (\alpha_{zy})^2\right] \qquad (2.7.10)$$

For non-totally symmetric modes in Raman scattering, $\bar{\alpha}^2 = 0$ and

$$\rho_l = \frac{3}{4} + \frac{5\gamma^2_{as}}{4\gamma^2_s} \qquad (2.7.11)$$

If $\gamma^2_{as} = 0$, we have the normal polarization with $\rho_l = \frac{3}{4}$. If $\gamma^2_{as} \neq 0$, then $\rho_l > \frac{3}{4}$, resulting in anamalous polarization provided $\gamma^2_s \neq 0$. If, however, $\gamma^2_s = 0$, then we have $\rho_l = \infty$ (inverse polarization). For totally symmetric modes where $\bar{\alpha}^2 \neq 0$, and $\gamma^2_{as} = 0$, the depolarization ratio is

$$\rho_l = \frac{3}{45\frac{(\bar{\alpha})^2}{\gamma^2_s} + 4} \qquad (2.7.12)$$

that is, the value of ρ_l can vary between and 0 and 3/4 according as

$$\infty \geq 45\frac{\bar{\alpha}^2}{\gamma^2_{as}} > 0 \qquad (2.7.13)$$

Group theoretical considerations provide information about the invariants which are non-zero for particular vibrational modes in molecules of a given symmetry. But this requires a knowledge of the symmetry properties of the general polarizability tensor. McClain[34] has given the symmetry of the scattering tensor for different molecular point groups which help in evaluating the contributions for a Raman process from any of the invariants transforming under particular irreducible representation of a point group pertinent to the molecule. The structural information about the symmetry of the molecule can often be obtained by studying the dispersion of ρ_l with exciting frequency. Experimentally the evaluation of all the three tensor invariants requires three independent intensity measurements: that of scattering at 90°, $(I_\perp + I_\parallel)$ and the depolarization ratio ρ_l may be supplemented by a measurement involving circularly polarized light. In this the reversal coefficient I_{contra}/I_{co}, which is the ratio of the intensity of contra-rotating light to that of the co-rotating light for the back scattering of purely circlarly polarized

incident radiation is usually measured. However, these are not sufficient to determine the point group symmetry of the molecule having modes which show a dispersion of ρ_l. Measurements of these above parameters at different values of exciting frequency ν_o would be required.

2.8 Antisymmetric scattering tensor contributions

The excitation of Raman scattering in the vicinity of the Q bands of the metalloporphyrins produce scattering mainly from the B term dominated by the vibrations that are effective in mixing the Q and the B transitions. The allowed vibrational modes are those whose irreducible representions are contained in the cross product of the symmetry representations of the two electronic states (E_u):

$$E_u \times E_u = A_{1g} + A_{2g} + B_{1g} + B_{2g} \qquad (2.8.1)$$

The A_{2g} modes are particularly interesting because of their rotational symmetry about the porphyrin four fold axis and antisymmetric scattering tensor property ($\alpha_{ij} = -\alpha_{ji}$). They couple the x and y components of the B transition to the y and x components respectively of the Q transition, thereby rotating the plane of polarization of the incident light by 90° and producing anamalous polarization. The A_{2g} modes are inactive in normal Raman scattering due to their antisymmetric tensors but are allowed in the region of resonance and give rise to inverse polarization.[35] This can be seen from the B term where the sign of the overlap integral reverses for the 0-0 (i = 0, v = 0, j = 1) and 0-1 (i = 0, v = 1, j = 1) resonances. Consequently the 0-0 and 0-1 contributions interfere destructively off resonance.

The first experimental evidence of inverse polarization in the RR studies of porphyrins and hemeproteins was provided by Verma and Bernstein[36] and Spiro and Strekas[13]. While antisymmetric scattering requires that the scattering intensity in parallel polarization should vanish, significant residual intensity in parallel scattering is observed in the anamalous scattering ($\rho > 3/4$).[13] Accidental degeneracy with the A_{2g} modes, that is, modes of the different symmetry coincident with the A_{2g} modes, or lowering of the effective four fold symmetry of the heme chromophore were suggested as possible explanation for the observation of anamalous polarization in these systems.[38] The antisymmetric scattering tensor gain some symmetric character.

The rigorous D_{4h} symmetry of Copper porphyrin in solution and the lowering of symmetry of Copper mesoporphyrins to C_s due to assymmetric substituent pattern in the latter has been demonstrated by Verma et al[37,38] through the measurements of depolarization ratio of selected Raman bands as a function of excitation wavelength.

REFERENCES

1. Küster, W.; *Hoppe Seyler's Z. Physiol. Chem.* 1912, 82, 463.

2. (a) Stern, A. Pruckner, F. *Z. Physik. Chem.* 1937, A180, 321.
   (b) Stern, A. Wenderlein, H. *Z. Physik. Chem.* 1936, A177, 165.
   (c) Stern, A. Pruckner, F. *Z. Physik. Chem.* 1937, A180, 321.

3. (a) Platt, J.R. In *Radiation Biology*; Hollander, A., Ed.; McGraw-Hill: New York, 1956; Vol.3, Chapter 2.
   (b) Gouterman, M. *J. Chem. Phys.* 1959, 30, 439.

4. Smith, W.T.; Williams, R.J.P. *Struct. Bonding* 1970, 7, 1.

5. Simpson, W.T. *J. Chem. Phys.* 1949, 17, 1218.

6. Gouterman, M. In *Excited States of Matter*; Shoppe, C.W., Ed.; Graduate Studies Tech. Univ: 1973; Vol.2, pp 1.

7. Longuet-Higgins, H.C.; Rector, C.W.; Platt, J.R. *J. Chem. Phys.* 1950, 18, 1174.

8. (a) Gouterman, M.; *J. Mol. Spectrosc.* 1961, 6, 138.
   (b) Platt, J.R. *J. Chem. Phys.* 1954, 18, 1174.

9. Perrin, M.H.; Gouterman, M.; Perrin, C.L. *J. Chem. Phys.* 1969, 50, 4137.

10. Eaton, W.E.; Hochstrasser, R.M. *J. Chem. Phys.* 1967, 46, 2533.

11. Eaton, W.E.; Hochstrasser, R.M. *J. Chem. Phys.* 1968, 49, 985.

12. Solov'ev, K.N. *Opt. Spectrosc.* 1961, 10, 389.

13. Spiro, T.G.; Strekas, T.G. *Proc. Natl. Acad. Sci. USA.* 1972, 69, 2622.

14. Friedman, J.M.; Hochstrasser, R.M. *J. Am. Chem. Soc.* 1976, 98, 4043.

15. Friedman, J.M.; Hochstrasser, R.M. *Chem. Phys.* 1973, 1, 457.

16. Albrecht, A.C. *J. Chem. Phys.* 1961, 34, 1476.

17. Reed, C.A.; Mashiko, T.; Bentley, S.P.; Kastner, M.E.; Scheidt, W.R.; Spartalian, K.; Lang, G. *J. Am. Chem. Soc.* 1979, 101, 2948.

18. Makinen, M.W.; Churg, A.K. In *Iron Porphyrins*; Lever, A.P.B.; Gray, H.B., Eds.; Addison-Wesley: Reading, 1983; Part 1, pp 101.

19. Owens, J,W.; O'Connor, C.J. *Coord. Chem. Rev.* 1988, 84, 1.

20. (a) Gouterman, M. In *The Porphyrins*; Dolphin, D., Ed.; Academic Press: New York, 1978; Vol. 3, pp 1.
(b) Adar, F.; Gouterman, M. Aronowitz, S. *J. Chem. Phys.* 1976, 80, 2184.

21. Herzberg, G. In *Infrared and Raman Spectra of Polyatomic Molecules*; Van Nostrand Reinhold Co: New York, 1945; Vol. 2.

22. Friedman, J.M.; Hochstrasser, R.M. *Chem. Phys.* 1974, 6, 155.

23. Jacon, M. In *Advances in Raman Spectroscopy*; Mathein, J.P. Ed.; 1973; Vol. 1.

24. Kramers, H.A.; Heisenberg, W. *Z. Physik.* 1925, 31, 681.

25. Dirac, P.A.M. *Proc. Roy. Soc. (London)*, 1927, 114, 710.

26. Verma, A.L. *Indian. J. Phys.* 1980, 54B, 54.

27. Albrecht, A.C. *J. Chem. Phys.* 1961, 34, 1476.

28. Krushinskie, L. L.; Shorygyn, P.P. *Opt. Spectrosc. USSR.* 1965, 19, 312.

29. Savin, F.A. *Opt. Spectrosc. USSR.* 1965, 19, 308.

30. Verlan, E.M. *Opt. Spectrosc. USSR.* 1966, 20, 341 and 447.

31. Tang, J.; Albrecht, A.C. In *Raman Spectroscopy*; Szymanski, H.A. Ed.; Plenum: New York, 1970; Vol. 2, pp 33.

32. Heitler, W. *The quantum theory of radiation*; 3rd ed. Oxford. Univ. Press (Clarendon): London and New York; 1954.

33. Tang, J.; Albrecht, A.C. *J. Chem. Phys.* 1968, 49, 1144.

34. McClain, W.M. *J. Chem. Phys.* 1971, 5, 2789.

35. Spiro, T.G. *Biochim. Biophys. Acta.* 1975, 415, 169.

36. Verma, A.L.; Bernstein, H.J. *J. Raman. Spectrosc.* 1974, 2, 163.

37. Verma, A.L.; Bernstein, H.J. *J. Chem. Phys.* 1974, 61, 2560.

38. Verma, A.L.; Mendelsohn, R.; Bernstein, H.J. *J. Chem. Phys.* 1974, 61, 383.

TABLE 2.3.1
Hamiltonians for y Polarized States[a]

	$(a_{2u}e_{qy})$	$(a_{1u}e_{qx})$	Dipole strength (q^2)
(a)			
$(a_{2u}e_{qy})$	$A'_{1g} + A_{1g}$	A''_{1g}	R_2^2
$(a_{1u}e_{qx})$	A''_{1g}	$A'_{1g} - A_{1g}$	R_1^2
	B_y^0	Q_y^0	
(a')			
$B_y^0 \equiv (2)^{-1/2}[(a_{2u}e_{qy}) + (a_{1u}e_{qx})]$	$A'_{1g} + A''_{1g}$	A_{1g}	$R^2 \equiv \frac{1}{2}(R_1 + R_2)^2$
$Q_y^0 \equiv (2)^{-1/2}[(a_{2u}e_{qy}) - (a_{1u}e_{qx})]$	A_{1g}	$A'_{1g} - A''_{1g}$	$r^2 \equiv \frac{1}{2}(R_2 - R_1)^2$
	B_y	Q_y	
(b) $[\tan 2v \equiv A_{1g}/A''_{1g}]$			
$B_y \equiv \cos v B_y^0 + \sin v Q_y^0$	$A'_{1g} + A''_{1g}\cos 2v$	0	$\frac{1}{2}(1 + \cos 2v)R^2 + Rr \sin 2v + \frac{1}{2}(1 - \cos 2v)r^2$
$Q_y \equiv -\sin v B_y^0 + \cos v Q_y^0$	0	$A'_{1g} - A''_{1g}/\cos 2v$	$\frac{1}{2}(1 - \cos 2v)R^2 - Rr \sin 2v + \frac{1}{2}(1 + \cos 2v)r^2$
(c) $[2v = A_{1g}/A''_{1g} \ll 1]$			
$B_y = B_y^0 + vQ_y^0$	$A'_{1g} + A''_{1g}(1 + 2v^2)$	0	$R^2 - v^2R^2 + 2vRr$
$Q_y = Q_y^0 - vB_y^0$	0	$A'_{1g} - A''_{1g}(1 + 2v^2)$	$(vR - r)^2$

[a] Table reproduced from Gouterman, [11c].

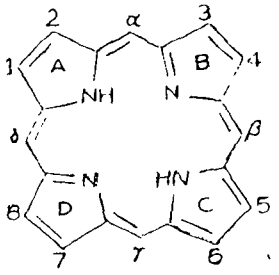

Porphyrin	1	2	3	4	5	6	7	8	α-γ
Protoporphyrin IX	M	V	M	V	M	P	P	M	H
Deuteroporphyrin IX	M	H	M	H	M	P	P	M	H
Mesoporphyrin IX	M	E	M	E	M	P	P	M	H
Haematoporphyrin IX	M	B	M	B	M	P	P	M	H
Etioporphyrin I	M	E	M	E	M	E	E	M	H
Octaethylporphyrin	E	E	E	E	E	E	E	E	H
Tetraphenylporphyrin	H	H	H	H	H	H	H	H	Ph

Side-chain abbreviations: M = CH_3 ; E = C_2H_5 ; V = $CH{=}CH_2$; B = $CHOHCH_3$
P = $(CH_2)_2COOH$; Ph = C_6H_5

Fig. 2.1.1. Structure and nomenclature of free-base and other porphyrin complexes.

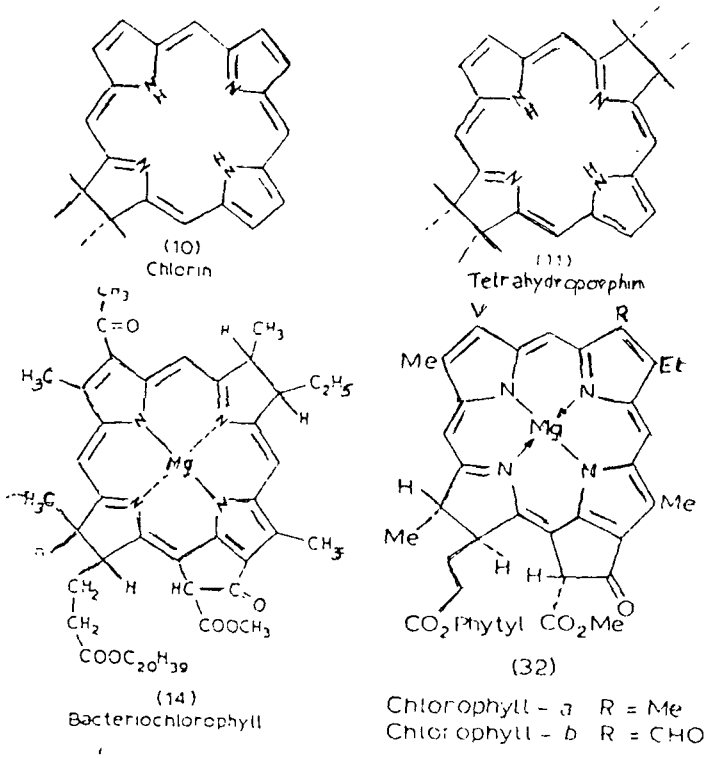

Fig. 2.1.2. Structures illustrating the hydroporphyrins with loss of double bonds at the pyrrole.

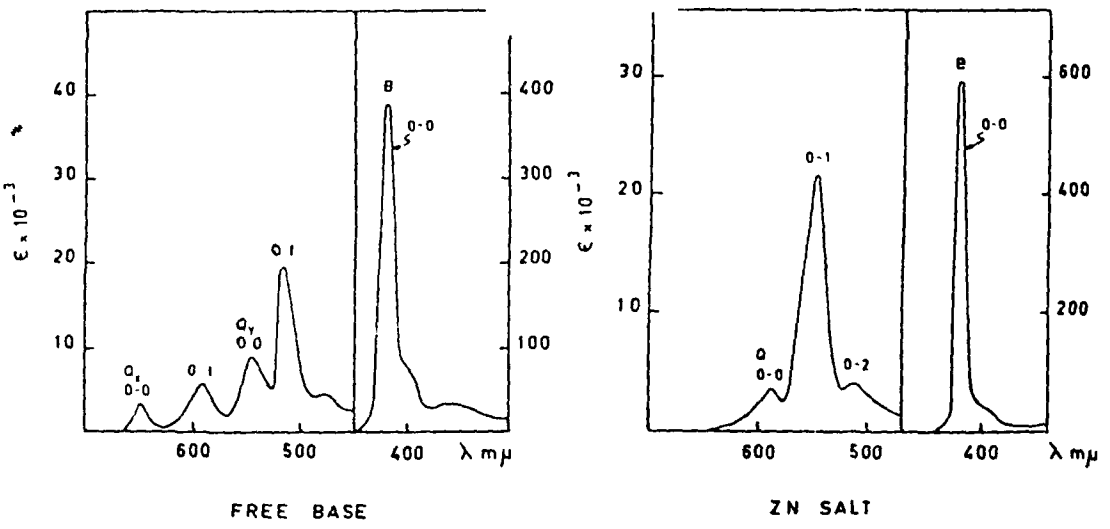

Absorption spectra of tetraphenyl porphin

Fig. 2.2.1. Absorption spectra of free base porphyrin and its metal derivatives.

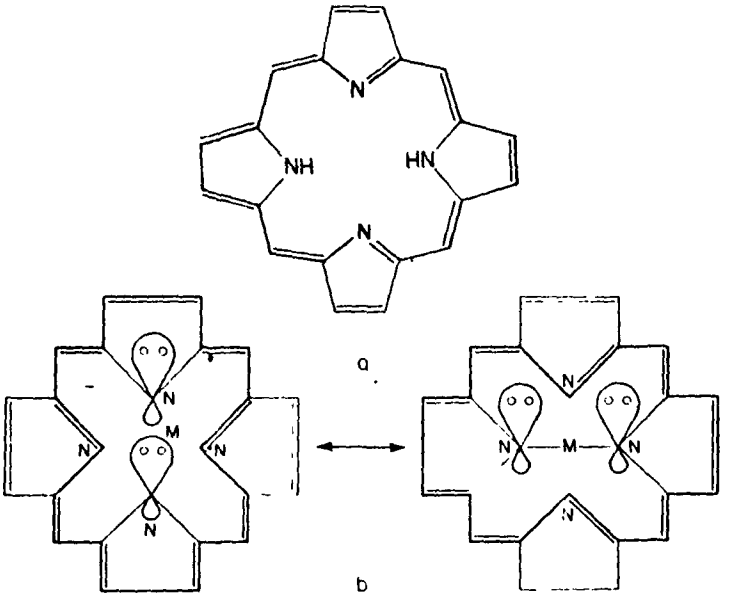

Fig. 2.3.1. (a) Resonance structure for free base porphyrin. (b) Resonance structures for metal-porphyrin complex; the out-of-plane electrons on the imino nitrogens are displayed in their orbitals.

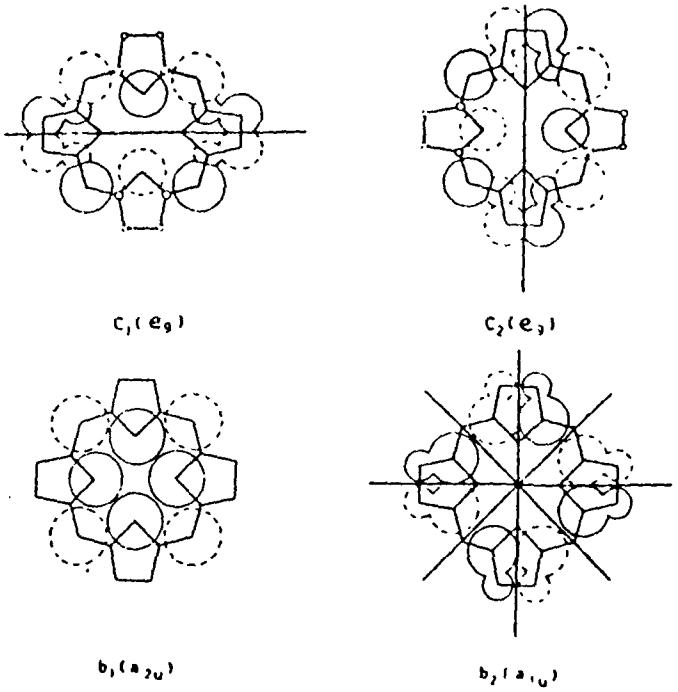

Fig. 2.3.2a Porphyrin top-filled MOs b_1 and b_2 and lowest empty MOs c_1 and c_2. The orbital coefficients are proportional to the size of the circles. Solid or dashed circles indicate sign. Symmetry nodes are drawn in heavy lines.

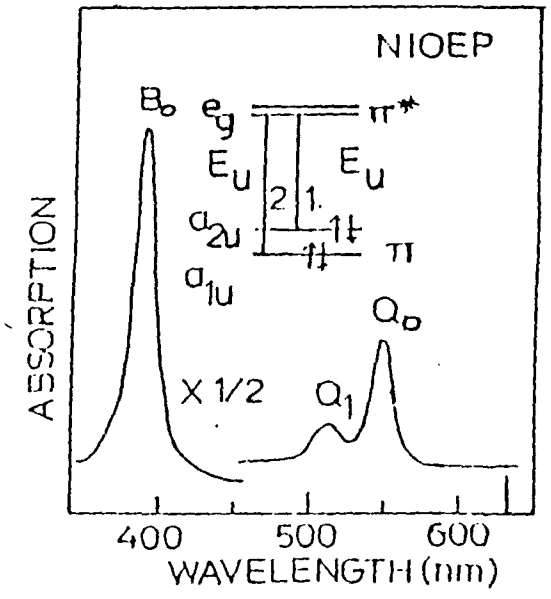

Fig. 2.3.2b Illustration of four-orbital model and absorption spectrum for a metalloporphyrin.

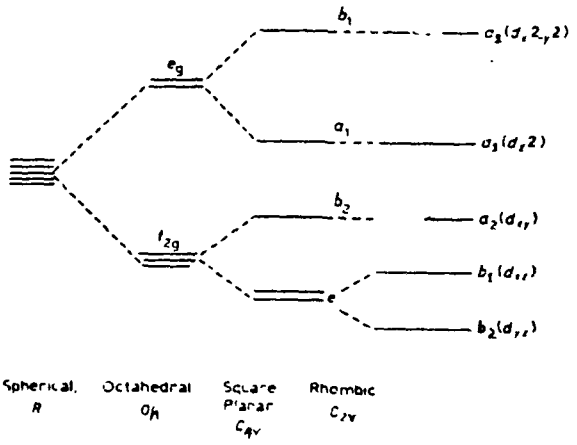

Fig.2.4.1. Diagram showing how the 3d electrons are split under the influence of changes in molecular symmetry.

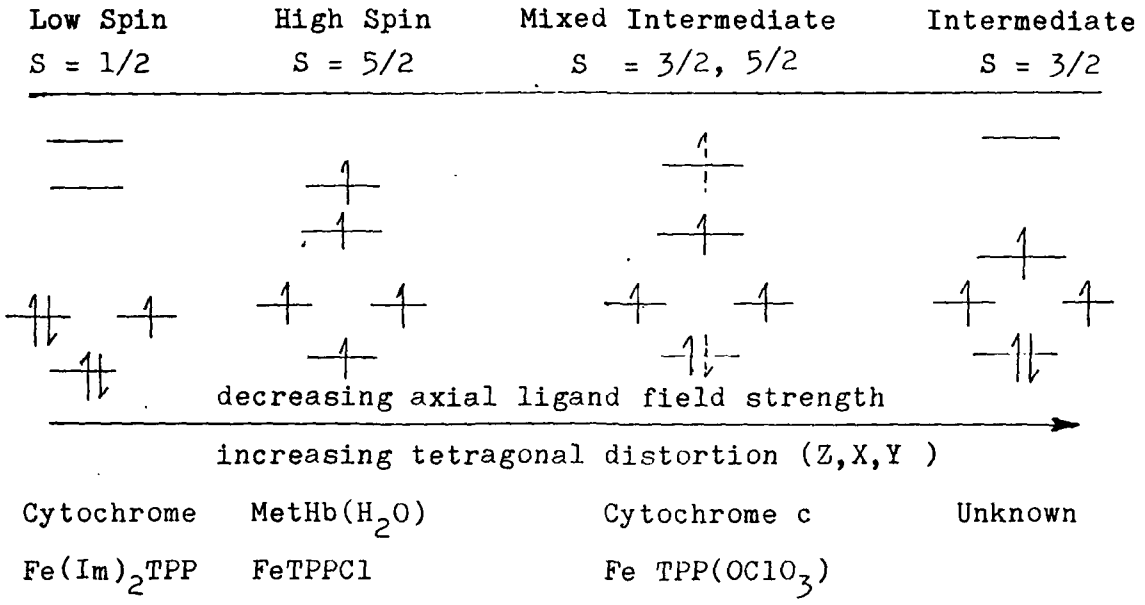

Fig.2.4.2. $3d^5$ splitting patterns for different spin states, with representative examples for protein and model systems.

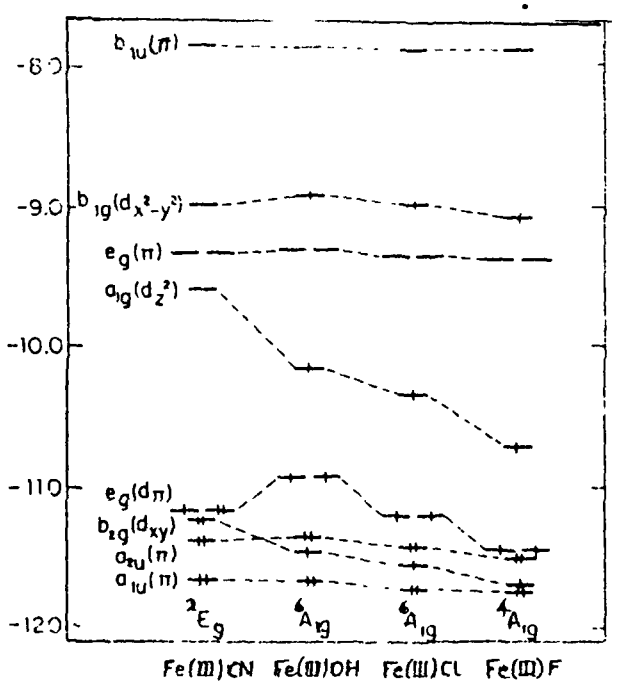

Fig.2.4.3. Top-filled and lowest-empty orbital energies by the IEH model for Fe(III) complexes. All are five coordinate with Fe 0.455 A out of plane.

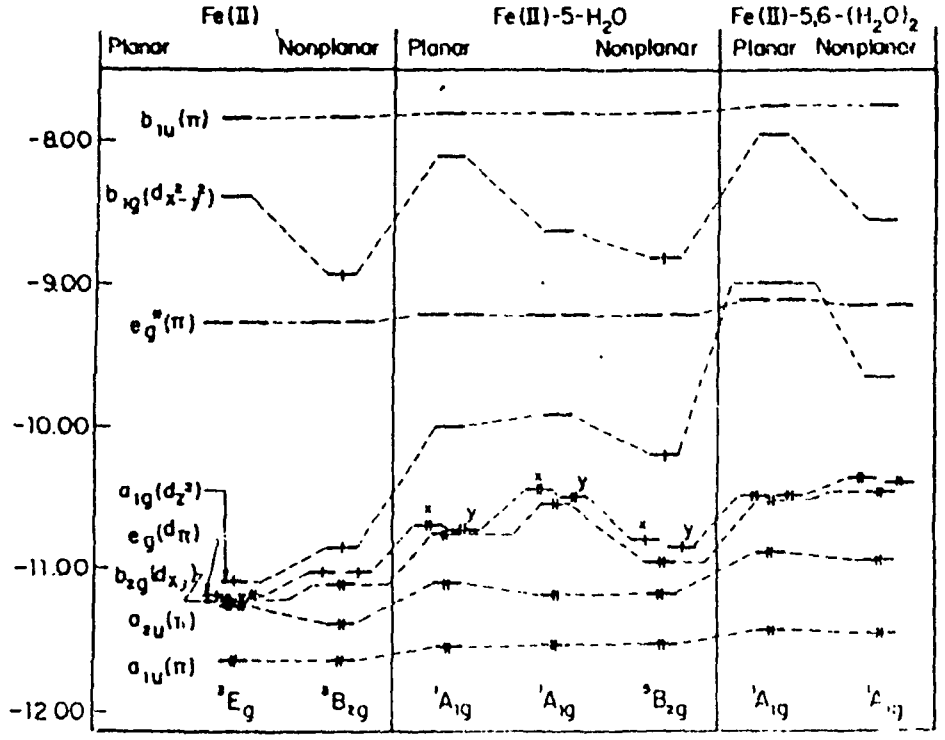

Fig.2.4.4. Top-filled and lowest empty orbital energies by the IEH model for Fe(II) complexes with none, one or two water molecules. Nonplanar structures have Fe 0.492 A out of plane: Cases V and VI differ by spin assignment.

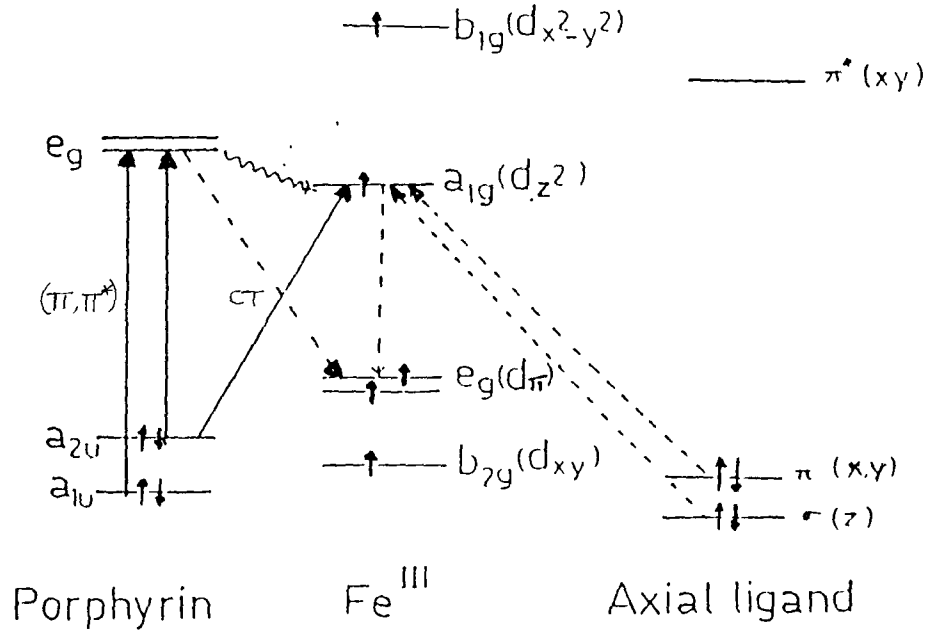

Fig.2.4.5. Schematic illustration of orbitals indicating CT transitions from the axial ligand in addition to porphyrin to metal CT transitions.

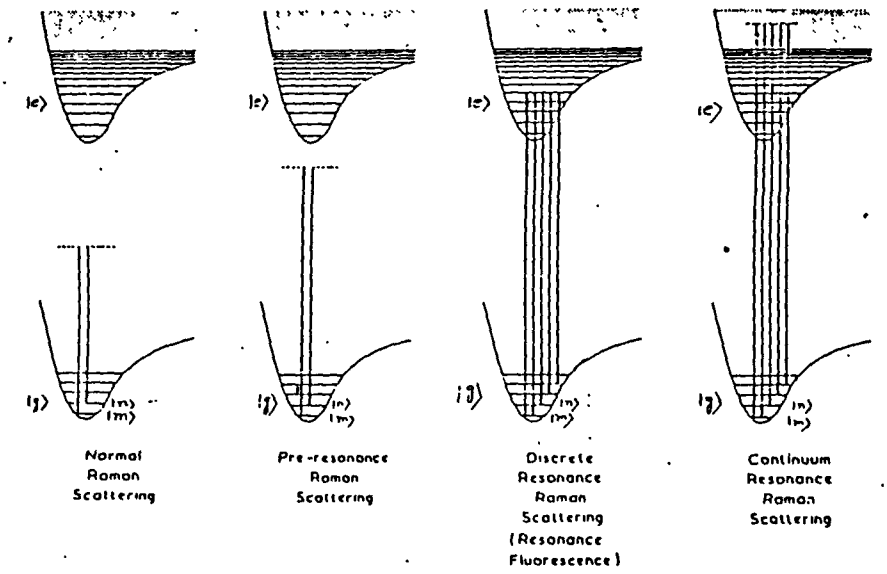

Fig. 2.5.1. Illustration of various light scattering processes.

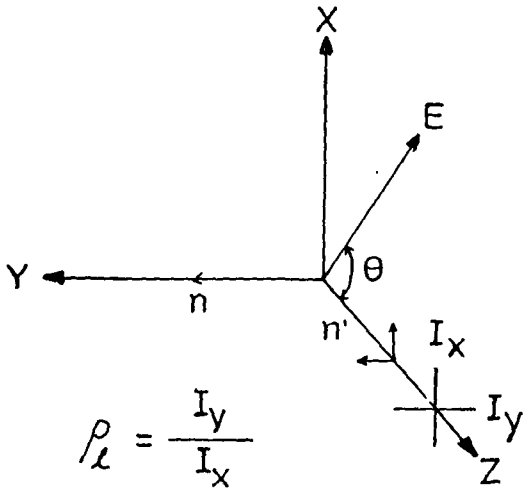

Fig.2.7.1. Raman scattering geometry. Light propogating along the Y direction is characterized by an electric vector E lying in the XZ plane. Scattered radiation is detected along the Z direction. Conventional scattering experiment has $\theta = 90^{0}$.

CHAPTER 3

EXPERIMENTAL TECHNIQUES

A brief description of methods of sample preparation, experimental techniques and the instruments used to obtain the vibrational and electronic spectra are presented in this chapter. We also give a brief account of the aqueous detergent micellar systems used in our work.

3.1. Preparation of samples

Iron protoporphyrin (IX) chloride (hemin) and Iron tetraphenylporphyrin chloride were purchased from Sigma Chemical Company, U.S.A. and Aldrich Co., U.S.A. respectively and were used without further purification. The nitrogenous ligand 2-methylimidazole (99%) and imidazole were obtained from Sigma Chemical Company, U.S.A. 1,2 dimethylimidazole was from purchased from Merck, Germany. All these compounds were used as recieved. The non-ionic detergent, Triton X-100, (TX-100) was obtained from Sigma Chemical Company, U.S.A. while the cationic cetyltrimethylammonium bromide (CTAB) and the anionic sodium dodecyl sulphate (SDS) (extra pure grade) detergents were purchased from BDH (England) and from SISCO laboratories respectively. All aqueous solutions were prepared with triple distilled, deionized water. Aqueous micellar solution of hemin was prepared as follows: An accurately weighed amount of hemin was dissolved in a small amount of dilute NaOH and mixed with the aqueous detergent solution so that the final concentration was 3% (v/v for Triton X-100 and w/v for SDS and CTAB) in the detergent and 0.5 mM for hemin. This solution was equilibrated at 40°C for about an hour after adjusting the pH. The nitrogenous ligands were added, when required,

before equilibration and their concentration was adjusted as per requirement. The pH was checked and adjusted just before carrying out the experiments and any loss of water was made up to restore the original concentration. To solubilize a water insoluble substrate in the micelle, an acetone solution of an accurately weighed amount of the substrate was first prepared and mixed with the aqueous detergent solution of known concentration. Acetone was then allowed to evaporate under slow heating and constant stirring of the solution with a magnetic stirrer. Any loss of water was made up to restore the required concentration.

The pH was measured with a Systronics Model 365 pH meter with a digital readout. Calibration of the pH meter was carried out using standard pH buffers. Dilute NaOH and HCl solutions were used to adjust the pH of the solutions.

All organic solvents used in this work were of spectroscopic grade and dried over molecular sieves when necessary.

3.2 Degassing of the solutions

Dissolved air from the solutions was removed using at least three freeze-pump-thaw cycles. The solution (approximately 1 ml) was first transferred to an arm of a specially designed glass apparatus with provision to fit the Raman quartz cell and other accesories for proper coupling to the vacuum line. The sample was frozen with liquid nitrogen and then connected to the vacuum line. When the pressure was about 10^{-4}-10^{-5} Torr, the vacuum line was cut off and the solution was allowed to warm up to room temperature. The solution was frozen again and the cycle was repeated at least three times to ensure removal of dissolved

oxygen from the solution. The solution was then transferred to the attached Raman cell under vacuum for recording the Raman spectra.

Alternatively, a stream of dry nitrogen or Argon gas was passed through the solution slowly for about 30 minutes in an airtight cuvette and the degassed solution was transferred with an airtight syringe to an airtight Raman cell, (or a capillary tube, for low temperature study) earlier purged with the inert gas.

3.3 Measurement of Raman Spectra

Raman spectra were recorded in a 90° scattering geometry with a Spex Ramalog 1403 triple monochromator equipped with a thermoelectrically cooled RCA-31034A photomultiplier and photon counting electronics. A microprocessor based Spex Datamate provided spectrometer control and data processing facility. Exciting laser lines were provided from Liconix Model 4240 He-Cd, Spectra-Physics Model 165-09 Argon ion and Spectra-Physics Model 375 jet stream dye lasers. AIR Products closed cycle helium cryo-cooler Model Displex CSA 202E was used to achieve low temperatures. The different instruments are described briefly here.

3.4 Liconix Model 4240 Helium-Cadmium Laser

This Model consists of two units: the laser tube and its power supply unit. Two mirrors mounted on adjustable plates and held at precise separation by three invar rods that run along the length of the laser tube made of pyrex glass, form the optical section of the laser tube. The mirrors are adjusted to reflect the laser light down the axis of the tube and allow emission through the partially reflecting mirror on one side.

Functionally the He-Cd laser is a helium filled plasma discharge tube containing cadmium metal within a reservoir. The tube terminates in vertically polarized Brewster windows of the resonator cavity. The coherent laser emission occurs by a mechanism similar to that of the Helium-Neon laser. The laser emission corresponds to the energy difference between the levels of cadmium atoms, while He gas aids in creating the population inversion in Cd atoms. Cooling by air is sufficient for this laser tube. The maximum power output at 441.6 nm was about 40 mW.

The power supply Model 4240 PS utilizes AC power from the primary source and converts to different DC levels for maintaining constant output power by controlling gas pressure (both He vapour and Cd vapour pressure) and associated current regulations in different electronic circuits.

3.5 Spectra-Physics Model 165-09 Argon Ion Laser

This model consists of the laser head with a CW output and Model 265 exciter. The laser head consists of a rugged beryllium oxide (BeO) plasma tube closed at both ends by fused silica Brewster windows, a solenoid for providing necessary magentic field and an optical resonator. The plasma tube is mounted in an optical cavity resonator formed by a spherical reflector at the output and a prism assisted by a flat mirror (to select the wavelength) at the high reflector end. The whole assembly of the resonator is held solidly against quartz rods with springs to minimize microphonic frequency shifts. The plasma tube is supported on a kinematically adjustable mount and is adjusted in such a way that the plasma tube is exactly centered. An external thumb wheel is provided for wavelength selection and for changing intracavity aperture. The plane of

polarization of the output beam can be changed to the desired plane by using the polarizer for recording the polarized Raman spectra.

The Spectra-Physics Model 265 exciter is fully equipped with the necessary electronic circuit to create, sustain and regulate the ion discharge in the plasma tube and to control the output power from the laser by simultaneously regulating the solenoid current. An arrangement is provided for a desired constant output optical power when operated in the "light control" mode. The 265 Exciter is fed with a stabilized three phase 380 V (phase to phase) power supply. This unit requires cooling of the transistor pass bank in the exciter, the solenoid and BeO plasma tube and is achieved by circulating distilled, deionized water at 15°C at 40 PSI from a closed cycle water chiller plant from Neslab, Model HX-500.

3.6. Spectra-Physics Model 375 Jet Stream Dye Laser

This model consists of a Model 375 dye laser along with a Model 376 dye circulator. The Spectra-Physics Argon ion laser source is used to pump the dye laser system to provide a continously tunable coherent laser. The laser gain medium is a solution of organic dye (Rhodamine 6G, in this case) which absorbs pump laser light focussed on it by an input mirror with a coating to provide maximum reflection at the Argon ion laser wavelengths. The dye emits light at longer wavelengths through fluorescence. The emitted light is passed many times through the dye stream using a set of mirrors, leading to stimulated emission of light at fluorescence wavelengths providing laser action. A tuning wedge, which is a Fabry-Perot etalon with a large free spectral range, tunes the cavity to any point within the broad fluorescence bandwidth. Finer control of the

output wavelength is provided with a fine tuning etalon which acts as a transmission filter, allowing the laser to operate only at those frequencies for which the etalon is tuned and provides continous wavelengths as it is tilted with respect to the dye laser beam.

The major components of the Model 376 dye circulator are the combination pump/motor, a reservoir bottle and a filter. The motor is magnetically coupled to the pump. A minimum pressure of 4.2 N/m^2 area is provided by the pump and the flow rate of the dye is $\approx$ 15 ml/sec. A stainless steel filter screen and a 10 μm teflon millipore filter through which the dye solution passes, ensure a clog-free nozzle for efficient dye laser action.

3.7 Spex Model Ramalog 1403 Laser Raman Spectrometer

Fig. 3.7.1 shows the relevant optical diagram of the instrument. This spectrometer (Spex 1403 double monochromator) is a f/7.8 instrument with a spectral coverage from 11000 cm^{-1} to 31000 cm^{-1} with an accuracy of ± 1 cm^{-1} in the 10000 cm^{-1} range. The spectral repeatablity of ± 0.2 cm^{-1} and the resolution of 0.15 cm^{-1} at 5791 Å (Hg line FWHM) can be achieved by this instrument. The holographic type grating used in the instrument has 1800 groves/mm blazed 5000 Å. The gratings are mounted on a modified Czerny-Turner mount using the fundamental grating equations:

$$d(\sin\alpha + \sin\beta) = n\lambda \qquad (3.7.1)$$

where n is the spectral order, λ the wavelength, d the grating spacing, α and β the angle of incidence and diffraction respectively. If $\alpha = \theta + \phi$ and $\beta = \theta - \phi$, where θ is the angle of rotation of the grating measured

from zero as shown in Fig. 3.7.2 and is a constant depending on the design of the instrument, then Equation 3.7.1. can be recast as

$$2d \, Sin\theta \, Cos\phi = n\lambda \qquad (3.7.2)$$

The Raman peaks are measured in terms of frequency shifts in cm^{-1} on a linear X-axis by utilizing a cosecant drive for grating rotation with $\phi = 10^{\circ}$ and thus $Cos\phi = 0.984$ (values supplied by manufacturers). To record the Raman spectra, the laser beam is passed through the Spex Model 1459 UVISIR illuminator after being diffracted from SPEX Model 1460 "Lasermate", which is a small unit consisting of a grating with 1200 lines/mm blazed at 5000 Å and a mirror assembly to isolate and filter the spurious plasma lines. The beam is then focussed on to the sample, after deflection (through 90°) by a mirror to a spot of diameter 10 μm by a fused silica condensing lens. Scattered radiation from the sample is then passed through the polarization analyser (optional) which works on the principle of birefringence and total reflection or of dichroism. The polarization state of the observed Raman bands can be obtained by using this analyser. The scattered radiation is then collected by an elliptical mirror (f/1.4) and focussed on to the entrance slit (S_3) of the spectrometer after reflection from the mirror (M_7) and passing through a polarization scrambler (Fig. 3.7.1). The polarization scrambler converts the plane-polarized scattered radiation to a randomly polarized radiation before it reaches the spectrometer and thus cancels any variation in spectrometer response that results from polarization-dependent efficiencies. The polychromtic scattered radiation which is focussed on to the entrance slit gets dispersed by the 1800 lines/mm holographic gratings (G_2 and G_3). Finally, a nearly monochromatic light signal of a particular

frequency selected by spectrometer control reaches the exit slit (S_7) of the double monochromator. This exit slit is coupled to the third monochromator Model Spex 1442 V.

3.8 The third Monochromator Model Spex 1442 V

This device is used for reducing stray light in Raman scattering where the weak spectral features are not clearly resolved in the vicinity of the intense Rayleigh line. This device which functions as a variable band monochromator is a modified Czerny-Turner spectograph attached to the exit slit of the double monochromator. The light entering the third monochromator is nearly monochromatic at the particular tuned frequency of the double monochromator with some stray light of the exciting frequency. This is further dispersed and only the desired component of the incoming monochromatic light is incident on the gap between the slit blades of the exit slit coupled to the photomultiplier tube. The stray radiation is blocked by the slit blades. The third monochromator can operate in the fixed mirror mode, in the scanning grating mode, or in the stationary grating mode. The fixed mirror mode converts the system to a double monochromator and so maximizes the signal intensity. It is ideal for high resolution work when the signal intensity is low. The scanning grating mode is uselful in cases where unwanted scattered light over the complete Raman spectrum hinders the obervation of the true signals. The stationary grating mode is especially valuable for identifying Raman lines close to the excitation frequency (Rayleigh line). In all the Raman measurements the third monochromator was used in the fixed mirror mode.

3.9 Spectrometer Control and Data Processing

The spectrometer control and data processing are achieved with a microcomputer based Spex "Datamate". The inbuilt software makes possible a host of oprations on the spectral data like differentiation, integration, change of frequency and intensity ranges, addition, subtraction, division etc,. The spectral data can be stored in the 4K data point storage in any of the eight variable length files. The stored data can be plotted on a strip chart recorder or transferred to external peripherals like floppy discs or to a PC through standard RS 232 port for further data manipulation. The unavoidable wavelength dependent distortions of the spectral data due to the spectrometer optics can be rectified by applying the radiometric corrections from the inbuilt 1K EAROM. Using programming options the entire spectrometer control as well as data collection and manipulation can be completely automated. The data storing facility could be bypassed and real time spectra can be directly recorded on the strip chart recorder.

The raw data is obtained from the output of the preamplifier (PC Dam). The anode of the photomultiplier tube is the input of the PC dam. The preamplifier gain is 400. The high voltage (-1750 volts) required for operating the photomultiplier tube is also supplied by the Datamate with a stability of ± 0.002% after 30 minutes of warm up.

The photomultiplier tube Model RCA 31034A used with the instrument is a 2" diameter head-on, 11-stage QUANTACON photomultiplier having a GaAs chip as its photocathode, an ultraviolet transmitting glass window and an in-line copper beryllium dynode structure. The tube is cooled to -30 $^{\circ}$C by a thermoelectric cooling device and has almost linear

absolute response in the 3000 Å to 8500 Å wavelength range. The operation is at a current gain of 10^6 with a maximum dark pulse summation of 12 CPC (counts per second).

3.10 Scanning of Raman Spectra

The recording of Raman spectra of coloured samples is associated with many problems which include: (a) optimization of concentration of the sample to minimize reabsorption of the scattered light and maximize scattering by the sample; (b) the local heating effect due to the high power laser focussing which may induce thermal decomposition of the sample and also give rise to thermal lens effect and; (c) the high background due to fluorescence from impurities in the compound or in the solvents or intrinsic fluorescence from the sample itself. The first of these can be overcome by a trial and error method using different concentrations of the sample until a good quality spectrum can be obtained. The local heating effect can be overcome by rotating the sample continuously in the laser beam so that the light scattering portion of the sample remains in the laser beam for a very short time and a fresh portion is presented to the beam everytime during the rotation. This technique due to Kiefer and Bernstein,[1,2] thus reduces local heating of the sample and consequent possible decomposition. Measuring Raman spectra in solid state or in KBr pellet reduces the flourescence background, but in solution, removal of possible impurities by purification of the sample or solvents helps minimize this problem.

The self absorption of the scattered light can be minimized by positioning the Raman cell (a cylindrical quartz cell) with the sample (0.5 to 1 ml) so that the laser beam strikes the bottom of the cell close to the inner perimeter of the cell. All the spectra were routinely calibrated with the standard lines of indene in the high frequency range 1200-1700 cm^{-1} and those of known lines of CCl_4 in the 100-500 cm^{-1} or the known Raman lines of solvents used. Other spectral parameters like laser power, integrating time, slit width, wavelength increment etc., are adjusted as required to optimize signal to noise ratio. Three to five scans were averaged for weak Raman signals with the help of Datamate.

3.11 Measurement of Raman Spectra at Low Temperatures

The Raman spectra of samples at low temperatures were obtained with the help of an AIR Products Helium cryo-cooler (Model Displex CSA 202E). This unit can cool the sample upto 10°K. Temperature control was achieved by a controller Model APD-E upto a precision of ± 0.5°K. A precalibrated gold/chrome thermocouple measured the temperature at the cryotip.

3.11.1 AIR Product Model CSA 202E closed cycle Helium Cryo-cooler

The closed cycle Helium cryo-cooler from AIR Products Duplex Model CSA 202E mainly consists of a compressor unit module 202 and expander module DE 202.

The compressor is an air cooled unit which supplies helium gas at a pressure of 260 PSI to the expander module. The gas under high pressure expands in the expander assembly. Joule-Thompson effect decreases

the temperature of the gas. The cooled gas returns to the compressor at 110 PSI pressure. With repeated cycles of this process a temperature of $10^{\circ}K$ can be achieved at the heat station with refrigeration capacity of 1.8 watts at $20^{\circ}K$. Higher temperatures can be obtained by a temperature controller Model APD-E unit.

The porphyrin solution under investigation was sealed in a quartz capillary tube and mounted on to the copper rod with the help of conducting glue. The rod is connected mechanically to the second heat station. Vacuum shroud Model DMX 1E is connected to a vacuum pump (Hind Hivac Oil diffusion pump) for thorough evacuation (upto 10^{-5} Torr) and to obtain necessary themal insulation. In addition to this, to obtain good thermal stability, a "radiation shield" is connected to the final stage of heat station. DMX-1X interface extension is used to obtain Raman spectra. A home made stand along with necessary arrangements for X-Y-Z movement of the expander module was used to align the sample in the beam path.

3.12. Electronic Absorption Spectra

The electronic absorption spectra were recorded on a Varian Carey 2300 UV-VIS-NIR Spectrphotometer and on a Shimadzu Model 160 A Spectrometer.

3.12.1 The Varian Carey 2300 UV-VIS-NIR Spectrophotometer

This spectrophotometer is a double-beam recording instrument for measuring light intensity at specified wavelengths in a continuous manner. The model employs two lamp sources: a tungsten-halogen lamp for VIS-NIR wavelengths (3152-340 nm) and a deuterium source for UV wavelengths (185-

340 nm). Light from the appropriate source is directed through a band pass or long wave pass filter to the single grating monochromator. The monochromatic beam is split into two components of equal intensity, one beam passing through the reference and the other through the sample. The intensity of light emerging from the reference/sample cells is detected by a photomultiplier tube for UV/VIS wavelengths and a lead sulphide detector for NIR wavelengths. The current pulses generated by light from the sample/reference cells are amplified and recorded in transmission or absorbance mode. In the absorbance mode the amplified signal is analysed by a log converter which transforms the light transmission current values to optical density and absorbance is equal to log 1/T (T = transmission). The resolution of this spectrometer is 0.07 nm with a wavelength repeatability of ± 0.05 nm and a wavelength accuracy of ± 0.2 nm. in the UV-VIS range. Fig. 3.12.1 shows the optical arrangement of the spectrometer.

3.13. Micellar systems

Micelles are aggregated structures formed by the interaction of several surfactant (detergent) molecules. The latter, called amphiphiles, are characterized by the presence of both a hydrophobic and a hydrophilic group within the same molecule. Aqueous solutions of detergents, at concentrations above their critical micellar concentration (CMC) provide microheterogenous fluids where the hydrophobic groups are held in close proximity due to hydrophobic bonds, a term given to the apparent attraction between non-polar groups held together due to strong attractive force between water molecules in the bulk phase.[3] The phenomena of micellization is a result of the fact that at a given temperature for a

given detergent only a certain amount of monomer detergents can be accomodated in a solution of a given volume and any further addition of the detergent in the solvent will be essentially transformed to micelles.[4] The micelle is also a dynamic structure in equilibrium with its monomer where the monomer-micelle exchange is taking place on a microsecond time scale.[5,6] However, the time scale of reactions in the micelle is much greater than the time required for monomer-micelle equilibrium.[6]

Condensed phase chemical rections are often strongly dependent upon solvation. In enzymes and lipid membranes, a coordinated local arangement of solvating molecule can completely control a reaction in a catalyic sense. These systems are often microscopically heterogenous in that a region of hydrophobic character exists within a few angstroms of a region of hydrophillic character. Much of the interest in micelle cataylsed reactions arises from structural similarities between micelles and the globular enzymes and to parallels between micellar enzymatic reactions and catalysis. A hydrocarbon like micellar interior of $\approx$ 40 Å in diameter is seperated from aqueous phase by an ionic double layer boundary region. A static potential gradient exists across the boundary (of opposite signs in cationic and anionic micelles) which is utilized in permanently separating charged species following ionization by radiation and to preferentially solubilize particular type of ions in the interior of the charged micelles.[7]

Fig. 3.13.1 illustrates the structure of ionic micelles where the polar head groups are either cationic or anionic. Fig. 3.13.2 shows the structure of non-ionic Triton X-100 micelles. The interfacial region or Stern layer (Fig.3.13.1) having a width of about the size of the

surfactant head group contains the ionic head groups of the amphiphile, a fraction of the counterions (0.6-0.9/ionic head group) and water.[8] The Stern layer is an extremely anisotropic region with properties intermediate between those of water and hydrocarbon (alcohol-like is the common description of its polarity). Thermal motion creates a diffuse electrical double layer, called Gouy-Chapman layer, which extends out into the aqueous phase and contains the remaining counterions.[7b] At the concentrations near and slightly above the CMC, the micelles are assumed to be approximately spherical in shape.

The subtrates solubilized in the micelles follow a Poisson distribution of occupancy in the micelles.[9] The probability of finding n number of substrates per micelle is given by

$$P(n) = \frac{e^{<q>}<q>^{n}}{n\ !} \qquad (2.13.1)$$

where <q> is the average number of substrates per micelle given by

$$<q> = \frac{[S]}{[M]} \qquad (2.13.2)$$

where [S] and [M] are the molar concentrations of the substrate and micelle respectively. The latter can be evaluated from

$$[M] = \frac{[C] - CMC}{N} \qquad (2.13.3)$$

where [C] and N are the total molar concentration of the surfactant and the aggregation number of the micelle respectively and CMC is the critical micelle concentration.

A given molecular species can be preferentially solubilized in the interior of the micelle or its boundary region (Stern layer) or adsorbed on to the micellar surface depending upon its hydrophilic-hydrophobic balance and the sign of the surface potential. Aromatic neutral molecules dissolve often in the hydrocarbon-like micellar interior. In the case of non-ionic TX-100 micelle (Fig. 3.13.2) the large aggregation number and the length of the hydrophilic chains along with the phenoxy chromophore prevents a clear boundary of the hydrophobic and hydrophilic regions of the micelle due to packing constraints. The hydration of oxyethylene groups is the primary reason that the non-ionic surfactant is soluble in water. However, the hydrophobic region is assumed to extend one oxyethylene chain length (16 Å) beyond the hydrophobic core making its total hydrophobic radius $\approx$ 27 Å and the micellar radius $\approx$ 43 Å in a spherical model. Incidentally, the hydrophilic region of this micelle forms 78-83% of the total volume of the micelle.[10]

Some of the important parameters of the micelles used in this work have been tabulated in Table 3.13.1. Many of these parameters, including the shape of the micelles, are sensitive to the experimental conditions like temperature, ionic strength, presence of alcohols and electrolytes, counter and co-ions, and the concentration of the surfactants themselves.[6,8]

The aggregation of porphyrins and metalloporphyrins in aqueous solutions is well known.[11-15] In order to study their properties in monomeric form, alcohols and alcohol containing solvent mixtures were also employed.[16,17] Simplicio et al[18] have shown that iron protoporphyrin can be solubilized and stabilized as monomers in both ionic and non-ionic

micelles. Several investigations have been carried out in these micellar systems on the metalloporphyrins and hemeproteins by various techniques like pulse radiolysis,[19] NMR,[20] UV-VIS,[21] Mössbauer[22] etc..

Fig. 3.13.3 illustrates the proposed[19b] orientation of iron protoporphyrin (hemin) in the anionic micelle, SDS. The hydrophilic propionic acid groups reside in the headgroup region and oriented towards the aqueous phase while the rest of the porphyrin moiety is well inside the micellar surface. Recent NMR[20c] studies show that the hemin is radially aligned with the iron centre about 5Å from the surface of the micelle, whereas the hydrophobic iron-octaethylporphyrin[20b] is embedded rather deeply near the core of the SDS micelle.

REFERENCES

1. Kiefer, W., Bernstein, H.J. App.Spectrosc. 1971, 25, 500.
2. Kiefer, W., Bernstein, H.J. App.Spectrosc. 1971, 25, 609.

3. Laidler, K.J.; Bunting, P.S. In *Chemical Kinetics of Enzyme Action*; 2nd ed. Clarendon Press: Oxford, 1973.

4. *Ulmins*, J.; *Wennerströmm*, H. Lennart, L.; Johansson, A.; Lindblom, G.; Gravasholt, S. *J. Phy. Chem.* 1979, 83, 2232.

5. (a) Aniansson, E.A.G.; Wall, S.; *J. Phys. Chem.* 1974, 78. 1024.
   (b) Aniansson, E.A.G.; Wall, S.; *J. Phys. Chem.* 1975, 78, 857.

6. (a) Fendler, J.H. Chem. Rev. 1987, 87, 877.
   (b) Fendler, J.H.; Fendler, E.H. *Catalysis in Micellar and Macromolecular Systems*; Academic Press: New York, 1975.
   (c) Rosen, M.J. *Surfactants and Interfacial Phenomena*; Wiley: New York, 1978.

7. (a) Turro, N.J.; Grätzel,M.; Braun, A.M. *Angew. Chemie.* Int. Ed. Eng. 1980, 19, 675.
   (b) Thomas, J.K. *Acc. Chem. Res.* 1977, 10, 133.

8. Bunton, C.A.; Nome, F.; Quina, F.H.; Romsted, L.S. *Acc. Chem. Res.* 1991, 24, 357.

9. (a) Nakagawa, T. In *Non-ionic Surfactants*; Shick, M.J. Ed.; Marcel Dekker: New York, 1968, pp 558.
   (b) Infelta, P.P.; Grätzel, M. *J. Chem. Phys.* 1979, 70, 179.

10. (a) Viseu, M.I.; Costa, S.M.B. *J. Chem. Soc., Farad. Trans.* 1993, 89, 1925.
    (b) Saitoh, T.; Hoshino, H.; Yotsuyanagi, T. *J. Chem. Soc., Farad. Trans.* 1994, 90, 479.

11. (a) White, W.I. In *The Porphyrins*; Dolphin, D., Ed.; Academic Press: New York, 1978; Vol. 5. Chapter 7.
    (b) Falk, E.J. In *Porphyrins and Metalloporphyrins*; Elsevier: Amsterdam, 1964.

12. Shelnutt, J.A. *J. Phys. Chem.* 1984, 219, 445.

13. (a) Chandrasekhar, T.K.; Van Willigen, H.; Ebersole, M.H. *J. Phys. Chem.* 1984, 88, 4326.

14. Kano, K.; Nakajima, T.; Takai, M.; Hashimoto, S. *Bull. Chem. Soc. Jpn.* 1987, 60, 1281.

15. Kadish, K.M.; Maiya, G.B.; Araullo, C.; Guillard, R. *Inorg. Chem.* 1989, 28, 2725.

16. Davies, T.H. *Biochim. Biophys. Acta.* 1973, 329, 108.

17. (a) Bartocci, C.; Scandola, F.; Ferri, A.; Carassiti, V. *J. Am. Chem. Soc.* 1980, 102, 7067.
(b) Bartocci, C.; Maldotti, A.; Varani, G.; Battioni, P.; Carassiti, V.; Mansuy, D. *Inorg. Chem.* 1991, 30, 1255.

18. (a) Simplicio, J. *Biochemistry*, 1982, 11, 2525.
(b) Simplicio, J.; Schwenzer, K. *Biochemistry*, 1973, 12, 1923.
(c) Simplicio, J; Schwenzer, K.; Maenpa, F. *J. Am. Chem. Soc.* 1975, 97, 7319.

19. (a) Brault, D.; Bizet, C.; Morliere, P.; Rougee, M.; Land, E.J.; Santus, R.; Swallow, A.J. *J. Am. Chem. Soc.* 1980, 102, 1015.
(b) Evers, E.L.; Jayson, G.G.; Swallow, A.J. *J. Chem. Soc., Farad. Trans.* 1. 1978, 74, 418.
(c) Bizet, C.; Morliere, P.; Brault, D.; Delgado, D.; Bazin, M.; Santus, R. *Photochem. Photobiol.* 1981, 34, 315.

20. (a) Muzumdar, S.; Medhi, O.K.; Mitra, S. *J. Chem. Soc., Dalton. Trans.* 1990, 1057.
(b) Muzumdar, S. *J. Chem. Soc., Dalton. Trans.* 1991, 2091.
(c) Muzumdar, S. *J. Phys. Chem.* 1990, 94, 5947.

21. Muzumdar, S.; Medhi, O.K.; Kannadaguili, N.; Mitra, S. *J. Chem. Soc., Dalton. Trans.* 1989, 1003.

22. (a) Medhi, O.K.; Silver. J. *J. Chem. Soc., Chem. Comm.* 1989, 1199.
(b) Medhi, O.K.; Houlton, A.; Silver, J. *Inorg. Chim. Acta.* 1989, 161, 213.

23. Robson R.J.,; Dennis, E.A. *Acc. Chem. Res.* 1983, 16, 251.

24. Tanford, C. in *The Hydrophobic Effect*; Wiley-Interscience: New York, 1973.

25. Sarpal, R.S.; Belletete, M.; Durocher, G. *J. Phys. Chem.* 1993, 97, 5007.

26. Darshaw, R.; Briggs, J; Bunton, C.A.; Nicoli, D.F. *J. Phys. Chem.* 1982, 86, 2388.

27. Malliaris, A.; Lang, J.; Zana, R. *J. Phys. Chem.* 1986, 90, 655.

28. Fendler, J,H. *Membrane Mimetic Chemistry*; Wiley: New York, 1982; pp 9.

29. Fernandez, M.S.; Fromherz, P. *J. Phys. Chem.* 1977, 81, 1755.

30. James, A.D.; Robinson, B.H. *J. Chem. Soc., Farad. Trans. 1.* 1978, 74, 10.

31. Cabane, B.; Duplessix, R.; Zemb, T. *J. Phys. Chem.* 1985, 46, 2161.

TABLE 3.13.1: Some important physical parameters of the micelles used in this work.

Surfactant	Dielectric constant[a]	CMC[b] at 25°C (mM)	Aggregation. Number[c]	Radius (Å)	Surface potential (mV)
TX-100	40	0.32[d]	143[d]	43[d]	—
CTAB	37	0.92[b]	84[e]	29[g]	+148[h]
SDS	43	8.1[b]	74[i]	25[g]	−134[h]

a, Ref.25; b, Ref.6b; c, in the abcence of salts.; d, Ref.23; e, Ref.27; f, Ref.24; g, Ref.26; h, Ref.29; i, Ref.31.

Triton X-100 $(CH_3)_3CCH_2C(CH_3)_2C_6H_4(OCH_2CH_2)_nOH$ n = 9,10

CTAB $CH_3(CH_2)_{14}CH_2(CH_3)_3N^+Br^-$

SDS $CH_3(CH_2)_{10}CH_2(SO_4)^-Na^+$

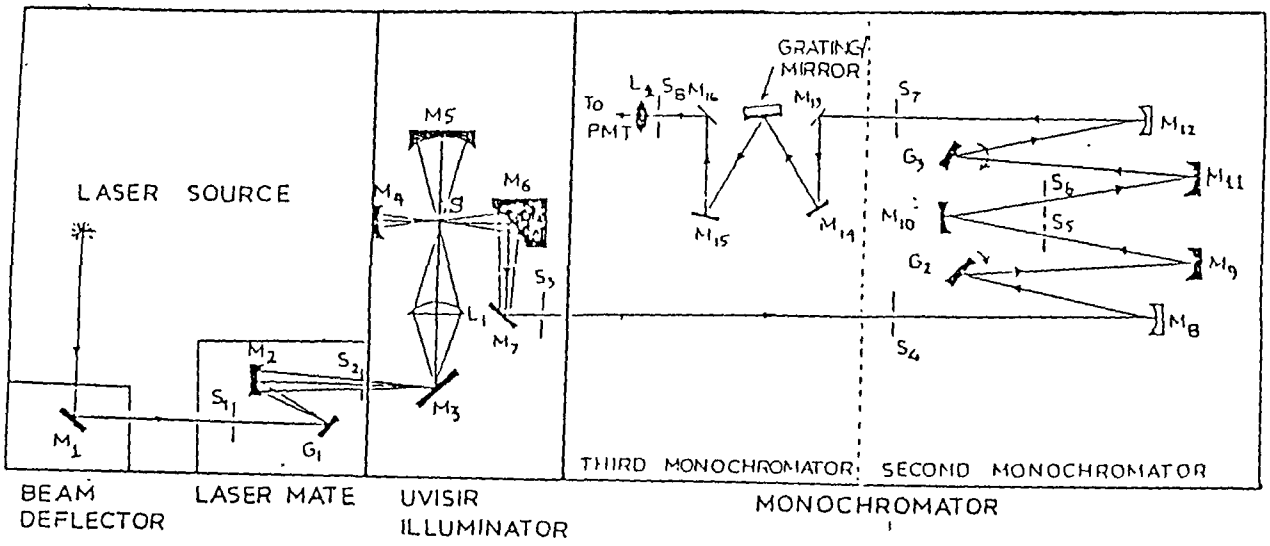

Fig.3.7.1 Optical diagram of a SPEX Model Ramalog 1403 laser Raman Spectrophotometer, including the laser mate, UVISIR illuminator and the third monochromator. (M_1,M_3,M_7,M_{13}-M_{16} are the plane mirrors: M_2,M_4,M_5,M_8,M_9-M_{12} are concave mirrors, M_6 is elliptical mirror, S_1-S_8 are slits: L_1 is fused silica condenser lens: L_2- field lens: S - sample: G_1-G_3 are the gratings and PMT is the photomultiplier tube).

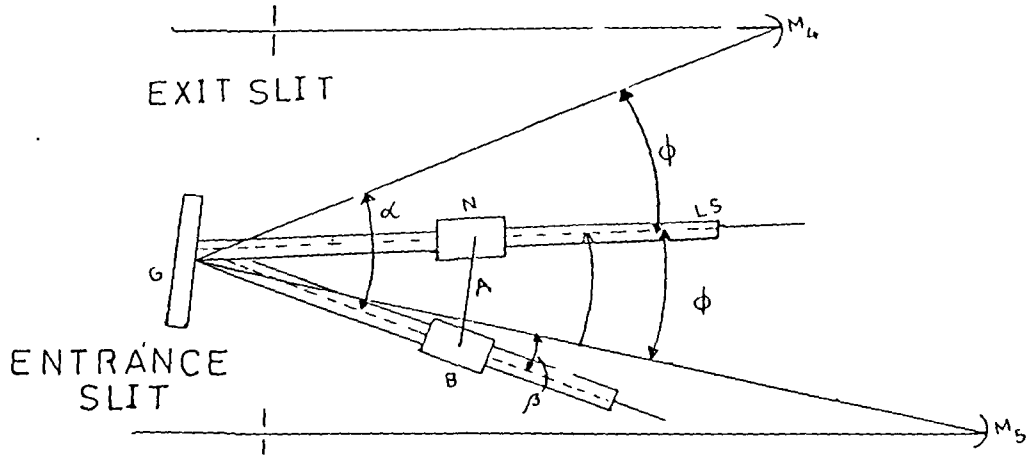

Fig. 3.7.2 Mechanical cosecant drive mechanism for the Czerny-Turner mount of gratings for the Spex Model 1403 Ramalog spectrometer. The nut N moves along lead screw LS while the slide B moves along a bar held at right angles to the grating G. The grating rotates as the arm A moves along the bar. Here M_4 and M_5 are the mirrors.

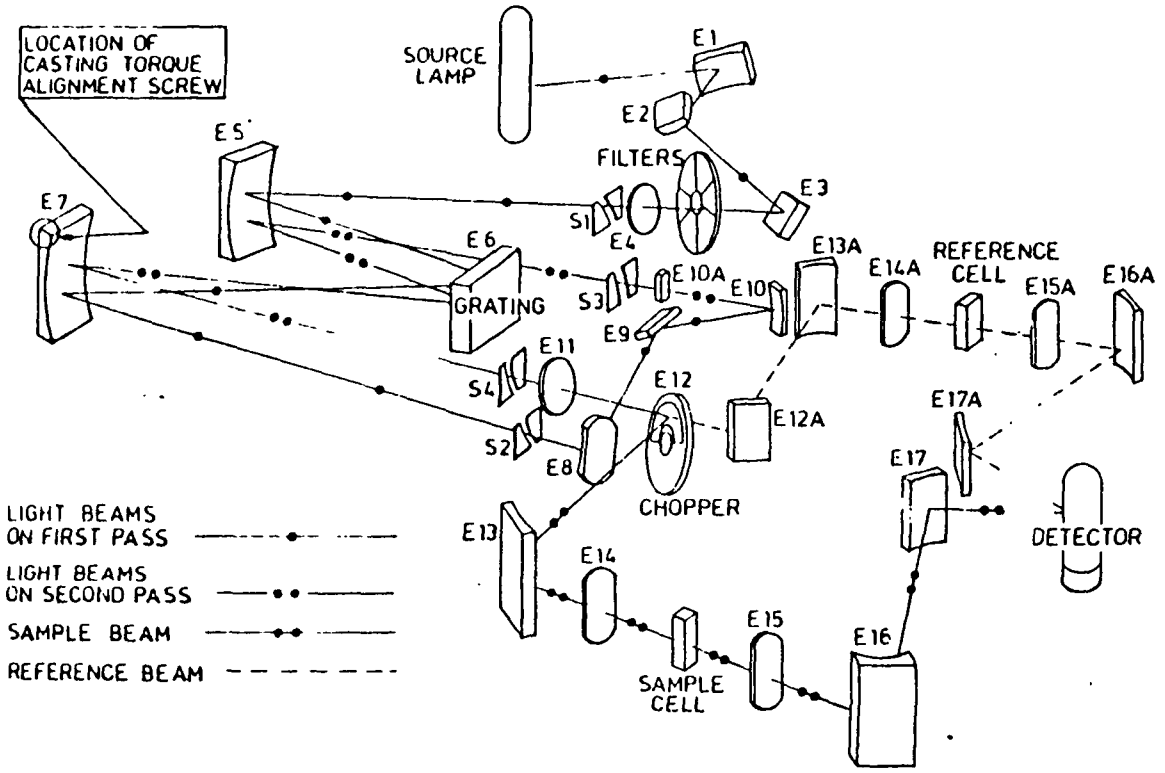

Fig. 3.12.1 Diagram of the Optical Arrangement

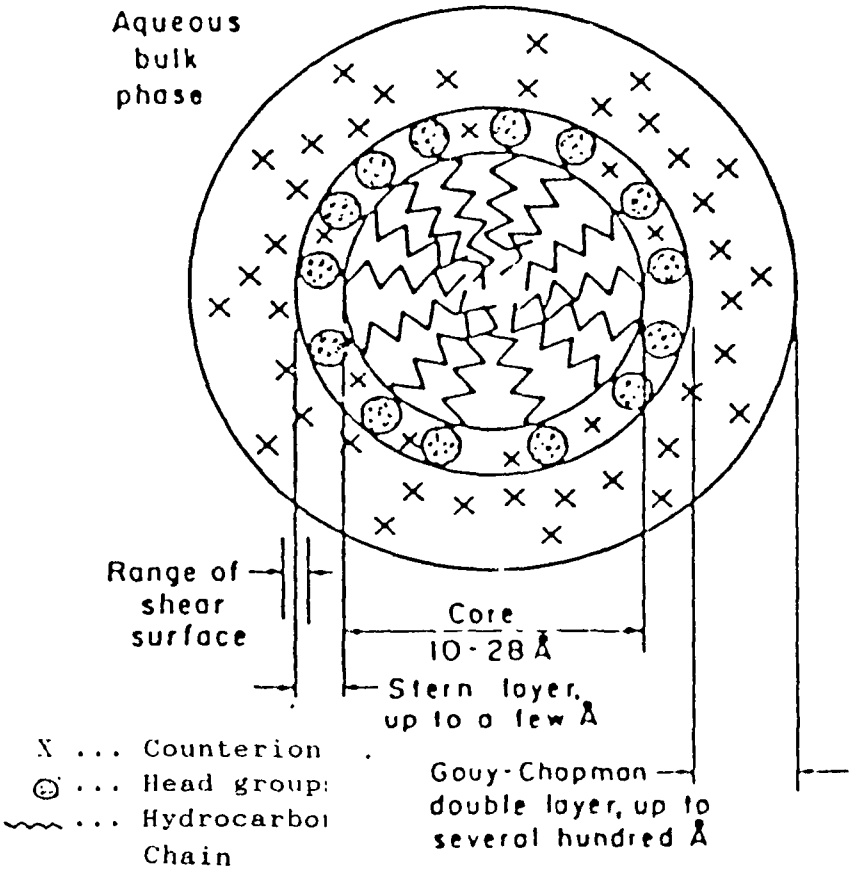

Fig. 3.13.1 A two-dimensional representation of the regions of a spherical ionic micelle.

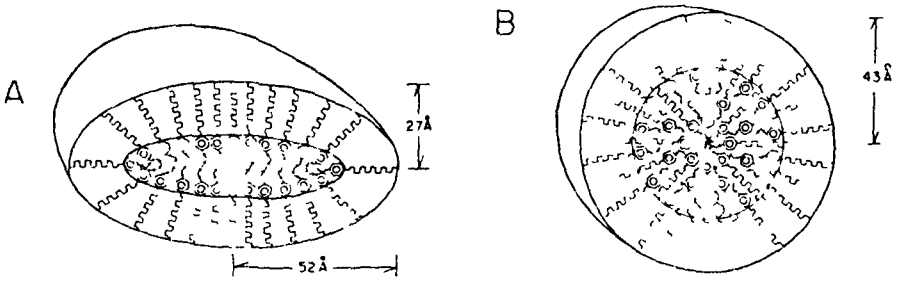

Fig. 3.13.2. Schematic view of the oblate ellipsoidal model (A) and spherical model (B) for a OPE-9 (Oxy Poly Ethylene) TX-100 micelle.

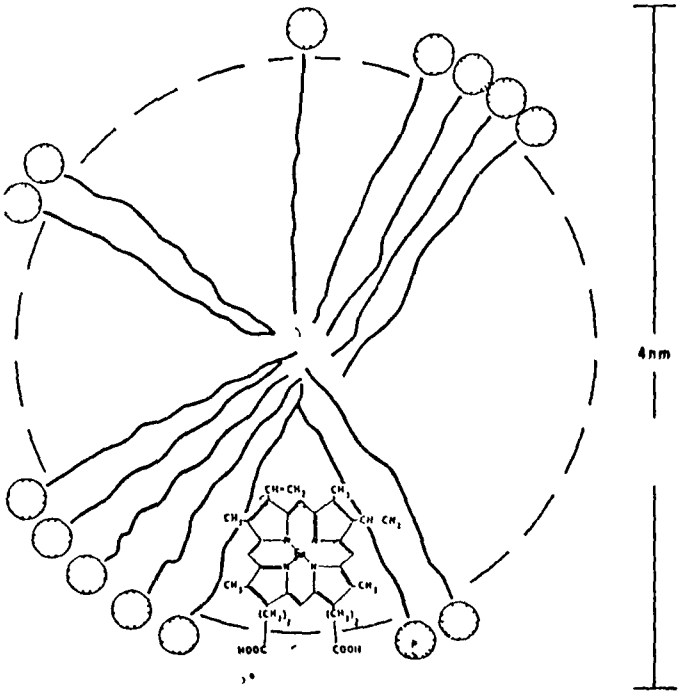

Fig.3.13.3 Two dimensional representation of the proposed orientation of in a spherical SDS micelle (charges are omitted) Only a few constituent SDS monomers (● hydrophyllic head group, ~~ hydrocarbon chain are shown The diagram shows the overall size relationship between the hemin and the micelle The axial ligands (not shown) would be placed above and below the plane of the porphyrin ring

CHAPTER 4

RESONANCE RAMAN STUDIES OF PHOTODISPROPORTIONATION OF THE μ-OXO DIMER, $Fe(TPP)_2O$, IN AQUEOUS DETERGENT MICELLE

We report in this chapter Resonance Raman (RR) studies of photodisproportionation of the μ-oxo dimer, $Fe(TPP)_2O$, obtained on solubilization of ferric tetraphenylporphyrin chloride, FeTPPCl, in aqueous alkaline Triton X-100 detergent micelle, as a result of laser irradiation at 441.6 nm. The oxoferryl tetraphenylporphyrin, $TPPFe^{IV}=O$, complex generated and stabilized at room temperature as one of the products of photofission has been characterized by its characteristic $\nu(Fe^{IV}=O)$ stretching frequency and the shift of this mode on coordination of dimethylformamide (DMF) as the sixth ligand trans to the ferryl oxygen, and by its other RR frequencies typical of its low spin character. The intensities of these bands are enhanced at low temperature consistent with the higher stability of this complex at low temperatures. The other photoproduct has been identified as a five coordinated, high spin, ferrous complex.

4.1 Introduction

Porphyrins containing metal-oxo bonds have been extensively studied[1-2] as models for the heme protein active sites of the peroxidases, catalases and cytochrome P-450s. Catalases reduce hydrogen peroxide to oxygen and water, while peroxidases oxidize organic and inorganic substrates via reaction with peroxides and other oxidants. The oxoferryl porphyrins, $PFe^{IV}=O$, have been postulated as reaction intermediates in the mechanism of action of peroxidases, oxygen donating species in cytochrome P-450,[1] cytochrome *c* oxidase[2] and in the auto-oxidation of Fe(II) porphyrins.[3] Several groups have reported the formation and characterization of iron(IV) oxo-porphyrin complexes by chemical, photochemical and electrochemical methods at low temperatures by various techniques.[4-6] On the other hand, room temperature stabilization and characterization of the oxoferryl species in only a few synthetic porphyrins and natural enzyme systems have been reported in the recent past.[6,7-9]

The photosensitivity of the oxygen bridged dimer, $(FeTPP)_2O$, and some water soluble iron porphyrin μ-oxo dimers have been studied recently[10] by transient absorption spectroscopy and the formation of oxoferryl species as one of the disproportionation products on photoexcitation was demonstrated. While some in-plane vibrations of the porphyrin macrocycle exhibit frequency shifts depending upon the delocalization of π-electrons between the iron atom and the porphyrin macrocycle, the frequency of the $\nu(Fe^{IV}=O)$ stretching vibration serves as the most direct probe of the $Fe^{IV}=O$ bond. Thus, this RR band has been

identified in Compound II of horseradish peroxidase (HRP),[9] Cytochrome *c* peroxidase (CcP) compound ES,[9e] compound B of Cytochrome oxidase[2c] and in several model compounds.[4-8]

In this chapter, we describe optical absorption and RR studies which showed that Fe(TPP)Cl in alkaline micellar medium exists as μ-oxo dimer, $(FeTPP)_2O$, which on photoexcitation with the 441.6 nm laser light at room temperature and at $-50^{\circ}C$, in anaerobic conditions, undergoes photodisproportionation yielding the oxoferryl $TPPFe^{IV}=O$ species and a five coordinated, high spin (5cHs) ferrous $Fe^{II}(TPP)L$ complex.

4.2 Experimental Section

2-methylimidazole (2-MeIm), N-methylimidazole (N-MeIm) and the detergent Triton X-100 (TX-100) were purchased from Sigma Chemical Company, U.S.A. and were used as recieved. FeTPPCl was obtained from Aldrich Chemical Company. 1,2-dimethylimidazole (1,2-MeIm) was purchased from Merck, Germany. Triple distilled water was used for preparing the aqueous micellar, NaOH, HCl and pH buffer solutions. Sample solutions were degassed by subjecting them to at least three freeze-pump-thaw cycles or by bubbling argon gas for at least thirty minutes. Raman lines were routinely calibrated with known lines of indene. The pH of the solutions was adjusted using aqueous NaOH and HCl solutions and was measured with a previously standardized pH meter (Systronics Model 335).

Resonance Raman Spectra were recorded at 90° scattering geometry with the SPEX Ramalog 1403 spectrometer equipped with a cooled RCA 31034A photomultiplier tube and photon counting electronics. Excitation line at 441.6 nm was provided by Liconix Model 4240 He-Cd laser.

4.3 Results and Discussion

The electronic absorption spectra of FeTPPCl solubilized in the aqueous detergent micelle TX-100 at alkaline and highly acidic conditions are shown in Fig. 4.3.1. At alkaline pH, the absorption bands at 408, 573 and 613 nm correspond to the Soret, and the Q bands respectively of the μ-oxo dimer and match very well with its absorption spectrum in organic solvents.[11,12,14a] No change was observed in the absorption spectrum when HCl was added till a pH of 2.9 was reached. At a pH of 1.8 and below, the 510 nm band gained intensity while the 573 nm band weakened considerably. The 613 nm band disappeared and the Soret band shifted to 419 nm. The new set of absorption bands (419, 510 and 573 nm) corresponds to the chloro complex, FeTPPCl, in agreement with the reported values.[11,12] The similarity of these spectra to those in non-coordinating organic solvents (Table 4.3.1) indicates that both these complexes, normally insoluble in water, get solubilized in the hydrophobic region of the micelle. The interconversion of these two complexes on reaction with strong alkali and HX acids is well known.[11,12] When nitrogenous ligands like 2-MeIm, 1,2-MeIm, N-MeIm or Im were added to the above micellar solution containing $(FeTPP)_2O$ at alkaline pH, no change in the absorption spectrum was observed indicating that these added ligands do not form complexes with the porphyrin ligand or coordinate to the iron centre. It is well known that the μ-oxo dimer, $(FeTPP)_2O$, does not generally coordinate axial ligands (i.e., $(L\text{-}FeTPP)_2O$ species is not formed) and has only one tetradentate ligand per metal. Further, it is also known that this complex shows no monomer-dimer equilibrium.[12a]

The major RR bands associated with the C-C, C-N and C-H skeletal deformation modes of the porphyrin macrocycle in iron tetraphenylporphyrin and its derivatives[13] appear in the 1000-1700 cm^{-1} and 100-600 cm^{-1} regions. The totally symmetric modes which appear within these frequency regions, among other in-plane porphyrin vibrations, and which are resonance enhanced via the porphyrin π-π^* transitions, are sensitive marker bands[13] of spin, coordination and oxidation states of the central metal atom. These modes show appreciable shift in frequency when any of these parameters change.

Figs. 4.3.2 and 4.3.3 depict the RR spectra in the high (1300-1650 cm^{-1}) and low frequency (150-550 cm^{-1}) regions respectively for the $(FeTPP)_2O$ complex in TX-100 micelle at pH 11 obtained with laser excitation at 441.6 nm under various experimental conditions. Trace A in both figures corresponds to the RR spectrum of $(FeTPP)_2O$ under aerobic conditions. Prominent RR bands at 1552 $cm^{-1}(\nu_2)$, 1450 $cm^{-1}(\nu_3)$, 1360 $cm^{-1}(\nu_4)$, 1237 $cm^{-1}(\nu_1)$, 390 $cm^{-1}(\nu_8)$, 199 $cm^{-1}(\phi_{10})$ are in perfect agreement with the values reported in literature for this complex in organic solvents.[14] A medium intensity band at 363 cm^{-1} can be attributed to the symmetric Fe-O-Fe stretching mode of the μ-oxo dimer. The absorption spectra of the complex present at this pH rules out the possibility of this RR band being due to the ν(Fe-Cl) stretching mode observed[13b] in FeTPPCl at nearly the same frequency. Although a hydroxide complex of an iron porphyrin,[11d] Fe(TMP)OH [ferric tetramesityl porphyrin hydroxide], displays an absorption spectrum similar to that of the μ-oxo dimer, $(FeTPP)_2O$, the presence of the 363 cm^{-1} band further supports the μ-oxo dimeric nature of the species in the micelle at this pH. The unprotected nature of the simple FeTPP ligand compared to that of FeTMP

ligand is responsible[11d] for dimerization of the ferric tetraphenyl porphyrin on contact with aqueous alkali.

The similarity of the Raman frequencies of $(FeTPP)_2O$ and FeTPPCl complexes has been attributed to the lack of exciton splitting interaction[14a] in the former due to the rather large spatial separation[15b] (5.2 Å) of the TPP units as well as to the extremely short excited state lifetime of iron porphyrins[15a,16] which is of the order of pico to subpicoseconds.

The low intensity of the ν_3 mode at 1450 cm^{-1} and the high intensity of the ν_3 mode at 1552 cm^{-1} in the TPP complexes compared to the octaethylporphyrin and protoporphyrin complexes has been attributed[13f] to the high degree of mixing of the $\nu_2(C_\beta C_\beta)$ and $\nu_3(C_\alpha C_m)$ vibrational modes in the former compared to the latter. Due to phasing of the mixed coordinates, the intensity adds up for the ν_2 mode and nearly cancels for the ν_3 mode in the case of the TPP complexes. The strong band at [illegible] cm^{-1} has been attributed[14b] to the ν_8 symmetric porphyrin core deformation mode involving in-phase vibrations of $Fe-N_4$ skeleton. Most $Fe^{III}TPP$ complexes exhibit this band in the range 386-392 cm^{-1} range and this is considerd to be a reliable oxidation state marker band.[14b] The observation of mostly polarized bands under near Soret excitation are typical of TPP complexes[14a] and indicate the effect of Franck-Condon scattering mechanism. However, the depolarization ratio for these polarized modes in $(FeTPP)_2O$ are lower than the expected values and show dispersion due to non-negligible contribution from the α_{zz} polarizability component to the scattering tensor. In metallo-tetraphenylporphyrins, the altered substituent patterns at the pyrrole β and methine bridges (as compared to

the physiological hemes), alter the ring substituent vibrational interactions. Several phenyl modes are also resonance enhanced with the π-π^* transition due to the interaction of the phenyl and porphyrin π-system in the excited state[14a] or due to the vibrational coupling[13f] between phenyl modes with nearby in-plane porphyrin skeletal modes.

Addition of moderate quantities (100 mM) of hindered imidazoles, 2MeIm or 1,2-MeIm, to a solution of $(FeTPP)_2O$ (0.1 mM) at alkaline pH had pronounced effect in both anaerobic and aerobic conditions. Traces B and C in Figs. 4.3.2.and 4.3.3. show new RR bands appearing at 1540, 1434, 1342 and 1229 cm^{-1} in the high frequency region and at 372 and 200 cm^{-1} in the low frequency region. A comparison of these frequencies with published data[14b-d,f] enables us to assign these to the ν_2, ν_3, ν_4, ν_1, ν_8 and ϕ_{10} modes respectively of the five coordinated, high spin (5cHS) Fe^{II}TPP(2-MeIm) and Fe^{II}TPP(1,2-MeIm) ferrous complexes. The enhanced intensity of the mode at 200 cm^{-1} in both the traces B and C in Fig. 4.3.3 may be due to overlapping of the Fe-axial ligand stretching modes of Fe^{II}TPP(2-MeIm) and Fe^{II}TPP(1,2-MeIm) complexes with the ϕ_{10} mode at about the same frequency. These have been identified[14g] in $Fe^{II}T_{piv}PP$(2-MeIm) and $Fe^{II}T_{piv}PP$(1,2-MeIm) complexes at 209 and 200 cm^{-1} respectively and at 206 cm^{-1} in Fe^{II}(TtButPP)(1,2-MeIm) complex.[14d] The weak shoulder in the ν_4 region around 1360 cm^{-1} indicates the presence of minor quantities of μ-oxo dimer in the photosteady state and also some contribution from the depolarized $\nu_{13}(B_{1g})$ mode[14c] of the 5cHS ferrous complex at the same frequency.

Addition of non-hindered imidazole, N-MeIm or Im to the TX-100 solution containing $(FeTPP)_2O$ yielded an RR spectrum characteristic of six coordinated, low spin (6cLS) ferrous species in even aerobic conditions on excitation at 441.6 nm. However, the RR spectra obtained with N-MeIm in anaerobic conditions are shown in Figs. 4.3.2D and 4.3.3D. The major RR bands at 1558, 1354, 1228, 382 and 199 cm^{-1} are consistent with the formation of 6cLS ferrous complex.[14a] It is interesting to note that the ν[Fe-(N-MeIm)] stretching mode has been identified at 255 cm^{-1} in the five coordinated $Fe^{II}T_{piv}PP$(N-MeIm) complex,[14f] but the symmetric axial mode for the 6cLS $Fe^{II}T_{piv}PP(N\text{-MeIm})_2$ complex could not be identified clearly. Nevertheless, the authors[14f] support the formation of the 6cLS complex with this ligand on the basis of the appearance of the ν_8 mode at 384 cm^{-1} as we also observe in our spectrum (trace D, Fig. 4.3.3). Table 4.3.2 summarizes the RR frequencies observed in the various complexes by us under diffferent experimental conditions.

From the above observations of the RR frequencies of $(FeTPP)_2O$ in TX-100 micelle, in the presence of hindered and unhindered imidazoles, and in their absence in anaerobic conditions, it is fairly clear that the 5cHS or 6cLS ferrous porphyrin species are formed due to irradiation of the μ-oxo dimer by laser light at 441.6 nm at room temperature. The similarity of the absorption spectra of $(FeTPP)_2O$ in the presence and absence of these nitrogenous ligands precludes the formation of iron porphyrin complexes having these ligands coordinated either to the iron centre or the oxygen atom of the μ-oxo bridge.

Fig. 4.3.4 shows the high frequency RR spectra of $(FeTPP)_2O$ in TX-100 micelle at alkaline pH obtained with laser excitation at 441.6 nm in aerobic (trace A) and anaerobic (trace B) conditions in the absence of added nitrogenous bases in different frequency regions of interest. Traces A and A' of Fig. 4.3.4 are identical to the traces A and A' of Fig. 4.3.2. On degassing the same solution, a complex RR spectral pattern develops at room temperature. The new RR bands at 1342, 1437, 1541, 1229 cm^{-1} (Fig. 4.3.2, trace A), and at 372 and 199 cm^{-1} in the low frequency region (spectrum not shown) can be identified with the ν_4, ν_3, ν_2, ν_1, ν_8 and ϕ_{10} modes respectively of a 5cHS ferrous complex, $Fe^{II}TPP(L)$. In addition to these, extra features at 1567 cm^{-1} in the high frequency region and 843 cm^{-1} in the usually sparce region between 700 and 900 cm^{-1} are also present in the room temperature spectra. The intensities of these new bands increase considerably in the spectra recorded at -50°C, along with the appearance of a clearly identifiable band at 1370 cm^{-1} (Figs. 4.3.4C and 4.3.4C''). These bands cannot be associated with the formation of a 6cLS ferrous complex as the bands observed by us for a typical representative of a 6cLS complex, $FeTPP^{II}(N\text{-}MeIm)_2$, shown in Fig. 4.3.2D at 1557 $cm^{-1}(\nu_2)$, 1354 $cm^{-1}(\nu_4)$ and 382 $cm^{-1}(\nu_8)$ (Fig. 4.3.3D) without any band at 843 cm^{-1} are quite distinct from the observed RR bands in our photoproduced spectra and thus rules out this possibility.

In order to identify the species responsible for the extra Raman features, it is pertinent to consider the results of recent time-resolved transient absorption studies,[10a-d] which have shown that $(FeTPP)_2O$ undergoes photodisproportionation in aprotic and protic solvents on near Soret excitation at $\approx$ 400 nm to yield the photoproducts according to the scheme[10a-d] proposed below:

$$TPPFe\text{-}O\text{-}FeTPP \xrightleftharpoons{h\nu} (TPPFe\text{-}O\text{-}FeTPP)^{*} \qquad (4.3.1)$$

$$(TPPFe\text{-}O\text{-}FeTPP)^{*} \longrightarrow TPPFe^{II} + TPPFe^{IV}{=}O \qquad (4.3.2)$$

$$(TPPFe\text{-}O\text{-}FeTPP)^{*} \longrightarrow TPPFe^{II} + TPP^{\bullet +}Fe^{III}{=}O \qquad (4.3.3)$$

$$TPPFe^{II} + TPPFe^{IV}{=}O \longrightarrow TPPFe\text{-}O\text{-}FeTPP \qquad (4.3.4)$$

$$Fe^{II}TPP + L \longrightarrow Fe^{II}TPP(L) \qquad (4.3.5)$$

where L is an external ligand.

Our RR data does not indicate the presence of $(TPP^{\bullet +})Fe^{III}{=}O$ species in the photoproducts of $(FeTPP_2)O$ as the RR marker bands for this species are quite distinct.[4a,7] The ν_2 mode for the π-cation radical of the ferric species appears[7] around 1526 cm^{-1} for the $Fe(TPP^{\bullet +})Cl$ and at 1509 cm^{-1} for[4a] the $Fe^{III}(TMP^{\bullet +})(ClO_4)_2$ complexes. Hence we can rule out the possibility given in Equation 4.3.3.

During the recent years, several groups[3-8] have reported the formation of oxo-ferryl porphyrin complexes in synthetic model systems by various techniques at low temperatures and identified their ν_2, ν_4 $\nu(Fe^{IV}{=}O)$ stretching modes (Table 4.3.3). The coincidence of our observed RR band at 843 cm^{-1} along with the other extra RR features in the spectra recorded at room temperature in Fig. 4.3.4 indicated formation of oxo-ferryl species and therefore we examined the RR spectra of our sample in anaerobic conditions at low temperature (-50°C) as shown in traces C, C' and C'' in Fig. 4.3.4. Once again the major RR features are identical to

those observed at room temperature indicating the formation of a 5cHS complex. However, the RR bands at 1570 cm^{-1} and 1370 cm^{-1} as well as at 843 cm^{-1} are enhanced considerably suggesting greater stabilization of the species at low temperature as expected for an oxoferryl porphyrin complex. In order to ascertain the formation of oxoferryl species, we carried out other control experiments.

Peterson and coworkers[10a-c] have presented strong evidence for the photodisproportionation of $(FeTPP)_2O$ in degassed benzene or pyridine and of $(FeTPPC)_2O$ (a water soluble iron porphyrin) in aqueous buffer solutions at alkaline pH on irradiation in the Soret region at room temperature. According to their scheme, the formation of a five coordinated ferrous complex in the presence of externally added nitrogenous ligand lead to the decay of the ferryl complex yielding the starting species according to the pattern:

$$Fe^{II}TPP + B \longrightarrow Fe^{II}TPP(B) \qquad (4.3.6)$$

$$Fe^{II}TPP(B) + TPPFe^{IV}=O \longrightarrow (FeTPP)_2O + B \qquad (4.3.7)$$

where B is an externally added nitrogenous ligand. This mechanism is in addition to the reverse reaction in equation 4.3.4. Observation of highly reduced yield of ferryl species on addition of 2-MeIm to the solution as indicated by the almost total diappearance of the RR bands characteristic of the ferryl species confirm the mechanism as proposed in Equations 4.3.6 and 4.3.7.

Further confirmation of the formation of $TPPFe^{IV}=O$ species is provided by Raman experiments as a function of laser power. The yield of photodisproportionation is expected to increase with an increase[10a-c] in the laser power (Equation 4.3.2). At low powers, the recombination of the photoproducts is negligible (Equation 4.3.4), which, however, becomes dominant at higher laser intensities.[10a] This effect, along with the instability of the oxoferryl species at higher temperatures as a result of local heating at higher powers[3b] would decrease the yield of this complex. We observed that the 843, 1370 and the 1570 cm^{-1} bands perceptibly weakened with an increase in laser power from 3 to 10 mW at 441.6 nm at $-50^{\circ}C$. When dimethylformamide (DMF) was added to the $(FeTPP)_2O$ solution at alkaline pH, the low frequency RR spectrum obtained at low temperature (Fig. 4.3.4D") showed clear shift of the 843 cm^{-1} band to 832 cm^{-1} on irradiation at 441.6 nm. The shift of the $\nu(Fe^{IV}=O)$ stretching frequency to lower value on formation of six coordinated oxoferryl complex has been reported in literature (Table 4.3.3) and clearly establishes the origin of the 843 cm^{-1} band as due to oxoferryl species. The decrease in the frequency on coordination with DMF can be understood as follows.

In the $Fe^{IV}=O$ structure, there is a strong σ interaction between the oxygen lone pair and the metal d_{z^2} orbital and a strong π overlap between the oxygen π^* and the metal d_π (d_{xz} and d_{yz}) orbitals. In both of these interactions, electron donation is from O^{2-} ligand to Fe^{IV}. In the absence of a strong ligand trans to the ferryl oxygen, the $\nu(Fe^{IV}=O)$ mode is observed in the 841-845 cm^{-1} range in solutions (Table 4.3.3). Coordination of a strong σ donor ligand trans to the ferryl oxygen tends to reduce the electron donation from oxygen to the iron atom leading to a weakening of the $Fe^{IV}=O$ bond with a concomitant decrease in its stretching

frequency. The observation of the lowering of the 843 cm^{-1} band to 832 cm^{-1} on coordination of a DMF molecule to oxoferryl porphyrin is in good accordance with the previously reported[4e] value (829 cm^{-1}).

All these experiments provide clear evidence for the formation of the oxo-ferryl species on photodisproportionation of $(FeTPP)_2O$. From a comparison of the previous work on oxoferryl complexes (Table 4.3.3), the RR bands observed in the present study at 843, 1370 and 1570 cm^{-1} on irradiation of $(FeTPP)_2O$ in detergent micelle can be associated, unambigously with the $\nu(Fe^{IV}=O)$ stretching, ν_4 and ν_2 modes respectively of the five coordinated low spin[4e,5b] oxoferryl complex. The intensity of these RR bands increases at -50°C consistent with the greater stability of the ferryl species at low temperatures.

In the absence of added nitrogenous ligands and under anaerobic conditions, both at room temperature and at low temperature, the expected RR spectrum for a four coordinated intermediate spin[17] $Fe^{II}TPP$ photoproduct was not observed by us. Instead we observed RR bands characteristic of a 5cHS ferrous $Fe^{II}TPP(L)$ complex with associated axial ligand L which may be a hydroxyl ion or a water molecule. Non-observation of the ν(Fe-OH) stretching mode[6b] around the reported value of 463 cm^{-1} at alkaline pH conditions by us and from the positions of other observed RR bands, we suggest that the ferrous photoproduct is coordinated[14d] axially by a water molecule. Extensive hydration of the ether groups of TX-100 micelle and the presence of water[18] within the micelle makes this a distinct possibility.

It is obvious that in aerobic conditions and in the absence of nitrogenous ligands, irradiation of $(FeTPP)_2O$ in TX-100 micelle leads to a regeneration of the starting complex due to autooxidation[3a] of $Fe^{II}TPP$.

$$4TPPFe^{II} + O_2 \longrightarrow 2(TPPFe\text{-}O\text{-}FeTPP) \qquad (4.3.8)$$

$$TPPFe^{II}O_2 + TPPFe^{IV}=O \longrightarrow TPPFe\text{-}O\text{-}FeTPP + O_2 \qquad (4.3.9)$$

Thus oxygen supresses the formation of the axial ligand-free $Fe^{II}TPP$ in aerobic conditions and also inhibits or reduces the formation of $TPPFe^{IV}=O$ complex. However, the observation of 5cHS or 6cLS complexes in aerobic conditions in the presence of nitrogenous ligands indicates higher affinity of $Fe^{II}TPP$ to these ligands than to oxygen as observed by others.[17]

In conclusion, we have presented evidence, for the first time, supported by separate control experiments, for the formation of a five coordinated oxoferryl complex, $TPPFe^{IV}=O$, via photodisproportionation of $(FeTPP)_2O$ in alkaline aqueous detergent micelle at room temperature under laser excitation at 441.6 nm. The complex has been characterized by its $\nu(Fe^{IV}=O)$ stretching, ν_4 and ν_2 modes at 843, 1370 and 1567 cm^{-1} respectively. The other photoproduct has been identified as a five coordinated high spin complex under the experimental conditions used.

REFERENCES

1. (a) Hewson, W.D.; Hager, L.P. In *The Porphyrins*; Dolphin, D., Ed.; Academic Press: New York, 1978; Vol. 7, pp 295.
   (b) Groves, J.T. In *Cytochrome P-450: Structure, Mechanism and Biochemistry*; Ortiz de Montellano, P.R , Ed.; Plenum: New York, 1986; Chapter 1.
   (c) Ortiz de Montellano, P.R. *Acc. Chem. Res.* 1987, 20, 289.
   (d) Dunford, H.B.; Stillman, J.S. *Coord. Chem. Rev.*, 1976, 19, 187.
   (e) Siraraja, M.; Goodwin, D.B.; Smith, M.; Hoffman, B.H. *Nature* (London), 1989, 245, 738.

2. (a) Witstrom, M. *Proc. Natl. Acad. Sci. USA*, 1981, 78, 4051.
   (b) Blair, D.F.; Witt, S.N.; Chan, S.I. *J. Am. Chem. Soc.* 1985, 107, 7389.
   (c) Ogura, T.; Takahashi, S.; Shinzawa-Itoh, K.; Yoshihara, S.; Kitagawa, T. *J. Bio. Chem.* 1990, 265, 14721.

(3) (a) Chin, D.H.; La Mar, G. N.; Balch, A. L. *J. Am. Chem. Soc.* 1980, 102, 4344.
   (b) Mizutani, Y.; Hashimoto, S.; Tatsuno, Y.; Kitagawa, T. *J. Am. Chem. Soc.* 1990, 112, 6809.
   (c) Paeng, I.R.; Shiwaku, H.; Nakamoto, K. *J. Am. Chem. Soc.* 1988, 110, 1995.
   (d) Ozawa, S.; Watanabe, Y.; Nakashima, S.; Kitagawa, T.; Morishima, I. *J. Am. Chem. Soc.* 1994, 110, 634.
   (e) Paeng, I.R.; Nakamoto, K. *J. Am. Chem. Soc.* 1990, 112, 3289.
   (f) Chin, D.H.; La Mar, G.N.; Balch, A.L. *J. Am. Chem. Soc.* 1980, 102, 5945.

(4) (a) Hashimoto, S.; Mizutani, Y.; Tatsuno, Y.; Kitagawa, T. *J. Am. Chem. Soc.* 1991, 113, 6542.
   (b) Schappacher, M.; Chottard, G.; Weiss, R. *J. Chem. Soc., Chem. Commun.* 1986, 93.
   (c) Oertling, W.A.; Kean, R.T.; Wever, R.; Babcock, G.T. *Inorg. Chem.* 1990, 29, 2633.
   (d) Hashimoto, S.; Tatsuno, Y.; Kitagawa, T. *J. Am. Chem. Soc.* 1987, 109, 8096.
   (e) Gold, A.; Jayaraj, K.; Doppelt, P.; Weiss, R.; Chottard, G.; Bill, E.; Ding, X.; Trautwein, A.X. *J. Am. Chem. Soc.* 1988, 110, 5756.

5. (a) Bajdor, K.; Nakamoto, K.; *J. Am. Chem. Soc.* 1984, 106, 3045.
   (b) Proniewicz, J.M.; Bajdor, K.; Nakamoto, K. *J. Phy. Chem.* 1986, 90, 1760.

6. (a) Czernuszewicz, R.S.; Macor, K.A.; *J. Raman. Spectrosc.* 1988, 19, 553.
   (b) Rodgers, K.T.; Reed, C.A.; Su, Y.O.; Spiro, T.G. *J. Am. Chem. Soc.* 1992, 31, 2688.

7. (a) Czernuszewicz, R.S.; Macor, K.A.; Li, X.Y.; Kincaid, J.R.; Spiro, T.G. *J. Am. Chem. Soc.* 1989, 111, 3860.
   (b) Li, X.Y.; Czernuszewicz, R.S.; Su, O.Y; Spiro, T.G. *J. Phy. Chem.* 1990, 94, 31.

8. (a) Shedbalkar, V.P.; Modi, S.; Mitra, S. *J. Chem. Soc., Chem. Comm.* 1988, 12, 38.
   (b) Bell, S.E.J.; Cooke, P.R.; Inchley, P.; Leonard, D.R.; Smith, L. J. R. *J. Chem. Soc., Perkin. Trans.* 1991, 2, 549.
   (c) Groves, J.T.; Gross, Z.; Stern, M.K. *Inorg. Chem.* 1994. 33, 5065.

9. (a) Terner, J.; Sitter, A.J.; Reczek, C.K. *Biochim. Biophys. Acta.* 1985, 828, 73.
   (b) Sitter, A.J.; Reczek, C.M.; Terner, J. *Biol. Chem.* 1985, 260, 7515.
   (c) Hashimoto, S.; Tatsuno, Y.; Kitagawa, T. *Proc. Natl. Acad. Sci. USA.* 1986, 83, 2417.
   (d) Sitter, A.J.; Reczek, C.M.; Terner, J. *Biochim. Biophys. Acta.* 1985, 828, 229.
   (e) Hashimoto, *S.*; Teraoka, J.; Inubushi, T.; Yonetani, T.; Kitagawa, T. *J. Biol. Chem.* 1986, 261, 11110.

10. (a) Peterson, M.W.; Rivers, D.S.; Richman, R.M. *J. Am. Chem. Soc.* 1985, 107, 2907.
    (b) Richman, R.M.; Peterson, M.W. *J. Am. Chem. Soc.* 1982, 104, 5795.
    (c) Peterson, M.W.; Richman, R.M. *Inorg. Chem.* 1985, 24, 722.
    (d) Guest C.R.; Straub, K.D.; Hutchins, J.A.; Rentzepis, P.M. *J. Am. Chem. Soc.* 1988, 110, 5276.

11. (a) Fleischer, E.B.; Srivastava, T.S. *J. Am. Chem. Soc.* 1969, 91, 2403.
    (b) Maricondi, C.; Swift, W.; Straub, D.K. *J. Am. Chem. Soc.* 1969, 91, 5205.
    (c) D'Souza, F.; Krishnan, V. *Proc. Ind. Acad. Sci. (Chem. Sci).* 1990, 102, 131.
    (d) Cheng, R.-J.; Latos-Grazynski, L.; Balch, A.L. *Inorg. Chem.* 1982, 21, 2412.
    (e) Groves, J.T.; Haushalter, R.C.; Nakamura, M.; Nemo, T.E.; Evans, B.J. *J. Am. Chem. Soc.* 1981, 103, 2884.
    (f) Mizutani, Y.; Watanabe, Y.; Kitagawa, T. *J. Am. Chem. Soc.* 1994, 116, 3439.

12. (a) Fleischer, E.B.; Palmer, J.M.; Srivastava, T.S.; Chatterjee, A. *J. Am. Chem. Soc.* 1971, 93, 3162.
    (b) Nappa, M.; Valentine, J.S.; Snyder, J.S. *J. Am. Chem. Soc.* 1977, 99, 5799.
    (c) Cohen, I.A. *J. Am. Chem. Soc.*,1969, 91, 1980.

13. (a) Spiro, T.G.; Czernuszewicz, R.S.; Li, X.Y. *Coord. Chem. Rev.* 1990, 100, 541.
    (b) Spiro, T.G.; Li, X.Y. In *Biological Applications of Raman Spectroscopy*; Spiro, T.G., Ed.; Wiley-Interscience: New York, 1988; Vol. 3, pp 1.

(c) Kitagawa, T.; Ozaki, Y. *Struct. Bonding* (Berlin) 1987, 64, 71.
(d) Spiro, T.G. In *Iron Porphyrins;* Lever, A.P.B.; Gray, H.B., Eds.; Addison-Wesley: Reading, MA.,1983; Vol. 2, p. 91.
(e) Büchler, J.W.; Kökisch, W.; Smith, W. *Struct. Bonding* (Berlin) 1978, 34, 79.

14. (a) Burke, J.M.; Kincaid, J.R.; Spiro, T.G. *J. Am. Chem. Soc.* 1978, 100, 6077.
(b) Burke, J.M.; Kincaid, J.R.; Peters, S.; Gagne, R.R.; Collman, J.P.; Spiro, T.G. *J. Am. Chem. Soc.* 1978, 100, 6083.
(c) Parthasarathi, N.; Hansen, C.; Yamaguchi, S.; Spiro, T.G. *J. Am. Chem. Soc.* 1987, 109, 3865.
(d) Leondiadis, L.; Momenteau, M.; Debois, A. *Inorg. Chem.* 1992, 31, 4691.
(e) Oshio, H.; Ama, T.; Watanabe, T.; Kincaid, J.; Nakamoto, K. *Spectrochim. Acta.* 1984, 40A, 863.
(f) Chottard, G.; Battioni, P.; Battioni,J.; Lange, M.; Mansuy, D. *Inorg. Chem.* 1981, 20, 718.
(g) Hori, H.; Kitagawa, T. *J. Am. Chem. Soc.* 1980, 102, 3608.

15. (a) Schick, G.A.; Bocian, D.F. *J. Am. Chem. Soc.* 1983, 105, 1830.
(b) Hoffman, H.B.; Collins, D.M.; Day, V.W.; Fleischer, E.B.; Srivastava, T.S.; Hoard, J.L. *J. Am. Chem. Soc.* 1972, 94, 3620.
(c) Moss, T.H.; Lillienthal, H.R.; Moleski, C.; Smythe, G.A.; Daniel, M.C.; Caughey, W.S. *J. Chem. Soc., Chem. Commun.* 1972, 263.

16. (a) Adar, F.; Gouterman, M.; Aronowitz, S. *J. Phys. Chem.* 1976, 80, 2184.
(b) Austin, J.C.; Bell, S.E.J.; Hester, R.E. *Chem. Phys. Lett.* 1990, 169, 342.
(c) Dixon, D.W.; Kirmaier, C.; Holten, D. *J. Am. Chem. Soc.* 1985, 107, 808.
(d) Hoshino, M.; Ozawa, K.; Seki, H.; Ford, P.C. *J. Am. Chem. Soc.* 1993, 115, 9568.
(e) Champion, P.M.; Lange, R. *J. Chem. Phys.* 1980, 73, 5947.

17. Collman, J.P.; Hoard, J.L.; Kim, N.; Lang, G.; Reed, C.A. *J. Am. Chem. Soc.* 1975, 97, 2676.

18. (a) Rösch, M. *Koll. Z.* 1956, 147: 78.
(b) Rösch, M. *Fette Seifen Anstrichmittel,* 1963, 65: 223.
(c) Robson, R.J.; Dennis, E.A. *Acc. Chem. Res.* 1983, 16, 251.
(d) Hinze, W.L. In *Solution Chemistry of Surfactants*; Mittal, K.L., Ed.; Plenum Press: New York, 1979; Vol. 1, pp. 79.
(e) Ribeiro, A.A.; Dennis, E.A. In *Non-ionic Surfactants*; Schick, M.J., Ed.; Marcel Dekker: New York, 1987; pp 971.

TABLE 4.3.1: Optical absorption bands of some selected iron porphyrin complexes.

Complex	Solvent	Absorption bands (nm)	Ref.
$(FeTPP)_2O$	CH_2Cl_2	406, 569, 612	12b
$(FeTPP)_2O$	CH_2Cl_2	408, 572, 612	12a
$(FeTPP)_2O$	Benzene	408, 572, 612	14a
$(FeTPP)_2O$	TX-100 (Aq)†	408, 573, 613	p
FeTPPCl	Toluene	369, 418, 506, 572, 648	12b
FeTPPCl	CH_2Cl_2	380, 417, 511, 577, 658	11a,b, 12a
FeTPPCl	CH_3CN	374, 418, 507, 574,	11c
FeTPPCl	TX-100 (Aq)§	378, 419, 510, 573, 648	p
FeTMPOH	Toluene	416, - 580, 633	11d
FeTMPOH	Toluene	333, 417, - 575, 633	11f

† at pH 11.5 : § at pH 1.8 : p this work.

TABLE 4.3.2 : Observed RR frequencies of FeTPPCl in 3% TX-100 at pH 11.

Assignment Symmetry	Mode	Aerobic RT	Anaerobic RT	Anaerobic $-50^{\circ}C$	Anaerobic, RT. +2-MeIm	+1,2-MeIm	+N-MeIm
$\nu(C_mC_{Ph}),A_{1g}$	ϕ_4	1597	1600	1599	1599	1599	1599
$\nu(C_\beta C_\beta), A_{1g}$	ν_2	1552	1541	1542	1541	1540	1558
$\nu(C_\alpha C_m), A_{1g}$	ν_3	1450	1437	1437	1434	1434	-
$\nu(C_mPh), A_{1g}$	ν_1	1237	1229	1231	1228	1228	1228
$\nu(NC_\alpha), A_{1g}$	ν_4	1360	1342	1342	1342	1342	1354
$\nu(FeN), A_{1g}$	ν_8	390	-	-	372	372	382
$\nu(C_mC_{Ph}),A_{1g}$	ϕ_{10}	199	-	-	200	200	199

Mode numbering according to ref.7.

TABLE 4.3.3 : Fe^{IV}=O stretching and few other Raman frequencies (cm^{-1}) for some selected iron porphyrin systems.

Species	$\nu(Fe^{IV}=O)$	ν_2	ν_4	Solvent: Temp.(°C)	Ref.
Fe^{IV}=O(TPP)	852	1575	1374	Ar:-250	5a
Fe^{IV}=O(OEP)	852	1551	1379	Ar:-258	5b
Fe^{IV}=O(TMP)	843	1570	1368	Toluene:-80	3b
Fe^{IV}=O(TMP)	845	-	-	Toluene:-46	3c
Fe^{IV}=O(TPP)	843	1570	1370	Micelle: RT,-50	p
(THF)Fe^{IV}=O(2,6-ClTPP)	841	-	-	THF: -50	4e
(DMF)Fe^{IV}=O(2,6-ClTPP)	829	-	1370	THF: -50	4e
(DMF)Fe^{IV}=O(TPP)	832	-	1371	Micelle, RT,-50	p
(1MeIm)Fe^{IV}=O(2,6-ClTPP)	818	-	1370	THF: -50	4e
(THF)Fe^{IV}=O(TPivPP)	829	1566	1370	THF: -50	4b
(N-MeIm)Fe^{IV}=O(TPivPP)	807	1566	1370	THF: -50	4b
(1-MeIm)Fe^{IV}=O(TPP)	820	1566	1369	Toluene: -120	4c
(1-MeIm)Fe^{IV}=O(OEP)	820	-	1385	Toluene: -120	4b
(OH)Fe^{IV}=O(TMPyP)	763	1577	1370	H_2O: pH 13, RT	6b
($TMP^{\bullet+}$)Fe^{IV}=O(MeOH)	831	1517	1335	CH_2Cl_2: -80	4a
Compound II of HRP	787	-	-	H_2O, pH 11, RT	9f
CCP Compound ES	767	-	-	H_2O, pH 4-11, RT,	9e
Ferryl Myoglobin	797	-	-	H_2O. pH 8.5, 20	9d

p This work: RT, Room Temperature.: Micelle, Alkaline aqueous TX-100.

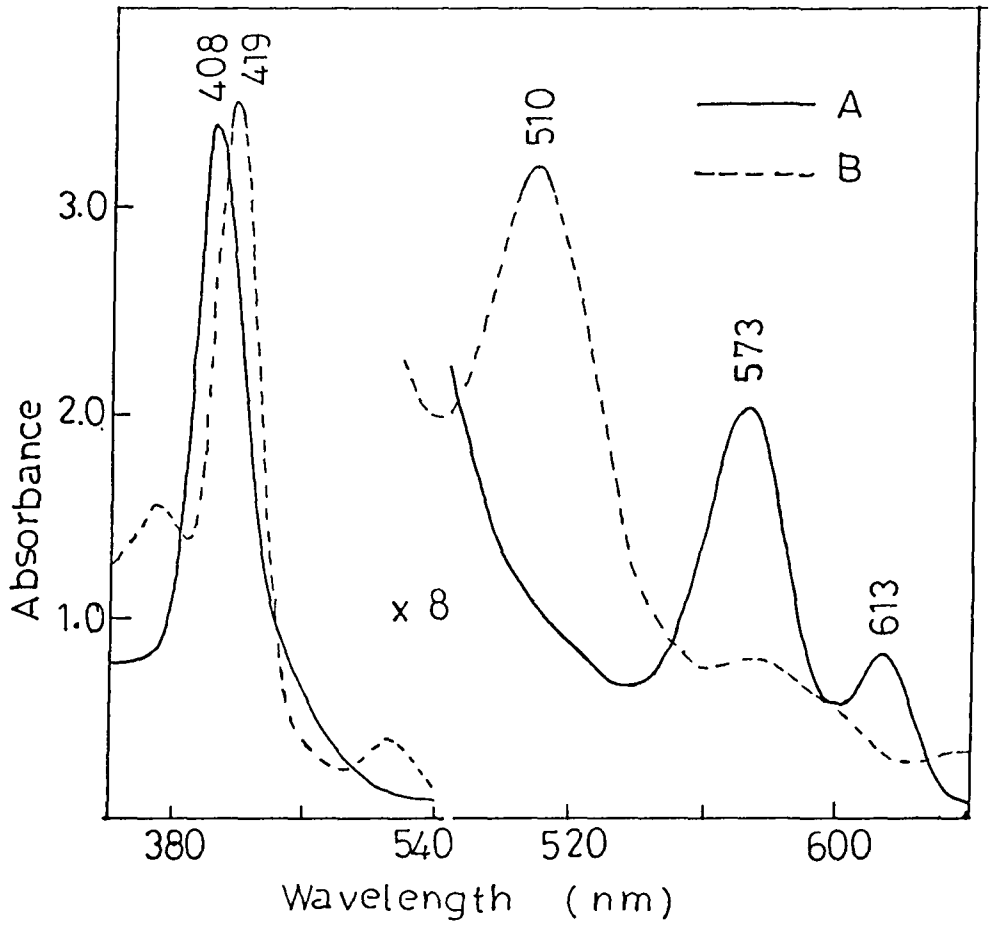

Fig. 4.3.1 Optical absorption spectra of FeTPPCl solubilized in 3% aqueous TX-100 micelle: (A) pH 11.5 (———); (B) pH 1.8 (----). Concentration = 30 μM: path length = 10 mm.

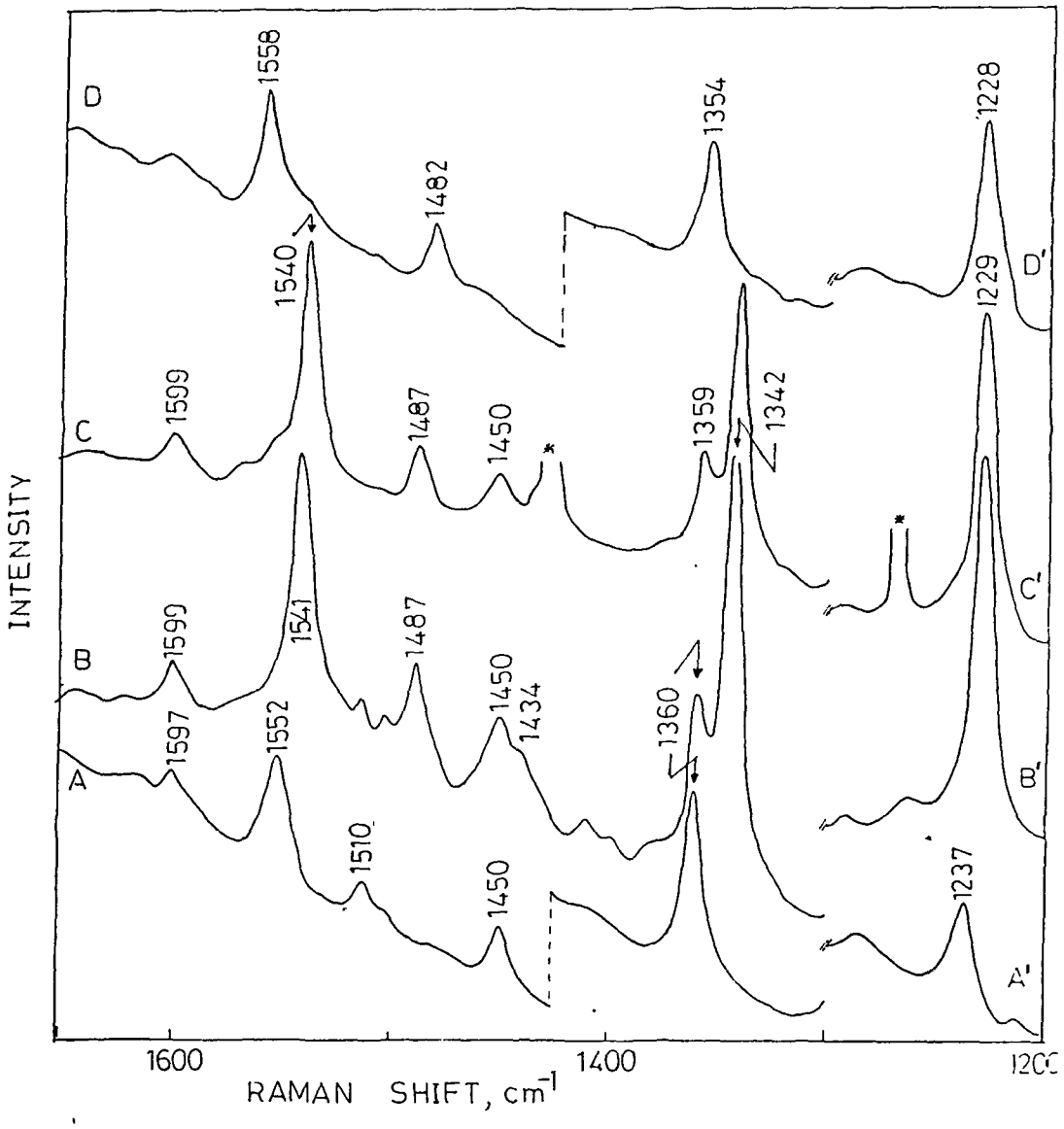

Fig. 4.3.2 High frequency RR spectra of FeTPPCl solubilized in 3% TX-100 micelle in the presence of imidazoles. pH = 11.5: Concentrations of FeTPPCl and imidazoles were as follows: (A) 0.1 mM, 0 mM; (B) 0.15 mM, 15 mM (2-MeIm); (C) 0.2 mM, 18 mM (1,2-MeIm); (D) 0.1 mM, 130 mM (N-MeIm): All spectra were recorded at room temperature; spectrum A in aerobic and spectra B-D in anaerobic conditions. λ_{exc} = 441.6 nm, 10 mW: scan speed 30 cm^{-1} per min. Asterisks denote plasma lines.

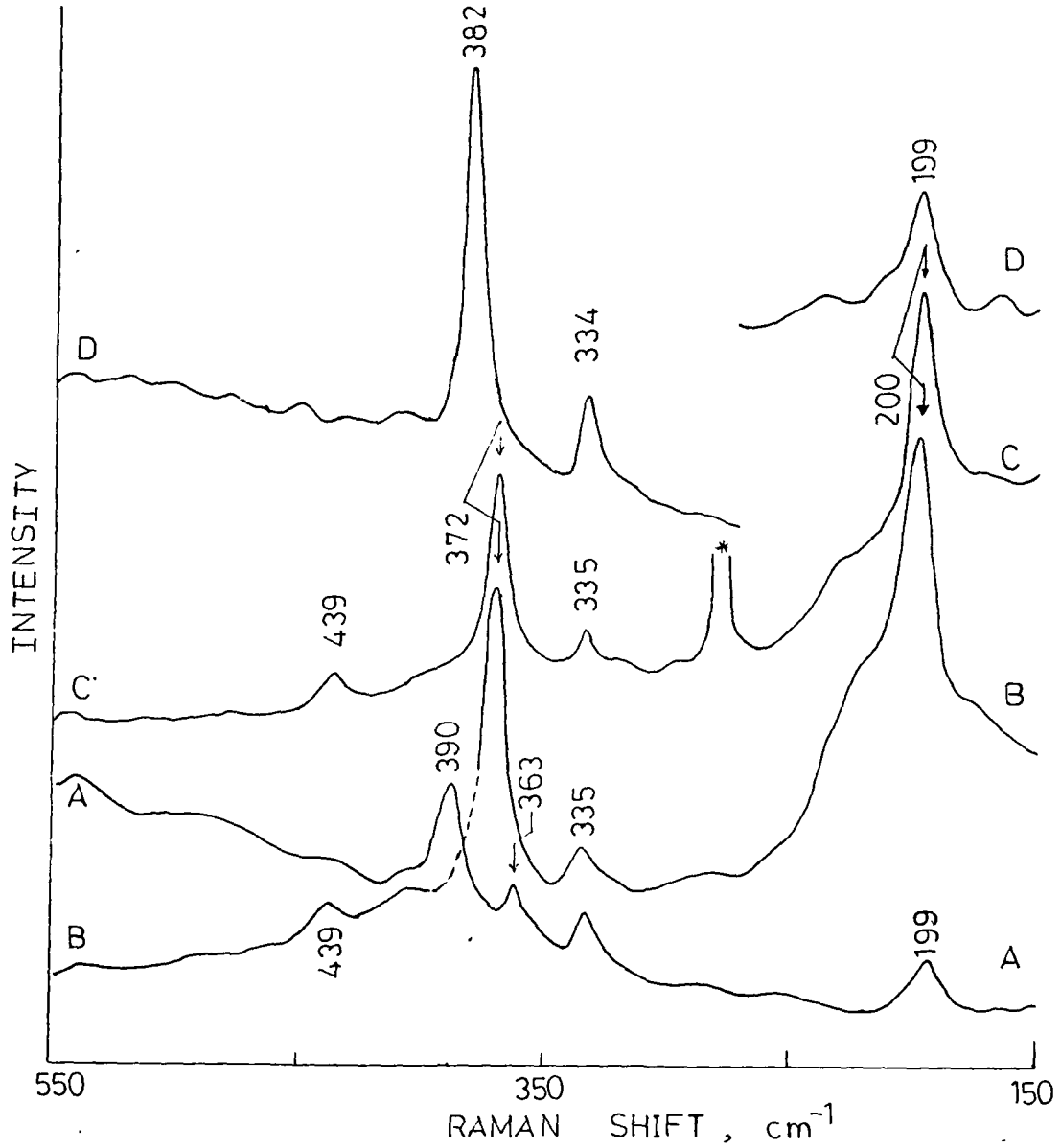

Fig. 4.3.3 Low frequency RR spectra of FeTPPCl solubilized in 3% TX-100 micelle in the presence of imidazoles. Experimental conditions are identical to those in Fig. 4.3.2.

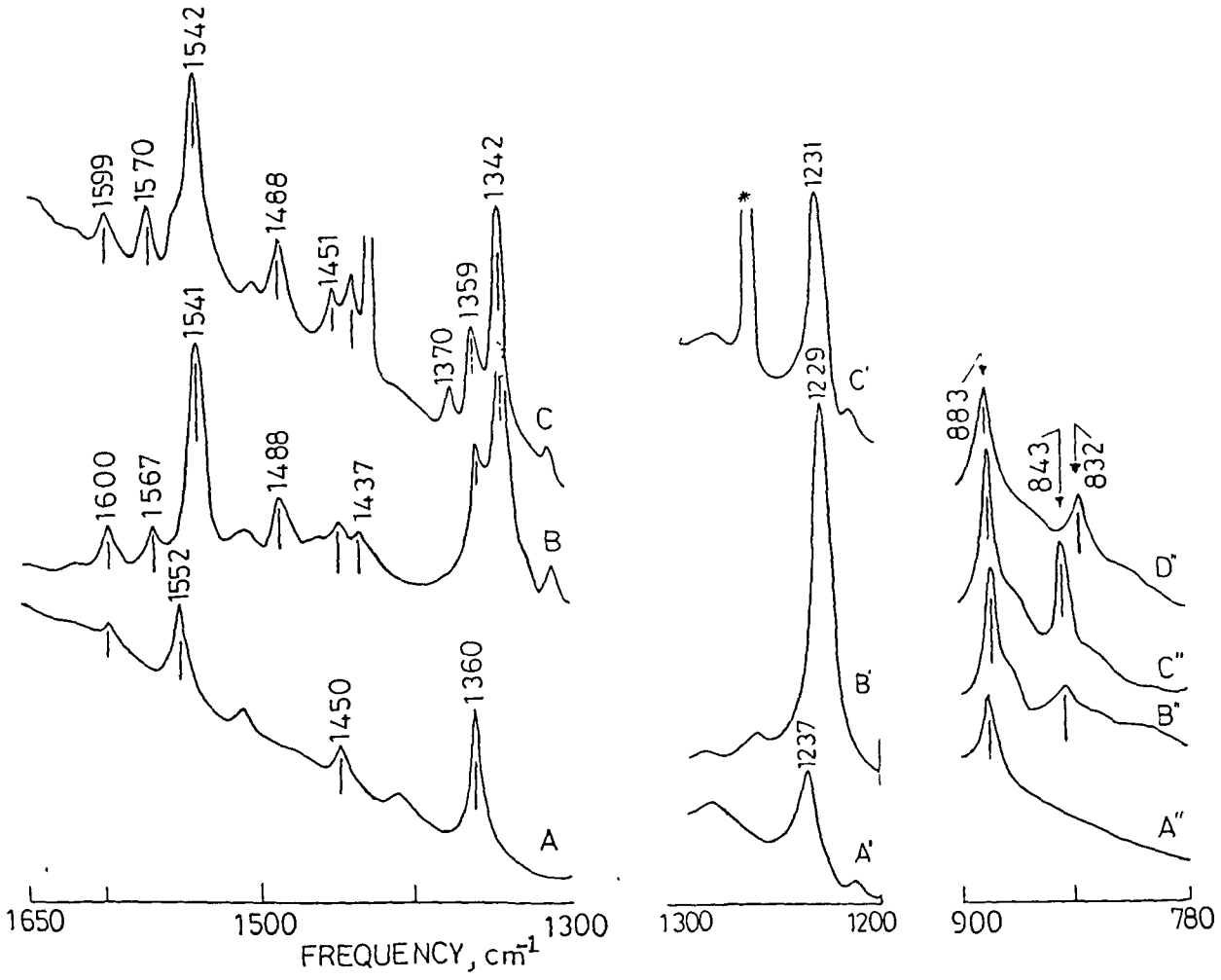

Fig. 4.3.4 RR spectra of FeTPPCl in 3% TX-100 micelle at pH 11: (A, A', A") in aerobic conditions at room temperature; (B, B', B") in anaerobic conditions at room temperature; (C, C', C") in anaerobic conditions at -50 °C ; (D') in anaerobic conditions at -50 °C in the presence of DMF (150 mM). Concentration of FeTPPCl = 0.1 mM: λ_{exc} = 441.6 nm, 10 mW at the source: Asterisks denote plasma line.

CHAPTER 5

PHOTOREDUCTION OF IRON TETRAPHENYLPORPHYRIN CHLORIDE IN DICHLOROMETHANE, DIMETHYLSULPHOXIDE IN THE PRESENCE OF, AND IN NEAT 1,2-DIMETHYLIMIDAZOLE WITHOUT ALCOHOL: EVIDENCE OF A PHOTOREACTIVE STATE BY RESONANCE RAMAN AND OPTICAL ABSORPTION STUDIES.

Coordination of 1,2-dimethylimidazole (1,2-MeIm) to iron tetraphenylporphyrin chloride (FeTPPCl) in CH_2Cl_2, DMSO and in neat 1,2-MeIm in the absence of alcohol resulted in clean reduction at the iron centre on photoexcitation at 441.6 nm. A similar photoreduction of FeTPPCl in CH_2Cl_2 was observed in the presence of low concentrations of 2-methylimidazole (2-MeIm) in anaerobic conditions with laser excitation at 406.7 and 441.6 nm. Systematic study of the optical absorption spectra of FeTPPCl in the above solvent systems under experimental conditions similar to those used for RR study revealed: (1) similar spectral changes on addition of (a) moderate concentrations of 1,2-MeIm in the absence of methanol, (b) lower concentrations of 1,2-MeIm and trace amounts ($\leq$ 1%) of methanol and (c) 1,2-MeIm to a solution of FeTPPCl in DMSO. (2) the appearance of a new absorption band in the 315-340 nm region for those species for which photoreduction was observed in our RR study. The latter indicates a possible link of the photoreduction process to a photoreactive state, localized in this region.

5.1 Introduction

As prosthetic groups of various heme proteins such as hemoglobin, myoglobin, cytochromes etc., iron porphyrins perform important biochemical functions such as electron transfer and oxygen transport in living systems.[1] The achievement and stabilization of the reduced state of iron, i.e., Fe^{II} (which is usually unstable outside the globin pocket in the biosystems)[1] in model iron porphyrins becomes important for understanding the mode of functioning of these basic biological molecules. Apart from the ususal chemical and electrochemical methods of reduction, photoinduced reduction of natural iron porphyrins and model iron porphyrin systems has been achieved and extensively studied[2-9] in recent times from the point of view of photochemistry,[6,7] chemical catalysis[6] etc.. Some of these studies have demonstrated among other things: (1) the electron transfer from axially coordinated ligands under photoexcitation[4-9] in solution and solid matrices, (2) the indispensability of primary alcohols in the solvent systems used either in trace amounts[8a,b] in the presence of nitrogenous ligands or in higher concentrations,[6,7] (3) the non-photoreducibility[8a] of iron porphyrin on laser excitation within the methanol ——> Fe charge transfer (CT) band at $\approx$ 585 nm, (4) the nature of the transient species involved in the process,[4-9] (5) simultaneous competition[8c] from photooxidation process on excitation at shorter wavelengths along with enhanced photoreduction yield. However, the nature of photoreactive state responsible for photoreduction and other subtle details are still not clear, although a charge transfer transition responsible for photoreduction within the intense Soret band region has been postulated.[8a]

We report here systematic Resonance Raman (RR) and UV-VIS absorption studies of FeTPPCl in coordinating and non-coordinating solvents in the presence of biologically relevant nitrogenous ligands like 2-MeIm and 1,2-MeIm under various experimental conditions. We have observed clean photoreduction of the iron centre in FeTPPCl in the presence of these hindered nitrogenous ligands in CH_2Cl_2 and in DMSO, in the absence of primary alcohols. In the UV-VIS absorption studies of FeTPPCl, we have detected certain features in the 315-340 nm region under solvent conditions similar to our RR work where we have observed photoreduction of the iron porphyrin. Further, enhanced photoreduction observed with 406.7 nm excitation compared to that at 441.6 nm under otherwise similar experimental conditions suggests that the photoreduction process is linked to the absorption band in the 315-340 nm range originating from a photoreactive state.

5.2 Experimental Section

FeTPPCl and 2-MeIm (99.9% pure) were purchased from Aldrich Chemical Company while 1,2-MeIm was from Merck, Germany, and were used without further treatment. The solvent CH_2Cl_2 was either from SD Chemicals (India) or Merck (India) Limited, and were of spectroscopic grade and contained no methanol as stabilizer or impurity. These were stored over Linde's molecular sieves (4 Å).

Resonance Raman spectra were recorded in the 90° scattering geometry using JEOL 400D and Spex 1403 Ramalog Spectrometers equipped with a cooled RCA-31034A photomultiplier, interfaced with Spex Datamate control unit. He-Cd (Liconix, Model 4240) laser and Krypton ion laser

(Spectra-Physics, Model 164) provided excitation lines at 441.6 and 406.7 nm respectively. Raman spectra were calibrated using the standard lines of indene or known solvent lines.

Optical absorption spectra were recorded with the help of the Varian Carey-2300 spectrophotometer using 10 mm path length quartz cuvettes. Fresh solution was prepared for each experiment directly in the quartz Raman cell. Anaerobic condition was achieved by bubbling argon gas into the solvent or the one containing 1% MeOH for about 15 minutes and transfering the required volume with the help of an air tight syringe to the Raman cell containing a weighed amount of FeTPPCl and the nitrogenous ligand. The cell was previously flushed with argon and capped with a rubber septum. Alternatively, a solutions of FeTPPCl in CH_2Cl_2 containing the ligand and 1% MeOH was flushed with Argon taking due care about the volatility of the solvents. Each spectrum corresponds to a sum of at least three scans. Typical concentration of the iron porphyrin was about 1 mM.

5.3 Results and Discussion

The vibrational modes in the high frequency 1200-1675 cm^{-1} and the low frequency 150-600 cm^{-1} regions are sensitive indicators of structure, oxidation and spin states of iron porphyrins.[10] The RR spectra of FeTPPCl in CH_2Cl_2 obtained with laser excitation at 441.6 nm under various experimental conditions are shown in Figs. 5.3.1 and 5.3.2. Traces A and B in Fig. 5.3.1 show the RR spectra of FeTPPCl (1 mM) in the absence and presence of 1,2-MeIm under aerobic conditions. The corresponding low frequency spectra are shown in Fig. 5.3.2. The two sets of spectra appear identical in major band positions with the RR bands at 1598, 1554, 1451,

1360 and 1233 cm^{-1} in the higher frequency region and at 200 and 390 cm^{-1} in the low frequency region. These are in accord with those reported in literature[11] for the five coordinated, high spin (5cHS) FeTPPCl complex. The spectrum is dominated by the intense ν_2 mode at 1554 cm^{-1} observed on excitation in the near Soret or Soret regions.[12] The anomalously low intensity of the ν_3 mode (at 1450 cm^{-1}) in the TPP complexes compared to that in octaethylporphyrin (OEP) or protoporphyrin (PP) complexes has been attributed to the large mixing[12a] of the $\nu_2(C_\beta C_\beta)$ and $\nu_3(C_\alpha C_m)$ modes in the former compared to the latter two complexes. The larger mixing of the in-phase and out-of-phase coordinates results in added intensity for the ν_2 mode and near cancellation for the ν_3 mode in the TPP complexes. A weak band appearing in both the traces A' and B' in Fig. 5.3.2 at 362 cm^{-1} can be attributed to the Fe-Cl stretching mode identified in the FeOEPCl[12c] and FeTPPCl[12b] complexes which is resonance enhanced on excitation close to the Cl ⟶ Fe charge transfer band around 350 nm.[12b] Although a band around the same frequency, 363 cm^{-1}, has been assigned to the out-of-plane symmetric stretching mode of the μ-oxo dimer, $(FeTPP)_2O$, in the absence of such a dimer in our work, as shown by the absorption spectra (vide infra), this weak band due to the ν(Fe-Cl) stretching mode indicates non-coordination or extremely weak coordination of 1,2-MeIm at the concentrations used. Anaerobic conditions at this stage and/or further addition of 1,2-MeIm upto 500 mM, i.e., upto a molar concentration ratio of 500, had no further effect on the RR spectra. (We shall denote the molar concentration ratio of 1,2-MeIm or 2-MeIm to FeTPPCl, as the case may be, by X in subsequent discussion). Nevertheless, a change in the relative intensity of the ν_2 mode at 1554 cm^{-1} was apparent from the traces A and B in Fig. 5.3.1. Similar effect was observed in the RR

spectra of FeTPPCl in CH_2Cl_2 obtained under laser excitation at 406.7 nm in the presence of 2-MeIm (Fig. 5.3.3, Traces A and B). This observation coupled with the decrease in intensity of the 376 nm CT band (Cl ——> Fe) on addition of these ligands indicate partial coordination of these hindered ligands to the iron centre by displacement of the strongly bound Cl^- ion.

Addition of a very small amount of methanol (MeOH, ≤ 0.5%) to the solution containing 100 mM of 1,2-MeIm and 1 mM FeTPPCl in CH_2Cl_2 had a dramatic effect on the RR spectra in both the high and the low frequency regions (Figs. 5.3.1C and 5.3.1C'). The earlier major RR bands shifted to lower fequencies; from 1554 to 1540 cm^{-1}, 1451 to 1434 cm^{-1}, 1360 to 1342 cm^{-1} and 391 to 372 cm^{-1}. The ν_8 and ϕ_{10} modes at 1233 cm^{-1} and 200 cm^{-1} showed enhanced intensity, the former shifting to 1229 cm^{-1}. These band positions are consistent with the formation of a 5cHS ferrous complex with 1,2-MeIm as axial ligand.[11a] Changing the ligand to 2-MeIm (100 mM) in the presence of ≤ 1% MeOH,resulted in a similar RR spectra with identical band positions as in the case of 1,2-MeIm. The relevant frequencies observed are summarized in Table 5.3.1. The mode numbering and vibrational assignments conform to published work.[12a] The 1360 cm^{-1} band continued to persist even at high concentrations of 1,2-MeIm or in neat 1,2-MeIm and/or under carefully degassed conditions irrespective of the absence or presence of MeOH. Polarization measurements indicated contribution to the intensity at this frequency from a depolarized mode at 1360 cm^{-1} consistent with the report of Parthasarathi et al[11b] who reported a $\nu_{13}(B_{1g})$ mode at 1358 cm^{-1} in the RR spectra of Fe^{II}TPP(2-MeIm) complex. Enhancement of the B_{1g} and B_{2g} modes in resonance with the B band excitation has been attributed to increased Jahn-Teller activity, which

correlates with the strength of the Q_o absorption band[11e] and hence on the strength of the configuration interaction. Similarly, the ν_3 mode at 1451 cm^{-1} corresponding to the ferric species may have contribution from the $\nu_{28}(B_{2g})$ mode at 1449 cm^{-1} of the Fe^{II}TPP(1,2-MeIm) complex.[11b] However, the ν_2 mode at 1540 cm^{-1} and ν_8 mode at 372 cm^{-1} indicate complete photoreduction under anaerobic conditions without any indication in the RR spectrum of the corresponding frequencies of the ferric complex.

RR results of the dependence of photoreduction of FeTPPCl in CH_2Cl_2 containing $\approx$ 1% MeOH on the concentration of the ligand, 1,2-MeIm, are shown in traces C-F and C'-F' of Figs. 5.3.1 and 5.3.2, in the high and low frequency regions respectively. The extent of photoreduction of the ferric species decreased as the concentration of this ligand decreased. This is clear from the change in the relative intensity of the RR bands associated with the ν_2, ν_3, ν_4 and ν_8 modes for the ferric and ferrous species at 1554 and 1540 cm^{-1}, 1451 and 1434 cm^{-1}, 1360 and 1342 cm^{-1}, and 390 and 372 cm^{-1} respectively.

The Fe-axial ligand stretching mode has been observed at 200 cm^{-1} for the Fe^{II}(TpivPP)(1,2-MeIm) complex[13a] and at 195 cm^{-1} for the Fe^{II}(PPDME)(1,2-MeIm) complex.[13b] The enormous intensity enhancement of the band at 200 cm^{-1} may indicate strong overlap of the ϕ_{10} mode with the Fe-axial ligand mode in the photoreduced Fe^{II}(TPP)(1,2-MeIm) complex.

With excess 1,2-MeIm ($X \geq 500$) in a solution of FeTPPCl in CH_2Cl_2 or in neat 1,2-MeIm, clean photoreduction of the iron centre was observed even in aerobic conditions and in the absence of methanol (Figs. 5.3.1G and 5.3.2G). Addition of MeOH in trace amounts or anaerobic conditions had no additional effect on the RR spectra except for a

marginal enhancement of the ν_4 mode at 1342 cm^{-1} and disappearance of the ν_8 and ν_2 modes of the ferric species at 390 cm^{-1} and 1554 cm^{-1} respectively. This observation contrasted strongly with the non-photoreducibility of FeTPPCl in CH_2Cl_2 in the presence of excess 2-MeIm ($X \geq 300$) in anaerobic conditions on excitation at 441.6 nm (spectra not shown). On the other hand, a deaerated solution of FeTPPCl in CH_2Cl_2, containing $\geq$ 25% MeOH, showed partial photoreduction even in the absence of 1,2-MeIm under 441.6 nm laser excitation. This last observation paralleled a similar observation reported for the Fe^{III}PPDME complex.[9a]

Excitation with laser light at 406.7 nm of an FeTPPCl solution in CH_2Cl_2 in the presence of 2-MeIm ($X \approx 100$) in anaerobic conditions led to clean photoreduction even without the presence of methanol. The RR spectra are shown in Fig. 5.3.3. The high frequency RR spectra of FeTPPCl in aerobic conditions in the absence (Trace A) and presence (Trace B) of 2-MeIm are identical in major band positions except for a decrease in the relative intensity of the ν_2 mode at 1554 cm^{-1} compared to the ν_4 mode at 1360 cm^{-1} as pointed out earlier. On degassing the solution, the spectrum shown in Trace C (Fig. 5.3.3) was obtained with characteristic RR bands of the reduced Fe^{II}(TPP)(2-MeIm) complex. As before, addition of methanol to the anaerobic solution of FeTPPCl in CH_2Cl_2 in the presence of 2-MeIm ($X \approx$ 100) did not significantly affect the RR spectrum further (Fig. 5.3.3D).

Fig. 5.3.4 shows the photoreduction of FeTPPCl in coordinating solvent, DMSO, in the presence of 1,2-MeIm at two different concentrations of the latter by laser excitation at 441.6 nm in anaerobic conditions. Enhanced yield of photoreduction is observed at the higher concentration of 1,2-MeIm ($X > 150$) as can be seen from the higher relative intensity of

the ν_4, ν_2 and ν_8 modes of the photoreduced complex at 1343, 1542 and 373 cm^{-1} compared to the 1360, 1555 and 389 cm^{-1} respectively of the ferric species. Earlier reports[14] suggest complete dissociation of the Cl^- ion from the iron centre (and lack of ion pairing in this solvent) and axial coordination of two molecules of DMSO giving a 6cHS complex in the absence of nitrogenous ligands. The major RR bands corresponding to the high spin $Fe^{III}TPP(DMSO)_2$ complex are reported[11b,c] in the 1541-1545 cm^{-1} (ν_2), 1438 cm^{-1} (ν_3), 1356-1360 cm^{-1} (ν_4), 1361 cm^{-1} (ν_{13}), 1486 cm^{-1} (ν_{12}) frequency ranges. This means that the concentration of the original complex FeTPPCl in the solution is negligible. Any RR band in our spectrum in the presence of 1,2-MeIm corresponding to a high spin ferric complex must be due to the species of the type $Fe^{III}TPP)(L)$ or $Fe^{III}TPP(L)(L')$ or $Fe^{III}TPP)(L')_2$ (where L and L' stand for 1,2-MeIm and DMSO respectively). Examples of mixed ligand complexes of $Fe^{III}TPP$ with DMSO and methoxide in DMSO have been reported.[15] Hence, it is likely that at the concentration of 1,2-MeIm used here ($X \approx 150$), we have mixed ligand complexes of the type $Fe^{III}TPP(L)(L')$ or $Fe^{III}TPP)(L')_2$ and/or a mixture of both. The former, interestingly has an absorption spectrum quite similar to that reported for $Fe^{III}TPP(OMe)(DMSO)$ complex.[15] However, in the light of extreme steric hindrance presented by the axially coordinated 1,2-MeIm for coordination to the iron centre of a sixth ligand at the concentration used, and due to the weak ligand field of DMSO molecule, the latter may be only loosely bound. Thus the RR bands observed at 1554 cm^{-1} (ν_2) and 389 cm^{-1}(ν_8) can be assigned to the complex $Fe^{III}TPP(1,2MeIm)$. It is interesting that we observed only partial photoreduction of FeTPP complex in neat DMSO (spectra not shown). However, photoreduction of $Fe^{III}PPDME$ in DMSO in the presence of 1,2-MeIm has been reported earlier.[9b]

In all the above studies in DMSO or in CH_2Cl_2 we did not observe any clear RR bands around 1565 and 1370 cm^{-1} corresponding to the ν_2 and ν_4 modes assignable to the four coordinated, intermediate spin (4cIS) ferrous complex, $Fe^{II}TPP$, which may be a transient species in the process of photoreduction.[8b,9a] This may indicate extreme affinity of $Fe^{II}TPP$ to nitrogenous ligands or to trace amounts of dissolved oxygen present in the solvents in the absence of the former. This is borne out by the observation of photoreduction of the ferric complexes in aerobic conditions in this work. Interestingly, the binding constants (K_1) of the hindered imidazoles, 1,2-MeIm[16a] and 2-MeIm[16b], to the ferrous porphyrins have been estimated to be of the same order ($\approx 10^4$ M^{-1}) as that of unhindered[16b] imidazoles ($\approx 10^4$ M^{-1}).

In order to understand the coordination state of FeTPPCl in CH_2Cl_2 and in DMSO, in the presence and absence of the nitrogenous ligands and methanol, and to throw further light on the nature of the photoreducible species under various experimental conditions, we carried out a series of systematic absorption spectral studies of FeTPPCl in various solvent systems under conditions similar to those used for RR experiments. However, the concentration of FeTPPCl used was of the order of 10^{-5} M compared to $\approx 10^{-3}$ M used in RR measurements.

The optical absorption spectra of FeTPP derivatives are significantly different from those of the physiological porphyrins in that there are shifts in band positions and absence of α-β splittings.[17a] Figs. 5.3.5 and 5.3.6 show the absorption spectra of FeTPPCl ($\approx 10^{-5}$M) in CH_2Cl_2 at various concentrations of 1,2-MeIm and 2-MeIm. The general features of trace 1 in both Figures are in good agreement with those of typical 5cHS

(S = 5/2) Fe^{III}TPP complexes[17b] with anionic axial ligand Y (Y = Cl^-, Br^-, I^-, SCN^-, etc.,) which exhibit the Soret and β[17c] bands at 416 and 510 nm respectively. The well defined band at ≈ 376 nm has been attributed to a CT band[4] from the coordinated Cl——>Fe. The spectral pattern of these high spin ferric porphyrins has been explained[17b] as arising from configuration interaction between the porphyrin singlet and triplet (π, π^*) states and the iron to porphyrin CT excited states.

Addition of increasing amounts of 1,2-MeIm to a solution of FeTPPCl in CH_2Cl_2 resulted, at first, in a steady increase in the intensity of the 574 nm band which shifted to 560 nm at higher concentrations of 1,2-MeIm. Concomitant decrease and the disappearance of the 376 and 510 nm bands indicated replacement of the axial chloride ion.[18a] Changing the ligand to 2-MeIm resulted in identical spectral changes (Fig. 5.3.6), although lower concentrations of this ligand was sufficient for the same spectral changes (Fig. 5.3.6). This may be due to the higher binding constant of 2-MeIm to FeTPPCl compared to that of 1,2-MeIm.[18a] A well defined band in the 316-318 nm region developed at higher concentrations of these nitrogenous ligands (Figs. 5.3.5 and 5.3.6). At lower concentrations (X ≈ 3700) the growth of a weak band in the 330-340 nm range was clearly visible. A rough estimate showed two sets of isosbestic points at 338, 496, and 532 nm at lower molar ratio (X ≈ 10^3), and at 334, 494, and 538 nm at higher molar ratios (X ≈ 10^4) corresponding to mono and bis adducts of 1,2-MeIm. Formation of mono and bis adducts of FeTPPCl with these hindered imidazoles have been reported.[18a]

Addition of MeOH (upto 1%) to an FeTPPCl solution in CH_2Cl_2 containing 1,2-MeIm at lower concentrations ($X \approx 10^3$) resulted in enhancement of intensity of the 574 nm band (trace 4 and 5, Fig. 5.3.7) and total disappearance of the 376 and 510 nm bands. A clear band, now at 334 nm, was observed at this stage. Reversing the order, when increasing amounts of 1,2-MeIm was added to an FeTPPCl solution in CH_2Cl_2 containing 1% MeOH, identical spectral changes were observed with the growth of bands at 334 and 578 nm along with the disappearance of the 510 and 376 nm bands (Fig. 5.3.8). The Soret band, however, remained unchanged around 416 nm.

While addition of upto 10% MeOH to a CH_2Cl_2 solution of FeTPPCl in the absence of 1,2-MeIm had no dramatic effect (Fig. 5.3.9) on the absorption spectra, higher amounts of MeOH ($\geq$ 25%) totally replaced the chloride ion as seen by the vanishing of the 376 and 510 nm bands. It is important to note the growth of the band at 334 nm at higher concentrations of MeOH without enhancement of the visible band at 578 nm in these spectra (Fig. 5.3.9) in the absence of 1,2-MeIm, or in its presence at much higher initial concentration of MeOH. While addition of 1,2-MeIm at lower initial concentration of MeOH (5% and 10%, Fig. 5.3.9) had the effect of enhancing the 574 nm band, such enhancement was weak or not observed in the presence of much higher initial concentrations of MeOH. A strong clear band at 330 nm was observed in the spectrum of FeTPPCl in pure MeOH (Fig. 5.3.6). A similar band has been reported in the spectrum of FeTPPCl in pure ethanol[19a] and was associated with the "base" form of the 6cHS species, FeTPP(EtO)(EtOH).

From the foregoing observations it emerges that the growth of an absorption band in the 574-578 nm range occured with, either higher concentrations of 1,2-MeIm ($X \geq 10^3$) or at lower concentrations of 1,2-MeIm ($X \approx 10^2$) but in the presence of small amounts of MeOH, while the development and enhancement of the band in the 330-340 nm range is observed at lower concentrations of 1,2-MeIm ($X \approx 10^2$), or at higher concentrations of MeOH in the presence and absence of 1,2-MeIm. In analogy with the spectra of FeTPPCl in pure ethanol,[19a] we associate the band around 330 nm with a species having a methoxy group coordinated to iron, and the growth of the band around 574-578 nm with a species having 1,2-MeIm as axial ligand.

The absorption spectra of FeTPPCl in DMSO (Fig. 5.3.10) revealed the steady growth of a new band at 572 nm as the concentration of the 1,2-MeIm was increased (from $X \approx 10^3$ to $X \approx 10^4$) suggesting that this band may be associated with its coordination to the iron centre. It is interesting that the 320 nm band seen in the spectrum of the 6cHS complex $FeTPP(DMSO)_2$ did not shift appreciably on addition of 1,2-MeIm.

Striking similarity of the absorption spectrum of FeTPPCl in neat 1,2-MeIm (Fig. 5.3.10) to its spectrum in CH_2Cl_2 in the presence of excess 1,2-MeIm ($X \geq 10^4$), to that of the spectrum of $Fe^{III}TPP(2\text{-MeIm})_2$ reported in literature[18a] helps us to associate these features with the six coordinated $FeTPP(1,2\text{-MeIm})_2$ ferric complex. A distinct band developed around 320 nm as observed before in Fig. 5.3.1. Throughout these experiments, the Soret band remained unchanged within the 416-418 nm range indicating no formation of any μ-oxo dimer.[11d] The latter usually shows distinct blue shifted Soret band at $\approx$ 408 nm.

From the above observations and in comparison to the absorption spectra of mixed ligand complexes,[15a] we can identify the species present in a CH_2Cl_2 solution of FeTPPCl in the absence of methanol and at low concentrations of 1,2-MeIm, as FeTPP(1,2-MeIm)$^+Cl^-$. In the presence of trace amount of methanol, the species would be FeTPP(1,2-MeIm) and/or FeTPP(1,2-MeIm)(OMe). The formation of the OMe moiety in the presence of hindered imidazoles may be promoted according to the scheme proposed recently by Uno et al[20] where the imine nitrogen of the hindered imidazole, engaging in a H-bonded interaction with MeOH, deprotonates the latter which then coordinates axially to the iron atom replacing the chloride ion. The chloride ion then forms a H-bond with the protonated hindered imidazole.

From the RR study of FeTPPCl under various conditions of solvents and axial ligands and from the study of optical absorption spectra so far, it is apparent that photoreduction has been observed under excitation at 441.6 nm in only those complexes which exhibited an absorption band in the 315-340 nm region suggesting that the state responsible for this absorption is a photoreactive state. Thus, we note that the methoxide coordinated mixed ligand complex FeTPP(1,2-MeIm)(MeO) exhibits a band around 334 nm, the DMSO complexed species FeTPP(1,2-MeIm)(DMSO) at 322 nm, the bis DMSO complex, FeTPP(DMSO)$_2$, around 320 nm, the species in pure methanol at 330 nm, the FeTPP(EtO)(EtOH) complex[19a] in pure ethanol at 335 nm. The monocoordinated FeTPP(1,2-MeIm) and FeTPP(2-MeIm) complexes show a weak band in the 330-340 nm region while the species in neat 1,2-MeIm exhibits this band at 318 nm. The clean photoreduction[19a] of only the "base" form of Fe^{III}TPP having an ethanolate group as axial ligand exhibiting this band at 335 nm

band in contrast to the "acid" form $FeTPP(EtOH)_2$ without any band in this region and also of the FeOEP(EtO)EtOH) complex[19b] with a band $\approx$ 340 nm supports our view. The relative yield of photoreduction would then depend on the extent of absorption of the complex due to this band at the wavelength of excitation, apart from other factors. This is clear from the observation of complete photoreduction of $Fe^{III}TPP(2\text{-MeIm})$ complex with excitation at 406.7 nm compared to only partial photoreduction at 441.6 nm excitation under otherwise similar experimental conditions as the absorption at the former exciting wavelength is higher. The observation of non-photoreducibility of FeTPPCl in the presence of pure ethanol even of the "base" form with $\lambda_{exc} > 400$ nm by Hoshino et al[19a] further supports our view.

Although the nature of this reactive state is not so clear at this stage, the most likely interpretation would be a charge transfer (CT) transition from the coordinated axial ligand to the iron atom. Such CT transitions have been clearly identified in the FeTPPCl complex[4] at 376 nm and in the ethoxo complex FeTPP(EtO)(EtOH) at 335 nm.[19a] It further emerges that only the high spin complexes of FeTPPCl formed with axial ligands like 1,2-MeIm, 2-MeIm, DMSO, primary alcohols exhibiting clear absorption band in the 315-340 nm region are photoreducible.

The facile photoreduction of FeTPPCl observed in CH_2Cl_2 in the presence of excess 1,2-MeIm but not in the presence of excess 2-MeIm in anaerobic conditions under excitation at 441.6 nm may be due to the formation of a 6cHS and a 6cLS complex in the former and latter cases respectively. The bis 2-MeIm complex of $Fe^{III}TPP$ is reported to show temperature dependent magnetic moment suggestive of a S = 1/2 and S = 5/2

spin equilibrium with the low spin state predominating at room temperature in solutions[21a] and in solid state.[21b] While no similar data is available for FeTPP(1,2-MeIm)$_2$ complex, NMR experiments[21c] have indicated 6cLS species for this complex at low temperature, but ESR data at 77°K revealed only high spin species. This was explained by invoking the relative stability of the high and the low spin species in frozen conditions. It is, thus, quite likely that with additional steric hindrance caused by the resistance of the 1-methyl group to the bending of the 2-methyl group, elongation of the Fe-axial bond distance[21b] helped by a favourable orientation cause the high spin state to predominate in this complex.

We can summarize the mechanism of photoreduction of FeTPPCl in CH_2Cl_2 or DMSO with different axial ligands as follows: Irradiation with 406.7 or 441.6 nm laser light excites the system to the photoreactive state having absorption in the 315-340 nm range, where the coordinated axial ligand (2-MeIm, 1,2-MeIm or OMe) dissociates donating its charge to the iron atom in the photoexcited state. The ligand-free, four coordinated, intermediate spin[22] ferrous complex generated as a result of photoreduction of 5cHS ferric complex is stabilized as a 5cHS ferrous species by coordination of a free nitrogenous ligand in solution. A 6cHS ferric complex of the type FeTPP(L_1)(L_2), (L_1 = 2-MeIm or 1.2-MeIm, L_2 = OMe; L_1 = L_2 = 1,2-MeIm) would be self stabilized following photoreduction depending on which of the two axial ligands acts as the electron donor in the photoexcited state.[8b] The likely role of methanol seems to be to provide a polar environment (akin to DMSO) in a solvent of low polarity (like CH_2Cl_2) to facilitate the removal of the halide ion from the coordination sphere of iron and in scavenging the photoproduced radicals, apart from its coordination to the iron centre.

REFERENCES

1. (a) Collman, J.P. *Acc. Chem. Res.* 1977,10, 265.
   (b) Scheidt, W.R.; Reed, C.A. *Coord. Chem. Rev.* 1981, 81, 543.
   (c) *Structure and Bonding*; Palme, G., Ed.; Springer: Berlin, 1991; Vol. 75.

2. Kitagawa, T.; Nagai, K. *Nature.* 1979, 281, 503.

3. Ogura,T.; Yoshikawa,S.; Kitagawa, T. *Biochemistry.*1985, 24, 7746.

4. Hendrickson, D.N.; Kinnaird M.G.; Suslick, K.S. *J. Am. Chem. Soc.* 1987, 109, 1243.

5 Suslick, K.S.; Bautista, J.F.; Watson, R.A. *J. Am. Chem. Soc.* 1991, 113, 6111.

6. (a) Bartocci, C,; Maldotti, A.; Varani, G.; Battioni, P.; Carassiti, V.; Mansuy, D. *Inorg. Chem.* 1991, 30, 1255.
   (b) Maldotti, A.; Bartocci, C.; Amadelli, B.; Polo, E.; Battioni, P. Mansuy, D. *J. Chem. Soc., Chem. Commun.* 1991, 1486.

7. (a) Bartocci, C,; Scandola, F.; Ferri, A.; Carassiti, V. *J. Am. Chem. Soc.* 1980, 102, 7067.
   (b) Harriman, A.; Porter,G. *J.Chem.Soc.*, Farad.Trans. 1979, 75, 1543.
   (c) Bizet, C.; Morliere, P.; Brault, D.; Delgado, O.; Bazin, M.; Santus, R. *Photochem. Photobiol.* 1981, 34, 315.

8. (a) Fidler, V.; Ogura, T; Sato, S.; Aoyagi, K; Kitagawa, T. *Bull. Chem. Soc. Jpn.* 1991, 64, 2315.
   (b) Sato, S.; Kamogawa, K.; Aoyagi, K.; Kitagawa, T. *J. Phys. Chem.* 1992, 96, 10676.
   (c) Gu, Y.; Li, P.; Sage, T.; Champion, P.M. *J. Am. Chem. Soc.* 1993, 115, 4993.

9. (a) Verma, A.L.; Chaudhuri, N.K. *J. Raman. Spectrosc.* 1991, 22, 427.
   (b) Chaudhuri, N.K.; Saini, G.S.S.; Verma, A.L. *Inorg. Chem.* 1995, 34, 346.

10. Spiro, T.G.; Czernuszewicz, R.S.; Li, X.Y. *Coord. Chem. Rev.* 1990, 100, 541.

11. (a) Burke, J.M.; Kincaid, J.R.; Peters, S.; Gagne, R.R.; Collman, J.P.; Spiro, T.G. *J. Am. Chem. Soc.* 1978, 100, 6083.
   (b) Parthasarathi, N.; Hansen, C.; Yamaguchi, S.; Spiro, T.G. *J. Am. Chem. Soc.* 1987, 109, 3865.
   (c) Chottard, G.; Battioni, P.; Collman, P.; Lange, M.; Mansuy, D. *Inorg. Chem.* 1981, 20, 1718.
   (d) Burke, J.M.; Kincaid, J.R.; Spiro, T.G. *J. Am. Chem. Soc.* 1978, 100, 6077.
   (e) Cheung, L.D.; Yu, N.-T.; Felton, R.H. *Chem. Phys. Lett.* 1978, 55, 527.

12. (a) Li, X.Y.; Czernuszewicz, R.S.; Kincaid, J.R.; Su, Y.O.; Spiro, T.G. *J. Phy. Chem.* 1990, 94, 31.
(b) Spiro, T.G.; Li, X.Y. In *Biological Applications of Raman Spectroscopy*. Spiro, T.G., Ed.; Wiley: New York, 1988; Vol. 3.
(c) Ogoshi, H.; Watanabe, E.; Yoshida, Z; Kincaid, J.R.; Nakamoto, K. *J. Am. Chem. Soc.* 1973, 95, 2845.

13. (a) Hori, H.; Kitagawa, T. *J. Am. Chem. Soc.* 1980, 102, 3608.
(b) Stein, P.; Mitchell, M.; Spiro, T.G. *J. Am. Chem. Soc.* 1980, 102, 7795.

14. (a) Brown, S.B.; Lantzke, I.R.; *Biochem. J.* 1969, 115, 279.
(b) Pasternak, R.F.; Gillies, B.S.; Stahlbush, J.R. *J. Am. Chem. Soc.* 1978, 100, 2613.
(c) Mashiko, T.; Kastner, M.E.; Spartalian, K.; Scheidt, W.R.; Reed, C.A. *J. Am. Chem. Soc.* 1978, 100, 6354.

15. (a) Otsuka, T.; Ohya, T.; Sato, M. *Inorg. Chem.* 1985, 24, 776.
(b) Otsuka, T.; Ohya, T.; Sato, M. *Inorg. Chem.* 1984, 23, 1777

16. (a) Tetreau, C. ; Leondiadis, L.; Lavalette, D.; Momenteau, M. *J. Chem. Soc., Perkin. Trans. 2.* 1992, 73.
(b) Brault, D.; Rougee, M. *Biophys. Biochem. Res. Comm.* 1974, 57, 654.

17. (a) Büchler, J.W.; Kökisch, W.; Smith, P.D. *Struct. Bonding* (Berlin) 1978, 34, 79.
(b) Kobayashi, H.; Yanagawa, Y.; Osada, H. *Bull. Chem. Soc. Jpn.* 1973, 46, 1471.
(c) Ciaccio, P.R.; Ellis, J.V.; Munson, M.E.; Kedderis, G.L.; McConville, F.X.; Duclos, J.M. *J. Inorg. Nucl. Chem.* 1976, 38, 1885.

18. (a) Walker, F.A.; Lo, M.W.; Ree, M.T. *J. Am. Chem. Soc.* 1976, 98, 5552.
(b) Yoshimura, T.; Ozaki, T. *Bull. Chem. Soc. Jpn.* 1979, 52, 2268.

19. (a) Hoshino, M.; Ueda, K.; Takahashi, M.; Yamaji, M.; Hama, Y. *J. Chem. Soc., Farad. Trans.* 1992, 88, 405.
(b) Maldotti, A.; Bartocci, C.; Amadelli, R.; Carassiti, V. *J. Am. Chem. Soc., Dalton. Trans.* 1989, 1197.

20. Uno, T.; Hatano, K.; Nishimura, Y. *J. Am. Chem. Soc.* 1994, 116, 4107.

21. (a) Geiger, D.K.; Lee, Y.J.; Scheidt, W.R. *J. Am. Chem. Soc.* 1984, 106, 6339.
(b) Scheidt, W.R.; Kirner, J.F.; Hoard, J.L.; Reed, C.A. *J. Am. Chem. Soc.* 1987, 109, 1963.
(c) Satterlee, J.D.; La Mar, G.N.; Frye, J.S. *J. Am. Chem. Soc.* 1976, 98, 7275.

22. Collman, J.P.; Hoard, J.L.; Kim, N.; Land, G.; Reed, C.A. *J. Am. Chem. Soc.* 1975, 97, 2676.

TABLE 5.3.1: RR frequencies of FeTPPCl (cm^{-1}) observed on photoreduction in the presence of hindered imidazoles.

Assignment† Symmetry	Mode	FeTPPCl in CH_2Cl_2	Fe^{II}(1,2-MeIm) in CH_2Cl_2	Fe^{II}(1,2-MeIm) in neat 1,2-MeIm	Fe^{II}(2-MeIm) in CH_2Cl_2
$\nu(C_mC_{Ph})$, A_{1g}	ϕ_4	1598	1599	1600	1599
$\nu(C_\beta C_\beta)$, A_{1g}	ν_2	1554	1539	1541	1542
$\nu(C_\beta C_\beta)$, B_{1g}	ν_{11}	-	1487	1489	1490
$\nu(C_\alpha C_m)$, A_{1g}	ν_3	1451	1434	1433	1434
$\nu(C_\alpha N)$, A_{1g}	ν_4	1360	1342	1343	1343
$\nu(C_mPh)$, A_{1g}	ν_1	1233	1229	1229	1229
$\nu(FeN_p)$, A_{1g}	ν_8	390	372	372	372
ν(Fe-ax), A_{1g}		362	200	200	200
Por. def.		331	336	336	336
$\nu(C_mC_{Ph})$ A_{1g}	ϕ_{10}	200	200	200	200

†Mode numbering according to ref. 16a.

TABLE 5.3.2: UV-VIS absorption bands for selected ferric tetraphenylporphyrin complexes.

Complex	Solvent systems	Spin state	Coord. Number	Absorption bands (nm)	Ref.
FeTPPCl	$CHCl_3$	HS	5	380, 417, 511, 577, 658	18a
$(FeTPP)_2O$	Benzene	HS	5	- 408, 572, 612	11d
FeTPP(EtO)(EtOH)	EtOH	HS	6	335, 413,	19a
FeTPP(MeO)(DMSO)	DMSO + MeO^-	HS	6	422, 530, 575, 615	15a
$FeTPP(DMSO)_2$	DMSO	HS	6	415, 497, 530, 660	15a
$FeTPP(DMSO)_2$	DMSO	HS	6	320, 418, 494, 530	p
FeTPP(MeO)(MeOH)	MeOH	HS	6	335, 414, 550, 596	p
FeTPP(DMSO)(L)	DMSO	HS	6	322, 418, 530, 572	p
FeTPP(MEO)(L)*	CH_2Cl_2	HS	6	334, 416, 574	p
$FeTPP(L)_2$	CH_2Cl_2	HS	6	318, 416, 525, 560, 610	p
$FeTPP(L)_2$	Neat L	HS	6	320, 416, 530, 560, 608	p
$FeTPP(L')_2$‡	CH_2Cl_2	LS	6	316, 416, 525, 560, 608	p

L = 1,2-MeIm: L' = 2-MeIm: ‡ In the presence of excess 2-MeIm. p present work.
* In the presence of L + 1% MeOH.

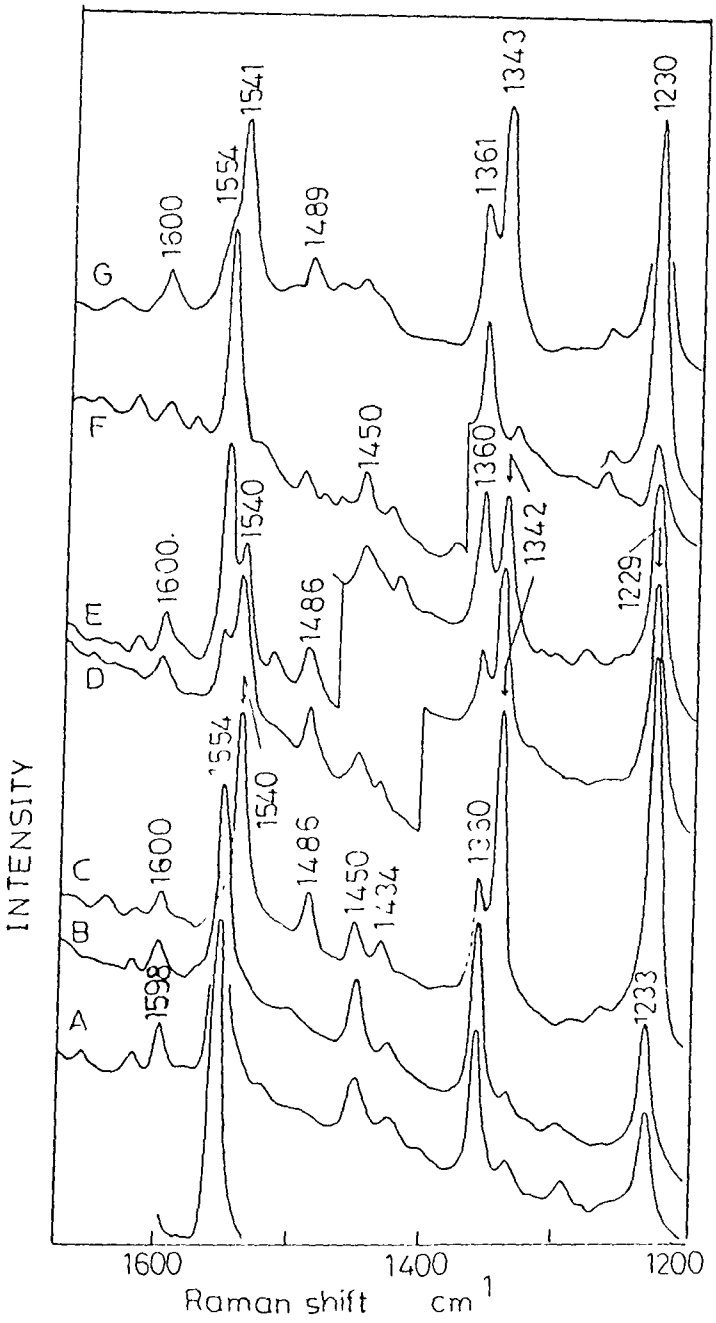

Fig. 5.3.1 High frequency (1200-1675 cm^{-1}) RR spectra of FeTPPCl (1.0 mM) in CH_2Cl_2 obtained with laser excitation at 441.6 nm, ≈ 10 mW. (A) FeTPPCl, (B) FeTPPCl + 1,2-MeIm (140 mM), in aerobic conditions; Spectra C-F recorded in the simultaneous presence of 1% MeOH; Concentration of 1,2-MeIm in (C) 100 mM, (D) 5 mM, (E) 0.5 mM, (F) 0.05 mM; (G) RR spectra of FeTPPCl (1 mM) in neat 1,2-MeIm in aerobic conditions. Scan speed, 30 cm^{-1}/min.

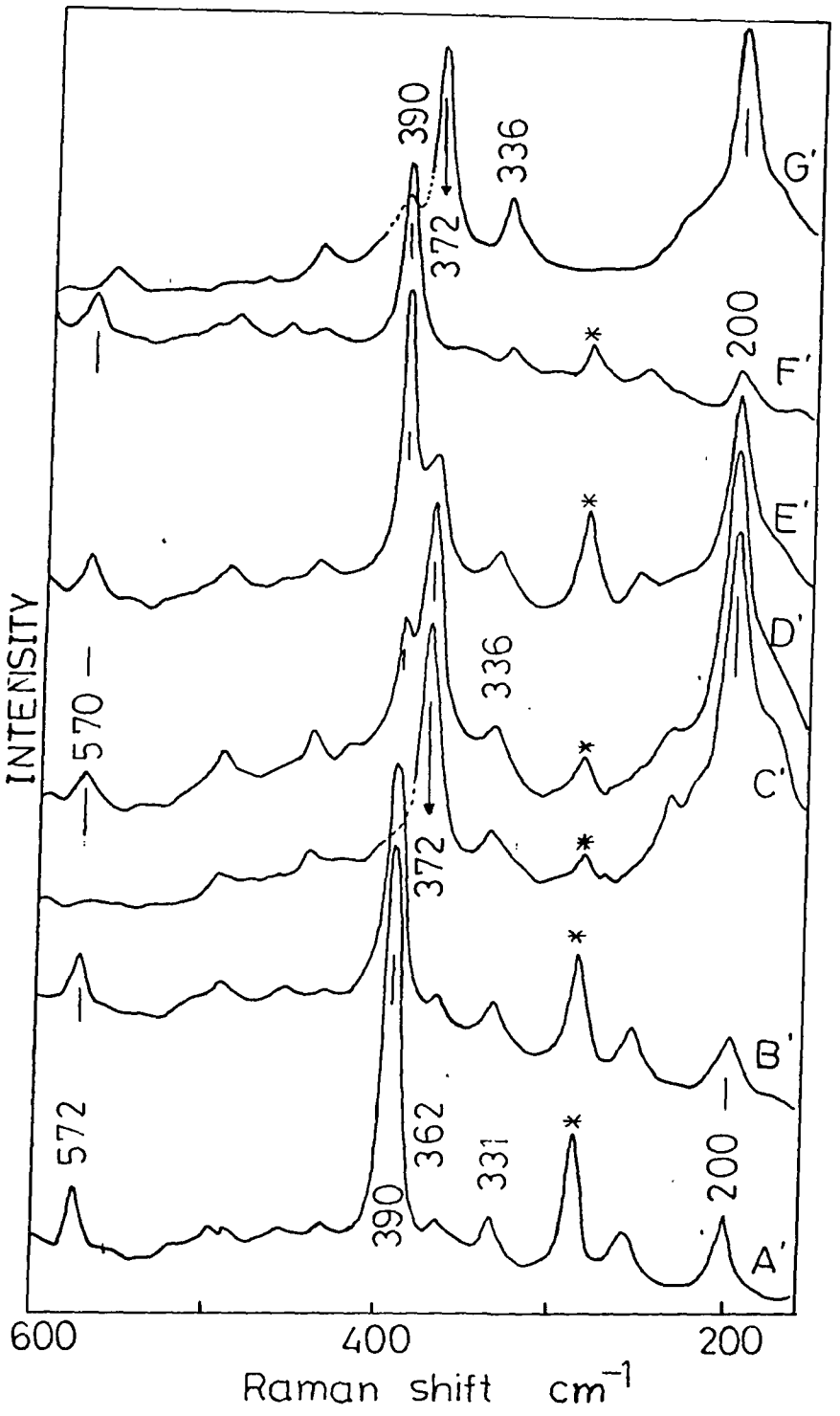

Fig. 5.3.2 Low frequency (150-600 cm^{-1}) RR spectra of FeTPPCl in CH_2Cl_2. Experimental conditions are identical to those in Fig. 5.3.1.

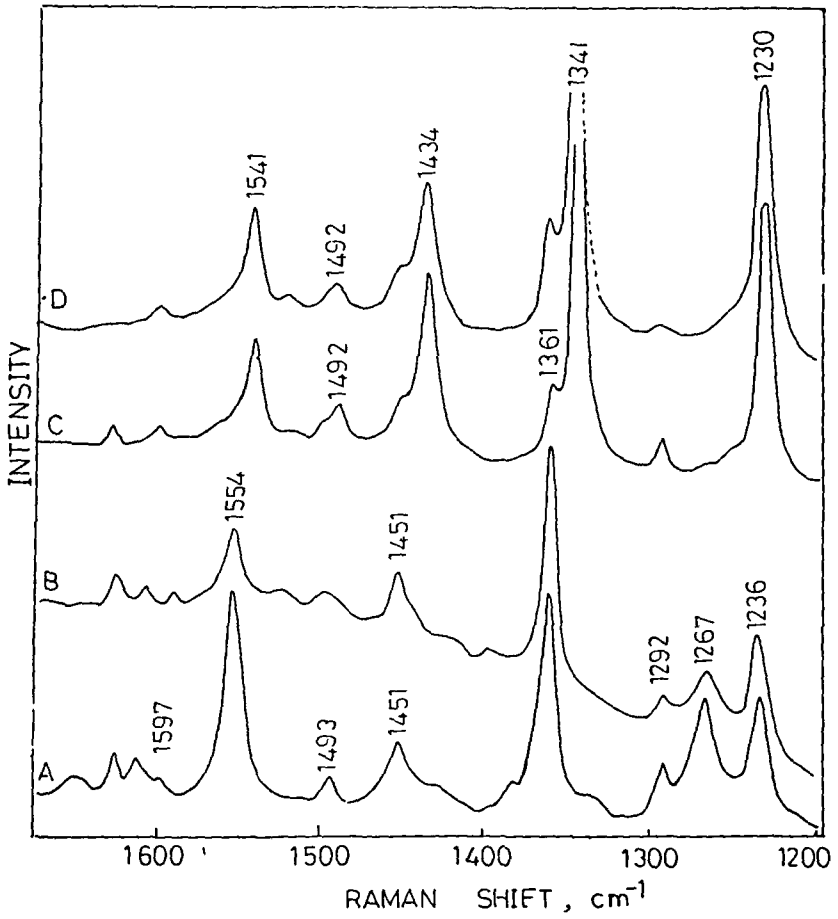

Fig. 5.3.3 High frequency (1200-1675 cm^{-1}) RR spectra of FeTPPCl (1.0 mM) in CH_2Cl_2 obtained with laser excitation at 406.7 nm, ≈ 10 mW.(A) FeTPPCl ; (B) FeTPPCl + 2-MeIm (100 mM), in aerobic conditions, (C) B in anaerobic conditions, (D) C + 1% MeOH. Scan speed 25 cm^{-1}/min.

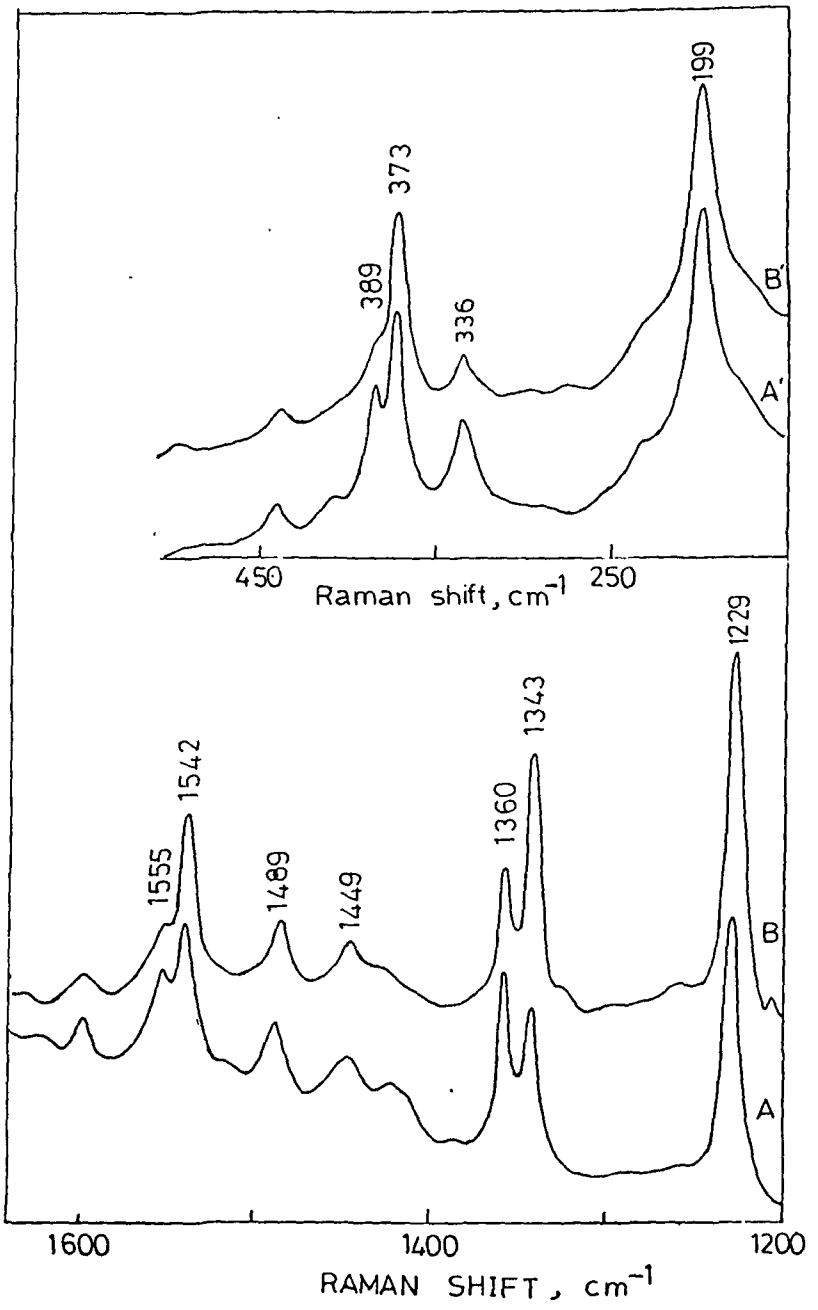

Fig. 5.3.4 RR spectra of FeTPPCl in DMSO in the presence of 1,2-MeIm in anaerobic conditions. Concentration of 1,2-MeIm; (A, A') 140 mM ,(B, B') 700 mM : Lower panel; 1200-1675 cm^{-1}: Upper panel; 150-500 cm^{-1}. λ_{exc} = 441.6 nm, power = 10 mW.

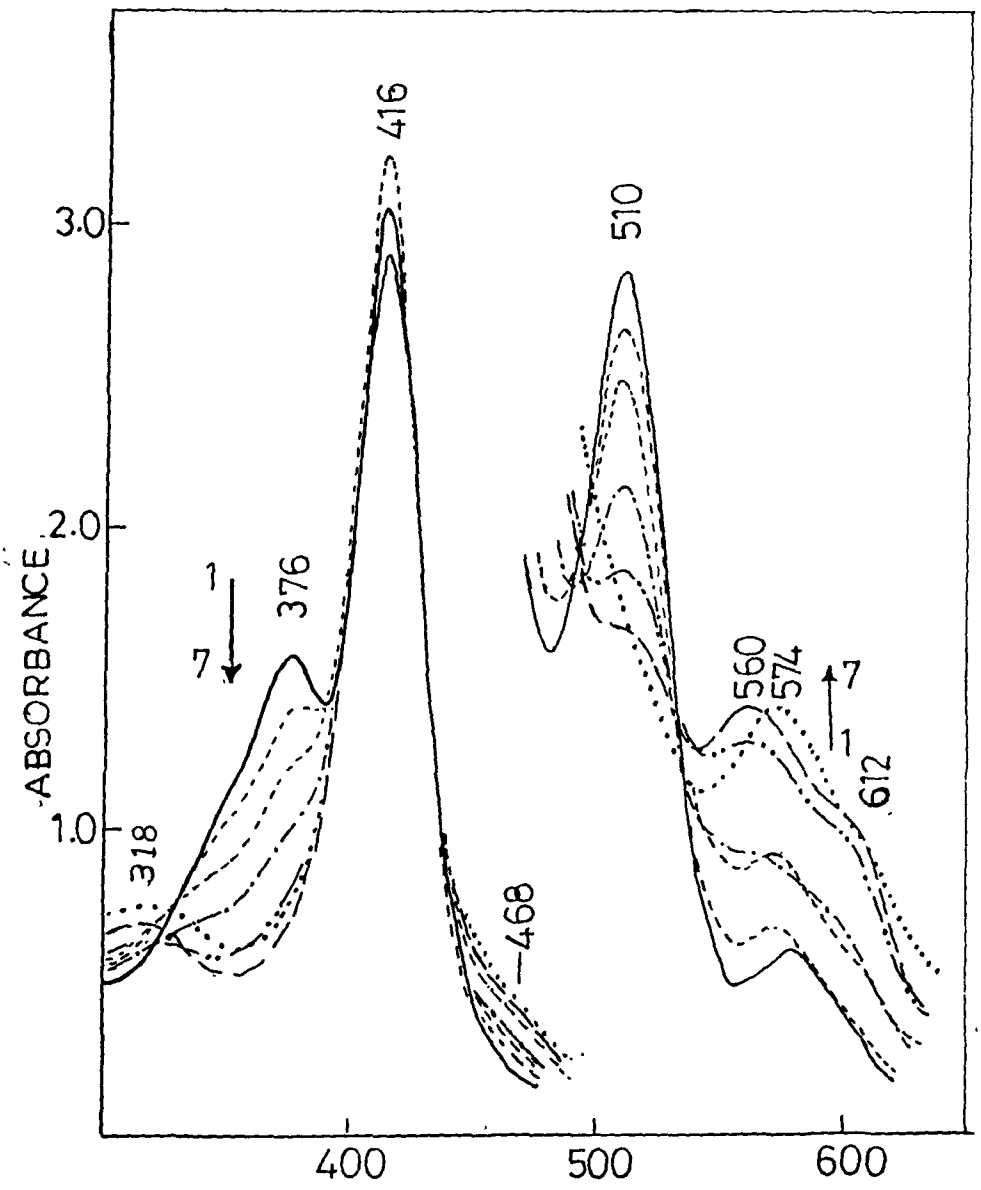

Fig. 5.3.5 Absorption spectra of (2×10^{-5} M) FeTPPCl in the presence of 1,2-MeIm in CH_2Cl_2. Concentration of 1,2-MeIm: (1) 0 mM (———); (2) 23 mM (- - - -); (3) 75 mM (- - - -); (4) 136 mM (—·—·—); (5) 272 mM (—···—); (6) 0.4 mM (— —); (7) 0.4 M + 1% MeOH (·····). Path length = 10 mm.

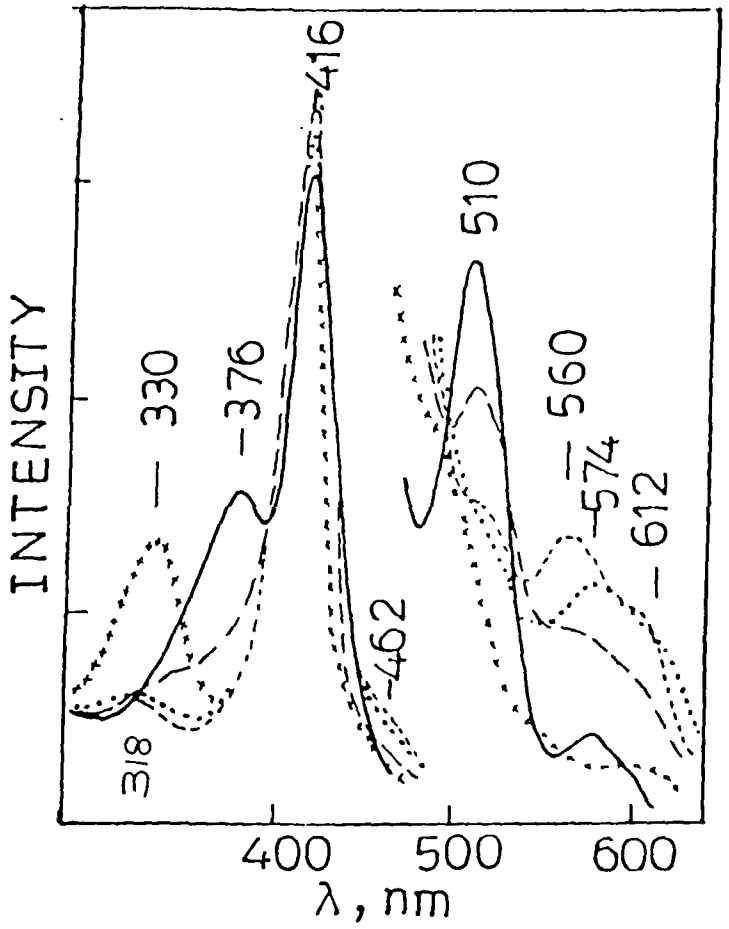

Fig. 5.3.6 Absorption spectra of (2×10^{-5}M) FeTPPCl in the presence of 2-MeIm in CH_2Cl_2. Concentration of 2-MeIm: (1) 0 mM (———); (2) 13 mM (— —); (3) 27 mM (- - -); (4) 27 mM + 1% MeOH (·····): (5) FeTPPCl (2×10^{-1}M) in pure MeOH (xxxxx). Optical path length 10 mm.

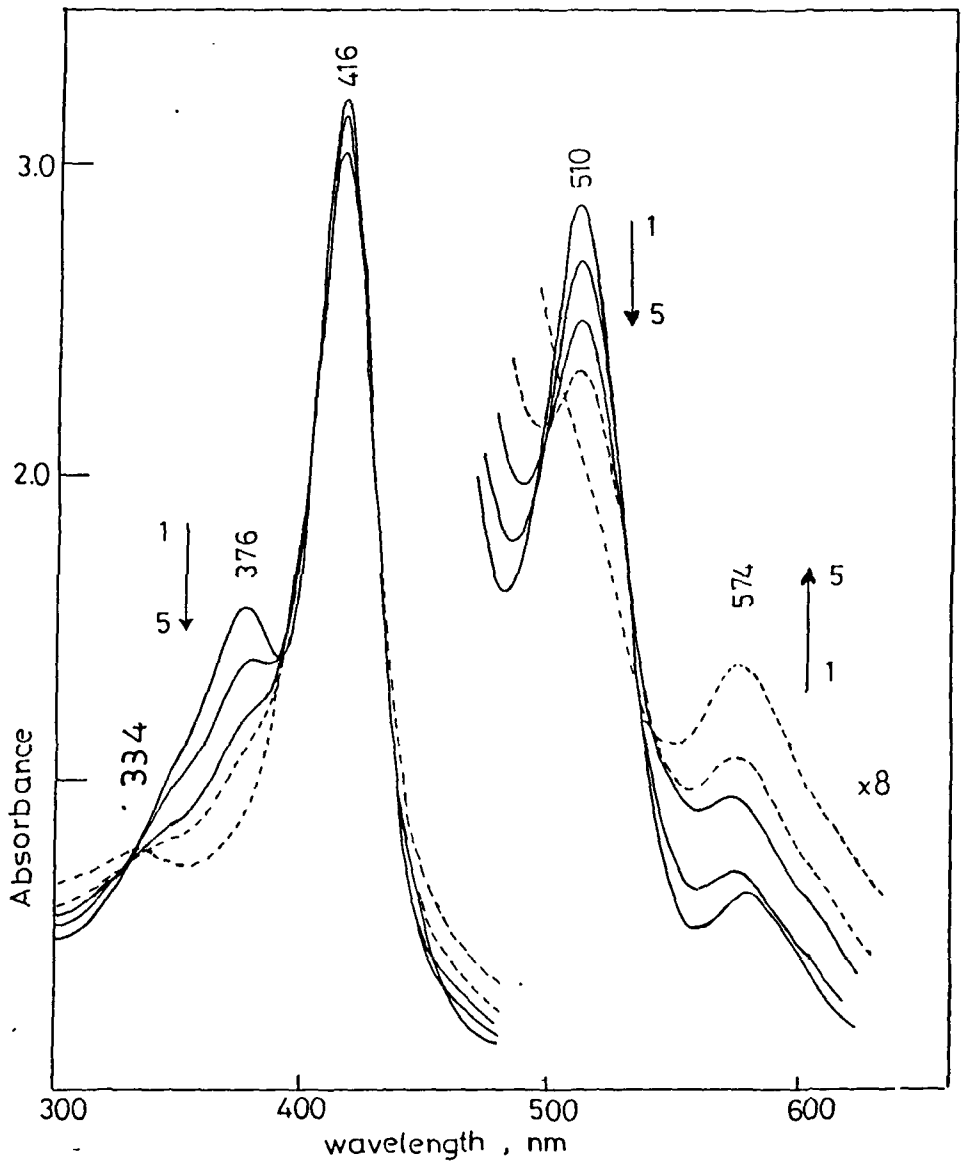

Fig. 5.3.7 Absorption spectra of (2×10^{-5}M) FeTPPCl in the presence of 1,2-MeIm and MeOH in CH_2Cl_2. Concentrations of 1,2-MeIm and MeOH : (1) 0 mM, 0% (———); (2) 23 mM, 0% (———); (3) 75 mM, 0% (———); (4) 75 mM, 0.1% (- - - -); (5) 75 mM, 1% (- - - - -). Path length 10 mm.

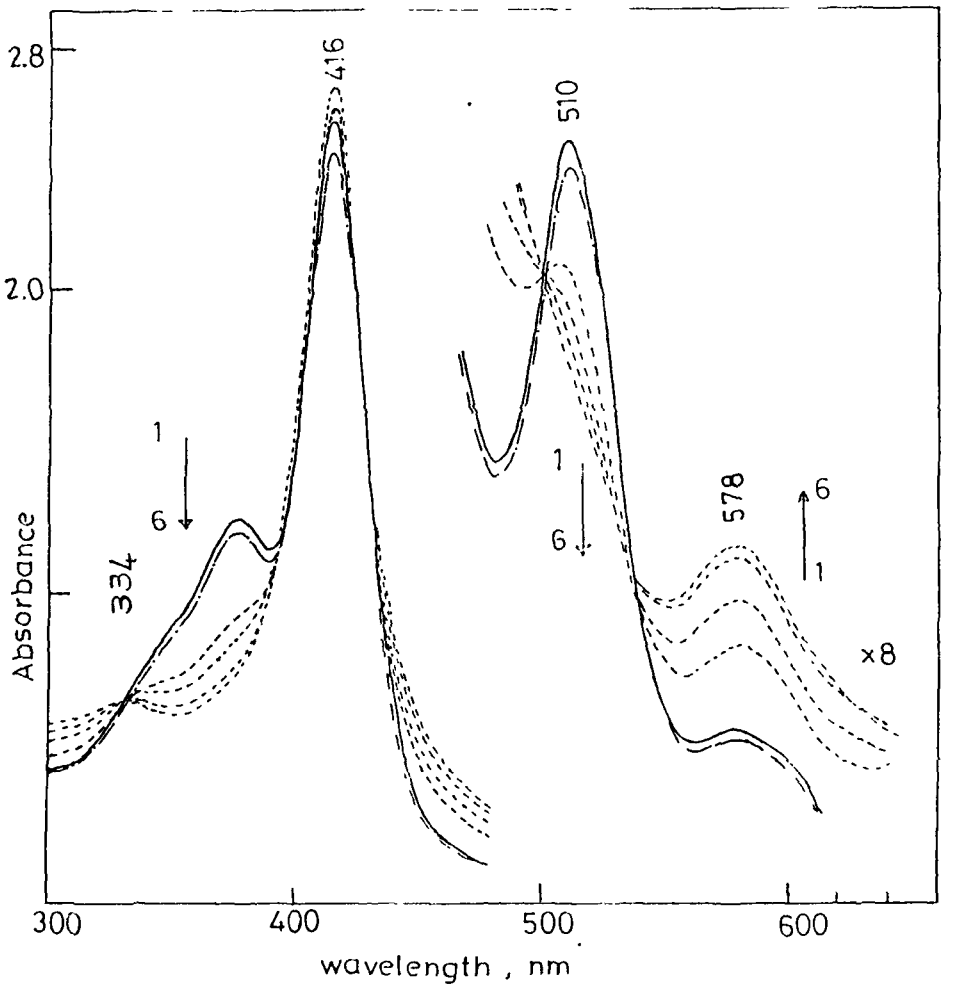

Fig. 5.3.8 Absorption spectra of (2×10^{-5}M) FeTPPCl in (1) CH_2Cl_2 (———): in the presence of 1% MeOH (—·—·—) and different concentrations of 1,2-MeIm (– – – –); (2) 0 mM, (3) 4 mM, (4) 11.8 mM, (5) 13 mM, (6) 16.4 mM. Path length 10 mm.

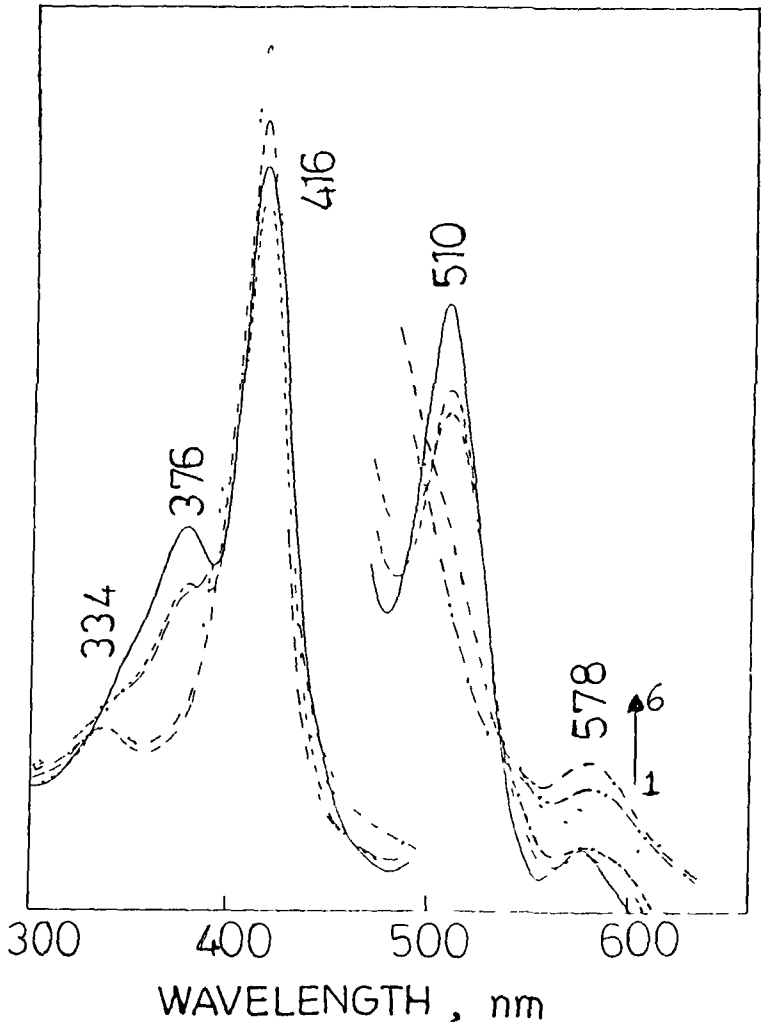

Fig. 5.3.9 Absorption spectra of (2×10^{-5}M) FeTPPCl in CH_2Cl_2 in the presence of different initial concentrations of MeOH and 1,2-MeIm respectively: (1) 0%, 0 mM (———); (2) 5%, 0 mM (- - - -); (3) 10%, 0 mM (— - · — - —); (4) ≥ 25%, 0 mM (· · · · ·); (5) 10%, 1.3 mM (— · · · — —); (6) 5%, 4 mM (— · — · —). Optical path length 10 mm.

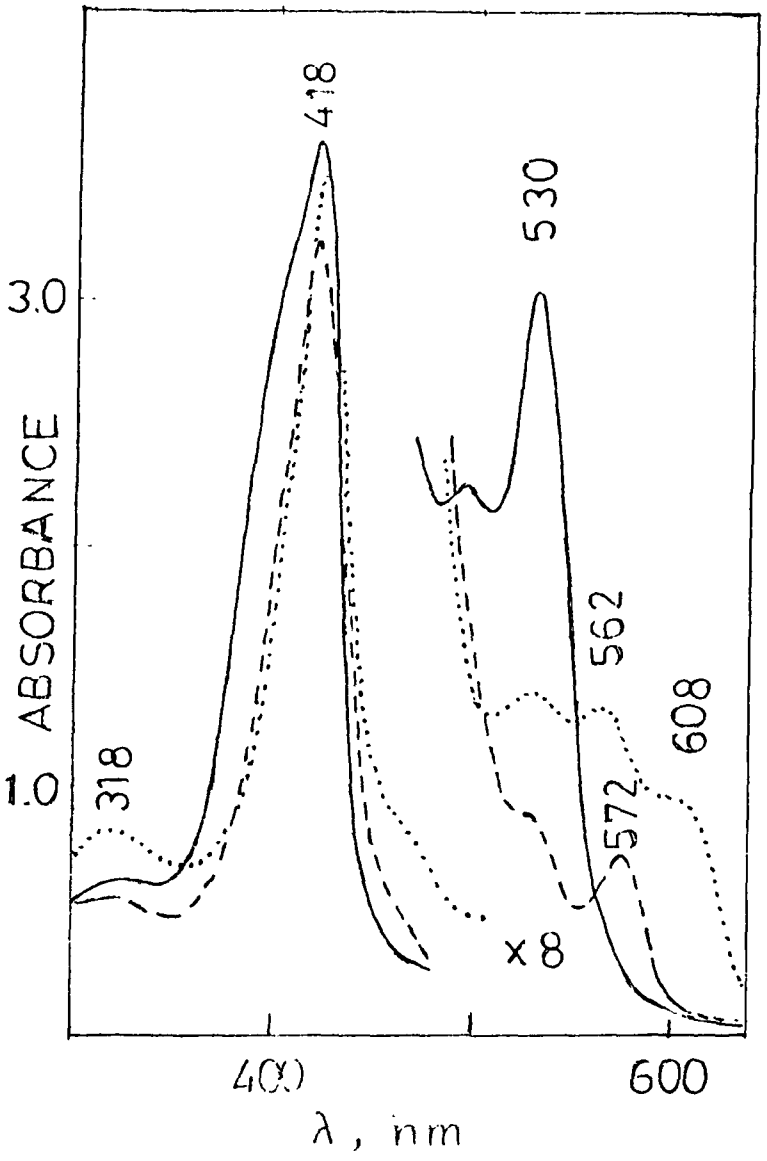

Fig 5.3.10 UV-VIS spectra of FeTPPCl in DMSO ($\approx 10^{-5}$M) in the absence (———) and in the presence (– – –) of 1,2-MeIm (280 mM); Absorption spectra of FeTPPCl ($\approx 10^{-5}$M) in neat 1,2-MeIm (·····). Path length = 10 mm. (in neat 1,2-MeIm, 2 mm).

CHAPTER 6

PHOTOREDUCTION OF IRON PROTOPORPHYRIN (IX) CHLORIDE IN IONIC AND NON-IONIC DETERGENT MICELLES PROBED BY RESONANCE RAMAN SPECTROSCOPY.

Resonance Raman studies of iron protoporphyrin (IX) Chloride (FePPCl, hemin) solubilized in aqueous detergent micelles in the absence and presence of hindered imidazoles, 2-methylimidazole (2-MeIm), 1,2-dimethylimidazole (1,2-MeIm) and unhindered imidazole (Im) under various experimental conditions are reported. In non-ionic Triton X-100 (TX-100) and cationic cetyltrimethylammonium bromide (CTAB) micelles, hemin was observed to undergo photoreduction at the metal centre, both in the absence and presence of the hindered imidazoles in anaerobic, alkaline and neutral pH conditions on photoexcitation with 441.6 and 457.9 nm laser light. The resulting ferrous complexes were characterized by their RR frequencies in comparison to the spectra of the chemically reduced species under similar experimental conditions and also by the $\nu(Fe\text{-}N_{axial})$ stretching frequencies in the presence of hindered imidazoles. From an RR study of photoreduction of hemin at different concentrations of the detergent (TX-100) it has emerged that only the monomer hemin encapsulated within the micelle at alkaline pH conditions is photoreducible.

In anionic sodium dodecyl sulphate (SDS) no photoreduction of hemin was observed in the presence of 2-MeIm in alkaline, anaerobic conditions on excitation at 441.6 nm or even on simultaneous addition of salts (NaCl or TMAB) to the micellar solution unless trace amount of ethanol was also present. The mechanism of photoreduction of hemin in TX-100 and CTAB micelles appears to be via an electron transfer in the photoexcited state from the coordinated hydroxyl ion to the iron atom and in SDS from the coordinated ethanolate anion.

6.1 Introduction

The stability of the reduced state of iron atom in such hemeproteins as hemoglobin, myoglobin etc., which is essential for the reversible binding of oxygen in the respiratory cycle is thought to be the result of the specially designed hydrophobic environment of the globin pocket where the iron protoporphyrin units are distributed as monomers with a single convalent link with the nitrogen atom of the hystidyl imidazole moiety.[1] Once outside the globin pocket, the heme units rapidly oxidize to the more stable ferric state. The axial coordination of the proximal and distal imidazoles play vital roles in controlling the heme-heme interactions in hemeproteins.[1] Extensive studies have been carried out over the last two decades in elucidating the kinetic and thermodynamics of axial ligation of imidazole and its derivatives to the natural and model iron porphyrins by optical spectroscopy,[2] NMR[3] and other techniques[4] in organic, coordinating[5] and non-coordinating solvents,[2] as well as in aqueous ethanolic solutions.[6] Several studies of hemin[7] and other iron porphyrins[8] have revealed the essentially monomeric nature of this metalloporphyrin when solubilized in aqueous detergent micellar solutions.

The photosensitivity of natural iron porphyrins[9a] and their model compounds,[11-14] and also of hemeproteins[10] in aqueous buffer or ethanol[9] and ethanol-mixed solvents[11] have been well documented in literature. Photoreduction of ferric porphyrins in these solvent systems on irradiation near the Soret region or at shorter wavelengths are believed to occur[8a,9,11] as a result of electron transfer from the axially coordinated alcoholate ligand to the metal centre in the photoexcited

state. However, other studies by Kitagawa et al[13,14] revealed the non-photoreducibility of iron porphyrin under excitation at ≈ 585 nm charge transfer CT (methanol —> Fe) band in the simultaneous presence of 2-MeIm and trace amount of methanol and also the possibility of multiple electron donors depending on the experimental conditions. While photoreduction of metalloporphyrins by electron transfer from the axially coordinated moiety was observed to be a general phenomena,[12] the possiblity of the coordinated hydroxyl ion as the electron donor under photoexcitation has also been pointed out.[9a,15c,d]

We report here a systematic RR study of hemin solubilized in ionic and non-ionic detergent micelles under various conditions of pH, concentrations, presence and absence of imidazole bases under different laser excitations. Absence of any change in the optical absorption spectra of hemin in the micelles on addition of hindered imidazoles indicated their non-coordination under the experimental conditions used. The studies have revealed that only the hydroxyl ion coordinated high spin monomer hemin is photoreducible on near Soret excitation in TX-100 and CTAB micelles in neutral to alkaline pH conditions. In SDS, photoreduction of hemin was observed only in the simultaneous presence of 2-MeIm and trace amount of ethanol on excitation at 441.6 nm at alkaline pH conditions.

6.2 Experimental Section

Iron protoporphyrin IX chloride, 2-MeIm, imidazole and the detergent TX-100 were purchased from Sigma Chemical Company, U.S.A. and were used as recieved. 1,2-MeIm was obtained from Merck, Germany. CTAB and SDS detergents were from BDH (England) and Sisco Laboratories (extra pure

grade) respectively. Triple distilled water was used in preparing all aqueous solutions. All alcohols used were of spectroscopic grade.

Raman spectra were recorded at 90° scattering geometry using Spex Ramalog 1403 triple monochromator equipped with a cooled photomultiplier coupled to photon counting electronics. A microprocessor based Spex Datamate provided spectrometer control, data aquisition and processing faclities.

Optical absorption spectra were recorded on a Shimadzu UV-VIS spectrophotometer and a Carey 2300 UV-VIS spectrophotometer using a 10 mm path length quartz cuvettes. Laser excitation at 441.6 and 457.9 nm were provided by He-Cd (Liconix Model 4240) and by Ar^+ (Spectra-Physics Model 165) lasers respectively. Typical laser powers at the source at 441.6 nm and 457.9 nm were 10-13 mW and 60-120 mW respectively. Raman shifts were calibrated with the standard lines of indene.

The pH of aqueous detergent solutions was adjusted using dilute HCl or NaOH solutions and measured with Systronics Model 355 digital pH meter which was calibrated previously using standard pH buffers. Micellar solutions of hemin was prepared by first dissolving an appropriate quantity of hemin in dilute NaOH and adding to the aqueous detergent solution. Equilibration was carried out at $\approx 40^{\circ}C$ in the dark for about an hour. Spectra were recorded immediately after adjusting the pH and degassing. Typical concentration of hemin for RR study was 0.5 mM in a 3% detergent solution (w/v or v/v). Nitrogenous ligands were added directly to the micellar solutions at typical concentration of 100 mM for the RR experiments.

A minimum of three freeze-pump-thaw cycles was employed to obtain anaerobic conditions of the solutions under study. Alternately, a stream of argon or nitrogen was passed into the solution for a mimimum of twenty minutes. Chemical reduction was carried out by mixing solid sodium dithionite was mixed with the air-evacuated detergent solution of hemin under vacuum in a special glass apparatus. The clear solution was then transfered under vacuum to the Raman cell for recording the Raman spectra.

6.3 Results and Discussion

As the Raman active vibrational modes of metalloporphyrins in the high frequency 1300-1700 cm^{-1} region provide sensitive marker bands for the spin and oxidation states of the central metal atom,[16] we concentrated our RR study in this region and also in the low frequency 100-250 cm^{-1} region, whenever relevant, where the metal-axial ligand stretching modes appear.[16] While hemin is normally dimeric in alkaline aqueous solutions,[6,17a,c] previous studies in aqueous detergent micelles[7] have shown that it exists in monomeric form over a large pH range within the hydrophobic region of the micelles and displays an acid-base equilibrium according to following equation:

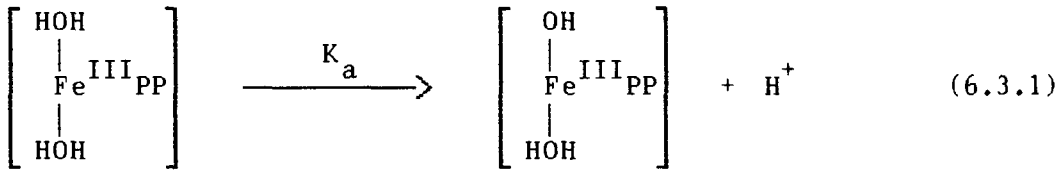

2 1 (6.3.1)

with pK_a values[7b] in TX-100, CTAB and SDS micelles being 4.7, 6.1 and 5.5 respectively. The slight differences in the absorption spectral features of hemin at alkaline pH in the above micellar systems have been

attributed[7b] to possible differences in the orientation or location of hemin within the cationic and anionic micelles, and to interaction of hemin with the hydrocarbon chain or the polyoxyethylene chain of the non-ionic detergent micelle. NMR studies[18a] on hemin in SDS micelles indicate a high spin (S = 5/2) configuration for both species 1 and 2 above in Equation 6.3.1. A comparison of the RR spectral features of hemin obtained in the other two micelles with its spectra in SDS and in organic solvents[17] suggests a similar high spin configuration for hemin in both the cationic and non-ionic micelles used.

6.3.1 TX-100 solutions

The absorption spectra of hemin in TX-100 at alkaline (pH 11) and acidic (pH 3) conditions are shown in Fig. 6.3.1. The solution at pH 11 displays absorption maxima at 360 nm (sh), 400 nm (Soret) and weak bands at 600 and 576 nm. In acidic conditions the bands appear at 388 nm (Soret), 510 and 542 nm (Q bands) and the charge transfer band at 644 nm. The band positions are in good agreement with those reported in literature.[7b] Addition of 250 fold excess of 2-MeIm did not have any significant effect on the absorption spectra of hemin in this micelle at alkaline or acidic conditions. This indicated non-coordination of 2-MeIm under these experimental conditions. Such a behaviour with this nitrogenous ligand has been observed by other workers[18b] in iron mesoporphyrin in CH_2Cl_2. It is pertinent to note that the absorption spectrum of hemin dimer, $(FePP)_2O$, is distinctly different,[17b-d] with a characteristic split Soret band[17b] at 368 and 385 nm and weak Q bands[17b] at 530 and 494 nm. Further, it is interesting to note that the absorption spectrum of hemin in acidic conditions in this micelle as well as in the

other two micelles used is very similar to the spectrum of iron protoporphyrindimethylester in acetonitrile,[17c] in CH_2Cl_2[17g] and in chloroform[2b] (Table 6.3.1).

The RR spectra of hemin in TX-100 in the absence of added nitrogenous ligands under various experimental conditions on laser excitation at 441.6 nm are shown in Fig. 6.3.2. The expected enhancement pattern of the near B band excited spectrum of hemin in aerobic conditions is seen in Trace A. In the spectral region recorded, the A_{1g} modes (ν_4, ν_3 and ν_2) appear at 1372, 1492 and 1570 cm^{-1}, as also the E_u modes (ν_{37} and ν_{38}) at 1594 and 1534 cm^{-1} which are activated by the asymmetric disposition of the vinyl substituents on the porphyrin periphery. There may be a strong overlap of the vinyl stretching frequency ($\nu_{C=C}$) and the ν_{10} mode at 1624 cm^{-1}. The variation in frequency of the ν_{10} mode in iron porphyrins with the nature and the coordination number of the axial ligands has been reported.[19b] The similarity of the RR spectral features to those of five coordinated, high spin (5cHS) iron protoporphyrin complexes,[16,17c] suggests that although a six-coordinated geometry has been proposed for hemin in alkaline aqueous micellar systems,[7b] water may be loosely bound in the sixth coordination site. Such a possiblity of one water molecule differently or loosely bound in iron porphyrins has been pointed out before[17e] even in bis-aquo complexes of hemin. Henceforth we shall refer to the species 1 shown in Equation 6.3.1 as a 5cHS complex.

On degassing the sample, the RR spectrum revealed the presence of a mixture of species. The shift in frequency of the totally symmetric mode ν_4 from 1372 to 1357 cm^{-1} clearly showed the reduction of the iron centre[17c] along with the lowering of the other frequencies of the ν_3, ν_2,

ν_{38} and ν_{10} modes to 1472, 1563, 1584 and 1605 cm^{-1}. Reduction of Fe(III) to Fe(II) without change in the spin state lowers[16] several frequencies by a few cm^{-1}. This has been interpreted as due to increased back donation of electrons from the Fe(II) d_{π} orbitals into the $e_g(\pi^*)$ antibonding porphyrin orbital with a slight reduction in the porphyrin bond strengths. Thus, the ν_4 mode, which is the C_{α}-N symmetric stretching vibration in which the four pyrrole nitrogens are displaced towards the iron ion in-phase during the vibration, decreases in frequency as the $e_g(\pi^*)$ orbital is antibonding with respect to C_{α}-N bond. A comparison with the published data[16,19a] suggest that the observed frequencies can be assigned to a 5cHS ferrous complex. The appearance of weak bands at 1503 $cm^{-1}(\nu_3)$ and 1643 $cm^{-1}(\nu_{10})$ indicate simultaneous presence of small amount of the four coordinated, intermediate spin (4cIS) ferrous[18,19] species in solution. RR spectrum identical to trace B was obtained on chemical reduction of hemin in anaerobic condition at pH 11 (Trace C). When the axial ligand is weak, as in the perchlorate complexes of ferric porphyrins,[18e] or absent as in the four coordinated ferrous porphyrin,[18f] the iron ion is in an intermediate spin state in which the d_{z^2} orbital is lowered in energy and is occupied but the $d_{x^2-y^2}$ orbital is empty. As a result, the in-plane Fe-N(pyrrole) bond is shortened and the core-size and RR frequencies are about the same as in low-spin ferric porphyrin complexes.[18b,19b] The intermediate spin nature of the chemically reduced hemin in the absence of added ligands in CTAB[18c,d] has been established.

The presence of some 5cHS species in the photoreduced (trace B) or chemically reduced (trace C) may be due to the coordination to the iron centre of a water molecule of the ether group of the TX-100 molecule. Such

a possibility has been pointed out[20a] in the Co^{II}(TPP) complex in TX-100 and in Fe^{II}(TPP) derivatives.[20c] The formation of bis aquo ferrous complex, $Fe^{II}PP(H_2O)_2$, on reduction of ferric protoporphyrin in SDS in alkaline conditions by hydrated electrons[8b] has been well documented. Although the RR spectrum of this complex is unavailable, it is remarkable to note that the RR spectrum reported[20d] of the bis hydroxo complex, $Fe^{II}PP(OH)_2$, in aqueous alkaline ethanol is very similar to the spectrum of 5cHS ferrous complex in that its ν_4, ν_3 and ν_2 modes appear at 1355, 1469, and 1559 cm^{-1}, although a six coordination geometry is postulated for this complex. A spectrum similar to trace B was obtained at pH 7 under excitation at 441.6 nm. The RR spectrum of hemin in anaerobic conditions at pH 3 (trace D) showed no indication of photoreduction as observed by others.[8a] The band positions at 1372 $cm^{-1}(\nu_4)$, 1494 $cm^{-1}(\nu_3)$, 1571 $cm^{-1}(\nu_2)$, 1591 $cm^{-1}(\nu_{37})$, 1631 $cm^{-1}(\nu_{10})$ indicate the major species present to be a high spin ferric complex and resemble strongly the RR spectrum of ferric protoporphyrin (IX) chloride in non-coordinating organic solvents[19a] with chloride ion as the axial ligand. Although acid-base equilibrium (equation 6.3.1) presumes coordination of the iron centre by two water molecules in acidic conditions, close association of the negatively charged chloride ion may be indicated by the ν_{10} mode at 1631 cm^{-1} which is close to 1626 and 1632 cm^{-1} reported for the same mode in the Fe^{III}PPCl complex by Choi et al[19a] and Spaulding et al.[19f] The charge neutralization of the bis aquo complex, $Fe^{III}PP(H_2O)_2$ with a single chloride ion may cause one axial water molecule to bind differently than the other giving a near five coordinated configuration. The absorption spectra of hemin in acidic conditions (Fig. 6.3.1) shows a band at 642 nm which is considered[17d] to involve incomplete electron transfer between Fe^{3+} and the chloride ion.

Further, the absorption spectrum[20e] of $FeTPP(H_2O)_2ClO_4$ also shows close similarity to that of FeTPPCl complex with both species exhibiting the β band at 510 nm characteristic of coordination by halide ions.[2a]

The effect of laser excitation at 441.6 nm on the hemin solution containing 2-MeIm in anaerobic and at different pH conditions is illustrated in Fig. 6.3.3, traces A to F. The RR bands at 1355, 1469, 1561, 1585, 1603, and 1623 cm^{-1} (trace C) correspond to the ν_4, ν_3, ν_2, ν_{37}, ν_{10} and the vinyl $\nu_{C=C}$ stretching modes of a 5cHS ferrous complex. An identical RR spectrum obtained on chemical reduction (trace A) confirm the formation of the 5cHS complex due to photoreduction at neutral and alkaline pH conditions (traces C and D). Appearance of a clear band at 205 cm^{-1} in the spectra A', C' and D' in the lower frequency region confirm the axial coordination by 2-MeIm to the ferrous complex.[13,16,21] The same axial mode appears at 195 cm^{-1} when 2-MeIm is replaced by 1,2-MeIm as expected (trace E'). The corresponding high frequency region RR spectrum (trace E) shows the formation of 5cHS ferrous complex $Fe^{II}PP(1,2\text{-MeIm})$ on photoreduction of hemin. Addition of 1% EtOH to the above solution slightly enhanced the intensities of the RR bands of the 5cHS ferrous complex. Trace F corresponds to the RR spectrum of hemin at pH 3 in anaerobic conditions in the presence of 2-MeIm, and as expected, shows no indication of photoreduction (trace D, Fig. 6.3.2). similar to that observed in the absence of 2-MeIm. Trace B in the high frequency region, identical to trace B in Fig. 6.3.2, is redrawn in Fig. 6.3.3 for better comparison purposes to emphasize the photoreduction of hemin at alkaline pH even in the absence of 2-MeIm. Accordingly there is no band corresponding to 205 cm^{-1} band in the lower frequency region. On excitation at 457.9 nm similar photoreduction of hemin was observed

although to a lesser extent but not on $\lambda_{exc} \geq 488$ nm. Table 6.3.2 lists the observed Raman frequencies under various experimental conditions.

From the observations so far, it is clear that the iron protoporphyrin complex coordinated by a hydroxyl ion at neutral and alkaline pH conditions in TX-100 micelle (pK_a = 4.7) is the species which undergoes photoreduction on laser excitation at wavelengths ≤ 458 nm. The following mechanism of photoreduction of hemin in this micelle may be suggested in view of the observation of photoreduction in the absence of 2-MeIm or 1,2-MeIm and their non-coordination in their presence (as inferred by the absorption apectra), under the experimental conditions used.

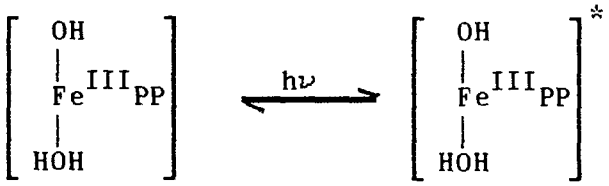

(6.3.2)

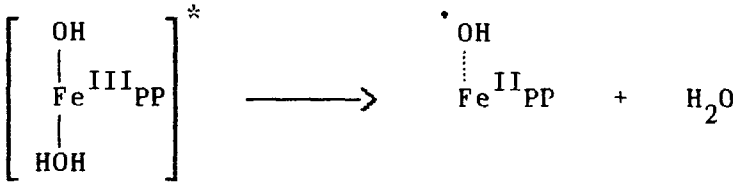

(6.3.3)

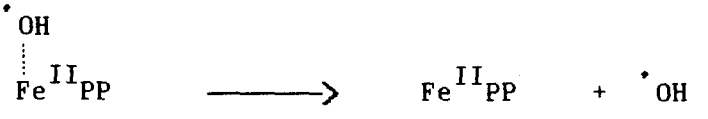

(6.3.4)

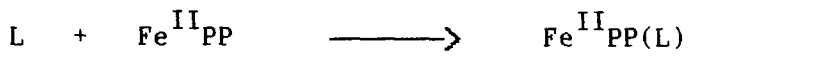

(6.3.5)

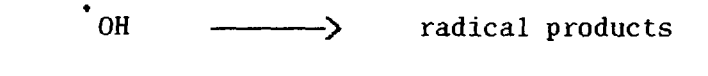

(6.3.6)

where L = H_2O, 2-MeIm or 1,2-MeIm.

In order to confirm our proposition we carried out further systematic UV-VIS and RR studies with hemin solubilized in this micelle in

the presence of imidazole and at different concentrations of the detergent. Fig. 6.3.4 shows the absorption spectra of hemin in 3% TX-100 under varying conditions of pH and concentrations of imidazole. Traces A and B were almost identical with respect to the band positions (398, 576 and 602 nm), although a 200 fold excess imidazole was present in the alkaline (pH 11.4) solution corresponding to the spectrum B. This implies non-coordination of imidazole under these experimental conditions of pH and concentrations. Addition of higher amounts of imidazole at the same pH or decreasing the pH of the solution to neutral conditions at the same or at slightly higher concentrations of imidazole reverted the spectrum to that of a low spin ferric species, $Fe^{III}PP(Im)_2$, indicating coordination of this strong field ligand. The new band positions at 418, 536 and 568 nm were in conformity to those reported in literature.[22a] It is interesting that Debois et al[22c] suggest the existence of an imidazole/imidazolate or bisimidazolate adduct of hemin in CTAB at this pH. However, they note that the RR skeletal frequencies are little affected by the deprotonation of the coordinated imidazole. At pH 3 no coordination is evident even at the highest concentration of imidazole used and the absorption spectrum of hemin has close similarity with its spectrum in the absence of imidazole (trace C, Fig. 6.3.1). It is of interest to note at this stage, that an acid-base equilibrium of hemin in aqueous[23a] solution or in detergent micelles[23b] in the presence of pyridine indicated a hydroxyl ion or water molecule coordinated trans to pyridine. It is unlikely that, imidazole, being a strong field would exhibit such an acid-base equilibrium. Attempts[22f] to stabilize a monoaquo complex in the presence of N-MeIm led to the formation of a 6cLS complex with this nitrogenous ligand. On the other hand, a similar non-coordination of 1-MeIm[22c] or pyridine to the

iron centre in hemin in a CTAB solution at a pH $\geq$ 9.5 has been proposed based on the absorption spectrum similar to that of the hydroxide coordinated species in the presence of these ligands at high alkaline pH. In view of these observations it is clear that even the strong field ligand like imidazole does not coordinate to the iron atom in hemin at low concentrations and alkaline pH conditions when the latter is encapsulated within the detergent micelle. It has been observed by other workers[22d] also that higher concentrations of imidazole than usual was neceassary to achieve complete formation of this low spin complex in detergent micelles. While the binding constant of imidazole to hemin is of the order of 10^6 M^{-2} in organic solvents,[2a] it is enormously reduced in detergent micelles[7c] (β_2 = 0,44 M^{-2}, in TX-100). However, the increase in the binding constants of imidazole to iron porphyrins as a function of its concentration has been demonstrated by Coyle et al.[24]

The RR spectra of hemin in TX-100 under various conditions of pH and other experimental conditions in the presence of imidazole under excitation at 441.6 nm is shown in Fig. 6.3.5. In aerobic conditions at pH 11 (trace A), the major RR bands at 1371, 1492, 1568 cm^{-1} corresponding to the ν_4, ν_3 and ν_2 modes respectively show the presence of 5cHS ferric species under these conditions (complex 1). However, presence of minor quanitities of 6cLS ferric species with imidazole as axial ligands is discernible from the weak shoulders at 1502 and 1640 cm^{-1}, and a band at 1580 cm^{-1} corresponding to the ν_3, ν_{10} and ν_2 modes of the latter. On degassing the solution, the RR spectrum (trace B) showed bands at 1359, 1491, 1583 cm^{-1} along with weak band at 1604 cm^{-1}. A comparison with the published data of RR frequencies of imdidazole complexes of hemin[22a] allows assignment of these Raman frequencies to ν_4, ν_3, ν_2 and ν_{10} modes

respectively. At pH 10 and 7 (traces C and D) the extent of formation of 6cLS ferrous complex decreased as seen by the decrease in the relative intensity of the ν_4 and ν_3 modes of the ferrous and the ferric low spin complexes at 1359 and 1372 cm^{-1}, and 1491 and 1503 cm^{-1} respectively. The enhanced intensity of the ν_{10} mode at 1640 cm^{-1} in trace C is another indicator larger presence of 6cLS species. Traces E and F show respectively the RR spectra of hemin in the presence of excess imidazole in 3% TX-100 and in simple aqueous alkaline solution in anaerobic conditions and indicate the predominant presence of 6cLS species which is not photoreduced. It has been, however, observed[22a] earlier that the RR frequencies of hemin complexes are essentially the same in water, detergent or organic solvents.

The dependence of photoreduction of hemin in TX-100 in the presence of imidazole at pH 11, as a function of the concentration of the detergent is depicted in Fig. 6.3.6. Since a 2% concentration of TX-100 corresponds to its critical micelle concentration, it is seen from traces B, C and D that as the concentration of the detergent is reduced from 3% to 0.0006%, the extent of formation of the 6cLS complex, $Fe^{II}PP(Im)_2$, on photoreduction of hemin, is also decreased as the proportion of the photoreducible monomeric ferric high spin species is reduced due to the non-availablity of sufficient number of micelles at lower concentration of the detergent. Simultaneously, the proportion of the non-photoreducible low spin ferric complex increases. This can be seen from the steady increase in the relative intensity of the 1371 $cm^{-1}(\nu_4)$, 1503 $cm^{-1}(\nu_3)$ and 1639 $cm^{-1}(\nu_{10})$ bands of the 6cLS species, $Fe^{III}PP(Im)_2$. Thus, it is clear that the observed RR spectra in Fig. 6.3.6 is due to increasing concentration of the low spin bisimidazole complex of hemin in the aqueous

phase and decreasing concentration of the monohydroxomonoaquo high spin species within the micellar phase as the concentration of the detergent is reduced. Since only the latter species is photoreducible, the extent of formation of the ferrous complex is proportional to the concentration of this species. Thus, this further supports the mechanism proposed by us in equations 6.3.2. to 6.3.6 for photoreduction of hemin in this micelle. Hence, in the presence of imidazole the process can be depicted, following Equations 6.3.2 to 6.3.4 as:

$$2L' + Fe^{II}PP \longrightarrow Fe^{II}PP(L')_2 \qquad (6.3.7)$$

where L' = imidazole.

Several workers[9,11] have observed the photoreducibility of only the "base" form of iron porphyrin in aqeuous ethanol or pyridine-water-ethanol mixed solvents in which the iron atom is coordinated by a hydroxyl or alcoholate anion along with either a pyridine or alcohol molecule but not under conditions when the hydroxyl or the alcoholate moiety was protonated. A CT band at $\approx$ 335 nm was suggested[11e] to be responsible for photoreduction of the alcoholate coordinated FeTPP complex on excitation at $\lambda_{exc} < 400$ nm. Interestingly, we observe a distinct shoulder around 360 nm in the absorption spectrum of the hydroxo complex of hemin at alkaline pH conditions in all the three micellar systems studied which is absent in acidic conditions. In the absence of alcohol, this band may have a CT (OH ——>Fe) character in hemin in micellar systems. Such a band is absent in the absorption spectrum of $Fe^{III}PPCl$ in organic solvents and the band in the 630-640 nm region is present indicative of association of the chloride ion with the iron centre.[17d]

Despite extensive observations that photoreduction of iron porphyrins in aqueous or mixed solvents containing pyridine or ethanol occured only at alkaline pH conditions, the role of the hydroxyl ion at the axial site in the photoreduction process has not been very clear. Nevertheless, photoreduction of iron porphyrins containing only hydroxyl ion in the axial positions have been reported by Tohara et al[15c] in the Fe^{III}(TMP)OH complex (which, interestingly exhibits a clear absorption band at ≈ 330 nm) on excitation at $\lambda > 300$ nm. Bartocci et al[15e] reported photoreduction of Fe(TDCPP)OH [iron(III) tetrakis (2, 2 dichlorophenyl) porphyrin] on excitation at 365 nm. Langford et al[15a] reported photoreduction of (non-porphyrin) hexaaquoFe(III) complex on excitation at 254 nm near the H_2O —> Fe^{III} CT transition at 240 nm (the CT transition OH —> Fe^{III} was believed[15a] to be at ≈ 300 nm). Electron transfer from the coordinated hydroxyl ion to the iron atom in hemin in aqueous ethanolic solvent containing pyridine was considered[9a] as one of the mechanisms of photoreduction of hemin on excitation at 365 nm but no clear conclusion was arrived at as the LMCT band (OH —> Fe^{III}) in the hydroxyl ion coordinated Fe^{III}PP(OH)(Py) complex was considered to be at lower wavelengths than 300 nm. Only the hydroxo species, Fe^{III}PP(OH)(Py) was, however, shown to be photoreducible[9a] in the presence of ethanol, although, as the ESR spin trapping experiments[9c] showed the formation of hydroxyethyl radical on photoexcitation, electron transfer from pyridine to iron was considered to be inefficient under the experimental conditions. Interestingly, the absorption spectrum[23b] of hemin in detergent micelles at alkaline pH conditions in the presence of pyridine shows a clear shoulder at ≈ 350 nm.

6.3.2 CTAB Solutions

The optical absorption spectra of hemin in aqueous CTAB solutions at alkaline and acidic conditions are shown in Fig. 6.3.7. The band positions are in good agreement with the reported values.[7] Addition of 200 to 2000 fold excess amount of 2-MeIm at pH 11 gave a spectrum identical to the one in its absence. This implies non-coordination of 2-MeIm under these experimental conditions. It is of interest to note that the absorption spectra of hemin in TX-100 and CTAB are very similar with almost identical band positions at corresponding pH conditions.

Fig. 6.3.8 shows the RR spectra of hemin in CTAB obtained with laser excitation at 441.6 nm. Trace A shows the spectrum at pH 11 in aerobic conditions with band positions at 1373, 1490, 1570, 1590 and 1626 cm^{-1} comparing well with those of 5cHS ferric complexes in organic solvents.[19a] These were also identical with the RR spectrum of hemin in TX-100 under identical conditions and are assignable to ν_4, ν_3, ν_2, ν_{37} and ν_{10} modes respectively. On degassing the sample, the spectrum developed new features. Bands at 1638 $cm^{-1}(\nu_{10})$, 1583 $cm^{-1}(\nu_2)$, 1505 $cm^{-1}(\nu_3)$ and 1372 $cm^{-1}(\nu_4)$ clearly indicates formation of 4cIS ferrous complex similar to that observed in TX-100 micelle and are identical to the RR spectrum obtained on chemical reduction[22e] of hemin in anaerobic conditions (trace B'). The weak intensity of these bands (in trace B') compared to the RR bands corresponding to the 5cHS ferric complex which also appear at 1570 $cm^{-1}(\nu_2)$, 1491 $cm^{-1}(\nu_3)$ and 1372 $cm^{-1}(\nu_4)$ may be due to not so perfect degassing of the solution. The shoulder at 1360 cm^{-1} and a weak band at 1605 cm^{-1} may indicate minor presence of 5cHS ferrous complex with a water molecule coordinated to the ferrous porphyrin. The RR

spectrum obtained in the presence of 2-MeIm in anaerobic conditions (trace C) shows the bands at 1604 $cm^{-1}(\nu_{10})$, 1585 $cm^{-1}(\nu_{37})$, 1562 $cm^{-1}(\nu_2)$, 1471 $cm^{-1}(\nu_3)$ and 1355 $cm^{-1}(\nu_4)$ corresponding to the formation of a 5cHS ferrous complex. Addition of trace amount of ethanol ($\approx$ 1%) had no further effect on the RR spectrum except the enhancement in the intensities of the bands corresponding to the 5cHS species (trace D). The RR band at 205 cm^{-1} in the low frequency region confirms the coordination of 2-MeIm at the axial position of the ferrous complex. The similarity of the RR spectra in traces C, C' and F, F' to the spectra obtained (trace E, E') on chemical reduction of hemin in the presence of 2-MeIm under otherwise identical conditions further confirm the photoreduction of hemin in CTAB on excitation at 441.6 nm under anaerobic, neutral and alkaline pH conditions. Similar photoreduction was observed in the presence of 1,2-MeIm. Under identical conditions similar photoeduction of hemin was observed on $\lambda_{exc} \leq 457.9$ nm . No photoreduction under acidic (pH 3) conditions was, however, observed in the presence of 2-MeIm or 1,2-MeIm. The observed RR frequencies are listed in Table 6.3.2.

When 2-MeIm was replaced by imidazole, the RR spectra of hemin in CTAB obtained at alkaline anaerobic conditions with laser excitation at 441.6 nm clearly showed bands corresponding to the formation of the low spin ferrous complex similar to our earlier observation in TX-100 micelle. (See Fig. 6.3.14, trace C) Excitation at 457.9 nm laser light (spectra not shown) of an anaerobic solution of hemin in CTAB in the presence of 2-MeIm at alkaline to neutral pH conditions resulted in the photoreduction of hemin confirmed by the appearance of the $\nu(Fe\text{-}N_{axial})$ stretching mode of the 2-MeIm coordinated ferrous complex at 205 cm^{-1} and by the other characteristic RR bands.

6.3.3 Aqueous alkaline solutions

Fig. 6.3.9 show identical high frequency RR spectra obtained on excitation at 441.6 nm at pH 11 of hemin solubilized in aqueous NaOH in the absence and presence of 2-MeIm in anaerobic conditions. Clearly, there is no photoreduction observed. The spectra correspond to the 5cHS μ-oxo dimer, $(FePP)_2O$. The RR frequencies of this ferric dimer is known to be identical[22a] to its monomer ferric complex, FePPCl. However, the aggregated nature of the species may be inferred[19c] from the higher ratio of the intensities of the ν_3 and ν_4 modes at 1494 and 1373 cm^{-1} in NaOH compared to that in CTAB or TX-100. In contrast to the hindered ligand, 2-MeIm, the presence of the strong field ligand, imidazole, results in the formation of the low spin complex in simple NaOH solution (Fig. 6.3.5, trace F).

6.3.4 SDS Solutions

The UV-VIS absorption spectra of hemin in SDS shown in Fig. 6.3.10 exhibit band positions are in conformity with the published values.[7,8a,18a] The porphyrin to metal charge transfer band occuring at higher energy in the hydroxo complex compared to the aquo complex has been attributed to the decreased positive charge on the iron centre and increased ligand basicity in the former.[18a] It is, however, pertinent to note that the absorption spectrum of hemin in SDS differs slightly from that observed in TX-100 and CTAB micelles (Table 6.3.1). The 576 nm band is very much weak or lacking in SDS and weak absoption bands are seen at 488 and 525 nm which are not found in the spectra of hemin in the other two micelles.

The RR spectra of hemin in 3% SDS under various experimental conditions obtained on laser excitation at 441.6 nm is shown in Fig. 6.3.11. Traces A and C show the spectra of hemin in the absence and presence of 2-MeIm respectively in anaerobic conditions at pH 11. The similarity of the band positions at 1629 $cm^{-1}(\nu_{10})$, 1592 $cm^{-1}(\nu_{37})$, 1572 $cm^{-1}(\nu_2)$, 1492 $cm^{-1}(\nu_3)$ and 1373 $cm^{-1}(\nu_4)$ characteristic of the ferric species in both the spectra indicate no photoreduction of hemin under these conditions. Addition of trace amount of ethanol ($\approx$ 1%) along with 2-MeIm in anaerobic conditions had a dramatic effect on the RR spectra. New RR bands appeared at 1624 cm^{-1} ($\nu_{C=C}$), 1604 cm^{-1} (ν_{10}), 1584 cm^{-1} (ν_{37}), 1562 cm^{-1} (ν_2), 1470 cm^{-1} (ν_3) and 1355 cm^{-1} (ν_4) corresponding to that of a 5cHS ferrous species confirmed by the identical spectrum obtained on chemical reduction of hemin (trace F) in the presence of 2-MeIm in SDS under similar experimental conditions. The axial coordination of 2-MeIm to the ferrous complex in both cases is confirmed by the $\nu(Fe\text{-}N_{ax})$ mode at 205 cm^{-1} as observed before in the other two micelles. No photoreduction of hemin was observed in the presence of 1% (or $\approx$ 2%) ethanol in the absence of 2-MeIm at alkaline pH (trace B), or at neutral or acidic pH conditions in the presence of 2-MeIm and ethanol (trace E). The photoreduction of hemin in SDS in the absence of nitrogenous ligands reported by Bizet et al[8a] may be due to the higher concentration of alcohol used (0.8M).

In order to understand the effect of ethanol on hemin in SDS micelle, we carried out some optical absorption studies. Traces A and B in Fig. 6.3.12 shows the essentially unaltered optical absorption spectra of hemin in the absence and presence of 200 fold excess of 2-MeIm or

1,2-MeIm. Addition of ethanol (1%) to the solution containing 2-MeIm did not affect the spectrum significantly. Addition of ethanol (10%) showed a slight shift of the 600 nm band to ≈ 590 nm (trace D). Similar effect was observed when ethanol (10%) was added in the absence of 2-MeIm (trace E). These parallel similar report by Bizet et al[8a] who observed a blue shift of the 600 nm band when pentanol (0.8 M) was added to an SDS solution containing hemin and associated the change to partial formation of alcoholate-alcohol coordinated hemin. This blue shift of the porphyrin to metal charge transfer band may indicate a further substantial decrease in the positive charge on iron with increased ligand basicity.[18a] We also note a remarkable similarity of our spectra of hemin (trace D and E) to the absorption spectra of hemin[9a] solubilized in aqueous pyridine-ethanol mixed solvent (concentration of ethanol = 40%) at pH 12.5 which was attributed[9c] to the complex, $Fe^{III}PP(OH)(EtO)$.

In order to investigate the effect of the surface charge of SDS on the photoreducibility of hemin, we carried out experiments in the presence of added salts like tetrabutylammonium chloride (TMAB) and NaCl. Earlier reports[7a] suggested that the charge neutralization of the surface charges of the SO_4^- ions of SDS micelles by the tetrabutylammonium cation of TMAB, was responsible for the enhanced formation of the dicyanohemin complex in SDS. The charge neutralization presumably facilitated the approach of the negatively charged CN^- ions to within the micelles for coordination to the iron centre in hemin intercalated within the micelles. Fig. 6.3.13 (traces E, C, and A) shows the RR spectra of hemin in 3% SDS in the presence of 2-MeIm (100 mM) in anaerobic conditions in the presence of 0.02, 0.08 and 0.1 M of TMAB respectively. They are identical in major RR bands at 1373, 1494, 1573, 1595 and 1627 cm^{-1} corresponding to ν_4, ν_3,

ν_2, ν_{37} and ν_{10} modes of the ferric high spin species and show no photoreduction at any concentration of TMAB used. Addition of 1% ethanol, however, had the same effect observed previously in the absence of TMAB. The new RR bands at 1355, 1471, 1562, 1584, 1604 and 1622 cm^{-1} corresponding to the ferrous five coordinated species ν_4, ν_3, ν_2, ν_{37} and ν_{10} and the $\nu_{C=C}$ modes of the ferrous high spin complex, Fe^{II}(PP)2-MeIm. Once again the ν(Fe-N_{ax}) stretching frequency confirm photoreduction of hemin and axial coordination by 2-MeIm (Traces B', D' and F'). No photoreduction of hemin was observed at pH 7 in the presence of TMAB and 2-MeIm even in the presence of ethanol similar to our previous observation in the absence of TMAB. Salts like NaCl when added to micellar solution decrease the electrostatic repulsion[25] between the charged head groups and reduce the surface potential.[25c] At high concentrations of NaCl, SDS micelle is suggested to behave like non-ionic ones.[25] However, the RR spectrum of hemin in SDS micelle containing 0.4 M NaCl and 2-MeIm at pH 11 under anaerobic conditions was identical to the spectrum shown in trace A, Fig. 6.3.11 and no photoreduction was observed. Hence the non-photoreducibility of hemin in the absence of added alcohol (at low concentrations) may be due to a more localized effect.

The binding constant of imidazole to hemin in micellar medium[7c] is enormously reduced compared to their values in organic solvents.[2a] However, the binding constant is larger[7c] by an order of magnitude in SDS than in TX-100 and CTAB micelles. The RR spectrum of an anaerobic alkaline solution of hemin (0.5 mM) in 3% SDS containing 50 mM imidazole showed typical features of 6cLS ferric species, $Fe^{III}PP(Im)_2$, under laser excitation at 441.6 nm (See Fig. 6.3.14, trace A). However, in the presence of ethanol, partial photoreduction of hemin was observed

indicated by the ν_4, and ν_2 modes appearing as shoulders at 1360 and 1491 cm^{-1}. This clearly shows that, as the 6cLS ferric complex, $Fe^{III}PP(Im)_2$, is not photoreducible[13a] there must be some ferric high spin species in SDS which are not converted to low spin complexes at the concentration of the imidazole used, but which were converted to photoreducible species on addition of ethanol. Coordination of free imidazoles to the photoreduced species stabilized the reduced complex.

Excitation at 457.9 nm of hemin in SDS under experimental conditions identical to those used earlier with 441.6 nm excitation did not result in photoreduction of hemin.

It is, at this, stage, pertinent to consider the location of hemin in the micelles. A radial type of alignment of hemin has been proposed by many workers.[7c,8b,26] NMR experiments[26a] on hemin in SDS suggested its location such that the iron atom lies 5 Å inside the micellar surface with the hydrophollic propionic acid groups directed towards the micellar surface. As the diameter[27a] of the sulphate head groups is 4.6 Å, the iron atom in hemin is close to the negatively charged oxygen atoms of the sulphate group in contrast to Fe(OEP) complex[26b] which is located within the core of the micelle. In cationic CTAB micelle a similar near surface location of hemin was postulated.[7c] In TX-100, the large aggregation number of the micelle does not permit well separated hydrophyllic and hydrophobic regions of the micelle.[27b] Extensive hydration of the ether groups of the polyoxyethylene chain of TX-100 molecule may facilitate intercalation of hemin such that the hydrophobic parts of hemin may be within the hydrophobic core of the micelle.

Although hemin was observed[8a] to undergo photoreduction in alkaline SDS only in the presence of primary alcohols, no explanation was put forward as to its non-photoreducibility in the absence of alcohols. In view of our observation of photoreduction of hemin in TX-100 and CTAB even in the absence of nitrogenous ligands and/or alcohol in anaerobic conditions, it becomes important to try to understand the possible factors governing such behaviour. In cationic CTAB micelle, the deprotonated propionic acid groups at neutral and alkaline conditions may be engaging in electrostatic interactions with the positive charges on the quarternary ammonium head groups of the micelle or in H-bond interactions with the water molecules in the Stern layer. In TX-100, hydrated ether groups or terminal hydroxo groups provide possible sites for similar H-bond interactions even within the micelle for the ionized carboxylic moiety (COO^-) of the propionic acid chain. On the other hand, in SDS, the negative charge on the sulphate head groups may repel the negatively charged COO^- groups causing a bending back of the propionic acid chain over the porphyrin ring to facilitate H-bond interactions with the axial hydroxo and/or the water molecule. Alternatively, the axial ligands may engage in similar H-bond interactions with the oxygen of the sulphate head groups of SDS due to their close proximity. Both situations, in SDS, effectively stabilize the higher positive charge on iron.

The effect of alcohols on SDS micelles has been extensively studied.[25,28] In general, it has been observed that addition of alcohols leads to increased water penetration[28b] into the micellar interface at low alcohol concentrations (< 25 mM) and a decrease[28c] in the dielectric constant at the surface.[28b,c] The surface charge density and the surface potential decreases on addition of alcohols.[25e]

Photoreduction of hemin in SDS in the presence of higher concentrations of ethanol (40%) may be influenced by these above factors, apart from coordination[8a,9] of the ethanolate anion to the iron centre. In our experiments with hemin in SDS, low concentrations of ethanol ($\approx$ 1%) in the absence of 2-MeIm had no appreciable effect on the RR spectrum. This may be due to the lower energy of excitation used in view of the established CT transition at $\approx$ 335 nm for the ethanolate coordinated iron porphyrins.[11e] However, in the presence of 2-MeIm, and 1% ethanol photoreduction of hemin was observed in anaerobic conditions. At low concentrations of ethanol in the presence of 2-MeIm a mechanism similar to the one proposed by Uno et al[29] may be operative. The formation of the ethanolate moiety and its coordination leading to photoreduction of hemin in SDS may be depicted by the following scheme:

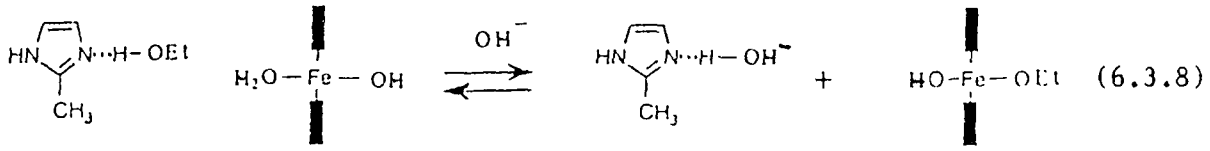

(6.3.8)

The added 2-MeImH may engage in H-bonding with ethanol and promote the formation of the ethanolate moiety which replaces the weakly bound water molecule at the iron atom. The high concentration of OH^- at alkaline pH deprotonates the 2-MeImH$_2$ complex (Equation 6.3.8). Absence of photoreduction of hemin in SDS at neutral pH even in the presence of ethanol may be due to the low pK_a[30] of 2-MeIm (7.56) and absence of formation of ethanolate coordinated hemin. Once the ethanolate moiety has coordinated, the photoreduction process may proceed according to the scheme proposed by Bartocci et al.[9]

(6.3.9)

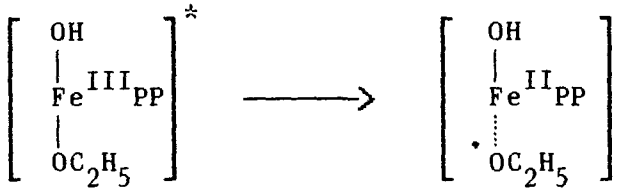

(6.3.10)

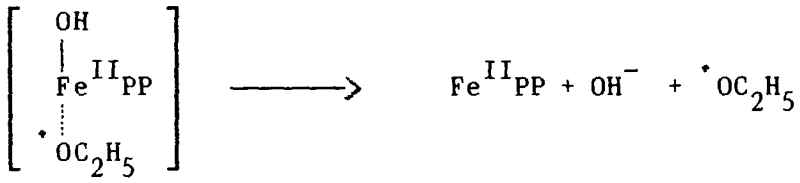

(6.3.11)

followed by equations 6.3.5 and 6.3.7. As before, the four coordinated, intermediate spin photoproduct is stabilized by coordination of available free imidazole ligand(s) in solution. The ethoxy radical can generate a hydroxyethyl radical, which being a strong reducing agent[31] causes secondary reductions increasing the yield of the ferrous porphyrin.

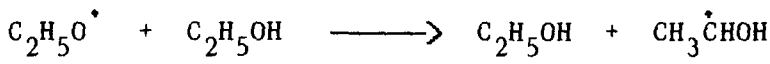

(6.3.12)

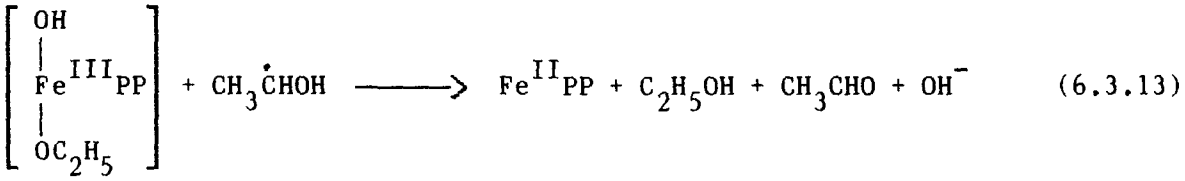

(6.3.13)

The low affinity[8c,32] of the hydroxyl ion to the ferrous porphyrin except at very high pH where there is evidence of dihydroxy species[8d,20b] is well documented.

In view of the above suggested mechanisms of photoreduction of hemin in SDS, non-photoreducibility of hemin in the absence of nitrogenous ligand like 2-MeIm even in the presence of ethanol (1%) may be due to the low concentration of the ethanolate coordinated hemin within the micelle and also due to the fast cage recombinations[11e] of the photoproducts to form the starting ferric complex. This is borne out by our RR experiments in the presence of imidazole and ethanol where a partial photoreduction of hemin was observed leading to the formation of the 6cLS ferrous complex, $Fe^{II}PP(Im)_2$, (Fig. 6.3.14), inspite of the predominant species being the non-photoreducible 6cLS ferric complex, $Fe^{III}PP(Im)_2$. This suggests that some hemin monomers within the SDS micelle are not converted to low spin ferric species at the concentration of the imidazole used and at the pH conditions employed but are converted to photoreducible species.

Absence of photoreduction of hemin in SDS micelle the presence of 2-MeIm and ethanol on excitation at 457.9 nm is consistent with the earlier report[9a] of decreasing quantum yield of photoreduction of hemin coordinated axially by the ethanolate moiety with increasing wavelength of excitation from 365 to 436 nm.

It is interesting to note that the behaviour of hemin and its derivatives in SDS micelle is very similar to that in simple alkaline solutions in many respects.. In the presence of 2-MeIm or small quanitity of ethanol the observed photochemical behaviour of hemin in SDS under alkaline ocnditions has been very similar to that in simple aqueous alkaline solutions. This may be due to the lesser hydrophobicity of SDS micelle compared to those of CTAB and TX-100 micelles. Kinetic studies[23b] of hemin and its derivatives in micellar systems in the presence of

pyridine have shown close similarity of SDS micelle and simple aqueous systems which was attributed to the difference in the hydrophobicity of the micelles.

We can summarize our main results as follows. Photoreduction of hemin in the cationic CTAB and non-ionic TX-100 micelles on near Soret excitation under alkaline anaerobic conditions is effected by electron transfer from the coordinated hydroxyl ion to the iron centre yielding a stable four coordinated, intermediate spin ferrous species. In the presence of imidazoles, the complex was stabilized as imidazole adduct. Only the monomer species coordinated by a hydroxyl ion and encapsulated within the micelle was photoreducible. In anionic SDS micelle, simultaneous presence of trace amount of ethanol and 2-MeIm was necessary for observation of photoreduction of hemin. Electron transfer under photoexcitation in this case is most likely from the coordinated ethanolate anion to the iron atom. No photoreduction was observed in any of the micelles under acidic conditions irrespective of the presence or absence of ethanol and/or imidazoles even at λ_{exc} = 441.6 nm. Higher relative yield of photoreduced species on excitation at 441.6 than at 457.9 nm indicates a possible coupling of the process to the Soret transition or to a CT transition in the 350 nm region.

REFERENCES

1. (a) Perutz, M.F. *Nature* (London), 1970, 228, 726.
   (b) Gisbon, Q.H. In *The Porphyrins*; Dophin, D., Ed.; Academic Press: New York, 1978; Vol. V, pp 153.
   (c) James B.R. In *The Porphyrins*; Dophin, D., Ed.; Academic Press: New York, 1978; Vol. V, pp 205.

2. (a) Walker, F.A.; Lo, M. W.; Ree, M.T. *J. Am. Chem. Soc.* 1976, 98, 5552.
   (b) Yoshimura, T.; Ozaki, Y. *Bull. Chem. Soc. Jpn.* 1979, 52, 2268.

3. (a) Walker, F.A. *J. Am. Chem. Soc.* 1979, 102, 3254.
   (b) Goff, G. *J. Am. Chem. Soc.* 1979, 102, 3252.
   (c) Satterlee, J.D.; La Mar, G.N.; Frye, J.S. *J. Am. Chem. Soc.* 1976, 98, 7275.
   (d) Satterlee, J.D.; La Mar, G.N. Bold, T.J. *J. Am. Chem. Soc.* 1977, 99, 1088.
   (e) Snyder, J.D.; La Mar, G.N. *J. Am. Chem. Soc.* 1976, 98, 4419. 100, 2400.

4. Kadish, K.M. In *Iron Porphyrins*; Lever, A.P.B.; Gray, H.B., Eds.; Addison-Wesley: Reading, MA, 1983; Part II, pp 161.

5. Pasternak, R.F.; Gilles, B.S.; Stahlbush, J.R. *J. Am. Chem. Soc.* 1978, 100, 2613.

6. (a) Davies, T.H. *Biochim. Biophys. Acta.* 1973, 329, 108.
   (b) Hasinoff, B.B.; Dunford, H.B.; Horne, D.G. *Can. J. Chem.* 1969, 47, 3225.

7. (a) Simplicio, J. *Biochemistry*, 1972, 11, 2525 and 2529.
   (b) Simplicio, J.; Schwenzer, K. *Biochemistry*, 1973, 12, 1923.
   (c) Simplicio, J.; Schwenzer, K.; Maenpa, F. *J. Am. Chem. Soc.* 1975, 97, 7319.
   (d) Minch, M.J.; La Mar, G. N. *J. Phys. Chem.* 1982, 86, 1400.

8. (a) Bizet, C.; Morliere, P.; Brault, D.; Delgado, O.; Bazin, M.; Santus, R. *Photochem. Photobiol.* 1981, 34, 315.
   (b) Evers, E.L.; Jayson, G.G.; Swallow, A.J. *J. Chem. Soc., Farad. Trans. 1.* 1978, 74, 418.
   (c) Philips, J.N. *Rev. Pur. Appl. Chem.* 1960, 10, 35.
   (d) Keilin, J. *Biochem. J.* 1949, 45, 448.

9. (a) Bartocci, C.; Scandola, F.; Ferri, A. Carassiti, V. *J. Am. Chem. Soc.* 1980, 102, 7067.
   (b) Bartocci, C.; Maldotti, A.; Traverso, O.; Bignozzi, C.A.; Carassiti, V. *Polyhedron.* 1983, 2, 97.
   (c) Maldotti, A.; Bartocci, C.; Amadelli, R.; Carassiti, V. *Inorg. Chim. Acta.* 1983, 74, 275.

(d) Bartocci, C.; Amadelli, R.; Maldotti, A.; Carassiti, V. *Polyhedron.* **1986**, 5, 1297.
(e) Maldotti, A.; Bartocci, C.; Chiorboli. C.; Ferri, A,; Carassiti, V. *J. Chem. Soc.*, Chem. Commun. 1985, 881.

10. (a) Kitagawa, T.; Chihara, S.; Fushitani, K.; Morimoto, H. *J. Am. Chem. Soc.* 1984, 106, 1860.
(b) Kitagawa, T.; Nagai, K. *Nature*, 281, 503.
(c) Adar, F.; Yonetani, Y. *Biochim. Biophys. Acta.* 1978, 502, 80.

11. (a) Maldotti, A.; Bartocci, C.; Amadelli, R.; Carassiti, V. *J. Chem. Soc., Dalton. Trans.* 1989, 1197.
(b) Hatano, K.; Ishida, Y. *Bull. Chem. Soc. Jpn.* 1982, 55, 3333.
(c) Hatano, K.; Usui, K.; Ishida, Y. *Bull. Chem. Soc. Jpn.* 1981, 54, 413.
(d) Bartocci, C.; Maldotti, A.; Varani, G.; Battioni, P.; Carassiti, V.; Mansuy, D. *Inorg. Chem.* 1991, 30, 1255.
(e) Hoshino, M.; Ueda, K.; Takahashi, M.; Yamaji, M.; Hama, Y. *J. Chem. Soc., Farad. Trans.* 1992, 88, 405.

12. (a) Hendrickson, D.N.; Kinnaird, M.G.; Suslick, K.S. *J. Am. chem. Soc.* 1987, 109, 1243.
(b) Suslick, K.S.; Bautista, J.F.; Watson, R.S. *J. Am. Chem. Soc.* 1991, 113, 6111.
(c) Imamura, T.; Jin, T.; Suzuki, T.; Fujimoto, M. *Chem. Lett.* 1985, 847.

13. (a) Ozaki, Y.; Iriyama, K.; Ogoshi, M.; Kitagawa, T. *J. Am. Chem. Soc.* 1987, 109, 5583.
(b) Fidler, V.; Ogura, T.; Ozaki, Y.; Kitagawa, T. *Chem. Phys. Lett.* 1990, 169, 457.
(c) Fidler, V.; Ogura, T.; Sato, S. Aoyagi, K.; Kitagawa, T. *Bull. Chem. Soc. Jpn.* 1991, 54, 2315.

14. (a) Gu, Y.; Li, P.; Sage, T.; Champion, P.M. *J. Am. Chem. Soc.* 1993, 115, 4993.
(b) Sato, S.; Kamogawa, K.; Aoyagi, K.; Kitagawa, T. *J. Phys. Chem.* 1992, 96, 10676.

15. (a) Langford, C.H.; Carey, J. *Can. J. Chem.* 1975, 53, 2430.
(b) Carey, J.; Langford, C.H. *Can. J. Chem.* 1975, 53, 2436.
(c) Tohara, A.; Sato, M. *Chem. Lett.* 1989, 153.
(d) Walling, C. *Acc. Chem. Res.* 1975, 8, 125.
(e) Maldotti, A.; Bartocci, C.; Amadelli, R.; Polo, E.; Battioni, P.; Mansuy, D. V. *J. Chem. Soc.*, Chem. Commun. 1991, 1486.

16. (a) Kitagawa, T.; Ozaki, Y. *Struct. Bonding (Berlin)* 1987, 64, 71.
(b) Spiro, T.G.; Czernuszewicz, R.S.; Li, X.Y. *Coord. Chem. Rev.* 1990, 100, 541.
(c) Spiro, T.G. In *Iron Porphyrins*; Lever, A.P.B.; Gray, H.B., Eds.; Addison-Wesley: Reading, MA, 1983; Part II, pp 91.
(d) Spiro, T.G.; Li, X.Y. In *Biological Applications of Raman Spectroscopy*; Spiro, T.G., Ed.; Wiley-Interscience: New York, 1988; Vol. 3. pp 1.

17. (a) Goff, H.; Morgan, L.O. *Inorg. Chem.* 1976, 15, 2062.
(b) DeVito V.; Asher, S.A. *J. Am. Chem. Soc.* 1989, 111, 9143.
(c) Sanchez, L.A.; Spiro, T.G. *J. Phys. Chem.* 1985, 89, 763.
(d) Momenteau, M. *Biochim. Biophys. Acta.* 1973, 304, 814.
(e) Brown, S.B.; Dean, T.C. Jones, P. *Biochem. J.* 1970, 117, 733.
(f) Brown, S.B.; Lantzke, I.R. *Biochem. J.* 1969, 115, 279.
(g) Chaudhury, N.K. Ph.D. Thesis, 1988, North-Eastern Hill University, Shillong, India.

18. (a) Mazumdar, S.; Medhi, O.K.; Mitra S. *Inorg. Chem.* 1988, 27, 2541.
(b) Spiro, T.G.; Burke, J.M. *J. Am. Chem. Soc.* 1976, 98, 5482.
(c) Medhi, O.K.; Mazumdar, S.; Mitra S. *Inorg. Chem.* 1989, 28, 3243.
(d) Medhi, O.K.; Silver, J. *J. Chem. Soc., Chem. Commun.* 1989, 1199.
(e) Kastner, M.E.; Scheidt, W.R.; Mashiko, T.; Reed, C.A. *J. Am. Chem. Soc.* 1978, 100, 666.
(f) Collman, J.P; Hoard, J.L.; Kim, N.; Lang, G.; Reed, C.A. *J. Am. Chem. Soc.* 1975, 97, 2676.

19. (a) Choi, S.; Spiro, T.G.; Lngry, K.C.; Smith, K.M.; Budd, D.L.; La Mar, G.N. *J. Am. Chem. Soc.* 1982, 104, 4345.
(b) Teroaka, J.; Kitagawa, T. *J. Phys. Chem.* 1980, 84, 1928.
(c) Verma, A.L.; Chaudhury, N.K. *J. Raman. Spectroscopy.* 1991, 22, 427.
(d) Kitagawa, T.; Teraoka, J. *Chem. Phys. Lett.* 1979, 63, 443.
(e) Spiro, T.G.; Strong, J.D.; Stern, P. *J. Am. Chem. Soc.* 1979, 101, 2648.
(f) Spaulding, L.D.; Chang, C.C. Yu, N-T.; Felton, R.H. *J. Am. Chem. Soc.* 1975, 97, 2517.

20 (a) Lerner, D.A.; Quintal, H.B.; Maillard, P.; Giannoti, C. *J. Chem. Soc., Perkin. Trans. 2,* 1990, 1105.
(b) Falk, J.E. In *Porphyrins and Metalloporphyrins*; Elsevier: Amsterdam, 1964;
(c) Leondiadis, L.; Momenteau, M.; Debois, A. *Inorg. Chem.* 1992, 31, 4691.
(d) Parthasarathi, N.; Hansen, C; Yamaguchi, S; Spiro, T.G. *J. Am. Chem. Soc.* 1987, 109, 3865.
(e) Gans, P.; Buisson, G.; Duce, E.; Marchon, J.C.; Erler, B.S.; Scholz, W.F.; Reed, C.A. *J. Am. Chem. Soc.* 1986, 108, 1223.

21. (a) Hori, H.; Kitagawa, T. *J. Am. Chem. Soc.* 1980, 102, 3608.
(b) Stein, P.; Mitchel, M.; Spiro, T.G. *J. Am. Chem. Soc.* 1980, 102, 7795.

22. (a) Choi, S.; Lee, J.J.; Wei, Y.H.; Spiro, T.G. *J. Am. Chem. Soc.* 1983, 105, 3692.
(b) Smith, D.W.; Williams, R.J.P. *Struct.Bonding (Berlin)* 1970, 7, Chapter 1.
(c) Debois, A.; Lutz, M. *Eur. Biophys. J.* 1992, 20, 321.
(d) Kitagawa, T.; Ozaki, Y.; Teraoka, J.; Kyogoku, Y.; Yamanaka, T. *Biochim. Biophys. Acta.* 1977, 494, 100.
(e) Nagai, K.; Kitagawa, T.; Morimoto, H. *J. Biol. Chem.* 1980, 136, 271.

(f) Mazumdar, S.; Dugad, L.B.; Medhi, O.K.; Mitra S. *J. Chem. Soc., Dalton. Trans.* 1988, 2797.

23. (a) Bartocci, C.; Scandola, F,; Ferri, A.; Carasiti, V. *Inorg. Chim. Acta.* 1979, 37, L473.
(b) Mazumdar, S.; Medhi, O.K.; Kannadaguili, N.; Mitra S. *J. Chem. Soc., Dalton. Trans.* 1989, 1003.

24. Coyle, C.L.; Rafson, P.A.; Abbot, E.H. *Inorg. Chem.* 1973, 12, 2007.

25. (a) Ikeda, S.; Hayashi, S.; Imae, T.*J. Phys. Chem.* 1981, 85, 106.
(b) Grand, D.; Hautecloque, S.; Bernas, A.; Petit, A. *J. Phys. Chem.* 1983, 87, 5236.
(c) James, A.D.; Robinson, B.H. *J. Chem. Soc., Farad. Trans.1* . 1978, 74, 10.
(d) Bunton, C.A.; Mhala, M.M.; Moffat, J.R. *J. Phys. Chem.* 1989, 93, 7851.
(e) Hartland, G.V.; Grieser, F.; White L.R. *J. Chem. Soc., Farad. Trans. 1* . 1987, 83, 591.

26. (a) Mazumdar, S. *J. Phys. Chem.* 1990, 94, 5947.
(b) Mazumdar, S. *J. Chem. Soc., Dalton. Trans.* 1989, 2091.
(c) Mazumdar, S.; Medhi, O.K. *J. Chem. Soc., Dalton. Trans.* 1990, 1057.

27. (a) Fendler, J.H. In *Membrane Mimetic Chemistry*; Wiley-Interscience: New York, 1982.
(b) Robson, R.J.; Dennis, E.A. *Acc. Chem. Res.* 1983, 16, 251.
(c) Ribeiro, A.A.; Dennis, E.A. In *Non-Ionic Surfactants*; Schick, M.J. Ed., Dekker: New York, 1987; Chapter 17, pp. 971.
(d) Bunton, C.A.; Ohmenzetter, K.; Sepulveda, L. *J. Phys. Chem.* 1977, 81, 2000.

28. (a) Almgren, M.; Swarup, S. *J. Colloid Interface. Sci.* 1981, 81, 536: *Ibid.* 1983, 91, 256: *Ibid.* 1982, 86, 4212.
(b) Baglioni, P.; Kevan, L. *J. Phys. Chem.* 1987, 91, 1516.
(c) Zana, R.; Yiv, S.; Strazielle, C.; Lianos, P. *J. Colloid Interface. Sci.* 1981, 80, 208.
(d) Stilbs, P. *J. Colloid Interface. Sci.* 1982, 87, 383: *Ibid.* 1982, 89, 547.
(e) Lianos, P.; Lang, J.; Strazielle, C.; Zana, R. *J. Phys. Chem.* 1982, 86, 1019.

29. Uno, T.; Hatano, K.; Nishimura, Y. *J. Am. Chem. Soc.* 1994, 116, 4107.

30. Katritzky, A.R.; Boulton, A.J. *Adv. Heterocycl. Chem.* 1970, 12, 103.

31. Swallow, A.J. *Progr. React. Kinet.* 1978, 9, 195.

32. Lexa, D.; Momenteau, M.; Seveant, J.M.; Xu, F. *Inorg. Chem.* 1985, 24, 122.

TABLE 6.3.1: UV-VIS absorption bands (nm) of hemin ($\approx 2\times10^{-5}$M) in aqueous detergent micelles and some selected organic solvents.

Micelle (3%)	pH 11.0 $FePP(OH)(H_2O)$	pH 3.0 $FePP(H_2O)_2$	Ref.
TX-100	360(sh), 398, 576, 600.	388, 512, 542, 644.	p
CTAB	360(sh), 400, 576, 600.	390, 512, 541, 645.	p
SDS	360(sh), 401, 488(sh), 525(sh), 604.	393, 508, 540, 635.	p
CH_3CN		385, 505, 540, 640.	17c
CH_2Cl_2		385, 510, 540, 640.	17g
$CHCl_3$		390, 510, 540, 642.	2b

p This work. * As dimethylester complex.

TABLE 6.3.2. : Observed Resonance Raman frequencies (cm^{-1}) of FePPCl in detergent micelles under various experimental conditions.

Micelle	Species	$C_\alpha N$ A_{1g} ν_4	$C_\alpha C_m$ A_{1g} ν_3	$C_\alpha C_m$ E_u ν_{38}	$C_\beta C_\beta$ A_{1g} ν_2	$C_\beta C_\beta$ E_u ν_{37}	$\nu_{C=C}$	$C_\alpha C_m$ B_{1g} ν_{10}	ν_{Fe-N}
TX-100	$PFe^{III}(OH)(H_2O)$	1371	1492	1534	1570	1594	1624	1624	-
	PFe^{II}(2-MeIm))	1355	1469	1524	1561	1585	1623	1603	205
	$PFe^{III}(Im)_2$	1371	1503	1552	1579	1602	1619	1639	-
	$PFe^{II}(Im)_2$	1359	1492	1559	1583	1604	1619	1619	-
	PFe^{II}	-	1503	-	-	-	1623	1643	-
	$PFe^{III}(H_2O)_2$	1372	1494	1534	1572	1594	-	1632	-
CTAB	$PFe^{III}(OH)(H_2O)$	1373	1490	-	1570	1590	1626	1626	-
	PFe^{II}(2-MeIm))	1355	1471	-	1562	1585	1625	1604	205
	$PFe^{II}(Im)_2$	1359	1492	1561	1582	1605	1618	1618	-
	PFe^{II}	1371	1505	-	1583	-	-	1638	-
	$PFe^{III}(H_2O)_2$	1372	1494	-	1572	1594	-	1632	-
SDS	$PFe^{III}(OH)(H_2O)$	1373	1492	-	1572	1592	-	1629	-
	†PFe^{II}(2-MeIm)	1355	1470	-	1562	1584	1624	1604	205
	$PFe^{III}(Im)_2$	1372	1502	-	1579	-	1621	1638	-
	†$PFe^{II}(Im)_2$	1360	1491	-	1581	-	1619	-	-
	$PFe^{III}(H_2O)_2$	1372	1492	-	1571	1593	-	1629	-

† in the presence of 1% ethanol.

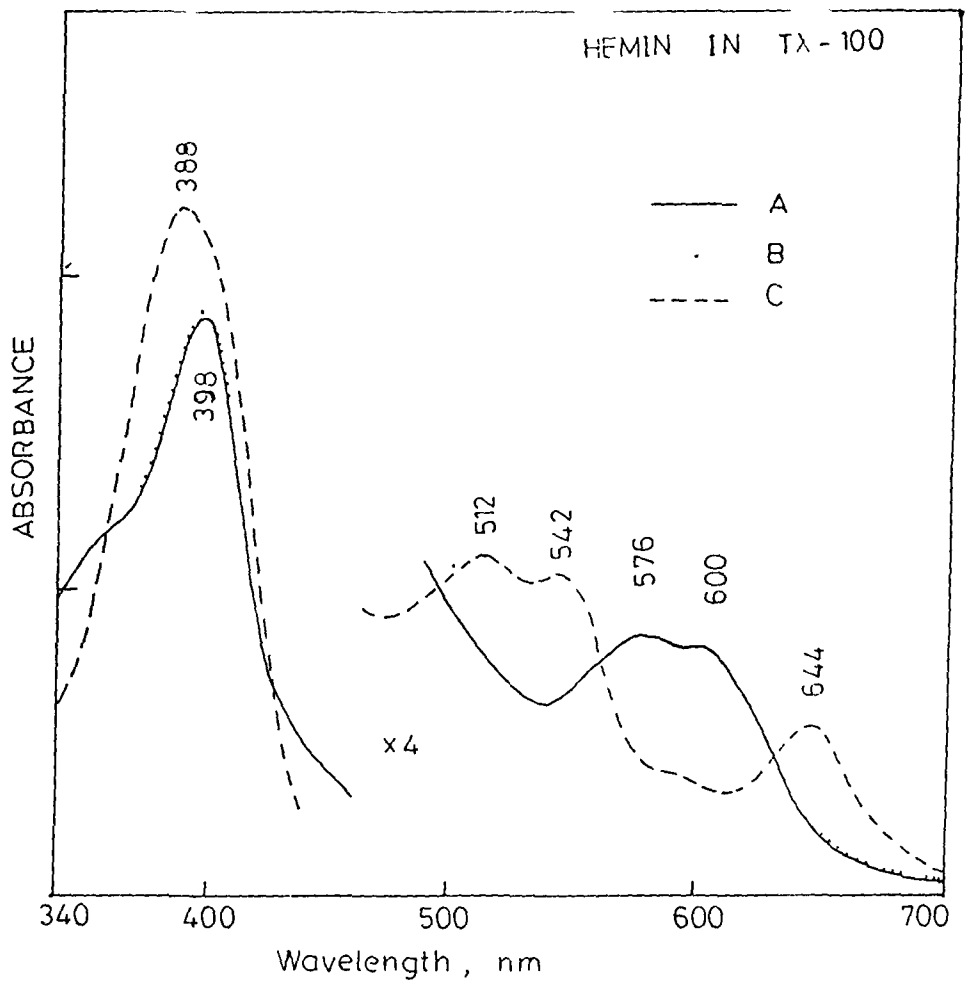

Fig. 6.3.1 Optical absorption spectra of FePPCl (2×10^{-5}M) in 3% TX-100: (A) pH 11, (——); (B) pH 11, A + 2-MeIm (5×10^{-3}M), (· · · ·); (C) pH 3, (– – –). Optical path length = 10 mm.

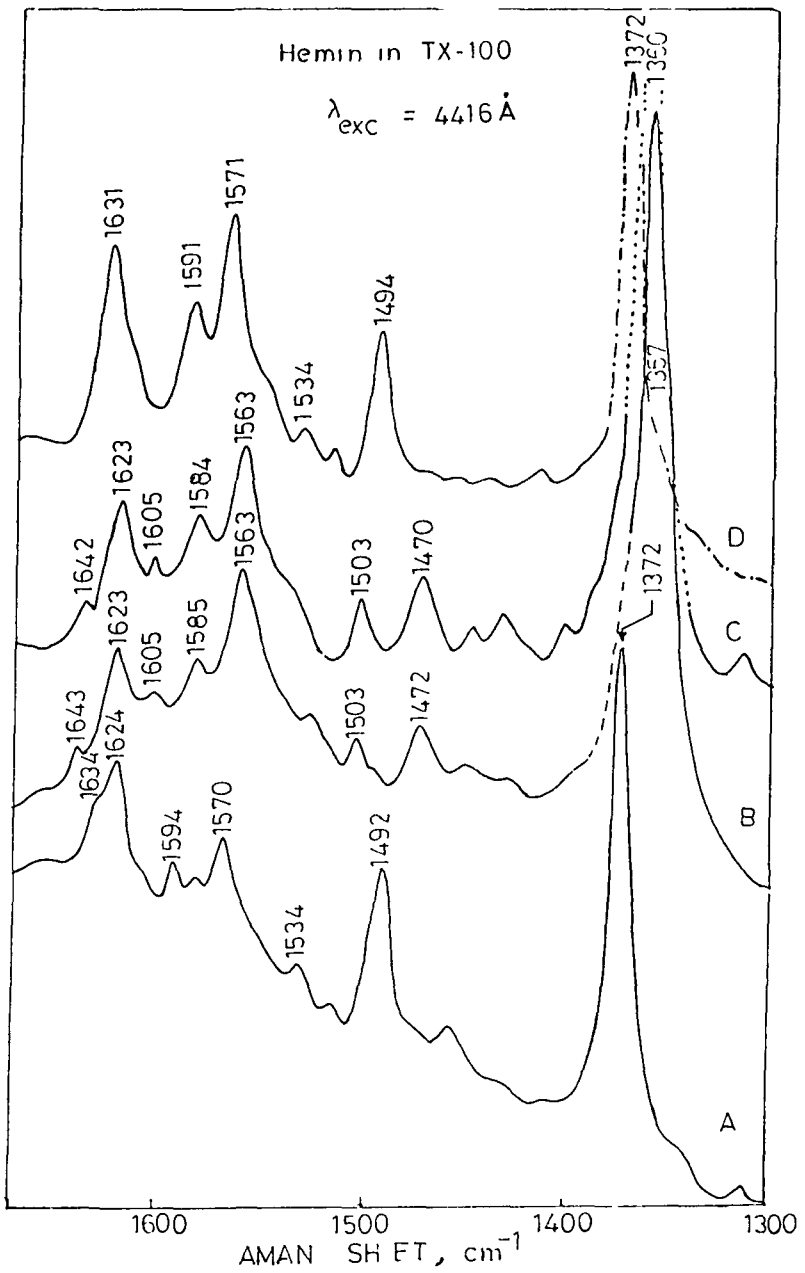

Fig. 6.3.2 RR spectra (1300-1675 cm^{-1}) of FePPC1 (0.5 mM) in 3% TX-100: (A) pH 11, aerobic: (B) pH 11, anaerobic conditions; (C) pH 11, chemically reduced, anaerobic; (D) pH 3, anaerobic conditions. λ_{exc} = 441.6 nm; power 13-18 mW. Scan rate 30 cm^{-1}/min.

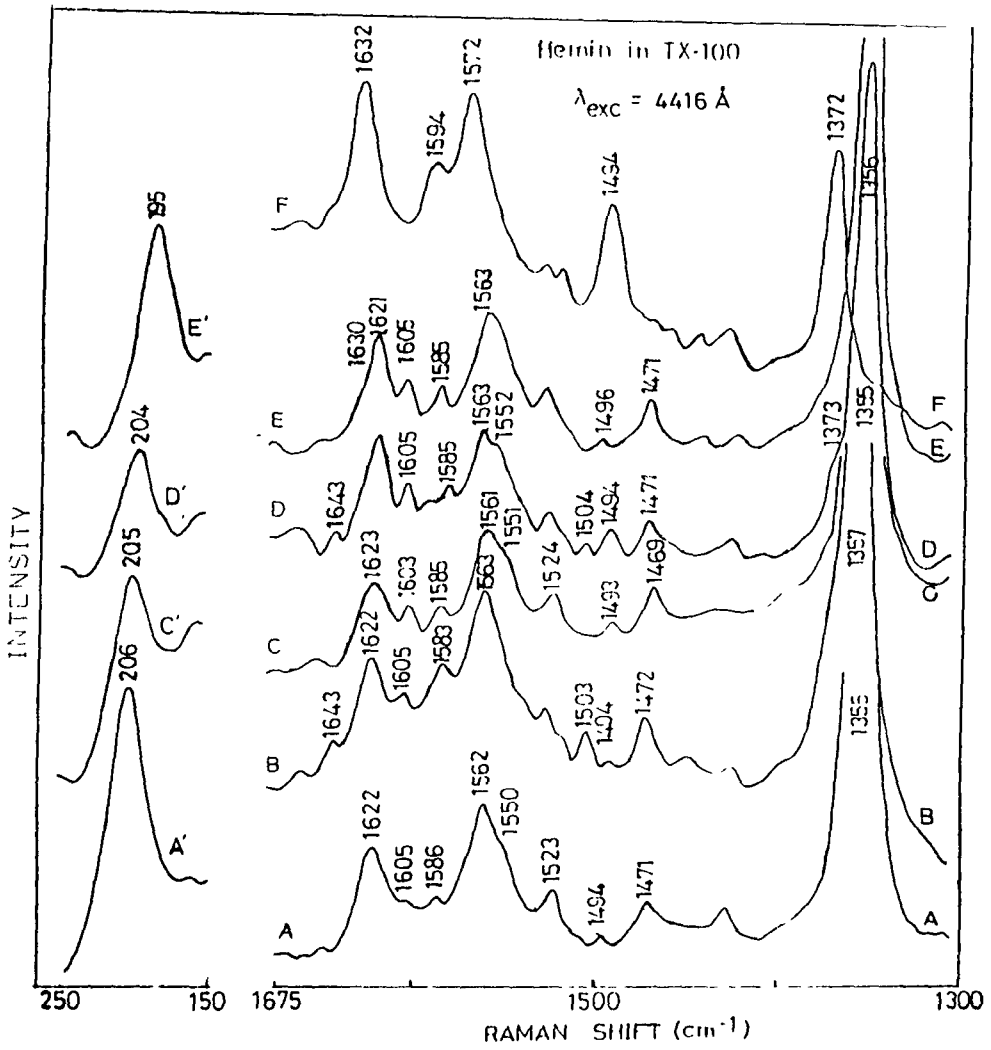

Fig. 6.3.3 RR spectra (1300-1675 cm^{-1}) of FePPCl (0.5 mM) in 3% TX-100 in the presence and absence of 2-MeIm (100 mM): (A) Chemically reduced, pH 11; (B) pH 11; (C) + 2-MeIm, pH 11; (D) + 2-MeIm, pH 7; (E) + 1,2-MeIm, pH 11;(F) + 2-MeIm, pH 3: Spectra A-F recorded in anaerobic conditions. The corresponding RR spectra in the 150-250 cm^{-1} region is shown in traces A'-F'. λ_{exc} = 441.6 nm. Power = 10-13 mW. Scan rate = 30 cm^{-1}/min.

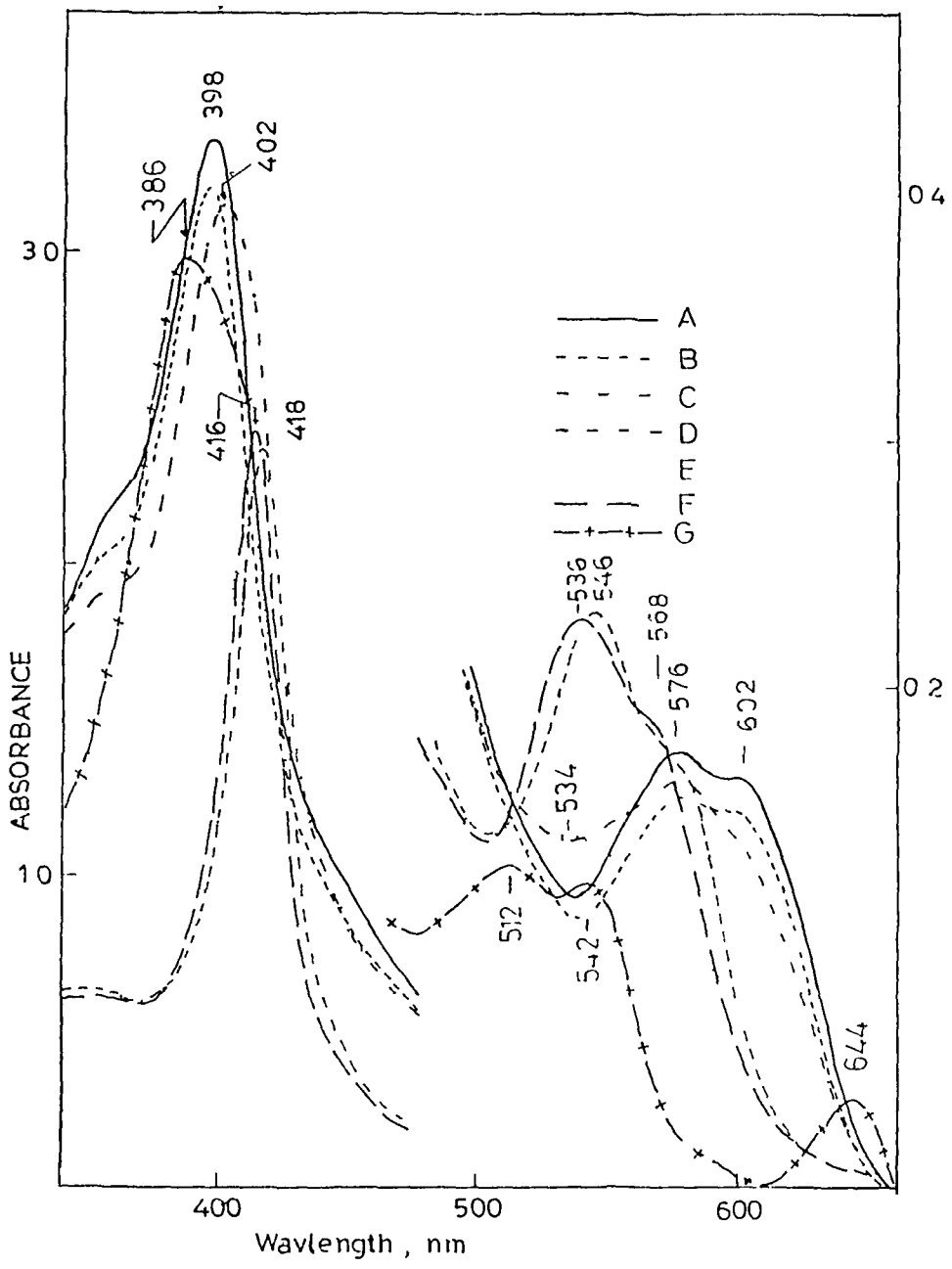

Fig. 6.3.4 UV-VIS spectra of FePPCl (2×10^{-5}M) in 3% TX-100 at different pH and concentrations of imidazole. (A) 11.4, 0 mM; (B) 11.4, 4 mM; (C) 11.4, 200 mM; (D) 11.4, 400 mM; (E) 7.1, 4 mM; (F) 7.1, 200 mM; (G) 3.0, 200 mM. Optical path length = 10 mm. For spectra A, B, C and G the ordinate scale in the Soret region is 0.5 units/div. For spectra D, E and F the scale is as shown.

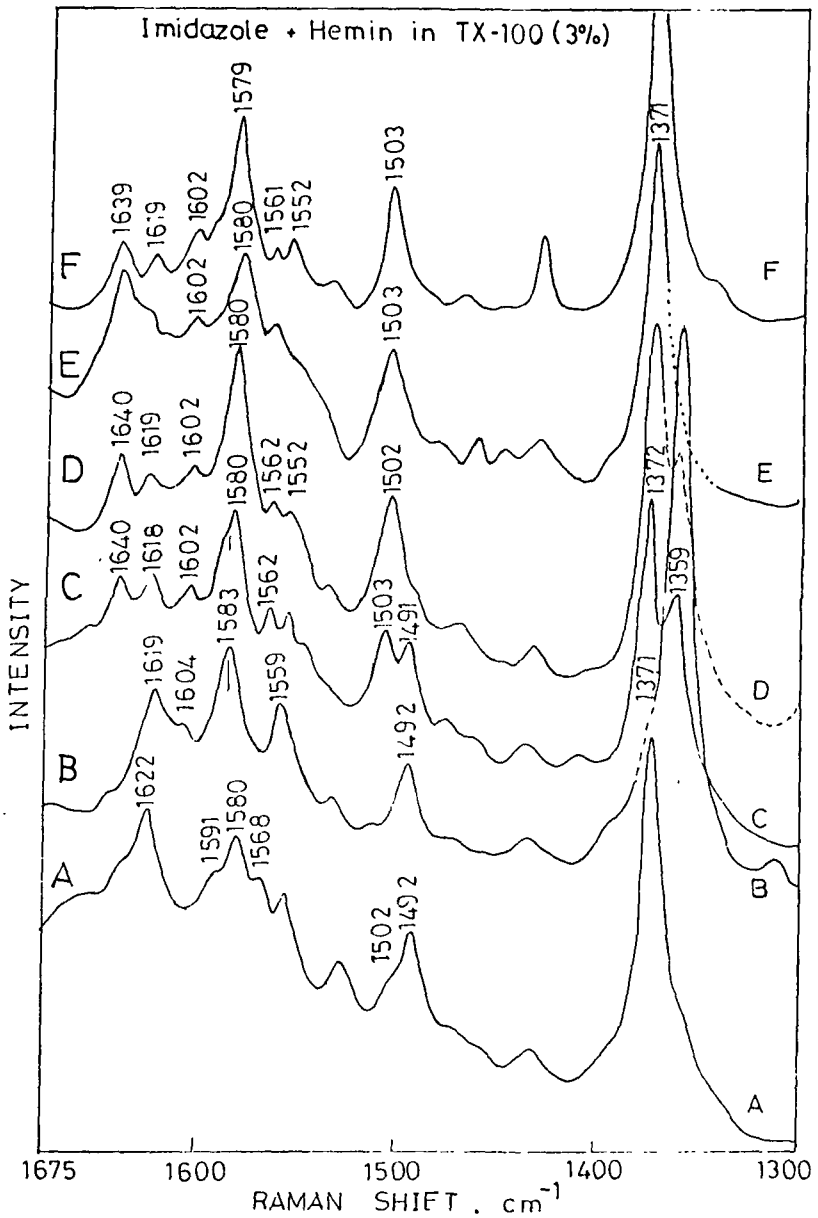

Fig. 6.3.5 RR spectra (1300-1675 cm^{-1}) of FePPCl (0.5 mM) in 3% TX-100 in the presence of imidazole: pH and imidazole concentrations are: (A) pH 11, 100 mM, aerobic; (B) pH 11, 100 mM, anaerobic; (C) pH 10, 100 mM, anaerobic; (D) pH 7, 100 mM anaerobic; (E) pH 11, excess imidazole, anaerobic: Spectrum F is of FePPCl + Im in dilute NaOH at pH 11 in anaerobic conditions. λ_{exc} = 441.6 nm, power = 11 mW. Scan rate 30 cm^{-1}/min.

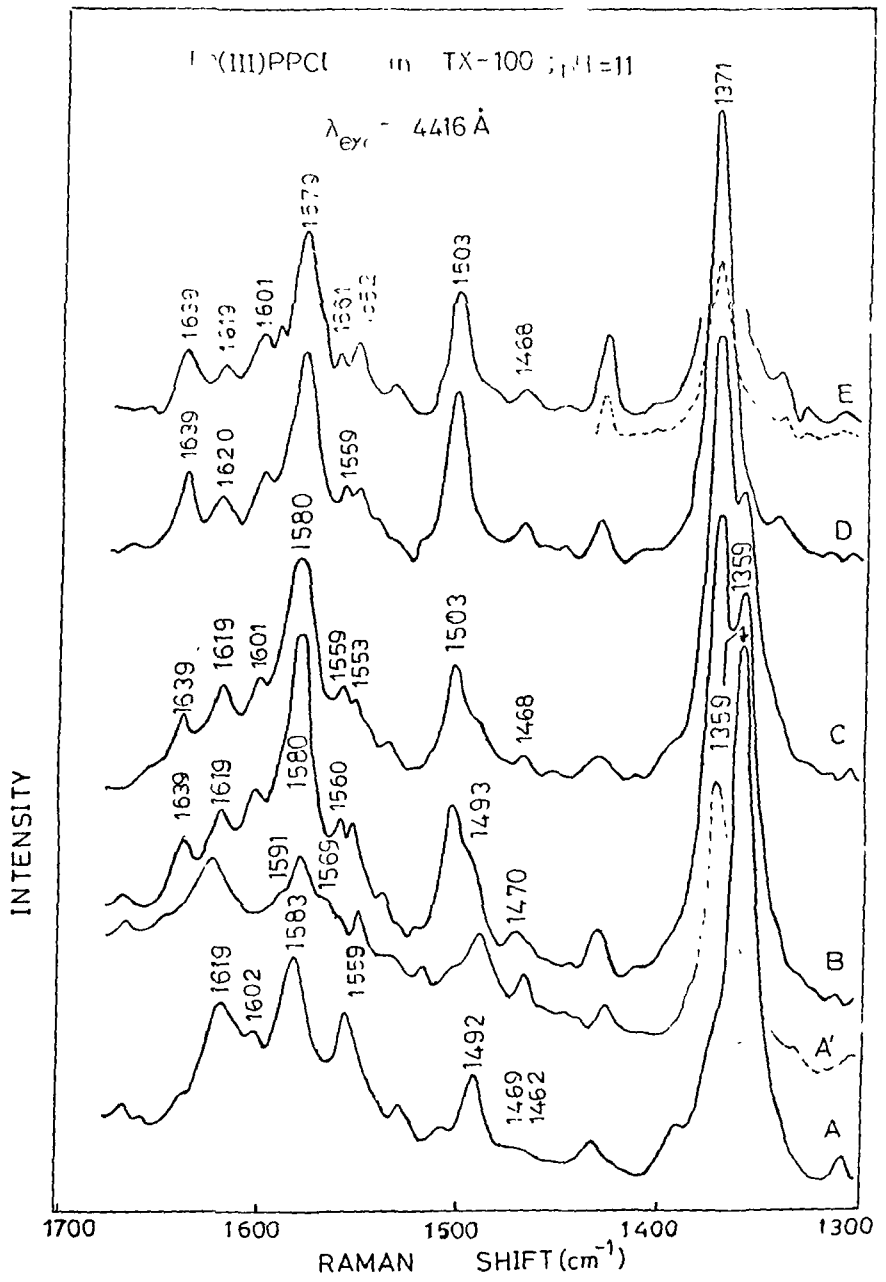

Fig. 6.3.6 RR spectra (1300-1675 cm^{-1}) of FePPCl (0.5 mM) in TX-100 in anaerobic conditions in the presence of imidazole (100 mM): Concentration of TX-100 in (A) 3%, (B) 0.06%, (C) 0.006%, (D) 0.0006%, (E) 0%. (A') 3% in aerobic condition. λ_{exc} = 441.6 nm; laser power = 11 mw; scan rate 30 cm^{-1}/min.

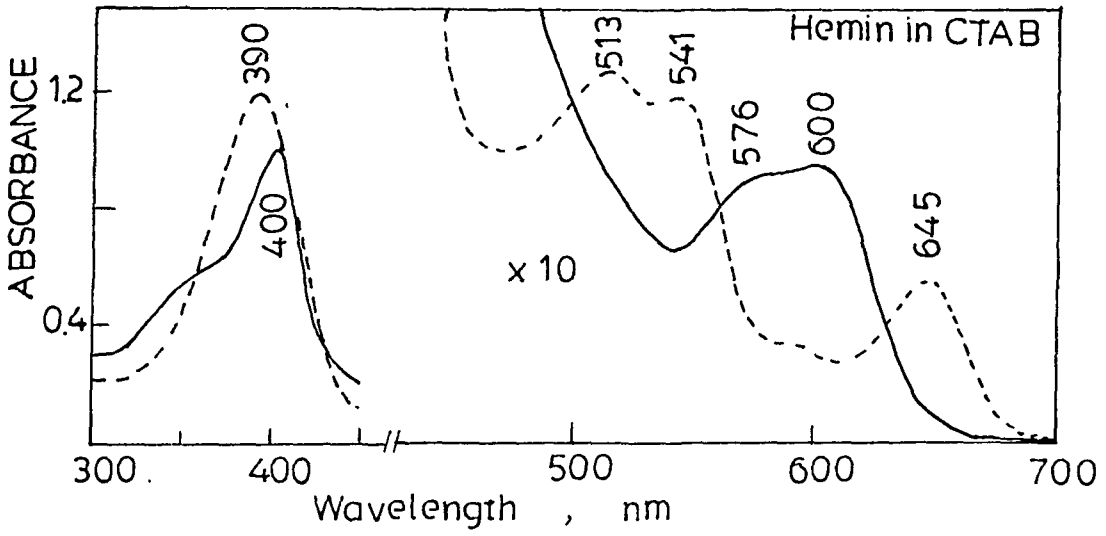

Fig. 6.3.7 UV-VIS spectra of FePPC1 ($\approx 10^{-5}$M) in 3% CTAB: (A) pH 11, (———); (B) pH 3, (----). Optical path length = 10 mm.

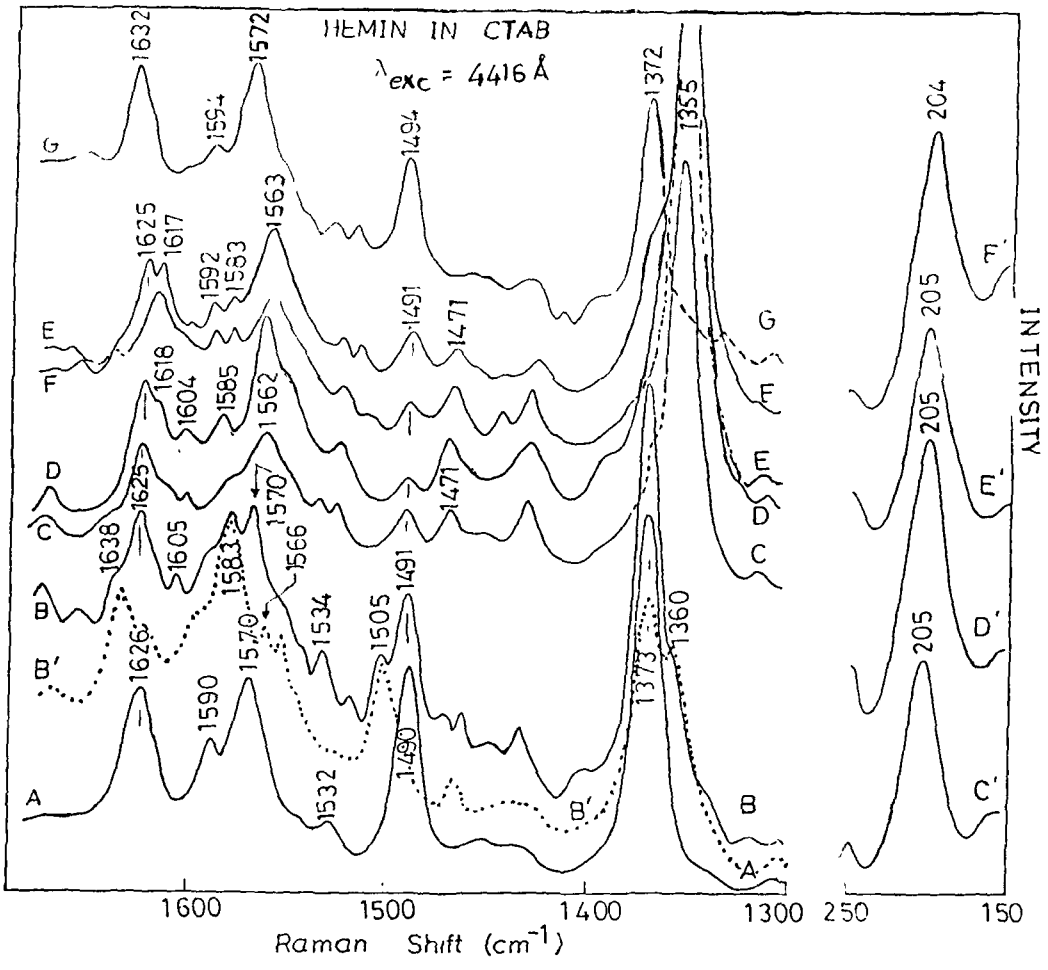

Fig. 6.3.8 RR spectra in the 1300-1675 cm^{-1} and 150-250 cm^{-1} region of FePPCl (0.5 mM) in 3% CTAB in the absence and presence of 2-MeIm (100 mM). (A) pH 11, aerobic; (B) pH 11, anaerobic; (B') pH 11, chemically reduced, anaerobic; (C) pH 11, + 2-MeIm, anaerobic; (D) C + 1% EtOH, anaerobic; (E) pH 11, + 2-MeIm, chemically reduced, anaerobic; (F) pH 7, + 2-MeIm, anaerobic; (G) pH 3, + 2-MeIm, anaerobic conditions. λ_{exc} = 441.6 nm; power = 10-13 mW. Scan rate 30 cm^{-1}/min.

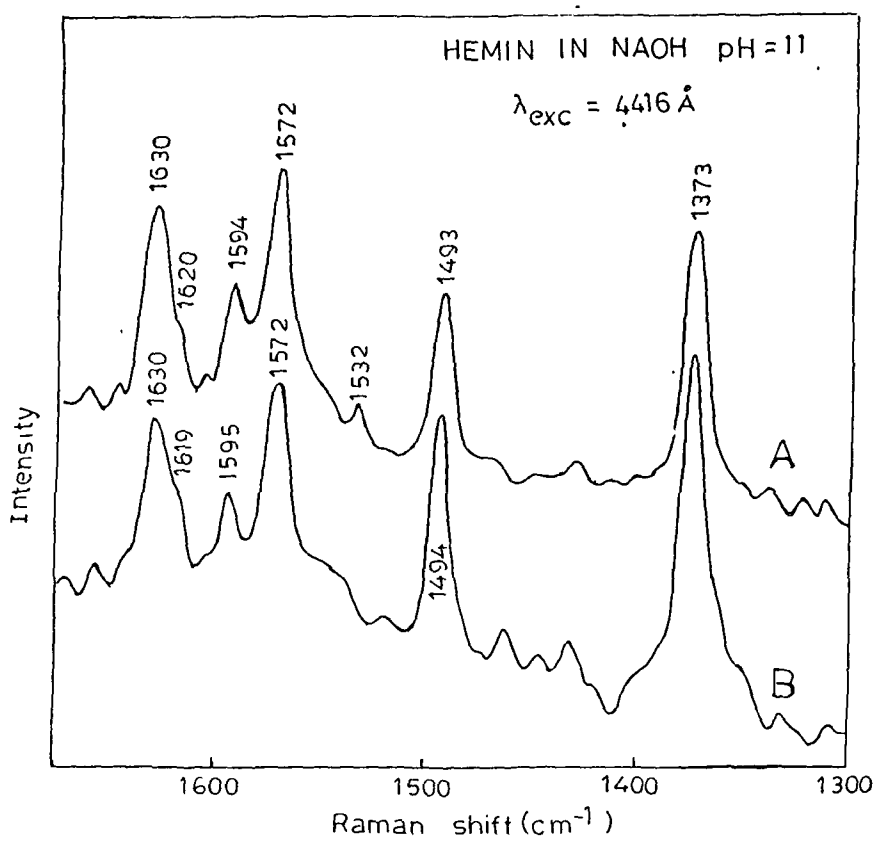

Fig. 6.3.9 RR spectra (1300-1675 cm^{-1}) of FePPCl (0.5 mM) in dilute NaOH at pH 11 in anaerobic conditions: (A) in the absence of 2-MeIm; (B) in the presence of 2-MeIm (100 mM). λ_{exc} = 441.6 nm at 12 mW: scan rate 30 cm^{-1}/min.

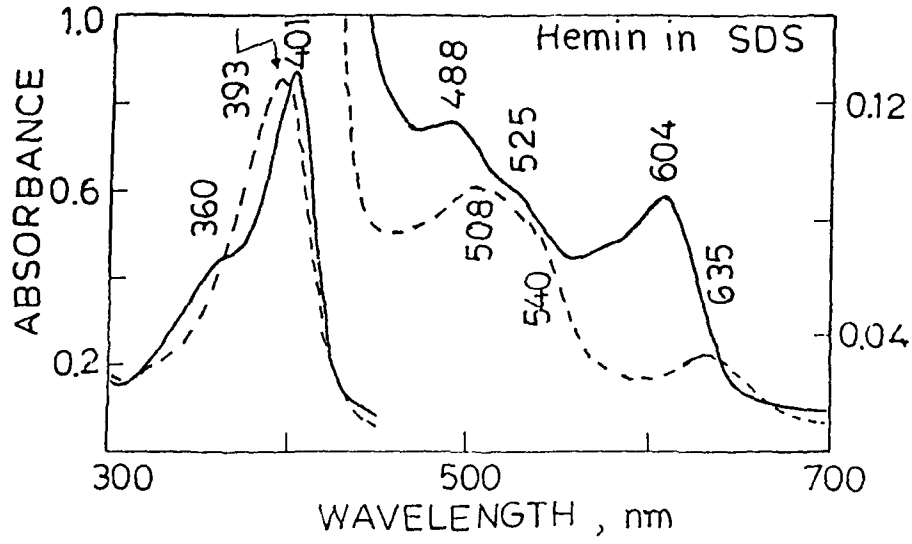

Fig.6.3.10 UV-VIS spectra of FePPCl (≈ 10^{-5}M) in 3% SDS: (A) pH 11, (———); (B) pH 3, (----). Optical path length = 10 mm.

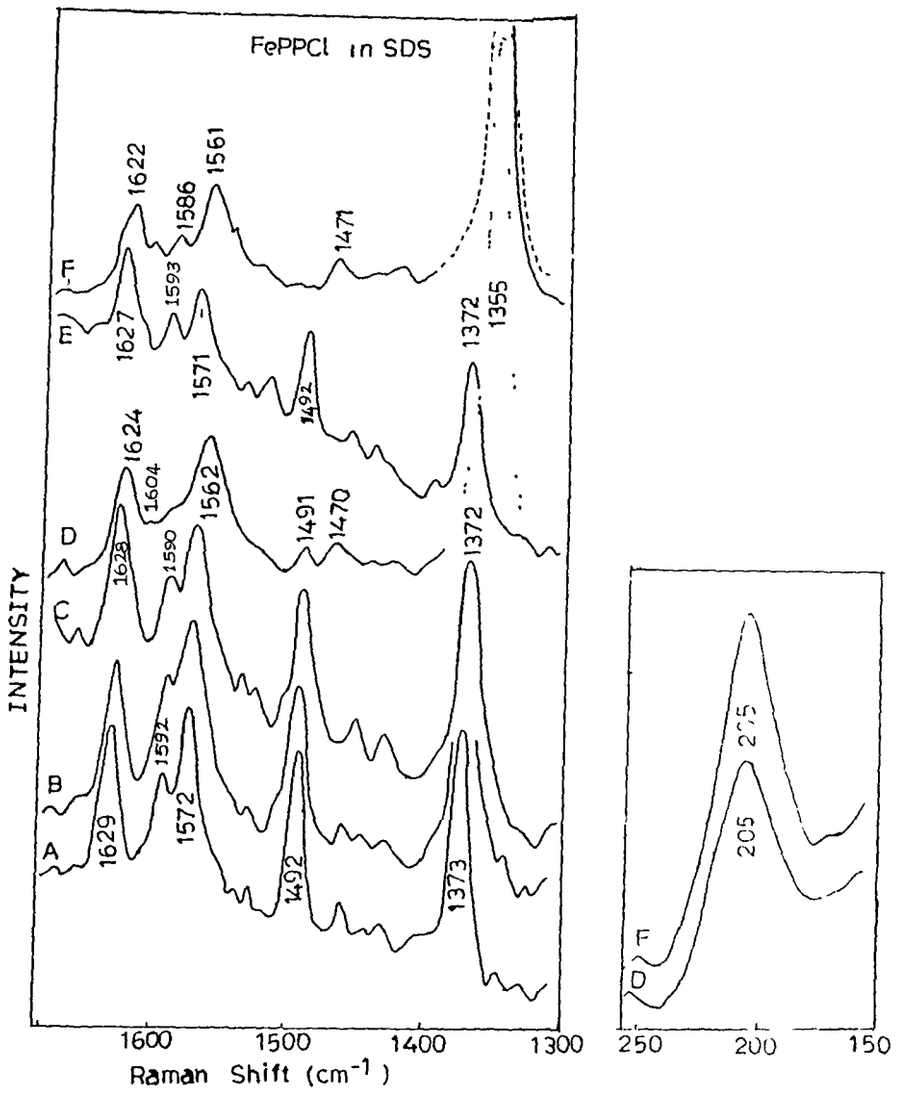

Fig.6.3.11 RR spectra in the 1300-1675 cm^{-1} and 150-250 cm^{-1} region of FePPCl (0.5 mM) in 3% SDS in the absence and presence of 2-MeIm (100 mM). (A) pH 11, anaerobic; (B) pH 11, + 1% EtOH, anaerobic; (C) pH 11, + 2-MeIm, anaerobic; (D) C + 1% EtOH, anaerobic; (E) pH 7, + 2-MeIm, + 1% EtOH, anaerobic; (F) pH 11, + 2-MeIm, chemically reduced, anaerobic; Traces D' and F' correspond to traces D and F in the lower frequency region. λ_{exc} = 441.6 nm; power = 10-13 mW. Scan rate 30 cm^{-1}/min.

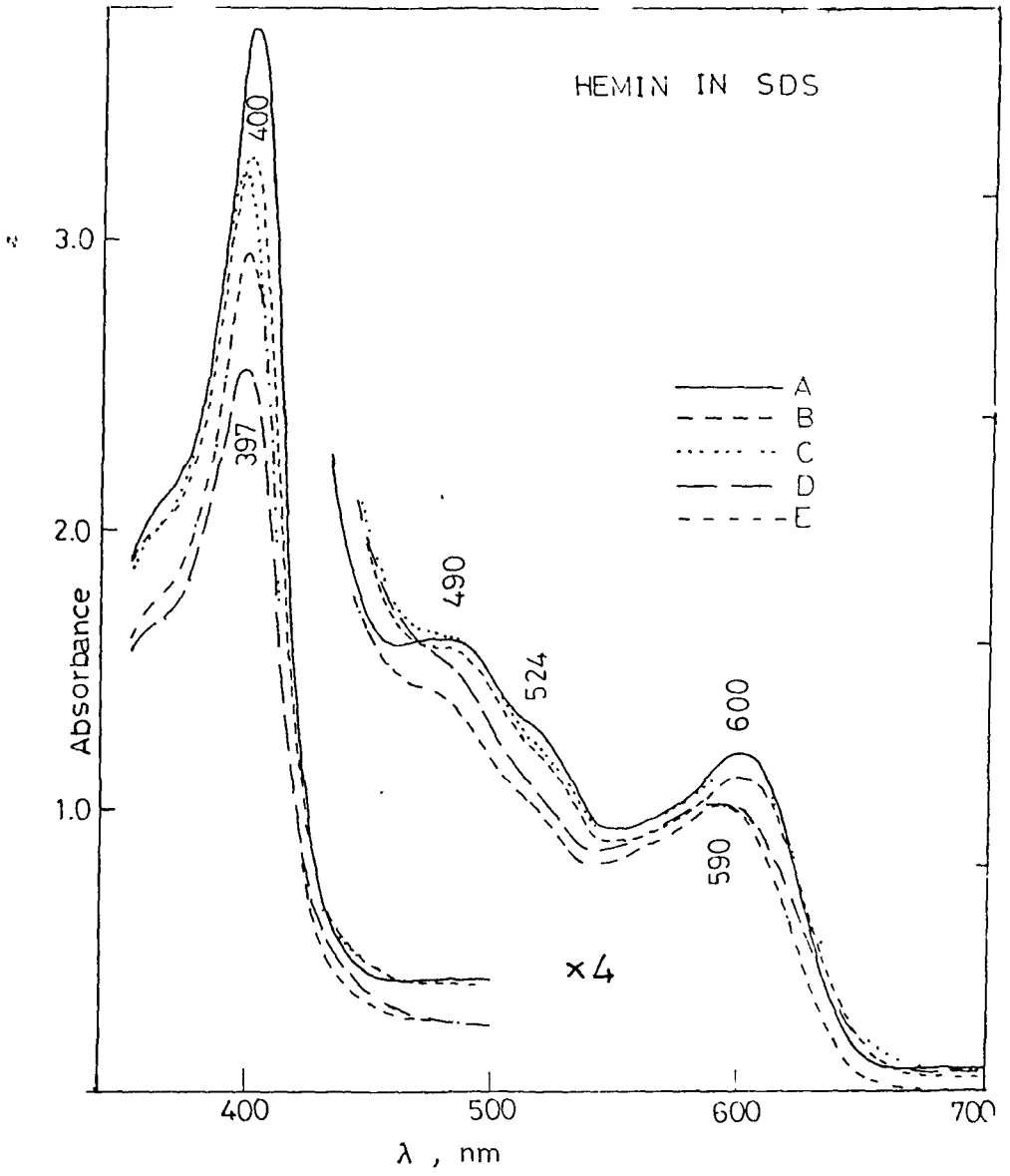

Fig.6.3.12 UV-VIS spectra of FePPCl (3×10^{-5}M) in 3% SDS in the presence and absence of 2-MeIm and EtOH at pH 11.(A) FePPCl only (———); (B) A + 2-MeIm (1 mM) (----); (C) B + 1% EtOH (·····); (D) B + 10 % EtOH; (E) A + 10% EtOH. Optical path length = 10 mm.

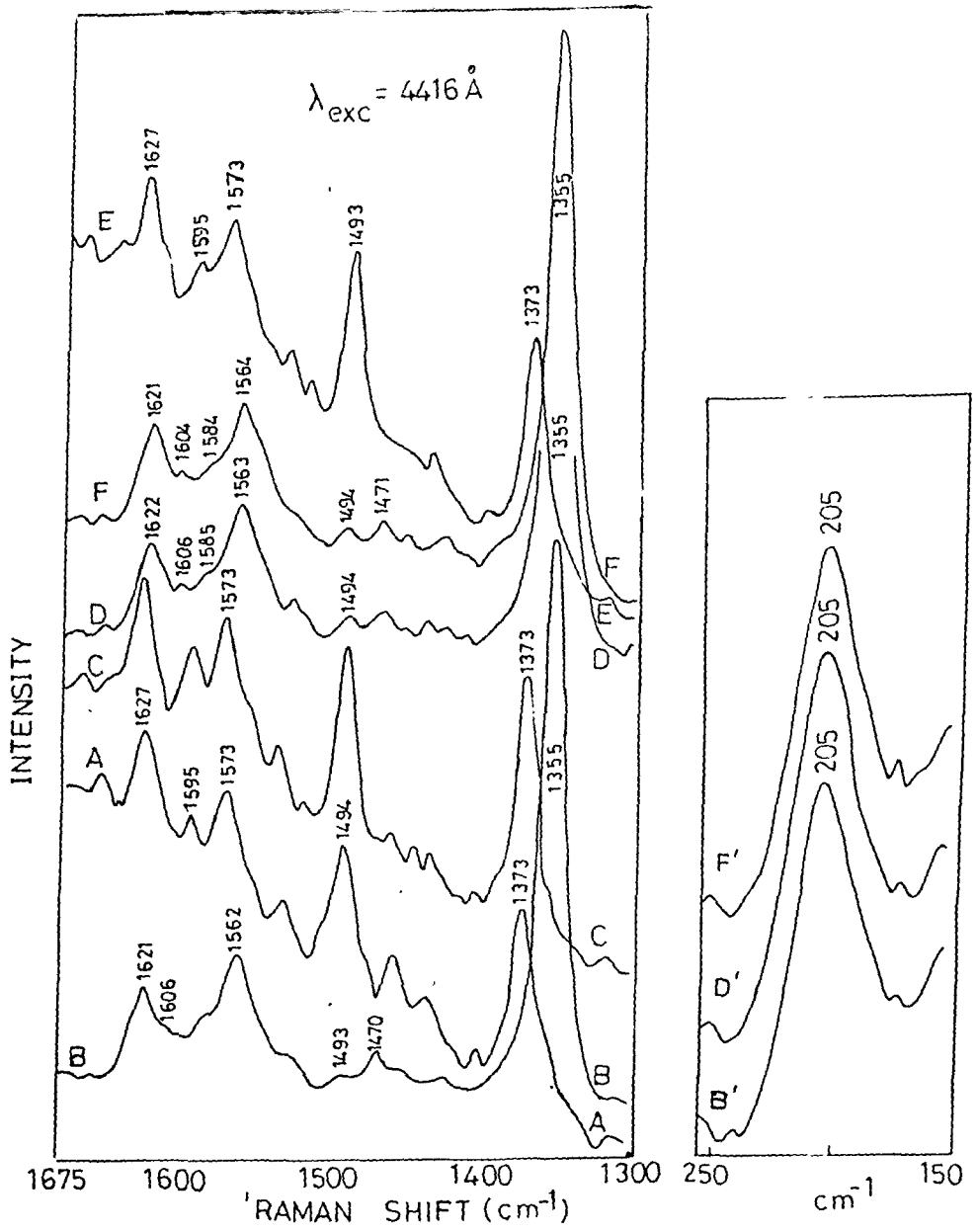

Fig.6.3.13 RR spectra in the 1300-1675 cm^{-1} and 150-250 cm^{-1} region of FePPCl (0.5 mM) in 3% SDS in the presence of TMAB and 2-MeIm (100 mM) in the absence and presence of 1% EtOH at pH 11 in anaerobic conditions. Concentration of TMAB in (A) 0.1 M; (B) 0.1 M + 1% EtOH; (C) 0.08 M; (D) 0.08 M + 1% EtOH; (E) 0.02 M; (F) 0.02 M + 1% EtOH. λ_{exc} = 441.6 nm; power = 10 mW. Scan rate 30 cm^{-1}/min.

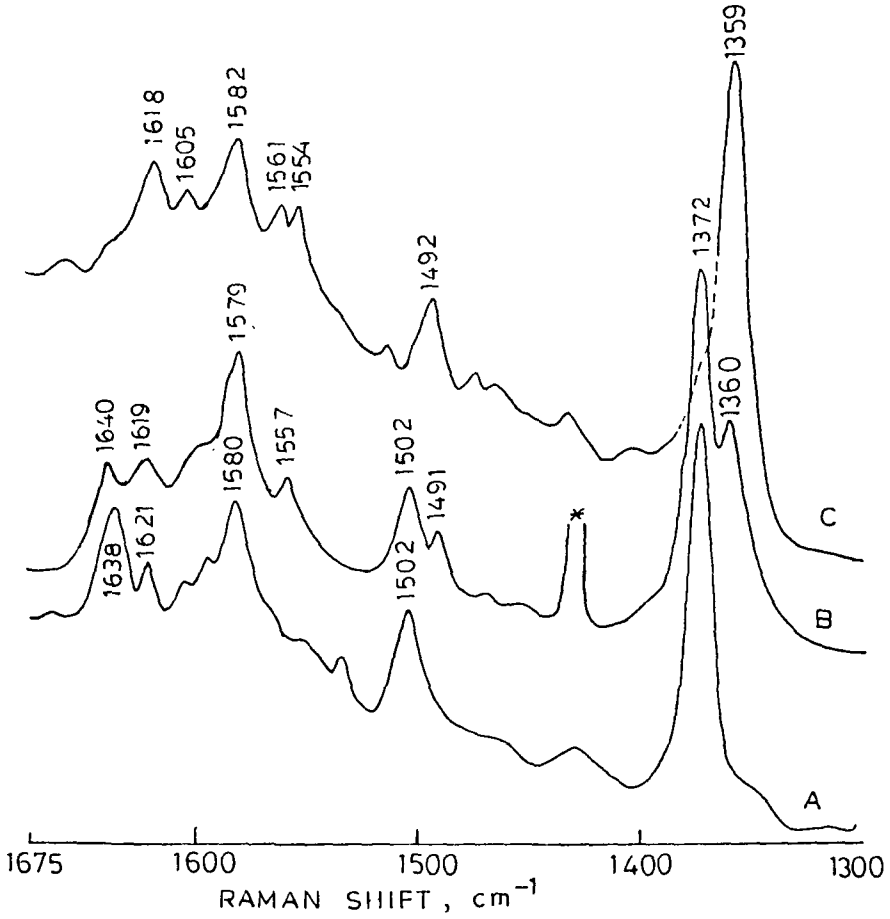

Fig.6.3.14 RR spectra of FePPCl (0.5 mM) in the 1300-1675 cm^{-1} region in anaerobic conditions at pH 11 in the presence of imidazole (50 mM) in: (A) 3% SDS; (B) A + 1% EtOH; (C) in 3% CTAB. λ_{exc} = 441.6 nm; power = 11 mW. Scan rate 30 cm^{-1}/min.

CHAPTER 7

SUMMARY AND CONCLUSION

The scope of this thesis is to elucidate the mechanism of photoinduced redox processes in some iron porphyrins in aqueous detergent micellar media and some other solvent systems which bring into play varied axial ligation at the iron centre and other structural changes using Resonance Raman and optical absorption technique as probes. The interest in micelle catalyzed reactions stems from the structural similarities between micelles and the globular enzyme proteins and parallels between micellar and enzymatic reactions and catalysis. These studies on simple model systems may be of great help in understanding some aspects of the redox processes in complex biological systems like redox cycle of cytochromes, photosynthetic reactions and in other hemeproteins where ligand exchange with metal ion often occurs at interfaces which exert environmental influences on the reactions.

We had undertaken systematic Resonance Raman studies on natural and model iron porphyrins such as iron protoporphyrin (IX) chloride (FePPCl, hemin) and iron tetraphenylporphyrin chloride (FeTPPCl) in different solvent systems in the presence of biologically relevant nitrogenous ligands like 2-methylimidazole (2-MeIm), 1,2-dimethylimidazole (1,2-MeIm) and imidazole (Im) to understand the mechanism of photoredox reactions in these systems and to provide further insight into the electron transfer processes and photoreactive states responsible.

Chapter 1 provided a general introduction to the importance of studies on iron porphyrins and on the photoreactivity of metalloporphyrins. Extensive reviews on photoreduction of iron porphyrins and the current level of understanding as to the mechanism, excited states responsible in some of the systems studied have been dealt with. The importance of RR studies on related model complexes was also emphasized. The basis of employing photoreduction technique and *in situ* monitoring of the redox processes probed by RR technique with various inherent advantages over conventional chemical and electrochemical techniques had been discussed in this chapter.

Sufficient and pertinent theoretical background to understand the absorption and Resonance Raman spectra of the porphyrins in general was presented in Chapter 2. Essential theoretical description of iron porphyrins was also incorporated in this chapter.

The details of different experimental techniques used in this study for recording Raman and absorption spectra were given in Chapter 3. Experimental details of sample preparation and techniques of degassing the solutions and a general introduction to the different micelles used in our study formed part of this chapter.

In Chapter 4 details of optical absorption and RR studies of the μ-oxo dimer, $(FeTPP)_2O$, obtained on dissolution of FeTPPCl in alkaline aqueous Triton X-100 detergent micelle was presented. In this study it was demonstrated that the μ-oxo dimer, located near the hydrophobic core of the micelle, undergoes photodisproportionation on excitation with 441.6 nm laser radiation at room temperature. One of the photoproducts has been identified as the oxoferryl tetraphenylporphyrin ($TPPFe^{IV}=O$) complex by

identifying its characteristic $\nu(Fe^{IV}=O)$ stretching frequency which also showed the expected enhancement in intensity at low temperatures along with those of other RR bands characteristic of low spin oxoferryl porphyrin species. This has been consistent with the expected higher stabilization of this complex at low temperatures. The enhancement of intensity of the RR bands corresponding to the ferryl species including that of the $\nu(Fe^{IV}=O)$ mode at lower laser powers along with the observed shift in the frequency of the axial mode, $\nu(Fe^{IV}=O)$, on coordination of dimethylformamide molecule trans to the ferryl oxygen, as well as the polarized nature of this mode has further confirmed this photoproduct as the $TPPFe^{IV}=O$ complex. Further studies by time-resolved Resonance Raman Spectroscopy and also by an isotope substitution experiment (where ^{16}O is substituted by ^{18}O isotope) can provide further confirmation for the oxoferryl photoproduct. Measurement of magnetic moment of the initial complex in the detergent micelle can shed further light on the nature of the complex in the hydrophobic core. A similar study in ionic detergent micelles like CTAB and SDS may be carried out to investigate the effect, if any, of the charged surface on photodisproportionation of $(FeTPP)_2O$.

Our RR and optical absorption studies of FeTPPCl in organic solvents like CH_2Cl_2, DMSO and in neat 1,2-MeIm in the presence of hindered imidazoles like 2-MeIm and 1,2-MeIm in the first two solvents were presented in Chapter 5. It has been shown that coordination of 1,2-MeIm to FeTPPCl replacing the chloride ion in CH_2Cl_2, DMSO and in neat 1,2-MeIm leads to clean reduction of the iron atom even in the absence of alcohol on photoexcitation at 441.6 nm. In CH_2Cl_2, FeTPPCl has been shown to be photoreduced in the presence of low concentrations of 2-MeIm in anaerobic conditions on excitation at 441.6 and 406.7 nm even in the

absence of alcohol. From optical absorption studies a distinct band has been identified in the 315-340 nm region under conditions where photoreduction of the concerned species was observed in the RR study. This band has been proposed as arising out of a photoreactive state, which is most likely a charge transfer (axial ligand to iron atom) transition state responsible for the observed photoreduction.

The identification of the radical species formed on photoreduction following electron transfer using radical spin traps by ESR technique would enable unambigous identification of the axial ligand responsible for the electron transfer in the photoreduction process. Further, excitation within the proposed CT transition and a study of the excitation profile of certain Raman bands can help establish the CT nature of the photoreactive state proposed.

In Chapter 6 detailed account of RR studies on photoreduction of iron-protoporphyrin IX chloride (hemin) solubilized in aqueous detergent micelles like TX-100, CTAB and SDS in the absence and presence of hindered and unhindered imidazole bases like 2-MeIm, 1,2-MeIm and imidazole was presented. It was shown that in non-ionic TX-100 and cationic CTAB micelles, hemin was photoreduced in anaerobic conditions in the absence of both nitrogenous ligand and primary alcohol on laser excitation at 441.6 nm yielding a four coordinated (ligand-free), intermediate spin (4cIS) transient species and minor quanitities of a mixture of 5cHS ferric and ferrous complexes. Identical absorption spectra of hemin observed in the presence and absence of the hindered imidazoles (2-MeIm or 1,2-MeIm) and in the presence of low concentrations of imidazole in alkaline conditions in these micellar systems was interpreted as indicative of

non-coordination of these nitrogenous ligands to the iron atom in hemin under the experimental conditions used and to propose an electron transfer mechanism from the coordinated hydroxyl ion to the iron atom under photoexcitation at $\lambda_{exc} \leq 458$ nm. Presence of nitrogenous bases lead to their coordination to the 4cIS transient species yielding the observed stable 5cHS or 6cLS complexes. The observation of photoreduction of hemin in SDS only in the simultaneous presence of 2-MeIm and trace amount of ethanol suggested the possible formation of ethanolate moiety via interaction of ethanol and 2-MeIm and eventual coordination of the ethoxy moiety to the iron atom in hemin. The observed photoreduction under these experimental conditions has been proposed as due to electron transfer from the ethanolate anion to the iron centre under photoexcitation at 441.6 nm. Absence of photoreduction of hemin at $\lambda_{exc} \geq 458$ nm in this micelle and also at neutral pH conditions provided further confirmation of this possibility. From a study of photoreduction yield on the concentration of the detergent used (TX-100) at constant concentration of hemin and imidazole it was shown that only those hemin molecules which were monodispersed in the micelles at alkaline pH conditions were photoreducible.

An excitation profile study of photoreduction of hemin in these detergent micelles may give us a clue to the location of the CT transition responsible for this phenomenon. An ESR spin trapping study may help in identifying the radical species and therefore confirm the nature of the electron donor under photoexcitation in different micelles under various experimental conditions.